

DISSERTATION

PART 1: FORMATION AND NUCLEOPHILIC INTERCEPTION OF α,β -UNSATURATED
PLATINUM CARBENES

PART 2: EFFORTS TOWARD CONTROLLING MAGNETIC PROPERTIES OF COBALT
AND IRON COORDINATION COMPLEXES

Submitted by

Tarik J. Ozumerzifon

Department of Chemistry

In partial fulfillment of the requirements

For the Degree of Doctor of Philosophy

Colorado State University

Fort Collins, Colorado

Fall 2017

Doctoral Committee:

Advisor: Matthew P. Shores

Alan J. Kennan
James R. Neilson
Jeffrey D. Achter

Copyright by Tarik J. Ozumerzifon 2017

All Rights Reserved

ABSTRACT

PART 1: FORMATION AND NUCLEOPHILIC INTERCEPTION OF α,β -UNSATURATED PLATINUM CARBENES

PART 2: EFFORTS TOWARD CONTROLLING MAGNETIC PROPERTIES OF COBALT AND IRON COORDINATION COMPLEXES

Presented in this dissertation are a series of studies describing the use of transition metals in several different applications. Part 1 concerns the development of novel platinum(II)-catalyzed reaction manifolds toward C-C bond formation, as well as the formal synthesis of a natural product. Meanwhile, Part 2 describes three separate efforts toward modulation of either single-molecule magnet properties in cobalt(II) or spin state control of iron(II) coordination complexes.

The first chapter is a general introduction to single-molecule magnetism (SMM) and spin crossover, as these topics specifically relate to Co(II) and Fe(II) complexes, respectively. The physical origins of both phenomena are discussed, as well as some general terminology that are used throughout Chapters 3-5.

Chapter 2 describes the use of Pt(II) salts in alkyne activation reactivity. The vinylogous addition of carbon nucleophiles into α,β -unsaturated platinum carbenes is discussed, and the optimization and scope of enol incorporation is provided. This is followed by a description of how Pt(II) catalysis enables the rapid formal synthesis of frondosin B, a sesquiterpene natural product.

In Chapter 3, the synthesis and characterization of several salts of a trigonal prismatic cobalt(II) complex are detailed. The capping ligand used in these podands is *cis-cis*-1,3,5-triaminocyclohexane (tach), a rigid backbone which dictates coordination geometry and the

iminopyridine contains pendant *tert*-butylamide moieties which are meant to enable guest association. The single-molecule magnet behavior (measured via slow magnetic relaxation) of these compounds is also explored, where the cation-binding tetraphenylborate salt shows slow magnetic relaxation at both zero and applied dc fields. A brief discussion of theoretical considerations of the effect of trigonal distortion on axial anisotropy is also presented, which suggests systems in an intermediate twisting geometry may give rise to guest-dependent magnetic properties in SMMs.

Chapter 4 presents initial efforts toward the development of an Fe(II) system which can undergo a spin-state switch upon addition of a reagent. The chemoselective process is intended to be the result of an irreversible ligand modification. The first target toward this goal is manifested in desilylation of a 5-siloxy substituted podand. Spectroscopic and spectrometric as well as electrochemical and magnetic data indicate qualitatively that ligand desilylation is occurring as a function of fluoride addition, affecting a decrease in high-spin:low-spin ratio.

Last, Chapter 5 details the systematic study of electronic character of 5-pyridyl substitution in the Fe(II) tren iminopyridine tripodal system. The Fe(II) species magnetic susceptibility and Ni(II) analog d-d transition energy data are compared to the Hammett parameter of the respective substituent, which define the complexes' electron-donating or -withdrawing properties. Overall, electron withdrawing substituents at this position lead to stabilization of the HS state. A comparison of these iminopyridine complexes to Fe(II) podands which undergo spin crossover is provided in an effort to explain the observed low-spin behavior of these complexes.

ACKNOWLEDGMENTS

If you ask me, any success I've had in graduate school has been a result of the mentorship and thoughtful conversations I've had with those I've had the luck of meeting at CSU. When I first got here, I remember running into Heemal outside of the building the week before classes started and he was still looking for a place to live. Luckily, one of the units in my complex was available and I told him he should move in. He did, and we became close friends. One of my biggest regrets is that we only got to spend a year together. Also that first year, I remember Phil(0) and Mike going through the organic chemistry "motions" together with us. Sadly, our time together also got cut short.

For only a year a half, I got to work for Eric Ferreira. Maybe I was that bad when I got here, but I was very quickly brought up to speed by the excellent chemists that were around me. Not only that, but we became friends, which I can't be thankful enough for. When I joined up, I got to work with Paul on projects that we were genuinely interested in while we became close friends. I also got to work in the same lab as Eric and Suzie, which was truly amazingly fun. Lil Mike used to set me straight, and while I may have hated him for it at the time, he is the biggest reason that I am even as remotely competent as I am. Suzie, my $C_2B_2F_2$, is a person that I can always call and chat with to ask for advice, or more importantly, talk about anything besides chemistry. Curtis, Oily Pete, Tim, Francisco and Phil, to all of you, I only wish we had been able to work together longer. Eric, you will always be a role model of mine. You were always extremely supportive of me, even when I didn't deserve it. Thank you for everything. Your sports allegiances suck, though.

Matt Shores in many ways saved me after the summer of 2014. I know you were on sabbatical, and you probably didn't even like me all that much, but you still accepted me into your group in the aftermath. I hope that the skills I was able to learn with Eric have benefited your group, because I certainly feel indebted to you, even if we might forget it from time to time. Christina, from the start, you were always honest with me. That is the trait that I appreciate most in you, and I thoroughly enjoyed working with you and taking over (some) of your projects. Justin, I see the enthusiasm you bring to the group and I am glad that things are working out for you. Romeo, while we haven't always seen eye to eye on things, you have been a consistently good friend and I wish you nothing but the best. Robert, of course, I've really got to thank you for everything. Your willingness to help literally everyone, your work ethic, your attitude and your humility all combine to make one amazing chemist. I'm glad we were able to become close friends.

While outside of the lab, trivia and softball were always fun. Dan and Trey, we have remained friends since the beginning, and it's always been fun to hang out with you guys. Especially because it meant we likely weren't in lab.

I've intentionally saved the most important for last, Stephanie, the love of my life. You have changed me so much for the better. And not only that, but we have Michael, the best doggy anyone could ask for. Thank you for your support over the past five years.

DEDICATION

For Stephanie and Michael, my two best friends.

TABLE OF CONTENTS

ABSTRACT.....	ii
ACKNOWLEDGMENTS	iv
DEDICATION.....	vi
TABLE OF CONTENTS.....	vii
LIST OF TABLES	xii
LIST OF FIGURES	xiii
LIST OF SCHEMES.....	xvii
Chapter 1: Controlling Spin Properties of First Row Transition Metals: Exploitation of Iron(II) and Cobalt(II) Magnetic Properties	1
1.1 Introduction.....	1
1.2 Single-Molecule Magnetism.....	1
1.3 Spin Crossover	4
1.4 Recent Efforts to Control SMM and Spin State Properties	5
1.5. Outline of Chapters	6
References.....	8
Chapter 2: Nucleophilic Interception of α,β -Unsaturated Platinum Carbenes	9
2.1 Introduction.....	9
2.2 Division of Labor	15
2.3 Experimental Details.....	16
2.3.1. Materials and Methods.....	16
2.3.2. Synthesis of Dicarbonyl-Incorporated Heterocycles	17
2.3.3. Synthesis of aniline and phenol carbene precursors	41
2.3.4. Competition Experiments	48

2.3.5. Synthesis of Frondosin B	49
2.4 Results and Discussion	58
2.4.1. Optimization and scope of dicarbonyl vinylogous additions.....	58
2.4.2. Competition Experiments	61
2.4.3. (4+3) cycloadditions enabled by diene incorporations	63
2.5 Conclusions.....	67
2.6 Acknowledgments.....	67
References.....	68
 Chapter 3: Toward Steric Control of Guest Binding Modality: a Cationic Co(II) Complex Exhibiting Cation Binding and Zero-Field Relaxation.....	
3.1 Introduction.....	71
3.2 Division of Labor	72
3.3 Experimental Details.....	72
3.3.1. Materials and Methods.....	72
3.3.2. Synthesis of ligands and cobalt complexes.....	74
3.3.4. Crystallographic Results	79
3.4 Results and Discussion	82
3.4.1. Synthesis of Co Complexes	82
3.4.2. DC Magnetic properties of 3-9 and 3-10	84
3.4.3. AC Magnetic Properties of 3-9 and 3-10.....	86
3.4.4. Theoretical Analysis of Anisotropy in Hexacoordinate System.....	89

3.5 Conclusions.....	90
3.6 Acknowledgments.....	91
References.....	92
Chapter 4: Progress Toward Spin-State Switching Induced by Chemical Modifications to Ligands in an Fe(II) Tripodal System.....	94
4.1 Introduction.....	94
4.2 Division of Labor.....	96
4.3 Experimental Details.....	97
4.3.1. Materials and Methods.....	97
4.3.2. Synthesis of Ligands and Fe Complexes.....	100
4.3.3 Crystallographic Results.....	104
4.4 Results and Discussion.....	105
4.4.1. Synthesis and Characterization of Fe Podands.....	105
4.4.2. Mass Spectrometry and NMR Analysis of Desilylation Reaction.....	107
4.4.3. Electrochemistry of 4-8 and 4-9.....	110
4.4.4. Discussion of Desilylation Reaction.....	113
4.5 Conclusions.....	115
4.6 Acknowledgments.....	115
References.....	116
Chapter 5: Investigation of Electronic Effect of 5-Pyridyl Substitution in Iron(II) Tren-Based Iminopyridines.....	119
5.1 Introduction.....	119

5.2 Division of Labor	121
5.3 Experimental Details.....	121
5.3.1. Materials and Methods.....	121
5.3.2. Syntheses of Ligands	123
5.3.3. Synthesis of Metal Complexes.....	128
5.3.4. Crystallographic Results	135
5.4 Results and Discussion	137
5.4.1. Synthesis of Fe complexes.....	137
5.4.2. Analysis of Ni(II) Analogs.....	139
5.4.3. Discussion of SCO Fe(II) tren Podands.....	143
5.5 Conclusions.....	146
5.6 Acknowledgments.....	146
References.....	147
Appendix 1: Supporting Information for Chapter 2	150
Cross referencing of dissertation numbering with numbering from published work.	150
Appendix 2: Supporting Information for Chapter 3	151
IR and Electronic Spectral Characterization of Co Complexes.....	151
Magnetic Data of Co Complexes.....	152
Appendix 3: Supporting Information for Chapter 4	155
A3.1. Mass Spectrometry Data	155
Electrochemical Data	166

Magnetic Data.....	168
NMR and IR Spectroscopic Data.....	169
Appendix 4: Supporting Information for Chapter 5	174

LIST OF TABLES

Table 2.4.1. Reaction optimization for enol incorporation.	59
Table 3.3.1. Crystallographic parameters for 3-9, 3-10, 3-11 and 3-12.	81
Table 3.4.1. Compiled crystallographic details regarding binding pockets in tripodal complexes.	83
Table 3.4.2. Anisotropy values acquired from fitting magnetic susceptibility data and calculations.	85
Table 4.3.1. Crystallographic parameters for 4-8.	105
Table 5.3.1. Crystallographic parameters for 5-14, 5-15, and 5-16.....	136
Table 5.4.1. Compiled relevant crystallographic details for 5-14, 5-15 and 5-16.	137
Table 5.4.2. Comparison of solution magnetic susceptibilities and Hammett parameters for Fe triflate salts.....	138
Table 5.4.3. Tabulated Ni(II) Dq values for 5-14a – 5-17a, 5-19a – 5-22a.....	142
Table 5.4.4. Summary of structural changes upon SCO in Fe(II) tren-capped tripodal systems.	145
Table A3.1. Major peaks in the ESI-MS spectra for 4-8 before and after addition of CsF.	162
Table A3.2. Major peaks in the ESI-MS spectra for 4-9 before and after addition of CsF.	162
Table A3.3. Relative abundance (%) of the major peaks in the ESI-MS spectra for 4-8 with different equivalents of CsF added.	163
Table A3.4. Relative abundance (%) of the major peaks in the ESI-MS spectra for 4-9 with different equivalents of CsF added.	163

LIST OF FIGURES

Figure 1.2.1. Schematic representing multiple relaxation pathways in SMMs.	3
Figure 1.3.1. Changes in electronic and physical structure between HS and LS Fe(II) ions.	4
Figure 3.3.1. Crystal structures of the cationic complexes 3-9.....	80
Figure 3.3.2. Crystal structure of 3-11	81
Figure 3.4.1. Short contacts in 3-9.....	82
Figure 3.4.2. Variable temperature dc magnetic susceptibility data for 3-9 and 3-10 collected between 1.8 and 300 K at an applied dc field of 1000 Oe.	84
Figure 3.4.3. Field dependence of magnetization for 3-10 collected at 2 K.....	85
Figure 3.4.4. DC field scan of 3-9.	87
Figure 3.4.5. DC field scan of 3-10.	87
Figure 3.4.6. Out-of-phase magnetic susceptibility for compound 3-10	88
Figure 3.4.7. Fit of out-of-phase χ'' maxima (1000 Oe).	89
Figure 3.4.8. Calculated energy of the second excited state in $[\text{Co}(\text{NH}_3)_6]^{2+}$ and ZFS parameters (D, E) as a function of torsion angle.	90
Figure 4.3.1. Crystal structure of the cationic complex 4-8.....	104
Figure 4.4.1. Temperature dependence of magnetic susceptibility for 4-9 measured with an applied dc field of 5000 Oe.....	106
Figure 4.4.2. Top: solution state magnetic properties for 4-8 upon addition of CsF. Bottom: relative abundance of Fe-containing desilylated ions, as determined by mass spectrometry for 4-8.....	108
Figure 4.4.3. Top: solution state magnetic properties for 4-9 upon addition of fluoride. Bottom: relative abundance of desilylated products as determined by mass spectrometry for 4-9.....	109
Figure 4.4.4. Cyclic voltammograms of 4-8 (bottom) and 4-9 (top) measured in 0.10 M Bu_4NPF_6 solutions in MeOH with scan rates of 0.10 V s^{-1} (solid) or 10 V s^{-1} (dashed).....	111
Figure 4.4.5. CV of 4-8 measured in a 0.10 M Bu_4NPF_6 solution of methanol with a scan rate of 0.10 V s^{-1} after addition of excess CsF.	112
Figure 4.4.6. Electrochemical data for 4-8 at ~0.001 M in a 0.1 M Bu_4NPF_6 MeOH solution scanning at 0.1 V s^{-1}	113
Figure 5.3.1. Crystal structures of the cationic complexes 5-14 (left) and 5-15 (right) depicted with 40% probability ellipsoids.	135
Figure 5.3.2. Crystal structure of 5-16 depicted with 40% probability ellipsoids.....	136
Figure 5.4.1. Plot of χ_{MT} as a function of Hammett parameter for the eight Fe complexes.	139
Figure 5.4.2. Dependence of the Ni(II) analog ligand field splitting (Dq) as a function of ligand substituent ($3\sigma_{\text{meta}}$).	140

Figure 5.4.3. Intramolecular π stacking in 5-16.....	141
Figure 5.4.4. Dependence of Ni(II) analog Dq as a function of $3\sigma_{\text{para}}$	142
Figure 5.4.5. Overlay of the HS (grey) and LS (black) crystal structures of $[\text{Fe}(\text{pz}_3\text{tren})](\text{NO}_3)_2 \cdot \text{CH}_3\text{NO}_2$	144
Figure A2.1. Stacked IR spectra of 3-9 and 3-10.	151
Figure A2.2. Stacked UV-Vis spectra of 3-9 and 3-10.....	151
Figure A2.3. Field dependence of magnetization for 3-9 collected at 100 K.....	152
Figure A2.4. Field dependence of magnetization for 3-10 collected at 100 K.....	152
Figure A2.5. Reduced magnetization of 3-10.....	153
Figure A2.6. χ' vs. ν under 0 applied DC field for 3-10.	153
Figure A2.7. χ' vs. ν under 1000 Oe applied DC field for 3-10.....	154
Figure A3.1. Full MS (positive ion mode) of 4-8 with 0 equivalents of CsF added in CD_3OD . 155	
Figure A3.2. Full MS (positive ion mode) of 4-8 with 0.5 equivalents of CsF added in CD_3OD	155
Figure A3.3. Full MS (positive ion mode) of 4-8 with 1 equivalent of CsF added in CD_3OD . . 156	
Figure A3.4. Full MS (positive ion mode) of 4-8 with 1.5 equivalents of CsF added in CD_3OD	156
Figure A3.5. Full MS (positive ion mode) of 4-8 with 2 equivalents of CsF added in CD_3OD . 157	
Figure A3.6. Full MS (positive ion mode) of 4-8 with 3 equivalents of CsF added in CD_3OD . 157	
Figure A3.7. Full MS (positive ion mode) of 4-8 with 5 equivalents of CsF added in CD_3OD . 158	
Figure A3.8. Full MS (positive ion mode) of 4-9 with 0 equivalents of CsF added in CD_3OD . 158	
Figure A3.9. Full MS (positive ion mode) of 4-9 with 0.5 equivalents of CsF added in CD_3OD	159
Figure A3.10. Full MS (positive ion mode) of 4-9 with 1 equivalent of CsF added in CD_3OD . 159	
Figure A3.11. Full MS (positive ion mode) of 4-9 with 1.5 equivalents of CsF added in CD_3OD	160
Figure A3.12. Full MS (positive ion mode) of 4-9 with 2 equivalents of CsF added in CD_3OD	160
Figure A3.13. Full MS (positive ion mode) of 4-9 with 3 equivalents of CsF added in CD_3OD	161
Figure A3.14. Full MS (positive ion mode) of 4-9 with 5 equivalents of CsF added in CD_3OD	161
Figure A3.15. Full MS (positive ion mode) of 4-8 in MeOH with excess TBAT added.	164
Figure A3.16. Full MS (positive ion mode) of 4-9 in MeOH with excess TBAT added.	164
Figure A3.17. Relative abundance of desilylated products as determined by MS for 4-8, desilylated fractions are normalized within each spectrum.	165

Figure A3.18. Relative abundance of desilylated products as determined by MS for 4-9, desilylated fractions are normalized within each spectrum.	165
Figure A3.19. Full CV of 4-8 measured in a 0.1 M Bu ₄ NPF ₆ solution of methanol with a scan rate of 0.10 V s ⁻¹	166
Figure A3.20. A portion of the SWV of 4-8 measured in a 0.10 M Bu ₄ NPF ₆ solution of methanol with a step size of 0.004 V.	166
Figure A3.21. Full CV of 4-9 measured in a 0.1 M Bu ₄ NPF ₆ solution of methanol with a scan rate of 0.10 V s ⁻¹	167
Figure A3.22. A portion of the SWV of 4-9 measured in a 0.10 M Bu ₄ NPF ₆ solution of methanol with a step size of 0.004 V.	167
Figure A3.23. Field dependence of magnetization for 4-9 collected at 100 K.	168
Figure A3.24. Zoom of field dependence of magnetization for 4-9 collected at 100 K.	168
Figure A3.25. ¹ H NMR spectrum of 4-3.	169
Figure A3.26. ¹³ C NMR (top) and IR (bottom) spectra of 4-3.	170
Figure A3.27. ¹ H NMR spectrum of 4-7.	171
Figure A3.28. ¹³ C NMR (top) and IR (bottom) spectra of 4-7.	172
Figure A4.1. ¹ H NMR spectrum of 5-2.	174
Figure A4.2. ¹ H NMR spectrum of 5-5.	175
Figure A4.3. ¹ H NMR spectrum of 5-6.	176
Figure A4.4. ¹ H NMR spectrum of 5-7.	177
Figure A4.5. ¹³ C NMR (top) and IR (bottom) spectra of 5-7.	178
Figure A4.6. ¹ H NMR spectrum of 5-8.	179
Figure A4.7. ¹³ C NMR (top) and IR (bottom) spectra of 5-8.	180
Figure A4.8. ¹ H NMR spectrum of 5-9.	181
Figure A4.9. ¹³ C NMR (top) and IR (bottom) spectra of 5-9.	182
Figure A4.10. ¹ H NMR spectrum of 5-11.	183
Figure A4.11. ¹³ C NMR (top) and IR (bottom) spectra of 5-11.	184
Figure A4.12. ¹ H NMR spectrum of 5-13.	185
Figure A4.13. Paramagnetic ¹ H NMR spectrum of 5-14.	186
Figure A4.14. IR spectrum of 5-14.	187
Figure A4.15. Paramagnetic ¹ H NMR spectrum of 5-16.	188
Figure A4.16. IR spectrum of 5-16.	189
Figure A4.18. IR spectrum of 5-17.	191
Figure A4.19. Paramagnetic ¹ H NMR spectrum of 5-19.	192
Figure A4.20. IR spectrum of 5-19.	193
Figure A4.21. Paramagnetic ¹ H NMR spectrum of 5-20.	194

Figure A4.22. IR spectrum of 5-20..... 195

LIST OF SCHEMES

Scheme 2.1.1. Formation of α,β -unsaturated platinum carbenes from propargylic esters.	9
Scheme 2.1.2. Examples of reported reactivity proceeding through an unsaturated Pt carbene. .	10
Scheme 2.1.3. Iwasawa's initial [3+2] cycloaddition report.	10
Scheme 2.1.4. Proposed mechanism of [3+2] cycloaddition with vinyl ethers.	11
Scheme 2.1.5. Proposed mechanistic alternative for [4+3] cycloadditions.	12
Scheme 2.1.6. Synthesis of heterocycles using internal N- and O-nucleophiles.	13
Scheme 2.1.7. Indole additions and bisheterocyclizations enabled by Pt carbenes.	14
Scheme 2.1.8. Formation of phenanthrenes, 1,3-oxazepines and 2,5-dihydropyridines with PtCl ₂	15
Scheme 2.4.1. Initial discovery of enol incorporation into α,β -unsaturated Pt carbene.	58
Scheme 2.4.2. Scope of compatible enol nucleophiles for the vinylogous addition reaction.	60
Scheme 2.4.3. Scope of compatible carbene substitution for the vinylogous addition reaction. .	61
Scheme 2.4.4. Competition experiments between dicarbonyl and alcohol substrates.	62
Scheme 2.4.5. Unlikely mechanistic possibility for dicarbonyl incorporation.	63
Scheme 2.4.6. (4+3)-containing cycloaddition strategy toward frondosin B.	64
Scheme 2.4.7. Synthetic route toward propargylic ether 2-87.	64
Scheme 2.4.8. Synthetic route toward diene 2-95.	65
Scheme 2.4.9. Initial attempt at (4+3) cycloaddition.	66
Scheme 2.4.10. Optimization of (4+3) cycloaddition en route to frondosin B.	67
Scheme 4.1.1. Ligand protonation affects Fe(II) spin state in a 4,4'-diaminobpy system	95
Scheme 4.1.2. Proposed method for spin state changing in Fe(II) podand complexes.	96
Scheme 4.4.1. (a) Depiction of ligand desilylation and (b) the effect on relative energies of metal d orbitals.	114
Scheme 5.1.1. Structure and substitution pattern of [Fe(bpp) ₂] ²⁺ complexes investigated by Halcrow and coworkers.	120

Chapter 1: Controlling Spin Properties of First Row Transition Metals:

Exploitation of Iron(II) and Cobalt(II) Magnetic Properties

1.1 Introduction

This chapter aims to introduce two important topics that are discussed throughout this dissertation, namely single-molecule magnetism (SMM) and spin crossover (SCO). Chapter 2, which details work included in two publications (*Org. Lett.* **2016**, *18*, 64 and *Org. Lett.* **2017**, *19*, 294), will not be introduced here; rather, an in-depth introduction is included in that chapter. Chapter one will focus mainly on fundamentals of phenomena rather than specific examples, though the potential for magnetic switching will be discussed.

1.2 Single-Molecule Magnetism

Single-molecule magnets (SMMs) are a unique class of molecules that exhibit magnetic bistability. That is, at zero field, an SMM can exist in either the $+M_s$ or $-M_s$ state, and there is an energy barrier U_{eff} to spin reorientation which can result in slow magnetic relaxation. The barrier U_{eff} is related to both the axial anisotropy D and spin S of the system: for integer spins, $U_{\text{eff}} = S^2|D|$; and for half-integer spins, $U_{\text{eff}} = (S^2 - 1/4)|D|$. “Classical” SMMs possess negative D values, which signify that M_s is maximized in the ground state. At low temperatures (below the blocking temperature) these materials exhibit remnant magnetization and coercivity, properties also displayed by ferro- and ferrimagnets. This means that upon application of a magnetic field, the spins will polarize to either the $+M_s$ or $-M_s$ state, and upon sweeping the field in the opposite direction to zero field, they exhibit a slow relaxation, to an equilibrium state. When magnetically characterized, this can be manifested as open hysteresis below the blocking temperature (in the absence of quantum tunneling of magnetization, QTM). Alternatively, an out-of-phase

susceptibility (χ'') measurement can also reveal slow magnetic relaxation, and is often used to quantify intrinsic SMM properties.

There are several different relaxation processes which can occur to affect spin reorientation in SMMs. Perhaps the easiest to envision is a thermal process, wherein the thermal barrier is overcome in the traditional sense before the molecule relaxes to the ground state (Figure 1.2.1, upper right red arrows). QTM (green and red arrows) is a process in which the spin tunnels through the thermal barrier and is most prevalent in systems possessing large rhombic anisotropy, E .¹ Meanwhile, direct, Orbach and Raman processes are also prominent in SMMs, however all of these arise from spin-lattice interactions resulting in phonon emission, and are thus not purely molecular processes. A direct process is a type of QTM which involves relaxation directly to the $+M_s$ state from a $-M_s$ state. In the latter two processes, the spin can be excited to either a low M_s state or a virtual state, respectively, before relaxation (via phonon emission) to the ground state. These four non-traditional processes result in deviation from Arrhenius behavior in the overall relaxation properties.

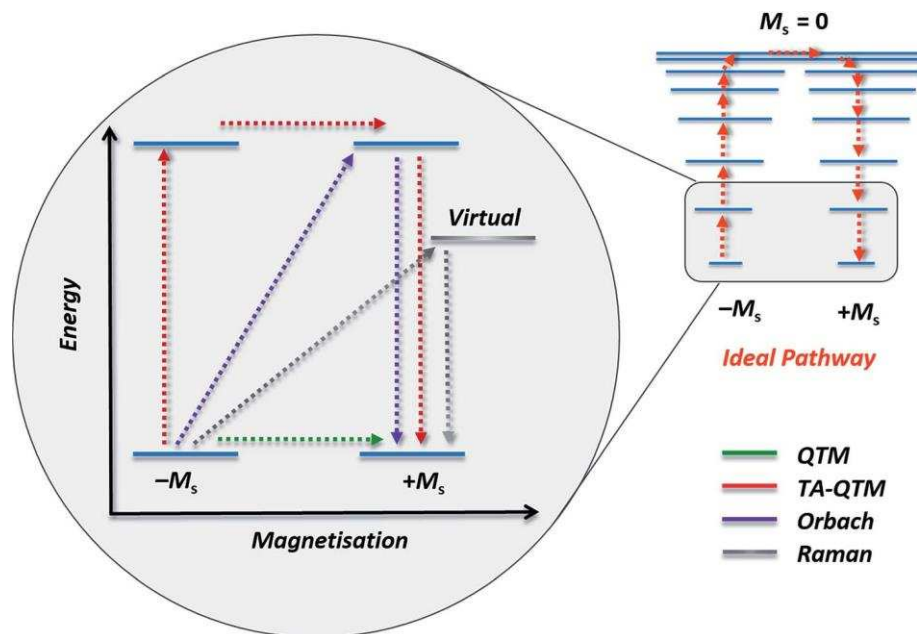


Figure 1.2.1. Schematic representing multiple relaxation pathways in SMMs. This figure is reproduced from reference 1.

While lanthanides (Dy, Tb) have dominated the field of high blocking temperature SMMs,² there is much interest in generating first-row transition metal complexes of this nature. Perhaps the most impressive first row transition metal SMM is the linear Fe(I) complex reported by Zadrozny *et al.* that exhibits a blocking temperature of 5 K and U_{eff} of 226 cm^{-1} .³ Among first row transition metals, high spin cobalt(II) ions are of particular interest for inclusion in mononuclear SMMs. This is because of the high intrinsic anisotropy associated with this ion, which gives rise to inherently larger barriers and makes their complexes more likely to exhibit slow magnetic relaxation.⁴

In fact, much work has been done to predict the sign and magnitude of anisotropy in mononuclear systems via computational methods.⁵ In a study by Ruiz and coworkers, it was suggested that d^7 systems such as Co(II) should possess either large negative or positive D values in almost all hexa- and lower coordinate geometries. Thus, our group has focused on the

development of novel hexacoordinate Co(II) systems and evaluation of the impact of geometric distortions on their anisotropies (Section 1.4), toward switching applications.

1.3 Spin Crossover

Spin crossover is the phenomenon of spin state interconversion between a high spin (HS) to a low spin (LS) state of a transition metal complex. In an octahedral ligand field, this is possible in d^4 - d^7 systems and is most commonly studied in Fe(II) (d^6) complexes. This interconversion process can be induced by external stimuli such as pressure or light, but is usually described as a thermal process. In order to exhibit SCO, the relative Δ (ligand field splitting) and P (electron pairing) energies must be close in magnitude (Figure 1.3.1).

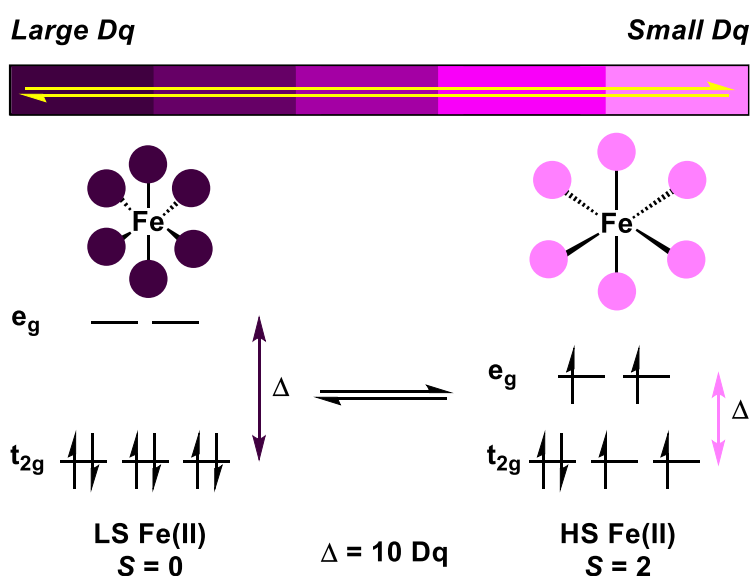


Figure 1.3.1. Changes in electronic and physical structure between HS and LS Fe(II) ions.

Along with a change in spin multiplicity, Fe(II) systems are unique in that the HS state is paramagnetic while the LS state is diamagnetic. This change in spin state is also accompanied by a stark color change (e.g., molar absorptivity and absorption wavelength), as there are high intensity charge transfer bands associated with the LS state. When SCO occurs near room temperature, these materials are of interest for applications in sensors and memory devices.⁶

Two of the most well-studied examples of Fe(II) SCO systems are $[\text{Fe}(\text{phen})_2(\text{NCS})_2]$ and $[\text{Fe}(\text{pic})_3]^{2+}$ (pic = 2-picolyamine). Both undergo SCO with a range of transition temperatures ($T_{1/2}$, where the occupation of the HS and LS states is equal) depending on co-crystallized solvents or anions.⁷ These studies showed that subtle effects such as hydrogen bonding alter the magnetic properties greatly, in addition to optimal first coordination environment (N_6) and ligand field strength.

1.4 Recent Efforts to Control SMM and Spin State Properties

Given the potential for single-molecule magnets and spin crossover compounds to impact device technology, there is great interest in controlling these magnetic properties and switching behavior. In fact, coordinated anion-dependent relaxation in a Co(II) system was also reported by Dunbar and coworkers,⁸ and examples of redox-dependent (both oxidative and reductive) Fe(II) SMMs have been recently reported by Harris and coworkers.⁹⁻¹⁰ The latter constitutes an example of “turn-on” slow magnetic relaxation, as a single electron redox event on the (metallo)ligand bridging the two Fe(II) centers can give rise to SMM properties in the system. Further, Winpenny and coworkers showed that a trigonal prismatic Co(II) system exhibited slow magnetic relaxation at zero field,¹¹ suggesting that hexacoordinate iminopyridine ligands which enforce a trigonal prismatic geometry may be conducive to SMM properties.

Our group has long aimed at developing Fe(II) systems which act as guest-dependent sensors. The seminal report of anion association-driven spin state switching in solution came in 2008 with the $[\text{Fe}(\text{H}_2\text{bip})_3]^{2+}$ system, where halide and perchlorate anions induce a LS state compared to when the anion is tetraphenylborate.¹² In fact, these properties were improved with a heteroleptic $[\text{Fe}(\text{H}_2\text{bip})_2(\text{phen})]^{2+}$ complex, which was shown to change color at room temperature in dichloromethane upon addition of bromide.¹³

In 2012, our group demonstrated that an Fe(II) tris(2-aminoethyl)amine (tren)-derived iminopyridine complex displayed anion-dependent SCO properties.¹⁴ This podand contained a 6-CH₂OH functional group which served two purposes: first, to allow for guest binding, but second and more importantly, to affect the ligand field such that a HS state was thermally accessible. In fact, it is well established that addition of steric bulk at the 6-pyridyl position in these systems results in the weakening of ligand field.¹⁵ Further, in 2013 our group showed that a ferrous 5-*tert*-butylamide-substituted iminopyridine complex remained LS, even though evidence was gathered that an anionic guest was associating within a binding pocket.¹⁶ This was shown *via* both crystallographic characterization of a $\{\text{Cl}[\text{FeL}^{5\text{-ONH}t\text{Bu}}]\}^+$ species, as well as NMR titration data indicating an increase in the chemical shift of the amide proton as a function of chloride added.

1.5. Outline of Chapters

Given these motivations, we are prompted to consider the possibility of installing guest binding moieties on a Co(II) *cis*-, *cis*-1,3,5-triaminocyclohexane (tach)-derived iminopyridine complex which would likely exhibit trigonal prismatic geometry.¹⁷ If guest association were to induce a severe enough distortion, we might be able to generate a new class of switchable SMMs. Our efforts toward testing this hypothesis are summarized in Chapter 3. Additionally, in Chapter 4 we consider an alternative switching manifold where, rather than guest association, an irreversible chemical modification to an iminopyridine ligand could induce a spin-state change. Based on our work with ferrous tren iminopyridine complexes, we predict that a severe change in electronic character of these ligands may enable switching of spin states, and so we began by installing a readily cleavable silyl ether moiety at the 5-pyridyl position. This would offer two advantages: first, chemoselectivity may be possible by reacting with fluoride; second (and more importantly), the large difference in electronic nature between a silyl ether and the hypothesized

product, a phenoxide, may be sufficient to induce a spin state change. In Chapter 5, we explore the potential for other switching manifolds by performing a systematic study varying electronic character at the 5-pyridyl position on Fe(II) spin state in tren iminopyridine complexes.

References

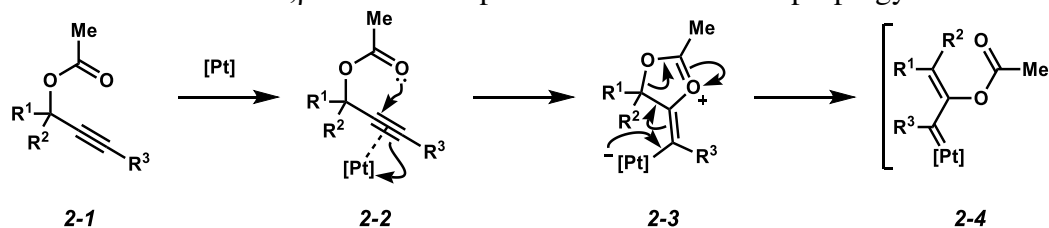
1. Frost, J. M.; Harriman, K. L. M.; Murugesu, M. *Chem. Sci.* **2016**, *7*, 2470.
2. Woodruff, D. N.; Winpenny, R. E. P.; Layfield, R. A. *Chem. Rev.* **2013**, *113*, 5110.
3. Zadrozny, J. M.; Xiao, D. J.; Atanasov, M.; Long, G. J.; Grandjean, F.; Neese, F.; Long, J. R. *Nat. Chem.* **2013**, *5*, 577.
4. Murrie, M. *Chem. Soc. Rev.* **2010**, *39*, 1986.
5. Gomez-Coca, S.; Cremades, E.; Aliaga-Alcalde, N.; Ruiz, E. *J. Am. Chem. Soc.* **2013**, *135*, 7010.
6. Kahn, O.; Martinez, C. J. *Science* **1998**, *279*, 44.
7. Halcrow, M. A. *Spin-crossover materials: properties and applications*; Wiley: West Sussex, UK, 2013.
8. Woods, T. J.; Ballesteros-Rivas, M. F.; Gómez-Coca, S.; Ruiz, E.; Dunbar, K. R. *J. Am. Chem. Soc.* **2016**, *138*, 16407.
9. Jeon, I.-R.; Park, J. G.; Xiao, D. J.; Harris, T. D. *J. Am. Chem. Soc.* **2013**, *135*, 16845.
10. Gaudette, A. I.; Jeon, I.-R.; Anderson, J. S.; Grandjean, F.; Long, G. J.; Harris, T. D. *J. Am. Chem. Soc.* **2015**, *137*, 12617.
11. Novikov, V. V.; Pavlov, A. A.; Nelyubina, Y. V.; Boulon, M.-E.; Varzatskii, O. A.; Voloshin, Y. Z.; Winpenny, R. E. P. *J. Am. Chem. Soc.* **2015**, *137*, 9792.
12. Ni, Z.; Shores, M. P. *J. Am. Chem. Soc.* **2009**, *131*, 32.
13. Ni, Z.; McDaniel, A. M.; Shores, M. P. *Chem. Sci.* **2010**, *1*, 615.
14. Klug, C. M.; McDaniel, A. M.; Fiedler, S. R.; Schulte, K. A.; Newell, B. S.; Shores, M. P. *Dalton Trans.* **2012**, *41*, 12577.
15. Wilson, L. J.; Georges, D.; Hoselton, M. A. *Inorg. Chem.* **1975**, *14*, 2968.
16. McDaniel, A. M.; Klug, C. M.; Shores, M. P. *Eur. J. Inorg. Chem.* **2013**, 943.
17. Wentworth, R. A. D.; Dahl, P. S.; Huffman, C. J.; Gillum, W. O.; Streib, W. E.; Huffman, J. C. *Inorg. Chem.* **1982**, *21*, 3060.

Chapter 2: Nucleophilic Interception of α,β -Unsaturated Platinum Carbenesⁱ

2.1 Introduction

In recent years, α,β -unsaturated platinum carbenes have become important synthetic intermediates in organic chemistry, and recent work has aimed at predictably generating these species. It is well understood that upon exposure of propargylic esters (**2-1**) to Pt(II) salts, a 1,2-acyloxy migration occurs, giving access to these putative intermediates (Scheme 2.1.1).¹⁻² This involves first activation of the alkyne and intramolecular attack of the acetate to give **2-3**, then Pt donation back in causes a rearrangement, giving α,β -unsaturated carbene **2-4**.

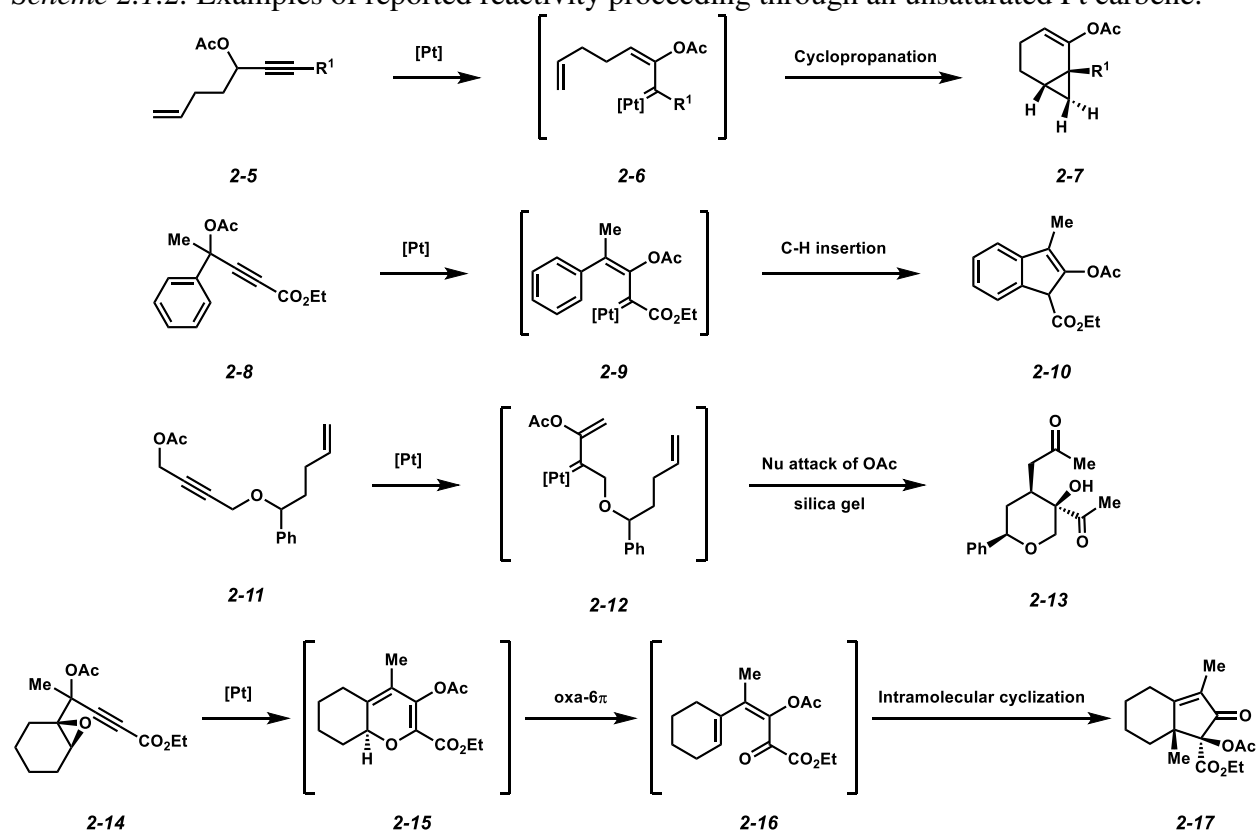
Scheme 2.1.1. Formation of α,β -unsaturated platinum carbenes from propargylic esters.



Once formed, these unsaturated platinum carbenes (**2-4**) can undergo various modes of reactivity, including cyclopropanation (e.g., Rautenstrauch-type), giving products similar to **2-7**,³⁻⁶ C-H insertion products (**2-10**)⁷ and nucleophilic interception by epoxides and alkenes (Scheme 2.1.2).⁸⁻⁹

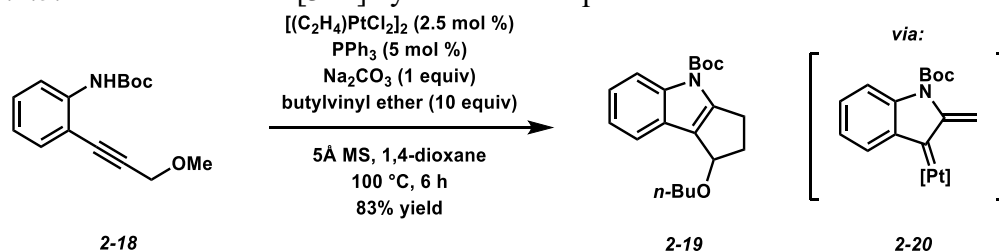
ⁱ Reproduced in part with permission from “Lewis Acid Mediated Vinylogous Additions of Enol Nucleophiles into an α,β -Unsaturated Platinum Carbene.” Allegretti, P. A.; Huynh, K.; Ozumerzifon, T. J.; Ferreira, E. M. *Org. Lett.* **2016**, *18*, 64 and “Platinum-Catalyzed α,β -Unsaturated Carbene Formation in the Formal Syntheses of Frondosin B and Liphagal.” Huynh, K. Q.; Seizert, C. A.; Ozumerzifon, T. J.; Allegretti, P. A.; Ferreira, E. M. *Org. Lett.* **2017**, *19*, 294. Copyright 2016 and 2017 American Chemical Society.

Scheme 2.1.2. Examples of reported reactivity proceeding through an unsaturated Pt carbene.



In 2011, the Iwasawa group reported a novel method for the formation of α,β -unsaturated platinum carbenes. They demonstrated that exposure of *N*-Boc anilines bearing propargylic ethers (**2-18**) to catalytic $[(C_2H_4)PtCl_2]_2$ (Zeise's dimer)¹⁰ in the presence of vinyl ethers gave access to annulated indole products (**2-19**), presumably proceeding through a carbene intermediate (**2-20**, Scheme 2.1.3).¹¹

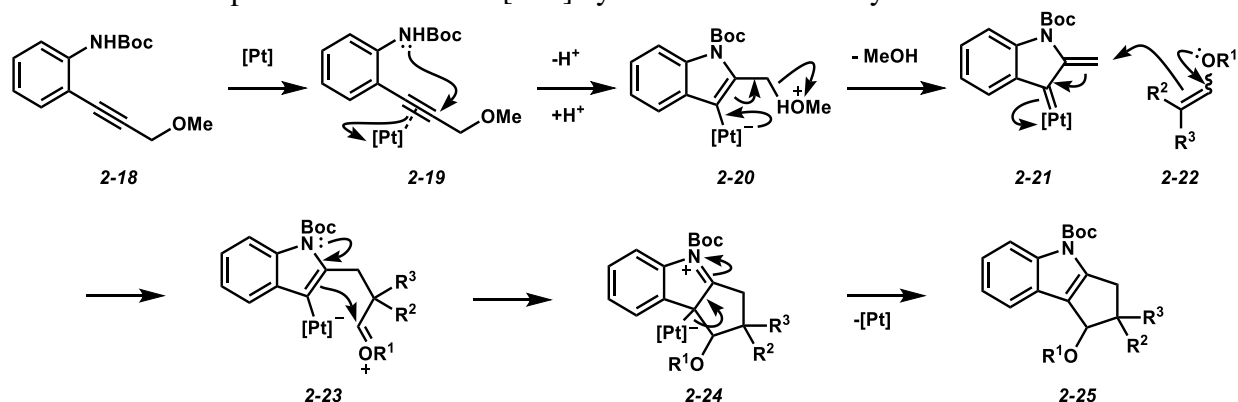
Scheme 2.1.3. Iwasawa's initial [3+2] cycloaddition report.



This reaction is hypothesized to proceed through a mechanism in which the Pt(II) salt activates the alkyne toward nucleophilic attack by the pendant aniline (Scheme 2.1.4). After 5-

endo-dig cyclization and subsequent proton transfer, the vinyl platinum species (**2-20**) is poised to extrude the propargylic leaving group, giving α,β -unsaturated carbene intermediate **2-21**. Nucleophilic addition of the vinyl ether then occurs at the β carbon (vinylogous), giving oxocarbenium **2-23**, which cyclizes concomitantly with deplatination to give substituted indole products **2-25**. Alternatively, this process may occur in a concerted fashion, where both carbon-carbon bonds are formed in one cyclization step. The generality of this reaction also allows for the formation of substituted naphthalenes and benzofurans from their respective *o*-alkynyl silyl enol ether or phenol substrates.

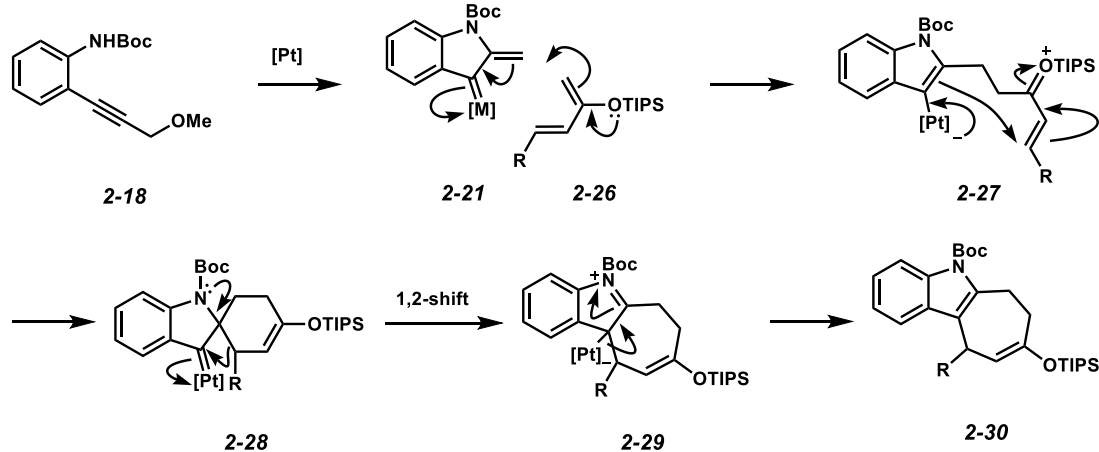
Scheme 2.1.4. Proposed mechanism of [3+2] cycloaddition with vinyl ethers.



In 2013 the Tang and Iwasawa groups independently showed that catalytically formed α,β -unsaturated platinum carbenes were also able to undergo [4+3] cycloadditions with siloxy dienes, furans and cyclic dienes.¹²⁻¹³ Expanding the product diversity obtainable from this carbenoid intermediate to cyclohepta[*b*]indoles, this reaction likely proceeds through a similar mechanism to the [3+2] reactivity, though other mechanisms were also proposed (Scheme 2.1.5). The contribution of a second mechanistic pathway is evidenced by isolation of differentially substituted derivatives of **2-30**, as secondary propargyl ether substrates bearing a *p*-tolyl substituent can exhibit a mixture of products derived from divergent migration of R groups in intermediate **2-28**. Regioselectivity was largely inconsequential in these reports, as the substrates were either

electronically biased or symmetric. In all, these three cycloaddition reports highlight a novel mode of reactivity of α,β -unsaturated Pt carbenes where an external nucleophile adds to the β -carbon.

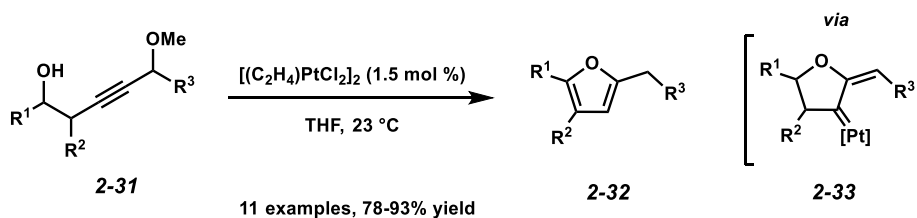
Scheme 2.1.5. Proposed mechanistic alternative for [4+3] cycloadditions.



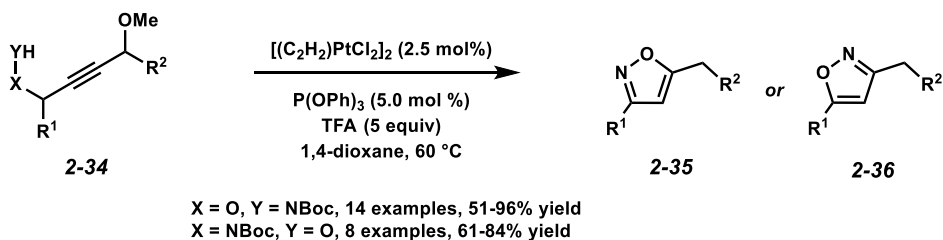
Meanwhile, reports from the Ferreira group in 2011 and 2012 highlight the utility of the vinyl carbene intermediate in terms of substituted heterocycle synthesis, namely furans (**2-32**) and isoxazoles (**2-35** – **2-36**, Scheme 2.1.6).¹⁴⁻¹⁵ Both transformations are postulated to proceed through a platinum carbene intermediate. Once formed, it is likely that a 1,2-hydride migration into the carbene occurs as supported by deuterium labeling experiments; isomerization (and Boc cleavage, where applicable) then gives the aromatic heterocycle. Notably, when R^2 is a *tert*-butyldimethylsilyl moiety in the furan syntheses, selective Si-migration can be favored over the typical hydride shift based on solvent and additive choice. Further, the Hashmi group showed that nitrones (**2-38**) are also competent nucleophiles in this reactivity, enabling the formation of [1,2]oxazino[5,4-*b*]indoles (**2-39**) by [3+3] cycloaddition.¹⁶ The utility of these annulated products was shown, as SmI_2 -mediated ring opening gives access to 1,4-amino alcohols.

Scheme 2.1.6. Synthesis of heterocycles using internal *N*- and *O*-nucleophiles.

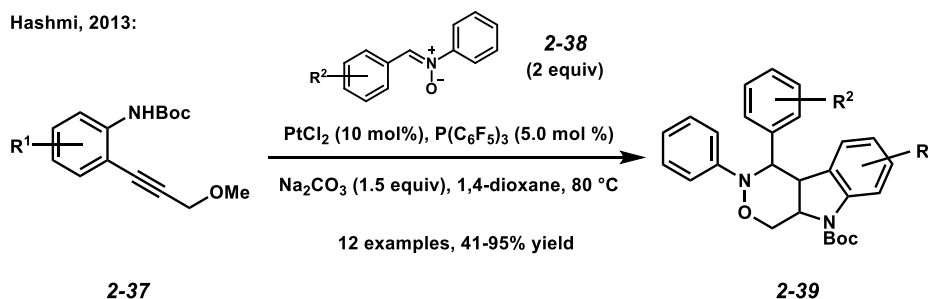
Ferreira, 2011:



Ferreira, 2012:

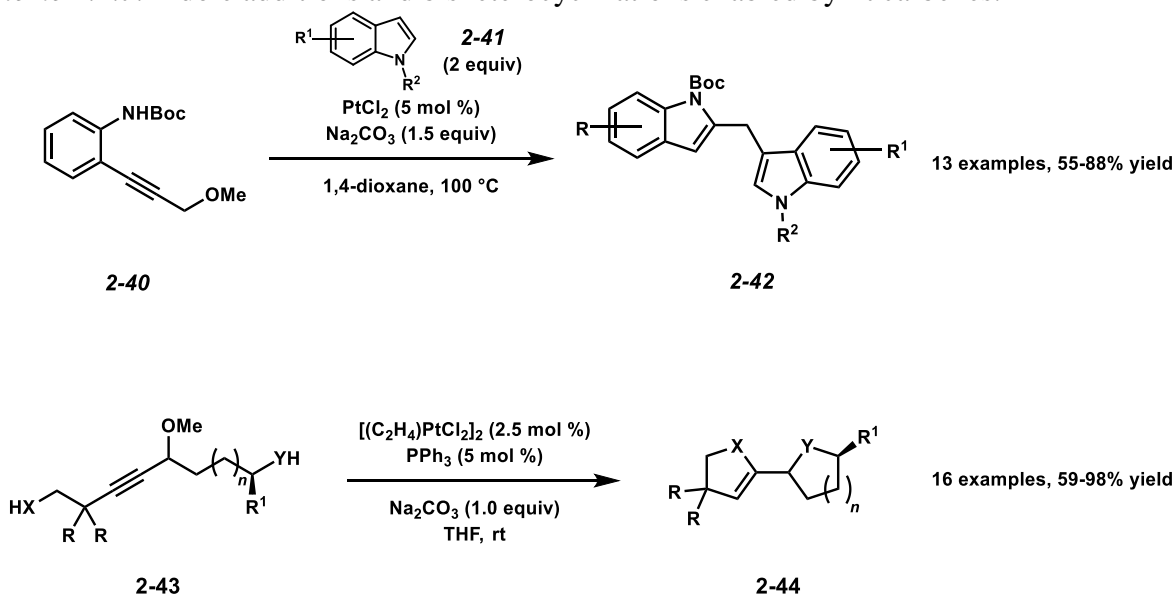


Hashmi, 2013:



Work to expand the types of nucleophiles compatible with this vinylogous reactivity has increased the impact of this methodology. For instance, in 2013, the Tang group showed that intermolecular nucleophilic interception by indoles was also possible, giving rise to diindolymethanes (**2-42**) which can be further converted to indolo[3,2-*b*]carbazoles (Scheme 2.1.7).¹⁷ Also, the Ferreira group demonstrated¹⁷ that treatment of substrates bearing two internal nucleophiles with Zeise's dimer gives rise to vicinal bisheterocycles (**2-44**).¹⁸ In the latter report, it was demonstrated that both *N* and *O*-nucleophiles are compatible in either cyclization event.

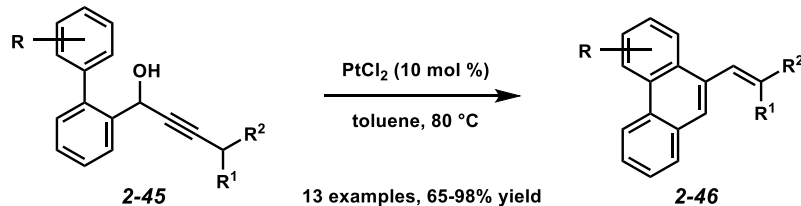
Scheme 2.1.7. Indole additions and bisheterocyclizations enabled by Pt carbenes.



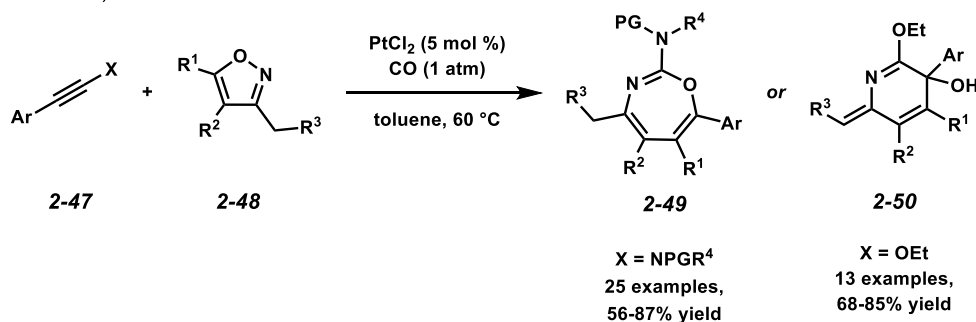
In recent years, reports of additions with carbon-based nucleophiles continue to expand the utility of this reactivity. For instance, the Kim group showed that substituted phenanthrenes can be formed by treating biphenyl propargyl alcohols to PtCl_2 .¹⁹ The alkene geometry in the phenanthrene products varied from 5:1 to 1:1, though substitution (R) on the biphenyl substrates were limited to electron rich ethers. Lastly, a creative use of isoxazoles (**2-48**) as nucleophiles masking an alkoxy leaving group in these processes was shown by Lu and Ye,²⁰ where 1,3-oxazapines (**2-49**) are obtained when using ynamides and 2,5-dihydropyridines (**2-50**) can be formed using alkynyl ethers (Scheme 2.1.8). These processes are hypothesized to proceed through an α -imino Pt carbene (**2-52**), which had been unprecedented until this report and the selectivity of the reaction is hypothesized to be sterically driven.

Scheme 2.1.8. Formation of phenanthrenes, 1,3-oxazepines and 2,5-dihydropyridines with PtCl₂.

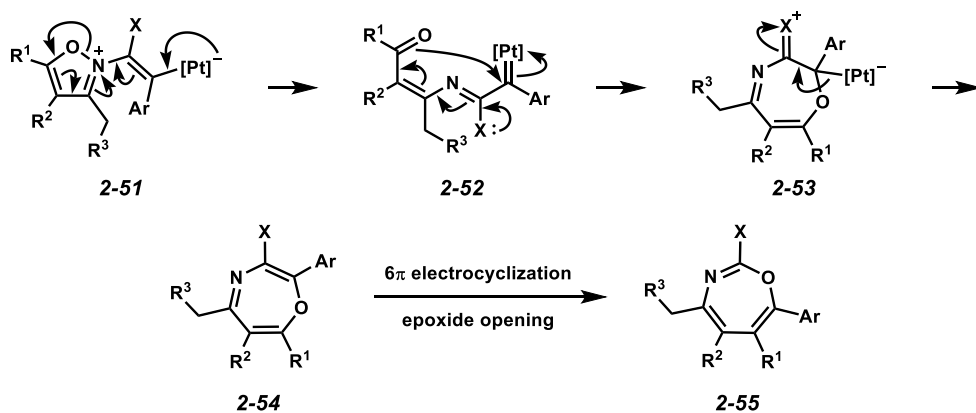
Kim, 2014:



Lu and Ye, 2017:



via:



Therefore, in our continuing efforts to examine the reactivity of α,β -unsaturated Pt carbenes, we set out to examine the possibility of incorporating novel carbon nucleophiles β to the carbene, as well as to explore the scope and limitations of concomitant annulations with various dienes in the context of natural product synthesis.

2.2 Division of Labor

Initial discovery and reaction optimization for dicarbonyl additions were performed by Dr. Paul Allegretti. Substrates **2-56** – **2-59** and **2-61** – **2-65** and starting materials **2-68c,e,i,k** and **2-76** – **2-78** were synthesized by Tarik Ozumerzifon. The remaining substrates were synthesized by Dr.

Khoi Huynh (at the University of Georgia). Dicarbonyl competition experiments were done by Dr. Khoi Huynh. The formal synthesis of frondosin B was done by Tarik Ozumerzifon with guidance from Dr. Paul Allegretti. Side product **2-97** was discovered by Dr. Khoi Huynh.

2.3 Experimental Details

2.3.1. Materials and Methods

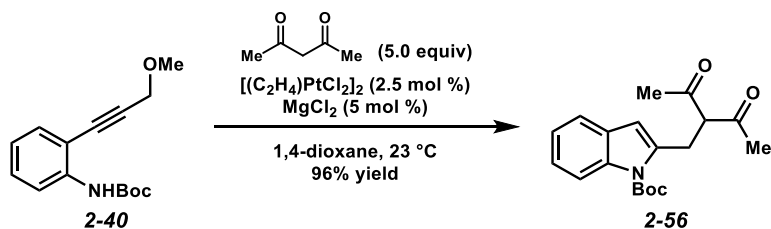
Reactions were performed under an argon atmosphere unless otherwise noted. Tetrahydrofuran, ether, dichloromethane and toluene were purified by passing through activated alumina columns. 1,4-dioxane was distilled over sodium/benzophenone. All other solvents used were ACS grade, and all other reagents were used as received, unless otherwise noted. Zeise's dimer ($[(C_2H_4)PtCl_2]_2$) was purchased from Strem Chemical Company. All other commercially available chemicals were purchased from Alfa Aesar (Ward Hill, MA), Sigma-Aldrich (St. Louis, MO), Oakwood Products, (West Columbia, SC), Strem (Newburyport, MA) and TCI America (Portland, OR). Qualitative thin layer chromatography (TLC) analysis was performed on 250 mm thick, 60 Å, glass backed, F254 silica (Silicycle, Quebec City, Canada). Visualization was accomplished with UV light and exposure to *p*-anisaldehyde or $KMnO_4$ stain solutions followed by heating. Flash chromatography was performed using Silicycle silica gel (230-400 mesh). 1H NMR spectra were acquired on either a Varian 400 MR (at 400 MHz), a Varian Mercury Plus (at 400 MHz), or a Varian Unity Inova 500 (at 500 MHz), and are reported relative to $SiMe_4$ (δ 0.00). ^{13}C NMR spectra were acquired on either a Varian 400 MR (at 100 MHz), a Varian Mercury Plus (at 100 MHz), or a Varian Unity Inova 500 (at 125 MHz), and are reported relative to $SiMe_4$ (δ 0.00). IR spectra were obtained on NaCl plates (film) with a Bruker Tensor 27 FT-IR or as a film on a Thermo Nicolet iS50 FT-IR, Thermo Nicolet 380 FT-IR or a Shimadzu IR Prestige 21 FT-IR. High resolution mass spectrometry data were acquired by the Colorado State University

Central Instrument Facility on an Agilent 6210 TOF LC/MS and by the Proteomics and Mass Spectrometry Core Facility at University of Georgia on a Thermo Scientific Orbitrap Elite Hybrid Ion Trap-Orbitrap MS.

2.3.2. *Synthesis of Dicarboxyl-Incorporated Heterocycles*

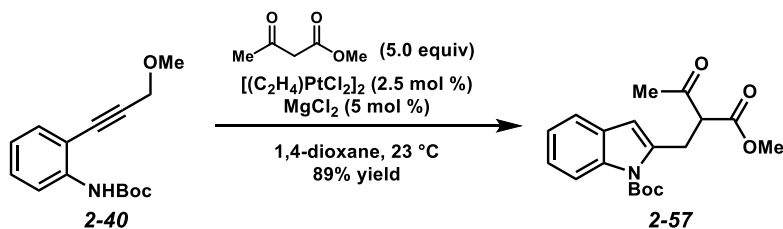
General procedure A for the platinum catalyzed indole synthesis. To a solution of *N*-Boc aniline (1.0 equiv) in 1,4-dioxane (0.1 M) was added the enol source (5.0 equiv) and MgCl₂ (5 mol %), and the resulting solution was stirred at 23 °C for 15 min. [(C₂H₄)PtCl₂]₂ (2.5 mol %) was then added, and the reaction mixture was stirred at 23 °C and monitored by TLC. Upon completion, the reaction mixture was filtered through a SiO₂ plug, washing with EtOAc (~2× reaction volume). The solvent was then removed by rotary evaporation, and the resulting residue was purified by flash chromatography on SiO₂.

General procedure B for the platinum catalyzed indole synthesis. A 2-dram vial equipped with a magnetic stir bar and MgCl₂ (5 mol %) was flame-dried under vacuum and cooled under a stream of argon. A solution of *N*-Boc aniline (1.0 equiv) and the enol source (5.0 equiv) in 1,4-dioxane (0.1 M in aniline) was added to the dried MgCl₂, and the resulting solution was stirred at 23 °C for 15 min. [(C₂H₄)PtCl₂]₂ (2.5 mol %) was then added, and the reaction mixture was stirred at 23 °C and monitored by TLC. Upon completion, the reaction mixture was filtered through a SiO₂ plug, washing with EtOAc (2× reaction volume). The solvent was then removed by rotary evaporation, and the resulting residue was purified by flash chromatography on SiO₂.



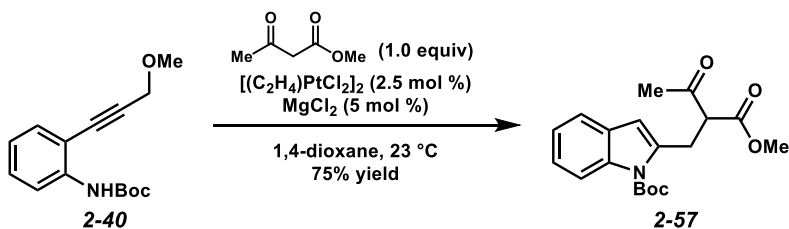
Indole 2-56. Following general procedure A, to a solution of *N*-Boc aniline **2-40**¹¹ (52.2 mg, 0.200 mmol) in 1,4-dioxane (2.00 mL, 0.1 M) was added 2,4-pentanedione (103 μ L, 1.00 mmol) and MgCl₂ (0.9 mg, 0.0100 mmol), and the solution was stirred at 23 °C for 15 min. Then, [(C₂H₄)PtCl₂]₂ (2.9 mg, 0.00500 mmol) was added, and the reaction mixture was stirred at 23 °C for 3 h. Upon completion, the reaction mixture was filtered through a plug of silica gel (0.5 \times 2.0 cm), washing with EtOAc (4 mL). The solvent was removed by rotary evaporation, and the resulting residue was purified by flash chromatography (9:1 hexanes/EtOAc eluent) to afford indole **2-56** (63.0 mg, 96% yield, R_f = 0.39 (enol), 0.66 (keto) in 4:1 hexanes/EtOAc) as an amber oil that solidified upon standing.

Indole 2-56: Characterized as a 2.5:1 enol-keto tautomer mixture (asterisk indicates keto tautomer). ¹H NMR (400 MHz, CDCl₃): δ 8.06 (d, J = 8.0 Hz, 0.71H), 8.02 (d, J = 8.0 Hz, 0.29H*), 7.43 (d, J = 7.6 Hz, 1H), 7.27 – 7.17 (comp. m, 2H), 6.34 (s, 0.29H*), 6.25 (s, 0.71H), 4.22 (t, J = 7.2 Hz, 0.29H*), 3.98 (s, 1.4H), 3.57 (d, J = 7.2 Hz, 0.58H*), 2.20 (s, 1.7H*), 2.11 (s, 4.3H), 1.73 (s, 6.4H), 1.71 (s, 2.6H*); ¹³C NMR (100 MHz, CDCl₃): δ 203.7, 192.3, 151.0, 140.8, 137.8, 137.1, 129.2, 129.1, 124.0, 123.8, 123.0, 120.4, 120.2, 115.8, 115.7, 110.2, 109.4, 107.8, 107.3, 84.5, 84.4, 77.4, 67.8, 29.6, 29.1, 28.6, 28.5, 28.4, 23.0; IR (film): 2978, 2932, 1721, 1453, 1369, 1323, 1301, 1155, 739 cm⁻¹; HRMS (ESI⁺) m/z calc'd for (M + Na)⁺ [C₁₉H₂₃NO₄ + Na]⁺: 352.1519, found 352.1511.



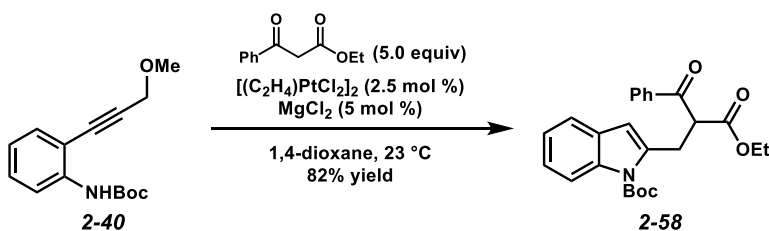
Indole 2-57. Following general procedure A, to a solution of *N*-Boc aniline **2-40** (52.2 mg, 0.200 mmol) in 1,4-dioxane (2.00 mL, 0.1 M) was added methyl acetoacetate (107 μ L, 1.00 mmol) and $MgCl_2$ (0.9 mg, 0.0100 mmol), and the solution was stirred at 23 °C for 15 min. Then, $[(C_2H_4)PtCl_2]_2$ (2.9 mg, 0.00500 mmol) was added, and the reaction mixture was stirred at 23 °C for 3 h. Upon completion, the reaction mixture was filtered through a plug of silica gel (0.5 \times 2.0 cm), washing with EtOAc (4 mL). The solvent was removed by rotary evaporation, and the resulting residue was purified by flash chromatography (4:1 hexanes/EtOAc eluent) to afford indole **2-57** (61.4 mg, 89% yield, R_f = 0.43 in 4:1 hexanes/EtOAc) as a colorless oil.

Indole 2-57: 1H NMR (400 MHz, $CDCl_3$): δ 8.03 (d, J = 8.4 Hz, 1H) 7.44 (d, J = 7.6 Hz, 1H), 7.24 – 7.17 (comp. m, 2H), 6.37 (s, 1H), 4.07 (dd, J = 8.4, 6.0 Hz, 1H), 3.70 (s, 3H), 3.57 (ABq, J = 15.2 Hz, $\Delta\nu$ = 29.2 Hz, 2H), 2.27 (s, 3H), 1.70 (s, 9H); ^{13}C NMR (100 MHz, $CDCl_3$): δ 202.4, 169.6, 150.6, 137.7, 136.6, 129.1, 123.9, 122.9, 120.3, 115.8, 109.5, 84.4, 59.2, 52.6, 29.6, 28.6, 28.4; IR (film): 2979, 2963, 2932, 2361, 2337, 1719, 1453, 1434, 1370, 1324, 1303, 1154, 1115, 742 cm^{-1} ; HRMS (ESI⁺) m/z calc'd for $(M + Na)^+$ $C_{19}H_{23}NO_5 + Na$: 368.1468, found 368.1472.



Indole 2-57 (using 1 equiv nucleophile). Following general procedure B, a 2-dram vial equipped with a magnetic stir bar and $MgCl_2$ (0.3 mg, 0.00274 mmol) was flame-dried under vacuum and

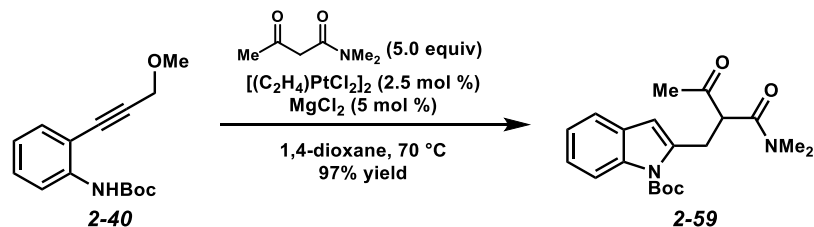
cooled under a stream of argon. A solution of *N*-Boc aniline **2-40** (14.3 mg, 0.0547 mmol) and methyl acetoacetate (6.0 μ L, 0.0556 mmol) in 1,4-dioxane (0.500 mL, 0.11 M in aniline) were added to the dried MgCl_2 , and the resulting solution was stirred at 23 $^\circ\text{C}$ for 15 min. Then, $[(\text{C}_2\text{H}_4)\text{PtCl}_2]_2$ (0.8 mg, 0.00137 mmol) was added, and the reaction mixture was stirred at 23 $^\circ\text{C}$ for 10 h. Upon completion, the reaction mixture was filtered through a plug of silica gel (0.5 \times 2.0 cm), washing with EtOAc (1 mL). The solvent was removed by rotary evaporation, and the resulting residue was purified by flash chromatography (4:1 hexanes/EtOAc eluent) to afford indole **2-57** (14.1 mg, 75% yield) as a colorless oil.



Indole 2-58. Following general procedure A, to a solution of *N*-Boc aniline **2-40** (52.2 mg, 0.200 mmol) in 1,4-dioxane (2.00 mL, 0.1 M) was added ethyl 3-oxo-3-phenylpropionate (172 μ L, 1.00 mmol) and MgCl_2 (0.9 mg, 0.0100 mmol), and the solution was stirred at 23 $^\circ\text{C}$ for 15 min. Then, $[(\text{C}_2\text{H}_4)\text{PtCl}_2]_2$ (2.9 mg, 0.00500 mmol) was added, and the reaction mixture was stirred at 23 $^\circ\text{C}$ for 20 h. Upon completion, the reaction mixture was filtered through a plug of silica gel (0.5 \times 2.0 cm), washing with EtOAc (4 mL). The solvent was removed by rotary evaporation, and the resulting residue was purified by flash chromatography (9:1 hexanes/EtOAc eluent) to afford indole **2-58** (69.2 mg, 82% yield, $R_f = 0.52$ in 4:1 hexanes/EtOAc) as a pale yellow oil.

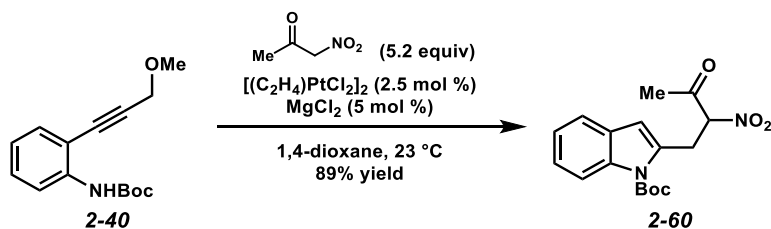
Indole 2-58: ^1H NMR (400 MHz, CDCl_3): δ 8.02 (t, $J = 9.2$ Hz, 3H), 7.57 – 7.51 (m, 1H), 7.46 – 7.39 (comp. m, 3H), 7.24 – 7.14 (comp. m, 2H), 6.37 (s, 1H), 4.94 (app. t, $J = 7.3$ Hz, 1H), 4.13 – 4.04 (comp. m, 2H), 3.77 – 3.67 (comp. m, 2H), 1.67 (s, 9H), 1.09 (t, $J = 7.2$ Hz, 3H); ^{13}C NMR (100 MHz, CDCl_3): δ 194.6, 169.3, 150.6, 137.7, 136.7, 136.4, 133.6, 129.1, 128.9, 128.8, 123.8,

122.8, 120.2, 115.7, 109.7, 84.3, 61.7, 53.9, 29.6, 28.4, 14.1; IR (film): 2979, 2934, 1726, 1687, 1452, 1369, 1325, 1304, 1153 cm^{-1} ; HRMS (ESI⁺) m/z calc'd for (M + Na)⁺ [$\text{C}_{25}\text{H}_{27}\text{NO}_5$ + Na]⁺: 444.1781, found 444.1770.



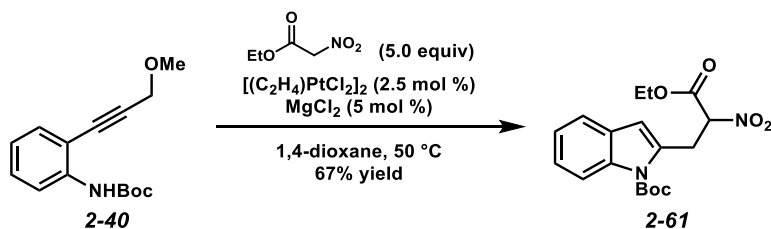
Indole 2-59. Following general procedure A, to a solution of *N*-Boc aniline **2-40** (52.2 mg, 0.200 mmol) in 1,4-dioxane (2.00 mL, 0.1 M) was added *N,N*-dimethylacetamide (129 mg, 1.00 mmol) and MgCl_2 (0.9 mg, 0.0100 mmol), and the solution was stirred at 23 °C for 15 min. Then, $[(\text{C}_2\text{H}_4)\text{PtCl}_2]_2$ (2.9 mg, 0.00500 mmol) was added, and the reaction mixture was heated to 70 °C and stirred for 72 h. Upon completion, the reaction mixture was cooled to 23 °C and filtered through a plug of silica gel (0.5 × 2.0 cm), washing with EtOAc (4 mL). The solvent was removed by rotary evaporation, and the resulting residue was purified by flash chromatography (2:1 hexanes/EtOAc eluent) to afford indole **2-59** (69.7 mg, 97% yield, R_f = 0.54 in 1:1 hexanes/EtOAc) as a colorless oil.

Indole 2-59: ^1H NMR (400 MHz, CDCl_3): δ 8.02 (d, J = 8.4 Hz, 1H), 7.44 (d, J = 7.6 Hz, 1H), 7.24 – 7.16 (comp. m, 2H), 6.38 (s, 1H), 4.25 (app. t, J = 7.2 Hz, 1H), 3.60 (ABq, J_{AB} = 15.2 Hz, $\Delta\nu$ = 41.6 Hz, 2H), 2.92 (s, 6H), 2.22 (s, 3H), 1.69 (s, 9H); ^{13}C NMR (100 MHz, CDCl_3): δ 204.0, 168.8, 138.0, 136.5, 129.2, 123.9, 123.0, 120.3, 115.7, 109.6, 84.4, 57.0, 37.6, 36.1, 29.5, 28.4, 27.8; IR (film): 2977, 2933, 1724, 1640, 1453, 1394, 1369, 1324, 1303, 1154, 1115, 746 cm^{-1} ; HRMS (ESI⁺) m/z calc'd for (M + Na)⁺ [$\text{C}_{20}\text{H}_{26}\text{N}_2\text{O}_4$ + Na]⁺: 381.1785, found 381.1791.



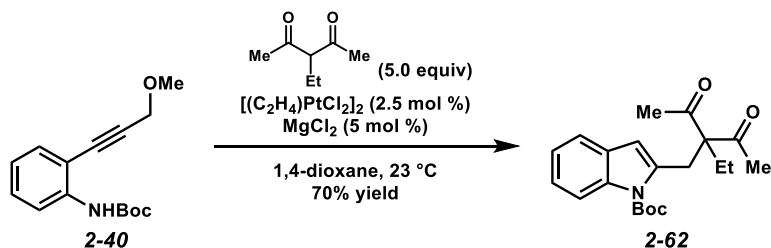
Indole 2-60. Following general procedure B, a 2-dram vial equipped with a magnetic stir bar and MgCl_2 (0.3 mg, 0.00281 mmol) was flame-dried under vacuum and cooled under a stream of argon. A solution of *N*-Boc aniline **2-40** (14.7 mg, 0.0562 mmol) and 1-nitropropan-2-one²¹ (30.0 mg, 0.291 mmol) in 1,4-dioxane (0.500 mL, 0.11 M in aniline) were added to the dried MgCl_2 , and the resulting solution was stirred at 23 °C for 15 min. Then, $[(\text{C}_2\text{H}_4)\text{PtCl}_2]_2$ (0.8 mg, 0.00141 mmol) was added, and the reaction mixture was stirred at 23 °C for 10 h. Upon completion, the reaction mixture was filtered through a plug of silica gel (0.5 × 2.0 cm), washing with EtOAc (1 mL). The solvent was removed by rotary evaporation, and the resulting residue was purified by flash chromatography (5:1 hexanes/EtOAc eluent) to afford indole **2-40** (16.7 mg, 89% yield, R_f = 0.31 in 5:1 hexanes/EtOAc) as a colorless oil.

Indole 2-40: ^1H NMR (400 MHz, CDCl_3): δ 7.97 (d, J = 8.4 Hz, 1H), 7.46 (d, J = 7.6 Hz, 1H), 7.30 – 7.26 (m, 1H), 7.24 – 7.19 (m, 1H), 6.49 (s, 1H), 5.79 (dd, J = 10.2, 3.7 Hz, 1H), 3.95 (dd, J = 15.3, 3.7 Hz, 1H), 3.75 (dd, J = 15.3, 10.2 Hz, 1H), 2.41 (s, 3H), 1.71 (s, 9H); ^{13}C NMR (100 MHz, CDCl_3): δ 196.2, 150.8, 136.1, 133.5, 128.7, 124.4, 123.1, 120.6, 115.7, 111.6, 93.9, 85.0, 30.1, 28.2, 27.2; IR (film): 2980, 2936, 1723, 1558, 1456, 1370, 1324, 1255, 1219, 1156, 1116, 1090, 770, 781 cm^{-1} ; HRMS (ESI⁺) m/z calc'd for $(\text{M} + \text{Na})^+$ [$\text{C}_{17}\text{H}_{20}\text{N}_2\text{O}_5 + \text{Na}$]⁺: 355.1264, found 355.1271.



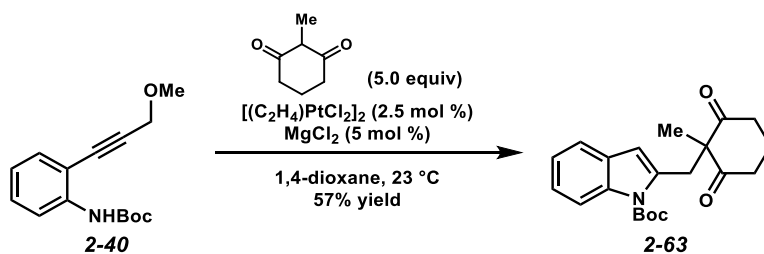
Indole 2-61. Following general procedure B, a 2-dram vial equipped with a magnetic stir bar and $MgCl_2$ (0.3 mg, 0.00291 mmol) was flame-dried under vacuum and cooled under a stream of argon. A solution of *N*-Boc aniline **2-40** (15.2 mg, 0.0582 mmol) and ethyl 2-nitroacetate (38.4 mg, 0.289 mmol) in 1,4-dioxane (0.500 mL, 0.12 M in aniline) were added to the dried $MgCl_2$, and the resulting solution was stirred at 23 °C for 15 min. Then, $[(C_2H_4)PtCl_2]_2$ (0.9 mg, 0.00146 mmol) was added, and the reaction mixture was heated to 50 °C and stirred for 3 h. Upon completion, the reaction mixture was cooled to room temperature and filtered through a plug of silica gel (0.5 × 2.0 cm), washing with EtOAc (1 mL). The solvent was removed by rotary evaporation, and the resulting residue was purified by flash chromatography (5:1 hexanes/EtOAc eluent) to afford indole **2-61** (14.2 mg, 67% yield, R_f = 0.53 in 5:1 hexanes/EtOAc) as a colorless oil.

Indole 2-61: 1H NMR (400 MHz, $CDCl_3$): δ 8.01 (d, J = 8.3 Hz, 1H), 7.46 (d, J = 7.7 Hz, 1H), 7.30 – 7.27 (m, 1H), 7.23 – 7.18 (m, 1H), 6.46 (s, 1H), 5.71 (dd, J = 9.5, 5.6 Hz, 1H), 4.32 – 4.24 (comp. m, 2H), 3.97 (dd, J = 15.2, 5.6 Hz, 1H), 3.88 (dd, J = 15.2, 9.5 Hz, 1H), 1.71 (s, 9H), 1.26 (t, J = 7.1 Hz, 3H); ^{13}C NMR (100 MHz, $CDCl_3$): δ 164.0, 150.5, 136.3, 133.2, 128.6, 124.4, 123.0, 120.5, 115.7, 111.3, 87.3, 84.9, 63.1, 31.1, 28.2, 13.8; IR (film): 1750, 1727, 1563, 1455, 1374, 1328, 1158, 1120, 749 cm^{-1} ; HRMS (ESI $^+$) m/z calc'd for $(M + H)^+$ [$C_{18}H_{22}N_2O_6 + H$] $^+$: 363.1551, found 363.1550.



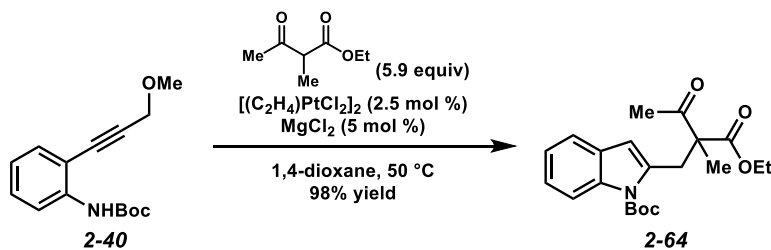
Indole 2-62. Following general procedure A, to a solution of *N*-Boc aniline **2-40** (52.2 mg, 0.200 mmol) in 1,4-dioxane (2.00 mL, 0.1 M) was added 3-ethyl-2,4-pentanedione (134 μL , 1.00 mmol) and MgCl_2 (0.9 mg, 0.0100 mmol), and the solution was stirred at 23 $^\circ\text{C}$ for 15 min. Then, $[(\text{C}_2\text{H}_4)\text{PtCl}_2]_2$ (2.9 mg, 0.00500 mmol) was added, and the reaction mixture was stirred at 23 $^\circ\text{C}$ for 3 h. Upon completion, the reaction mixture was filtered through a plug of silica gel (0.5 \times 2.0 cm), washing with EtOAc (4 mL). The solvent was removed by rotary evaporation, and the resulting residue was purified by flash chromatography (9:1 hexanes/EtOAc eluent) to afford indole **2-62** (50.0 mg, 70% yield, $R_f = 0.48$ in 4:1 hexanes/EtOAc) as an amber oil that solidified upon standing.

Indole 2-62: ^1H NMR (400 MHz, CDCl_3): δ 8.04 (d, $J = 8.4$ Hz, 1H), 7.42 (d, $J = 8.0$ Hz, 1H), 7.25 – 7.16 (comp. m, 2H), 6.23 (s, 1H), 3.77 (d, $J = 1.2$ Hz, 2H), 2.17 (q, $J = 7.6$ Hz, 2H), 2.13 (s, 6H), 1.72 (s, 9H), 0.77 (t, $J = 7.6$ Hz, 3H); ^{13}C NMR (100 MHz, CDCl_3): δ 207.0, 150.8, 136.5, 136.4, 129.1, 123.9, 122.9, 120.2, 115.6, 108.7, 84.5, 71.1, 29.8, 28.4, 27.1, 23.7, 8.6; IR (film): 2976, 2932, 1729, 1696, 1453, 1369, 1324, 1301, 1154, 1083, 731 cm^{-1} ; HRMS (ESI $^+$) m/z calc'd for $(\text{M} + \text{H})^+$ [$\text{C}_{21}\text{H}_{27}\text{NO}_4 + \text{H}$] $^+$: 358.2013, found 358.2019.



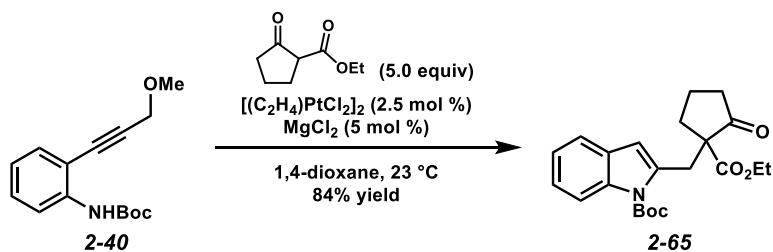
Indole 2-63. Following general procedure A, to a solution of *N*-Boc aniline **2-40** (52.2 mg, 0.200 mmol) in 1,4-dioxane (2.00 mL, 0.1 M) was added 2-methyl-1,3-cyclohexanedione (126 mg, 1.00 mmol) and MgCl_2 (0.9 mg, 0.0100 mmol), and the mixture was stirred vigorously at 23 °C for 15 min. Then, $[(\text{C}_2\text{H}_4)\text{PtCl}_2]_2$ (2.9 mg, 0.00500 mmol) was added, and the reaction mixture was stirred at 23 °C for 10 h. Upon completion, the reaction mixture was filtered through a plug of silica gel (0.5 × 2.0 cm), washing with EtOAc (4 mL). The solvent was removed by rotary evaporation, and the resulting residue was purified by flash chromatography (4:1 hexanes/EtOAc eluent) to afford indole **2-63** (40.2 mg, 57% yield, $R_f = 0.31$ in 4:1 hexanes/EtOAc) as an amber oil that solidified upon standing.

Indole 2-63: $^1\text{H NMR}$ (400 MHz, CDCl_3): δ 7.96 (d, $J = 8.4$ Hz, 1H), 7.42 (d, $J = 7.6$ Hz, 1H), 7.24 – 7.14 (comp. m, 2H), 6.18 (s, 1H), 3.68 (s, 2H), 2.80 – 2.72 (comp. m, 2H), 2.68 – 2.61 (comp. m, 2H), 2.08 – 1.98 (m, 1H), 1.96 – 1.86 (m, 1H), 1.70 (s, 9H), 1.29 (s, 3H); $^{13}\text{C NMR}$ (100 MHz, CDCl_3): δ 210.2, 150.9, 136.7, 136.5, 128.8, 123.9, 122.8, 120.2, 115.7, 110.4, 84.4, 64.7, 38.5, 35.6, 28.4, 21.1, 17.5; IR (film): 2979, 2934, 2254, 1726, 1694, 1452, 1370, 1327, 1156, 906, 726 cm^{-1} ; HRMS (ESI $^+$) m/z calc'd for $(\text{M} + \text{Na})^+$ [$\text{C}_{21}\text{H}_{25}\text{NO}_4 + \text{Na}$] $^+$: 378.1676, found 378.1679.



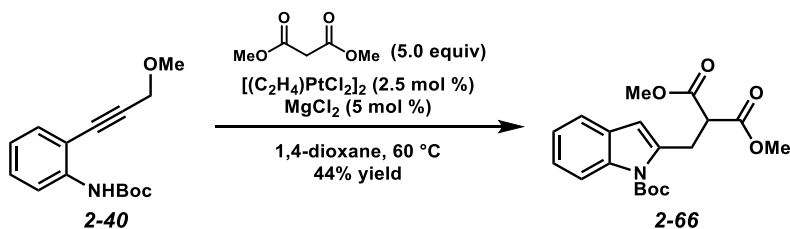
Indole 2-64. Following general procedure B, a 2-dram vial equipped with a magnetic stir bar and $MgCl_2$ (3.7 mg, 0.0331 mmol) was flame-dried under vacuum and cooled under a stream of argon. A solution of *N*-Boc aniline **2-40** (0.173 g, 0.661 mmol) and ethyl 2-methyl-3-oxobutanoate (0.550 mL, 3.89 mmol) in 1,4-dioxane (6.60 mL, 0.10 M in aniline) were added to the dried $MgCl_2$, and the resulting solution was stirred at 23 °C for 15 min. Then, $[(C_2H_4)PtCl_2]_2$ (10.2 mg, 0.0173 mmol) was added, and the reaction mixture was heated to 50 °C and stirred for 15 h. Upon completion, the reaction mixture was cooled to room temperature and filtered through a plug of silica gel (0.5 × 2.0 cm), washing with EtOAc (13 mL). The solvent was removed by rotary evaporation, and the resulting residue was purified by flash chromatography (5:1 hexanes/EtOAc eluent) to afford indole **2-64** (0.242 g, 98% yield, $R_f = 0.47$ in 5:1 hexanes/EtOAc) as a colorless oil.

Indole 2-64: 1H NMR (400 MHz, $CDCl_3$): δ 8.03 (d, $J = 8.1$ Hz, 1H), 7.43 (d, $J = 7.5$ Hz, 1H), 7.27 – 7.14 (comp. m, 2H), 6.35 (s, 1H), 4.23 – 4.14 (comp. m, 2H), 3.79 (ABq, $J_{AB} = 16.0$ Hz, $\Delta\nu = 32.2$ Hz, 2H), 2.20 (s, 3H), 1.69 (s, 9H), 1.41 (s, 3H), 1.21 (t, $J = 7.1$ Hz, 3H); ^{13}C NMR (100 MHz, $CDCl_3$): δ 205.0, 172.5, 150.6, 136.7, 136.4, 128.9, 123.6, 122.6, 120.0, 115.6, 109.7, 84.2, 61.6, 60.4, 33.0, 28.2, 26.2, 18.8, 13.9; IR (film): 2926, 2233, 1730, 1716, 1457, 1376, 1329, 1163, 1120, 1085, 748 cm^{-1} ; HRMS (ESI⁺) m/z calc'd for $(M + Na)^+$ $[C_{21}H_{27}NO_5 + Na]^+$: 396.1781, found 396.1781.



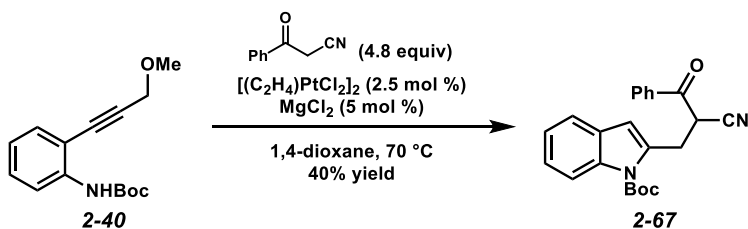
Indole 2-65. Following general procedure A, to a solution of *N*-Boc aniline **2-40** (52.2 mg, 0.200 mmol) in 1,4-dioxane (2.00 mL, 0.1 M) was added ethyl 2-oxocyclopentanecarboxylate (156 mg, 1.00 mmol) and MgCl₂ (0.9 mg, 0.0100 mmol), and the solution was stirred at 23 °C for 15 min. Then, [(C₂H₄)PtCl₂]₂ (2.9 mg, 0.00500 mmol) was added, and the reaction mixture was stirred at 23 °C for 3 h. Upon completion, the reaction mixture was filtered through a plug of silica gel (0.5 × 2.0 cm), washing with EtOAc (4 mL). The solvent was removed by rotary evaporation, and the resulting residue was purified by flash chromatography (2:1 hexanes/EtOAc eluent) to afford indole **2-65** (64.4 mg, 84% yield, R_f = 0.53 in 4:1 hexanes/EtOAc) as a colorless oil.

Indole 2-65: ¹H NMR (400 MHz, CDCl₃): δ 8.05 (d, *J* = 8.0 Hz, 1H), 7.44 (d, *J* = 7.6 Hz, 1H), 7.25 – 7.16 (comp. m, 2H), 6.35 (s, 1H), 4.17 (qd, *J* = 7.2, 1.6 Hz, 2H), 4.00 (d, *J* = 15.6 Hz, 1H), 3.51 (d, *J* = 15.6 Hz, 1H), 2.66 – 2.60 (m, 1H), 2.46 – 2.38 (m, 1H), 2.19 – 2.10 (m, 1H), 2.03 – 1.90 (comp. m, 2H), 1.88 – 1.80 (m, 1H), 1.69 (s, 9H), 1.22 (t, *J* = 7.2 Hz, 3H); ¹³C NMR (100 MHz, CDCl₃): δ 214.4, 170.8, 150.8, 137.2, 136.5, 129.1, 123.8, 122.8, 120.2, 115.8, 109.8, 84.3, 61.8, 61.2, 38.3, 32.9, 32.7, 28.4, 19.8, 14.2; IR (film): 2979, 2936, 2906, 2255, 1726, 1452, 1369, 1325, 1155, 1117, 908, 727 cm⁻¹; HRMS (ESI⁺) *m/z* calc'd for (M + NH₄)⁺ C₂₂H₂₇NO₅ + NH₄⁺: 403.2227, found 403.2227.



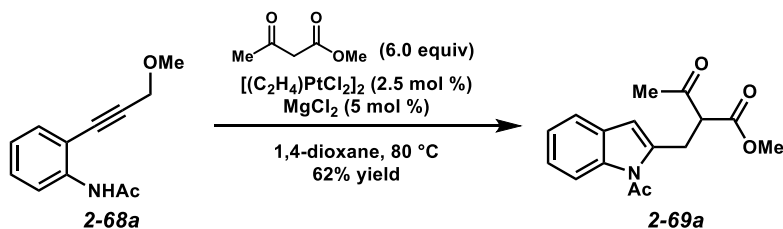
Indole 2-66. Following general procedure B, a 2-dram vial equipped with a magnetic stir bar and $MgCl_2$ (0.3 mg, 0.00287 mmol) was flame-dried under vacuum and cooled under a stream of argon. A solution of *N*-Boc aniline **2-40** (15.0 mg, 0.0574 mmol) and dimethyl malonate (33.0 μ L, 0.289 mmol) in 1,4-dioxane (0.500 mL, 0.11 M in aniline) were added to the dried $MgCl_2$, and the resulting solution was stirred at 23 °C for 15 min. Then, $[(C_2H_4)PtCl_2]_2$ (0.8 mg, 0.00144 mmol) was added, and the reaction mixture was heated to 60 °C and stirred for 12 h. Upon completion, the reaction mixture was cooled to room temperature and filtered through a plug of silica gel (0.5 \times 2.0 cm), washing with EtOAc (1 mL). The solvent was removed by rotary evaporation, and the resulting residue was purified by flash chromatography (5:1 hexanes/EtOAc eluent) to afford indole **2-66** (9.2 mg, 44% yield, R_f = 0.26 in 5:1 hexanes/EtOAc) as a colorless oil.

Indole 2-66: 1H NMR (400 MHz, $CDCl_3$): δ 8.06 (d, J = 8.2 Hz, 1H), 7.44 (d, J = 7.5 Hz, 1H), 7.25 – 7.15 (comp. m, 2H), 6.38 (s, 1H), 3.98 (t, J = 7.6 Hz, 1H), 3.71 (s, 6H), 3.63 (d, J = 7.6 Hz, 2H), 1.69 (s, 9H); ^{13}C NMR (100 MHz, $CDCl_3$): δ 169.1, 150.4, 137.1, 136.5, 128.9, 123.8, 122.7, 120.1, 115.7, 109.1, 84.3, 52.6, 51.4, 29.4, 28.2; IR (film): 2976, 2956, 1732, 1753, 1457, 1373, 1329, 1158, 1119, 1088, 1029, 751 cm^{-1} ; HRMS (ESI $^+$) m/z calc'd for $(M + Na)^+$ [$C_{19}H_{23}NO_6 + Na$] $^+$: 384.1418, found 384.1418.



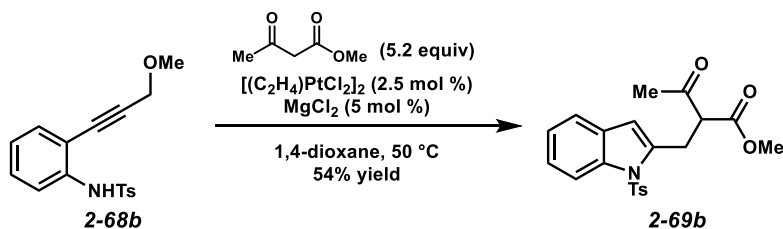
Indole 2-67. Following general procedure B, a 2-dram vial equipped with a magnetic stir bar and MgCl_2 (0.3 mg, 0.00268 mmol) was flame-dried under vacuum and cooled under a stream of argon. A solution of *N*-Boc aniline **2-40** (14.0 mg, 0.0536 mmol) and 3-oxo-3-phenylpropanenitrile (37.6 mg, 0.259 mmol) in 1,4-dioxane (0.500 mL, 0.11 M in aniline) were added to the dried MgCl_2 , and the resulting solution was stirred at 23 °C for 15 min. Then, $[(\text{C}_2\text{H}_4)\text{PtCl}_2]_2$ (0.8 mg, 0.00134 mmol) was added, and the reaction mixture was heated to 70 °C and stirred for 15 h. Upon completion, the reaction mixture was cooled to room temperature and filtered through a plug of silica gel (0.5 × 2.0 cm), washing with EtOAc (1 mL). The solvent was removed by rotary evaporation, and the resulting residue was purified by flash chromatography (5:1 hexanes/EtOAc eluent) to afford indole **2-67** (8.1 mg, 40% yield, $R_f = 0.31$ in 5:1 hexanes/EtOAc) as a colorless oil.

Indole 2-40: ^1H NMR (400 MHz, CDCl_3): δ 8.07 (d, $J = 8.2$ Hz, 2H), 7.98 (d, $J = 8.2$ Hz, 1H), 7.63 (t, $J = 7.0$ Hz, 1H), 7.54 – 7.47 (comp. m, 3H), 7.30 – 7.24 (m, 1H), 7.21 (t, $J = 7.3$ Hz, 1H), 6.63 (s, 1H), 5.08 (dd, $J = 9.7, 5.6$ Hz, 1H), 3.84 (dd, $J = 14.5, 5.6$ Hz, 1H), 3.49 (dd, $J = 14.5, 9.7$ Hz, 1H), 1.70 (s, 9H). ^{13}C NMR (125 MHz, CDCl_3): δ 190.4, 150.7, 136.2, 134.9, 134.5, 134.2, 128.99, 128.98, 128.8, 124.3, 123.0, 120.6, 117.0, 115.6, 111.8, 84.8, 39.8, 30.2, 28.3. IR (film): 2980, 2935, 2361, 1699, 1455, 1370, 1329, 1262, 1221, 1161, 1120, 1089 cm^{-1} ; HRMS (ESI⁺) m/z calc'd for $(\text{M} + \text{H})^+$ [$\text{C}_{23}\text{H}_{22}\text{N}_2\text{O}_3 + \text{H}$]⁺: 375.1703, found 375.1703.



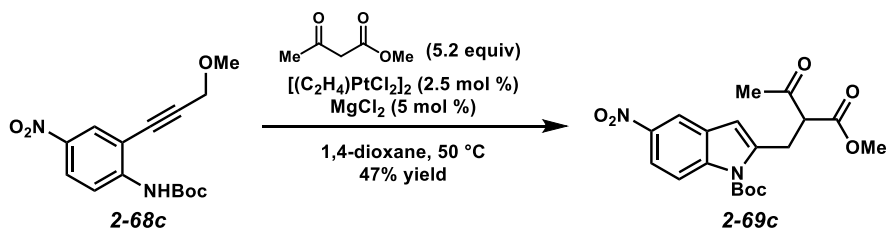
Indole 2-69a. Following general procedure B, a 2-dram vial equipped with a magnetic stir bar and $MgCl_2$ (0.3 mg, 0.00295 mmol) was flame-dried under vacuum and cooled under a stream of argon. A solution of *N*-acetyl aniline **2-68a**²² (12.0 mg, 0.0590 mmol) and methyl acetoacetate (38.0 μ L, 0.352 mmol) in 1,4-dioxane (0.500 mL, 0.12 M in aniline) were added to the dried $MgCl_2$, and the resulting solution was stirred at 23 °C for 15 min. Then, $[(C_2H_4)PtCl_2]_2$ (0.9 mg, 0.00148 mmol) was added, and the reaction mixture was heated to 80 °C and stirred for 11 h. Upon completion, the reaction mixture was cooled to room temperature and filtered through a plug of silica gel (0.5 \times 2.0 cm), washing with EtOAc (1 mL). The solvent was removed by rotary evaporation, and the resulting residue was purified by flash chromatography (3:1 hexanes/EtOAc eluent) to afford indole **2-69a** (10.5 mg, 62% yield, R_f = 0.23 in 3:1 hexanes/EtOAc) as a white solid.

Indole 2-69a: 1H NMR (400 MHz, $CDCl_3$): δ 7.65 (d, J = 8.3 Hz, 1H), 7.49 (d, J = 7.7 Hz, 1H), 7.30 – 7.21 (comp. m, 2H), 6.46 (s, 1H), 4.12 (dd, J = 8.3, 5.9 Hz, 1H), 3.69 (s, 3H), 3.58 (dd, J = 14.8, 5.9 Hz, 1H), 3.50 (dd, J = 14.8, 8.3 Hz, 1H), 2.82 (s, 3H), 2.28 (s, 3H); ^{13}C NMR (100 MHz, $CDCl_3$): δ 202.4, 170.4, 169.5, 138.7, 135.8, 129.8, 123.9, 123.1, 121.0, 114.2, 111.0, 59.0, 52.5, 29.5, 29.0, 27.7; IR (film): 2953, 1742, 1700, 1459, 1433, 1374, 1299, 1208, 1146, 749 cm^{-1} ; HRMS (ESI⁺) m/z calc'd for (M + H)⁺ [$C_{16}H_{17}NO_4$ + H]⁺: 288.1230, found 288.1230.



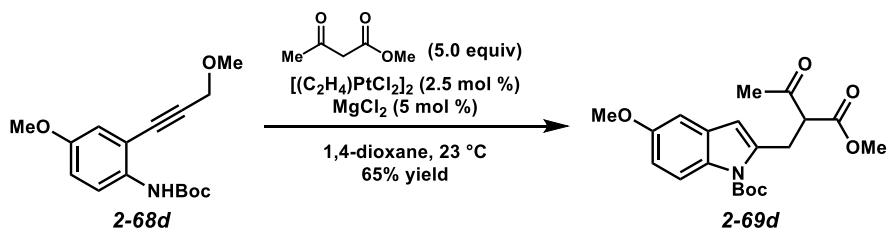
Indole 2-69b. Following general procedure B, a 2-dram vial equipped with a magnetic stir bar and $MgCl_2$ (0.3 mg, 0.00247 mmol) was flame-dried under vacuum and cooled under a stream of argon. A solution of *N*-tosyl aniline **2-68b**²³ (15.6 mg, 0.0495 mmol) and methyl acetoacetate (28.0 μ L, 0.259 mmol) in 1,4-dioxane (0.500 mL, 0.10 M in aniline) were added to the dried $MgCl_2$, and the resulting solution was stirred at 23 °C for 15 min. Then, $[(C_2H_4)PtCl_2]_2$ (0.8 mg, 0.00136 mmol) was added, and the reaction mixture was heated to 50 °C and stirred for 11 h. Upon completion, the reaction mixture was cooled to room temperature and filtered through a plug of silica gel (0.5 \times 2.0 cm), washing with EtOAc (1 mL). The solvent was removed by rotary evaporation, and the resulting residue was purified by flash chromatography (5:1 hexanes/EtOAc eluent) to afford indole **2-69b** (10.6 mg, 54% yield, R_f = 0.30 in 5:1 hexanes/EtOAc) as a white solid.

Indole 2-69b: 1H NMR (400 MHz, $CDCl_3$): δ 8.14 (d, J = 8.4 Hz, 1H), 7.61 (d, J = 8.4, 2H), 7.39 (d, J = 7.9 Hz, 1H), 7.30 – 7.25 (m, 1H), 7.22 – 7.17 (comp. m, 3H), 6.42 (s, 1H), 4.27 (t, J = 7.1 Hz, 1H), 3.70 (s, 3H), 3.56 – 3.48 (comp. m, 2H), 2.32 (s, 3H), 2.28 (s, 3H); ^{13}C NMR (100 MHz, $CDCl_3$): δ 202.2, 169.1, 145.0, 137.4, 137.3, 135.5, 129.9, 129.5, 126.3, 124.5, 123.7, 120.5, 114.9, 111.7, 59.1, 52.6, 30.0, 27.7, 21.6; IR (film): 1746 1719, 1454, 1366, 1213, 1173, 1148, 1092, 1049, 811, 749, 670 cm^{-1} ; HRMS (ESI⁺) m/z calc'd for $(M + H)^+$ [$C_{21}H_{21}NO_5S + H$]⁺: 400.1213, found 400.1213.



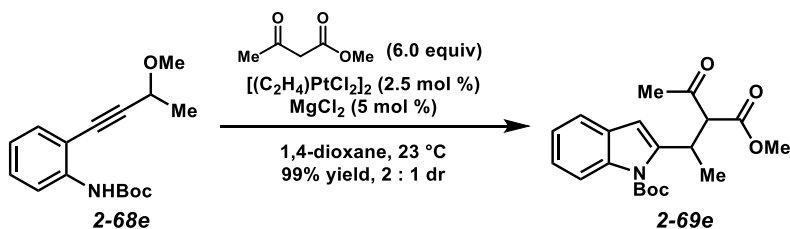
Indole 2-69c Following general procedure B, a 2-dram vial equipped with a magnetic stir bar and MgCl_2 (0.3 mg, 0.00263 mmol) was flame-dried under vacuum and cooled under a stream of argon. A solution of *N*-Boc aniline **2-68c** (15.3 mg, 0.0499 mmol) and methyl acetoacetate (28.0 μL , 0.260 mmol) in 1,4-dioxane (0.500 mL, 0.10 M in aniline) were added to the dried MgCl_2 , and the resulting solution was stirred at 23 $^\circ\text{C}$ for 15 min. Then, $[(\text{C}_2\text{H}_4)\text{PtCl}_2]_2$ (0.8 mg, 0.00136 mmol) was added, and the reaction mixture was heated to 50 $^\circ\text{C}$ and stirred for 10 h. Upon completion, the reaction mixture was cooled to room temperature and filtered through a plug of silica gel (0.5 \times 2.0 cm), washing with EtOAc (1 mL). The solvent was removed by rotary evaporation, and the resulting residue was purified by flash chromatography (5:1 hexanes/EtOAc eluent) to afford indole **2-69c** (9.2 mg, 47% yield, $R_f = 0.27$ in 5:1 hexanes/EtOAc) as a white solid.

Indole 2-69c: $^1\text{H NMR}$ (400 MHz, CDCl_3): δ 8.36 – 8.32 (m, 1H), 8.13 (app. s, 2H), 6.50 (s, 1H), 4.04 (dd, $J = 8.6, 6.0$ Hz, 1H), 3.72 (s, 3H), 3.62 (dd, $J = 15.6, 6.0$ Hz, 1H), 3.53 (dd, $J = 15.6, 8.6$ Hz, 1H), 2.30 (s, 3H), 1.71 (s, 9H); $^{13}\text{C NMR}$ (100 MHz, CDCl_3): δ 201.4, 169.2, 149.6, 143.7, 141.1, 139.5, 128.7, 119.0, 116.2, 115.7, 109.3, 85.9, 58.7, 52.7, 29.3, 28.3, 28.1; IR (film): 2984, 1729, 1719, 1519, 1449, 1372, 1345, 1322, 1152, 1091, 671 cm^{-1} ; HRMS (ESI $^+$) m/z calc'd for $(\text{M} + \text{Na})^+$ [$\text{C}_{19}\text{H}_{22}\text{N}_2\text{O}_7 + \text{Na}$] $^+$: 413.1319, found 413.1319.



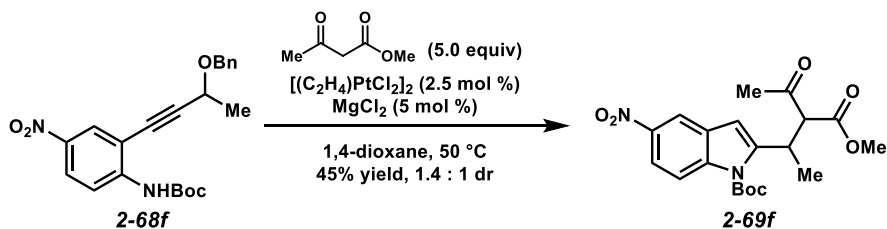
Indole 2-69d. Following general procedure B, a 2-dram vial equipped with a magnetic stir bar and MgCl_2 (0.3 mg, 0.00263 mmol) was flame-dried under vacuum and cooled under a stream of argon. A solution of *N*-Boc aniline **2-68d** (15.0 mg, 0.0515 mmol) and methyl acetoacetate (28.0 μL , 0.259 mmol) in 1,4-dioxane (0.500 mL, 0.10 M in aniline) were added to the dried MgCl_2 , and the resulting solution was stirred at 23 °C for 15 min. Then, $[(\text{C}_2\text{H}_4)\text{PtCl}_2]_2$ (0.8 mg, 0.00129 mmol) was added, and the reaction mixture was stirred at 23 °C for 10 h. Upon completion, the reaction mixture was filtered through a plug of silica gel (0.5 \times 2.0 cm), washing with EtOAc (1 mL). The solvent was removed by rotary evaporation, and the resulting residue was purified by flash chromatography (5:1 hexanes/EtOAc eluent) to afford indole **2-69d** (12.6 mg, 65% yield, $R_f = 0.29$ in 5:1 hexanes/EtOAc) as a pale yellow oil.

Indole 2-69d: ^1H NMR (400 MHz, CDCl_3): δ 7.90 (d, $J = 9.0$ Hz, 1H), 6.90 (s, 1H), 6.84 (d, $J = 9.0$ Hz, 1H), 6.30 (s, 1H), 4.06 (t, $J = 7.2$ Hz, 1H), 3.82 (s, 3H), 3.69 (s, 3H), 3.58 (dd, $J = 15.2$, 5.7 Hz, 1H), 3.49 (dd, $J = 15.2$, 8.5 Hz, 1H), 2.26 (s, 3H), 1.68 (s, 9H); ^{13}C NMR (100 MHz, CDCl_3): δ 202.3, 169.5, 155.8, 150.3, 138.2, 131.0, 129.8, 116.4, 112.4, 109.3, 102.6, 84.1, 58.9, 55.6, 52.5, 29.5, 28.5, 28.2; IR (film): 2982, 2951, 1721, 1618, 1480, 1449, 1373, 1314, 1211, 1160, 1125, 1091, 1035, 768 cm^{-1} ; HRMS (ESI $^+$) m/z calc'd for $(\text{M} + \text{Na})^+$ [$\text{C}_{20}\text{H}_{25}\text{NO}_6 + \text{Na}$] $^+$: 398.1574, found 398.1573.



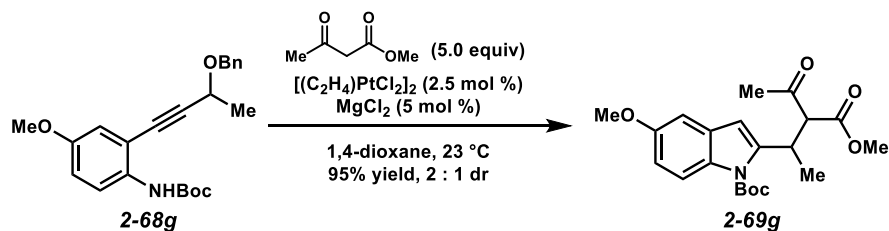
Indole 2-69e. Following general procedure A, to a solution of *N*-Boc aniline **2-68e**¹¹ (55.0 mg, 0.200 mmol) in 1,4-dioxane (2.00 mL, 0.1 M) was added methyl acetoacetate (128 μ L, 1.19 mmol) and MgCl₂ (0.9 mg, 0.0100 mmol), and the solution was stirred at 23 °C for 15 min. Then, [(C₂H₄)PtCl₂]₂ (2.9 mg, 0.00500 mmol) was added, and the reaction mixture was stirred at 23 °C for 7 h. Upon completion, the reaction mixture was filtered through a plug of silica gel (0.5 \times 2.0 cm), washing with EtOAc (4 mL). The solvent was removed by rotary evaporation, and the resulting residue was purified by flash chromatography (9:1 hexanes/EtOAc eluent) to afford indole **2-69e** (71.1 mg, 99% yield, *R*_f = 0.59 in 4:1 hexanes/EtOAc) as a pale yellow oil.

Indole 2-69e: Characterized as a 2:1 mixture of diastereomers. ¹H NMR (400 MHz, CDCl₃): δ 8.07 (d, *J* = 8.4 Hz, 0.33H), 8.04 (d, *J* = 8.4 Hz, 0.67H), 7.45 – 7.42 (m, 1H), 7.27 – 7.16 (comp. m, 2H), 6.40 (s, 0.33H), 6.38 (s, 0.67H), 4.62 – 4.53 (m, 1H), 4.02 – 3.98 (m, 1H), 3.71 (s, 2H), 3.59 (s, 1H), 2.25 (s, 1H), 2.17 (s, 2H), 1.72 (s, 9H), 1.36 (d, *J* = 6.8 Hz, 2H), 1.29 (d, *J* = 6.8 Hz, 1H); ¹³C NMR (100 MHz, CDCl₃): δ 202.2, 202.1, 169.0, 168.8, 150.4, 150.3, 143.9, 143.5, 136.5, 136.4, 128.9, 128.8, 123.84, 123.79, 122.74, 122.68, 120.2, 120.1, 115.6, 106.9, 106.1, 84.4, 84.3, 65.2, 65.1, 52.5, 52.3, 32.7, 32.6, 30.2, 28.6, 28.2, 19.3, 18.9; IR (film): 2978, 2934, 1724, 1453, 1433, 1370, 1322, 1301, 1152, 1113 cm⁻¹; HRMS (ESI⁺) *m/z* calc'd for (M + NH₄)⁺ [C₂₀H₂₅NO₅ + NH₄]⁺: 377.2071, found 377.2074.



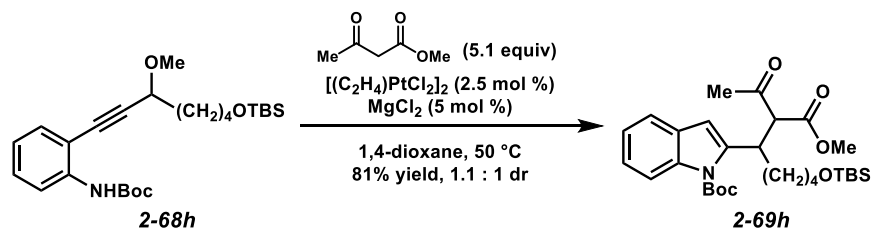
Indole 2-69f. Following general procedure B, a 2-dram vial equipped with a magnetic stir bar and $MgCl_2$ (0.3 mg, 0.00263 mmol) was flame-dried under vacuum and cooled under a stream of argon. A solution of *N*-Boc aniline **2-68f** (20.5 mg, 0.0517 mmol) and methyl acetoacetate (28.0 μ L, 0.259 mmol) in 1,4-dioxane (0.500 mL, 0.10 M in aniline) were added to the dried $MgCl_2$, and the resulting solution was stirred at 23 °C for 15 min. Then, $[(C_2H_4)PtCl_2]_2$ (0.8 mg, 0.00129 mmol) was added, and the reaction mixture was heated to 50 °C and stirred for 5 h. Upon completion, the reaction mixture was cooled to room temperature and filtered through a plug of silica gel (0.5 \times 2.0 cm), washing with EtOAc (1 mL). The solvent was removed by rotary evaporation, and the resulting residue was purified by flash chromatography (5:1 hexanes/EtOAc eluent) to afford indole **2-69f** (9.4 mg, 45% yield, R_f = 0.24 in 5:1 hexanes/EtOAc) as a pale yellow oil.

Indole 2-69f: Characterized as a 1.4:1 mixture of diastereomers. 1H NMR (400 MHz, $CDCl_3$): δ 8.37 – 8.33 (m, 1H), 8.20 – 8.10 (comp. m, 2H), 6.51 (s, 0.42H), 6.49 (s, 0.58H), 4.62 – 4.51 (m, 1H), 4.02 – 3.96 (m, 1H), 3.73 (s, 1.7H), 3.58 (s, 1.3H), 2.30 (s, 1.3H), 2.18 (s, 1.7H), 1.73 (s, 9H), 1.37 (d, J = 6.9 Hz, 1.7H), 1.29 (d, J = 6.9 Hz, 1.3H); ^{13}C NMR (100 MHz, $CDCl_3$): δ 201.32, 201.30, 168.6, 168.4, 149.6, 149.5, 147.4, 147.2, 143.6, 139.6, 139.5, 128.6, 127.6, 127.0, 119.0, 116.2, 115.73, 115.71, 106.8, 106.1, 86.0, 85.9, 65.2, 64.9, 52.7, 52.5, 32.6, 32.3, 30.3, 29.1, 28.1, 19.6, 18.7; IR (film): 2982, 1743, 1719, 1520, 1451, 1374, 1317, 1151, 1085 cm^{-1} ; HRMS (ESI $^+$) m/z calc'd for $(M + Na)^+$ [$C_{20}H_{24}N_2O_7 + Na$] $^+$: 427.1476, found 427.1480.



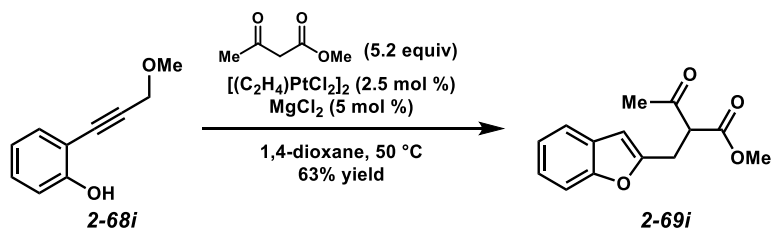
Indole 2-69g. Following general procedure B, a 2-dram vial equipped with a magnetic stir bar and MgCl_2 (0.3 mg, 0.00263 mmol) was flame-dried under vacuum and cooled under a stream of argon. A solution of *N*-Boc aniline **2-68g** (19.9 mg, 0.0522 mmol) and methyl acetoacetate (28.0 μL , 0.259 mmol) in 1,4-dioxane (0.500 mL, 0.10 M in aniline) were added to the dried MgCl_2 , and the resulting solution was stirred at 23 $^\circ\text{C}$ for 15 min. Then, $[(\text{C}_2\text{H}_4)\text{PtCl}_2]_2$ (0.8 mg, 0.00131 mmol) was added, and the reaction mixture was stirred at 23 $^\circ\text{C}$ for 24 h. Upon completion, the reaction mixture was filtered through a plug of silica gel (0.5 \times 2.0 cm), washing with EtOAc (1 mL). The solvent was removed by rotary evaporation, and the resulting residue was purified by flash chromatography (5:1 hexanes/EtOAc eluent) to afford indole **2-69g** (19.3 mg, 95% yield, $R_f = 0.31$ in 5:1 hexanes/EtOAc) as a colorless oil.

Indole 2-69g: Characterized as a 2:1 mixture of diastereomers. ^1H NMR (400 MHz, CDCl_3): δ 7.96 (d, $J = 9.2$ Hz, 0.33H), 7.92 (d, $J = 9.1$ Hz, 0.67H), 6.91 (d, $J = 2.6$ Hz, 1H), 6.85 (dd, $J = 9.2$, 2.6 Hz, 1H), 6.33 (s, 0.33H), 6.31 (s, 0.67H), 4.60 – 4.49 (m, 1H), 3.99 (m, 1H), 3.82 (s, 3H), 3.70 (s, 2H), 3.59 (s, 1H), 2.24 (s, 1H), 2.17 (s, 2H), 1.70 (s, 9H), 1.34 (d, $J = 7.0$ Hz, 2H), 1.28 (d, $J = 7.0$ Hz, 1H); ^{13}C NMR (100 MHz, CDCl_3): δ 202.2, 202.1, 169.0, 168.8, 155.81, 155.79, 150.3, 150.2, 144.5, 144.1, 131.2, 131.0, 129.7, 129.6, 116.5, 112.5, 112.4, 106.8, 106.0, 102.7, 84.2, 84.1, 65.1, 65.0, 55.6, 52.5, 52.3, 32.73, 32.68, 30.1, 28.6, 28.2, 19.2, 18.8; IR (film): 2979, 2955, 1720, 1450, 1371, 1308, 1122, 1085, 1036, 849, 801, 770 cm^{-1} ; HRMS (ESI $^+$) m/z calc'd for (M + H) $^+$ [$\text{C}_{21}\text{H}_{27}\text{NO}_6 + \text{H}$] $^+$: 390.1911, found 390.1911.



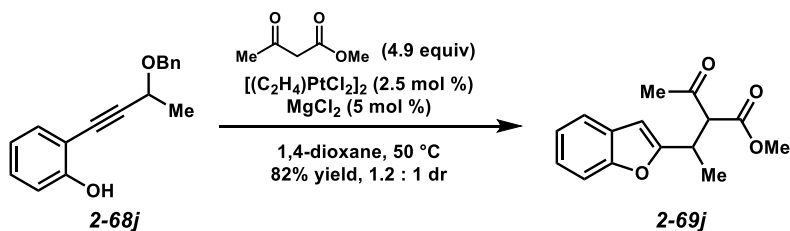
Indole 2-69h. Following general procedure B, a 2-dram vial equipped with a magnetic stir bar and $MgCl_2$ (0.3 mg, 0.00263 mmol) was flame-dried under vacuum and cooled under a stream of argon. A solution of *N*-Boc aniline **2-68h** (22.8 mg, 0.0509 mmol) and methyl acetoacetate (28.0 μ L, 0.259 mmol) in 1,4-dioxane (0.500 mL, 0.10 M in aniline) were added to the dried $MgCl_2$, and the resulting solution was stirred at 23 °C for 15 min. Then, $[(C_2H_4)PtCl_2]_2$ (0.8 mg, 0.00136 mmol) was added, and the reaction mixture was heated to 50 °C and stirred for 15 h. Upon completion, the reaction mixture was cooled to room temperature and filtered through a plug of silica gel (0.5 \times 2.0 cm), washing with EtOAc (1 mL). The solvent was removed by rotary evaporation, and the resulting residue was purified by flash chromatography (5:1 hexanes/EtOAc eluent) to afford indole **2-69h** (22.0 mg, 81% yield, R_f = 0.32 in 5:1 hexanes/EtOAc) as a colorless oil.

Indole 2-69h: Characterized as a 1.1:1 mixture of diastereomers. 1H NMR (400 MHz, $CDCl_3$): δ 8.05 (m, 1H), 7.44 (d, J = 7.4 Hz, 1H), 7.23 – 7.19 (comp. m, 2H), 6.40 (s, 0.48H), 6.38 (s, 0.52H), 4.79 – 4.66 (m, 1H), 3.94 (d, J = 8.2 Hz, 1H), 3.72 (s, 1.5H), 3.54 – 3.46 (comp. m, 3.5H), 2.26 (s, 1.5H), 2.12 (s, 1.5H), 1.72 (s, 9H), 1.51 – 1.36 (comp. m, 3H), 1.29 – 1.23 (comp. m, 3H), 0.80 (s, 9H), -0.04 (s, 6H); ^{13}C NMR (100 MHz, $CDCl_3$): δ 202.1, 169.0, 168.6, 150.5, 150.4, 141.7, 136.6, 136.4, 128.8, 123.7, 123.6, 122.6, 122.5, 120.1, 120.0, 115.6, 115.5, 107.5, 107.0, 84.4, 84.3, 65.0, 62.8, 52.4, 52.3, 36.9, 36.6, 32.9, 32.8, 30.1, 28.8, 28.2, 25.8, 22.6, 22.5, 18.2, -5.3, -5.4; IR (film): 2957, 2930, 1731, 1655, 1454, 1371, 1327, 1256, 1157, 1117, 1085, 837, 773, 741 cm^{-1} ; HRMS (ESI+) m/z calc'd for $(M + Na)^+$ [$C_{29}H_{45}NO_6Si + Na$] $^+$: 554.2908, found 554.2909.



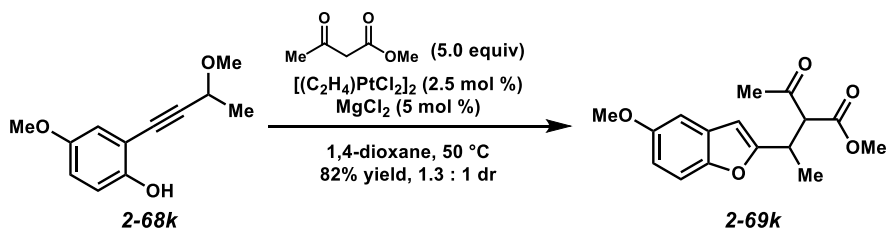
Benzofuran 2-69i. Following general procedure B, a 2-dram vial equipped with a magnetic stir bar and $MgCl_2$ (0.3 mg, 0.00324 mmol) was flame-dried under vacuum and cooled under a stream of argon. A solution of phenol **2-68i**²⁴⁻²⁵ (10.5 mg, 0.0647 mmol) and methyl acetoacetate (36.0 μ L, 0.335 mmol) in 1,4-dioxane (0.500 mL, 0.13 M in aniline) were added to the dried $MgCl_2$, and the resulting solution was stirred at 23 °C for 15 min. Then, $[(C_2H_4)PtCl_2]_2$ (0.9 mg, 0.00161 mmol) was added, and the reaction mixture was heated to 50 °C and stirred for 12 h. Upon completion, the reaction mixture was cooled to room temperature and filtered through a plug of silica gel (0.5 \times 2.0 cm), washing with EtOAc (1 mL). The solvent was removed by rotary evaporation, and the resulting residue was purified by flash chromatography (5:1 hexanes/EtOAc eluent) to afford benzofuran **2-69i** (10.0 mg, 63% yield, R_f = 0.22 in 5:1 hexanes/EtOAc) as a pale yellow oil.

Benzofuran 2-69i: 1H NMR (400 MHz, $CDCl_3$): δ 7.47 (d, J = 7.6 Hz, 1H), 7.39 (d, J = 7.6 Hz, 1H), 7.27 – 7.15 (comp. m, 2H), 6.45 (s, 1H), 4.03 (t, J = 7.4 Hz, 1H), 3.75 (s, 3H), 3.34 (dd, J = 7.4, 3.9 Hz, 2H), 2.28 (s, 3H); ^{13}C NMR (100 MHz, $CDCl_3$): δ 201.5, 169.0, 154.8, 154.7, 128.5, 123.7, 122.7, 120.6, 110.8, 103.8, 57.6, 52.7, 29.6, 27.0; IR (film): 1748, 1719, 1455, 1436, 1356, 1254, 1215, 1147, 752 cm^{-1} ; HRMS (ESI⁺) m/z calc'd for $(M + H)^+$ [$C_{14}H_{14}O_4 + H$]⁺: 247.0965, found 247.0965.



Benzofuran 2-69j. Following general procedure B, a 2-dram vial equipped with a magnetic stir bar and MgCl_2 (0.3 mg, 0.00264 mmol) was flame-dried under vacuum and cooled under a stream of argon. A solution of phenol **2-68j** (13.3 mg, 0.0527 mmol) and methyl acetoacetate (28.0 μL , 0.259 mmol) in 1,4-dioxane (0.500 mL, 0.11 M in aniline) were added to the dried MgCl_2 , and the resulting solution was stirred at 23 °C for 15 min. Then, $[(\text{C}_2\text{H}_4)\text{PtCl}_2]_2$ (0.8 mg, 0.00132 mmol) was added, and the reaction mixture was heated to 50 °C and stirred for 12 h. Upon completion, the reaction mixture was cooled to room temperature and filtered through a plug of silica gel (0.5 \times 2.0 cm), washing with EtOAc (1 mL). The solvent was removed by rotary evaporation, and the resulting residue was purified by flash chromatography (5:1 hexanes/EtOAc eluent) to afford benzofuran **2-69j** (11.3 mg, 82% yield, $R_f = 0.25$ in 5:1 hexanes/EtOAc) as a colorless oil.

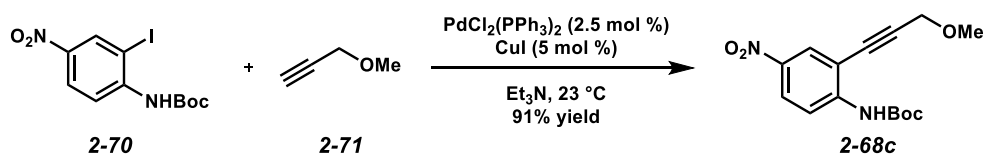
Benzofuran 2-69j: Characterized as a 1.2:1 mixture of diastereomers. ^1H NMR (400 MHz, CDCl_3): δ 7.48 (dd, $J = 7.7, 2.0$ Hz, 1H), 7.40 (d, $J = 7.7$ Hz, 1H), 7.26 – 7.15 (comp m, 2H), 6.46 (s, 0.45H), 6.44 (s, 0.55H), 3.99 (d, $J = 2.1$ Hz, 0.45H), 3.97 (d, $J = 2.1$ Hz, 0.55H), 3.86 – 3.78 (m, 1H), 3.76 (s, 1.7H), 3.60 (s, 1.3H), 2.27 (s, 1.3H), 2.11 (s, 1.7H), 1.39 (d, $J = 6.9$ Hz, 1.7H), 1.36 (d, $J = 6.9$ Hz, 1.3H). ^{13}C NMR (100 MHz, CDCl_3) δ 201.7, 201.5, 168.5, 159.2, 158.9, 154.6, 154.5, 128.34, 128.32, 123.8, 123.7, 122.7, 122.6, 120.7, 120.6, 110.9, 102.8, 102.5, 63.7, 52.6, 52.5, 33.6, 33.5, 30.3, 29.7, 17.3, 16.9. IR (film): 1748, 1721, 1453, 1436, 1359, 1250, 1167, 942, 810, 753 cm^{-1} ; HRMS (ESI+) m/z calc'd for $(\text{M} + \text{Na})^+$ [$\text{C}_{15}\text{H}_{16}\text{O}_4 + \text{Na}$] $^+$: 283.0941, found 283.0941.



Benzofuran 2-69k. Following general procedure B, a 2-dram vial equipped with a magnetic stir bar and MgCl_2 (0.3 mg, 0.00263 mmol) was flame-dried under vacuum and cooled under a stream of argon. A solution of phenol **2-68k** (10.8 mg, 0.0524 mmol) and methyl acetoacetate (28.0 μL , 0.259 mmol) in 1,4-dioxane (0.500 mL, 0.10 M in aniline) were added to the dried MgCl_2 , and the resulting solution was stirred at 23 $^\circ\text{C}$ for 15 min. Then, $[(\text{C}_2\text{H}_4)\text{PtCl}_2]_2$ (0.9 mg, 0.00153 mmol) was added, and the reaction mixture was heated to 50 $^\circ\text{C}$ and stirred for 5 h. Upon completion, the reaction mixture was cooled to room temperature and filtered through a plug of silica gel (0.5 \times 2.0 cm), washing with EtOAc (1 mL). The solvent was removed by rotary evaporation, and the resulting residue was purified by flash chromatography (5:1 hexanes/EtOAc eluent) to afford benzofuran **2-69k** (12.4 mg, 82% yield, $R_f = 0.29$ in 5:1 hexanes/EtOAc) as a colorless oil.

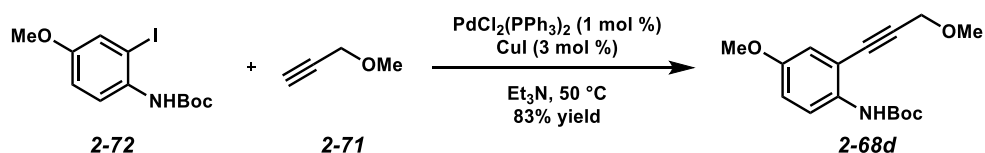
Benzofuran 2-69k: Characterized as a 1.3:1 mixture of diastereomers. ^1H NMR (400 MHz, CDCl_3): δ 7.32 – 7.23 (m, 1H), 6.94 (dd, $J = 4.1, 2.5$ Hz, 1H), 6.83 (d, $J = 2.5$ Hz, 0.56H), 6.81 (d, $J = 2.5$ Hz, 0.44H), 6.39 (s, 0.44H), 6.37 (s, 0.56H), 3.95 (d, $J = 9.5$ Hz, 1H), 3.81 (s, 3H), 3.80 – 3.74 (m, 1H), 3.75 (s, 1.7H), 3.59 (s, 1.3H), 2.26 (s, 1.3H), 2.10 (s, 1.7H), 1.37 (d, $J = 6.9$ Hz, 1.7H), 1.34 (d, $J = 6.9$ Hz, 1.3H); ^{13}C NMR (100 MHz, CDCl_3): δ 201.7, 201.5, 168.50, 168.49, 160.1, 159.7, 155.9, 155.8, 149.6, 149.5, 128.91, 128.89, 112.3, 112.2, 111.27, 111.25, 103.4, 103.0, 102.7, 63.76, 63.75, 55.9, 52.6, 52.5, 33.7, 33.6, 30.3, 29.7, 17.3, 16.8; IR (film): 2979, 2955, 2937, 1720, 1620, 1592, 1478, 1308, 1222, 1146, 1160, 1122, 1085, 1036, 849, 801, 770 cm^{-1} ; HRMS (ESI $^+$) m/z calc'd for $(\text{M} + \text{Na})^+$ [$\text{C}_{16}\text{H}_{18}\text{O}_5 + \text{Na}$] $^+$: 313.1046, found 313.1046.

2.3.3. Synthesis of aniline and phenol carbene precursors



Alkyne 2-68c. To a mixture of *N*-tert-butoxycarbonyl-2-iodo-4-nitroaniline²⁶ (**2-0**, 728 mg, 2.00 mmol), $\text{PdCl}_2(\text{PPh}_3)_2$ (35.0 mg, 0.0499 mmol), and CuI (19.0 mg, 0.100 mmol) in Et_3N (4.00 mL, 0.5 M) at room temperature was added 3-methoxypropyne (**2-71**, 0.186 mL, 2.20 mmol) dropwise. After the mixture was stirred for 12 h, it was diluted with 1.0 M aq. HCl (1 mL) and extracted with Et_2O (3×20 mL). The combined organic layers were washed with brine (10 mL) and dried over MgSO_4 . The solvent was removed by rotary evaporation, and the residue was purified by flash column chromatography (5:1 hexanes/ EtOAc eluent) to afford alkyne **2-68c** (558 mg, 91% yield, $R_f = 0.57$ in 5:1 hexanes/ EtOAc) as a yellow solid.

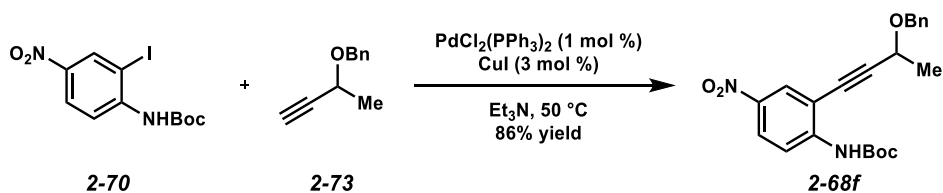
Alkyne 2-68c: $^1\text{H NMR}$ (400 MHz, CDCl_3): δ 8.37 (d, $J = 9.3$ Hz, 1H), 8.28 (d, $J = 2.4$ Hz, 1H), 8.17 (dd, $J = 9.3, 2.4$ Hz, 1H), 7.50 (s, 1H), 4.42 (s, 2H), 3.49 (s, 3H), 1.55 (s, 9H); $^{13}\text{C NMR}$ (100 MHz, CDCl_3): δ 151.5, 145.1, 141.7, 127.7, 125.4, 116.9, 110.6, 94.1, 82.3, 79.6, 60.3, 58.0, 28.2; IR (film): 3397, 2983, 2931, 1738, 1579, 1539, 1513, 1344, 1237, 1149, 1098, 903 cm^{-1} ; HRMS (ESI^+) m/z calc'd for $(\text{M} + \text{Na})^+ [\text{C}_{15}\text{H}_{18}\text{NO}_5 + \text{Na}]^+$: 329.1108, found 329.1109.



Alkyne 2-68d. To a mixture of *N*-tert-butoxycarbonyl-2-iodo-4-methoxyaniline²⁷ (**2-72**, 0.259 g, 0.742 mmol), $\text{PdCl}_2(\text{PPh}_3)_2$ (5.2 mg, 0.00742 mmol), and CuI (4.2 mg, 0.0223 mmol) in Et_3N (0.700 mL, 1.1 M) at 50 °C was added 3-methoxypropyne (**2-71**, 60.8 mg, 0.867 mmol) dropwise. After the mixture was stirred for 12 h, it was diluted with 1.0 M aq. HCl (30 mL) and extracted

with Et₂O (3 × 20 mL). The combined organic layers were washed with brine (30 mL) and dried over MgSO₄. The solvent was removed by rotary evaporation, and the residue was purified by flash column chromatography (5:1 hexanes/EtOAc eluent) to afford alkyne **2-68d** (0.180 g, 83% yield, R_f = 0.27 in 5:1 hexanes/EtOAc) as a white solid.

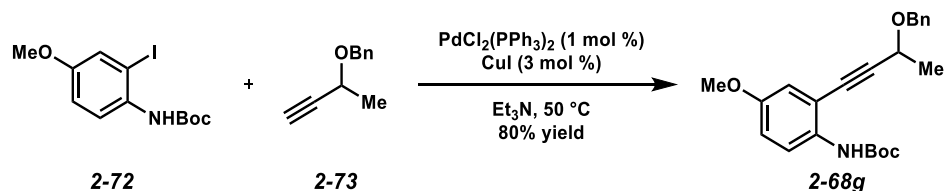
Alkyne 2-68d: ¹H NMR (400 MHz, CDCl₃): δ 7.99 (d, *J* = 8.5 Hz, 1H), 7.00 (s, 1H), 6.93 – 6.85 (comp. m, 2H), 4.39 (s, 2H), 3.76 (s, 3H), 3.47 (s, 3H), 1.51 (s, 9H); ¹³C NMR (100 MHz, CDCl₃): δ 154.4, 152.6, 133.4, 119.5, 116.3, 116.2, 111.7, 91.4, 81.9, 80.6, 60.4, 57.7, 55.5, 28.3; IR (film): 3416, 2989, 2934, 1728, 1519, 1160, 1242, 1211, 1098, 1023, 1038 cm⁻¹; HRMS (ESI⁺) *m/z* calc'd for (M + Na)⁺ [C₁₆H₂₁NO₄ + Na]⁺: 314.1363, found 314.1362.



Alkyne 2-68f. To a mixture of *N*-*tert*-butoxycarbonyl-2-iodo-4-nitroaniline²⁷ (**2-70**, 0.630 g, 1.73 mmol), PdCl₂(PPh₃)₂ (12.1 mg, 0.0173 mmol), and CuI (9.9 mg, 0.0520 mmol) in Et₃N (1.70 mL, 1.0 M) at 50 °C was added 3-benzyloxybutyne²⁸ (**2-73**, 0.304 g, 1.90 mmol) dropwise. After the mixture was stirred for 12 h, it was diluted with 1.0 M aq. HCl (30 mL) and extracted with Et₂O (3 × 20 mL). The combined organic layers were washed with brine (30 mL) and dried over MgSO₄. The solvent was removed by rotary evaporation, and the residue was purified by flash column chromatography (5:1 hexanes/EtOAc eluent) to afford alkyne **2-68f** (0.590 g, 86% yield, R_f = 0.56 in 5:1 hexanes/EtOAc) as a yellow oil.

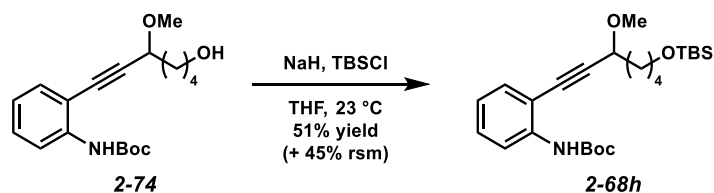
Alkyne 2-68f: ¹H NMR (400 MHz, CDCl₃): δ 8.37 (d, *J* = 9.4 Hz, 1H), 8.27 (d, *J* = 2.1 Hz, 1H), 8.17 (dd, *J* = 9.4, 2.7 Hz, 1H), 7.54 (s, 1H), 7.42 – 7.28 (comp. m, 5H), 4.85 (d, *J* = 11.7 Hz, 1H), 4.60 (d, *J* = 11.7 Hz, 1H), 4.52 (q, *J* = 6.6 Hz, 1H), 1.62 (d, *J* = 6.6 Hz, 3H), 1.53 (s, 9H); ¹³C NMR

(100 MHz, CDCl₃): δ 151.5, 145.0, 141.7, 137.3, 128.5, 128.02, 128.00, 127.5, 125.3, 116.8, 110.8, 98.5, 82.3, 78.4, 71.1, 64.8, 28.1, 22.1; IR (film): 3391, 2983, 2936, 1738, 1579, 1534, 1508, 1457, 1344, 1231, 1144, 1093, 1052, 1022, 898, 842, 750 cm⁻¹; HRMS (ESI⁺) m/z calc'd for (M + H)⁺ [C₂₂H₂₄N₂O₅ + H]⁺: 397.1758, found 397.1758.



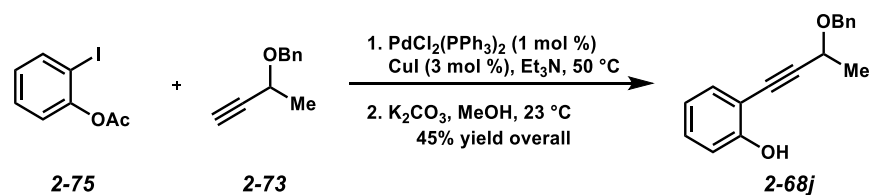
Alkyne 2-68g. To a mixture of *N*-tert-butoxycarbonyl-2-iodo-4-methoxyaniline²⁷ (**2-72**, 0.286 g, 0.819 mmol), PdCl₂(PPh₃)₂ (5.8 mg, 0.00819 mmol), and CuI (4.7 mg, 0.0246 mmol) in Et₃N (0.800 mL, 1 M) at 50 °C was added 3-benzyloxybutyne²⁸ (**2-73**, 0.145 mg, 0.905 mmol) dropwise. After the mixture was stirred for 12 h, it was diluted with 1.0 M aq. HCl (30 mL) and extracted with Et₂O (3 × 20 mL). The combined organic layers were washed with brine (30 mL) and dried over MgSO₄. The solvent was removed by rotary evaporation, and the residue was purified by flash column chromatography (5:1 hexanes/EtOAc eluent) to afford alkyne **2-68g** (0.250 g, 80% yield, R_f = 0.52 in 5:1 hexanes/EtOAc) as a pale yellow oil.

Alkyne 2-68g: ¹H NMR (400 MHz, CDCl₃): δ 7.99 (d, J = 9.1 Hz, 1H), 7.42 – 7.30 (comp. m, 5H), 7.03 (s, 1H), 6.90 (d, J = 11.6 Hz, 2H), 4.85 (d, J = 11.6 Hz, 1H), 4.59 (d, J = 11.6 Hz, 1H), 4.49 (q, J = 6.5 Hz, 1H), 3.77 (s, 3H), 1.60 (d, J = 6.5 Hz, 3H), 1.50 (s, 9H); ¹³C NMR (100 MHz, CDCl₃): δ 154.4, 152.6, 137.6, 133.3, 128.5, 128.1, 127.9, 119.5, 116.15, 116.12, 111.8, 95.7, 80.7, 80.5, 70.8, 64.9, 55.6, 28.3, 22.2; IR (film): 3411, 2981, 1734, 1519, 1416, 1366, 1310, 1242, 1211, 1155, 1027 cm⁻¹; HRMS (ESI⁺) m/z calc'd for (M + Na)⁺ [C₂₃H₂₇NO₄ + Na]⁺: 404.1832, found 404.1830.



Alkyne 2-68h. To a solution of alcohol **2-74**¹⁸ (0.273 g, 0.819 mmol) in THF (4.10 mL, 0.2 M) at 0 °C was added NaH (40.0 mg, 60% dispersion in mineral oil, 1.00 mmol). The reaction mixture was stirred at 0 °C for 30 min, then warmed to 23 °C and stirred for 2 h. TBSCl (0.138 g, 0.916 mmol) was then added, and the solution was stirred at 23 °C for 14 h. The reaction mixture was poured into water (20 mL) and extracted with Et₂O (2 × 30 mL). The combined organic phases were dried over MgSO₄, and the solvent was removed by rotary evaporation. The resulting residue was purified by flash chromatography (5:1 hexanes/EtOAc eluent), producing alkyne **2-68h** (0.186 g, 51% yield, R_f = 0.67 in 5:1 hexanes/EtOAc) as a colorless oil. Unreacted alcohol **2-74** (0.122 g, 45% yield) was also recovered as a colorless oil.

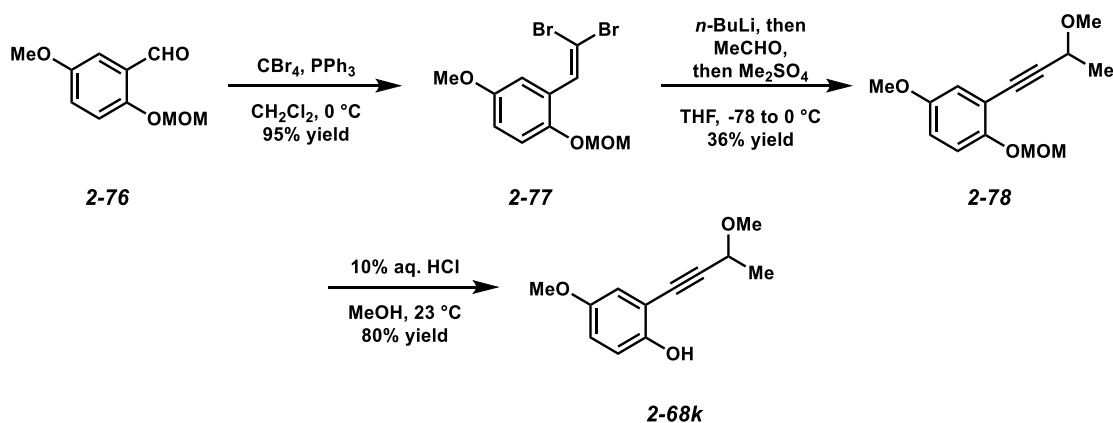
Alkyne 2-68h: ¹H NMR (500 MHz, CDCl₃) δ 8.14 (d, *J* = 8.3 Hz, 1H), 7.40 (dd, *J* = 7.7, 1.3 Hz, 1H), 7.35 – 7.30 (m, 1H), 7.27 (s, 1H), 7.00 – 6.95 (m, 1H), 4.27 (t, *J* = 6.6 Hz, 1H), 3.67 (t, *J* = 6.2 Hz, 2H), 3.52 (s, 3H), 1.94 – 1.83 (comp. m, 2H), 1.65 – 1.59 (comp. m, 4H), 1.55 (s, 9H), 0.91 (s, 9H), 0.07 (s, 6H); ¹³C NMR (125 MHz, CDCl₃) δ 152.4, 139.6, 131.7, 129.7, 122.0, 117.5, 110.7, 95.1, 81.3, 80.7, 71.8, 63.0, 56.6, 35.5, 32.5, 28.3, 26.0, 21.7, 18.4, -5.3; IR (film): 3406, 2929, 2856, 1737, 1516, 1448, 1238, 1155, 1097, 908, 835, 732 cm⁻¹; HRMS (ESI⁺) *m/z* calc'd for (M + Na)⁺ [C₂₅H₄₁NO₄Si + Na]⁺: 470.2697, found 470.2697.



Alkyne 2-68j. To a mixture of 2-iodophenyl acetate²⁹ (**2-75**, 1.50 g, 5.68 mmol), PdCl₂(PPh₃)₂ (44.9 mg, 0.0640 mmol), CuI (35.4 mg, 0.186 mmol) in Et₃N (6.00 mL, 0.95 M) at 50 °C was added 3-benzyloxybutyne²⁸ (**2-73**, 1.00 g, 6.24 mmol) dropwise. After the mixture was stirred for 12 h, it was diluted with 1.0 M aq. HCl (60 mL) and extracted with Et₂O (3 × 50 mL). The combined organic layers were washed with brine (50 mL) and dried over MgSO₄. The solvent was removed by rotary evaporation.

To a solution of the crude residue (assumed 5.68 mmol) in MeOH (16.0 mL, 0.35 M) was added K₂CO₃ (0.875 g, 6.33 mmol) and stirred overnight at 23 °C. MeOH was removed by rotary evaporation, and the crude residue was diluted with Et₂O (60 mL), washed sequentially with H₂O (30 mL) and brine (30 mL), and dried over MgSO₄. The solvent was removed by rotary evaporation and the crude residue was purified by flash column chromatography (5:1 hexanes/EtOAc eluent) to afford alkyne **2-68j** (0.646 g, 45% yield, R_f = 0.27 in 5:1 hexanes/EtOAc) as a pale yellow oil.

Alkyne 2-68j: ¹H NMR (400 MHz, CDCl₃): δ 7.44 – 7.32 (comp. m, 5H), 7.35 – 7.22 (comp. m, 2H), 6.96 (d, *J* = 8.3 Hz, 1H), 6.89 (t, *J* = 7.5 Hz, 1H), 5.74 (s, 1H), 4.84 (d, *J* = 11.7 Hz, 1H), 4.60 (d, *J* = 11.7 Hz, 1H), 4.50 (q, *J* = 6.6 Hz, 1H), 1.60 (d, *J* = 6.6 Hz, 3H). ¹³C NMR (100 MHz, CDCl₃): δ 156.7, 137.7, 131.9, 130.6, 128.5, 128.0, 127.9, 120.3, 114.7, 108.9, 96.5, 79.3, 70.8, 65.0, 22.3; IR (film): 3365, 2986, 2933, 2864, 2658, 1611, 1576, 1489, 1454, 1328, 1292, 1236, 1091, 1057, 751 cm⁻¹; HRMS (ESI⁺) *m/z* calc'd for (M + Na)⁺ [C₁₇H₁₆O₂ + Na]⁺: 275.1043, found 275.1043.



Alkyne 2-68k. To a solution of 5-methoxy-2-(methoxymethoxy)benzaldehyde³⁰ (**2-76**, 3.00 g, 15.3 mmol) in CH_2Cl_2 (51.0 mL) at $0\text{ }^\circ\text{C}$ was added carbon tetrabromide (10.1 g, 30.6 mmol) followed by triphenylphosphine (16.0 g, 61.2 mmol). The mixture was removed from the ice bath and allowed to stir for 10 min, whereupon TLC indicated full consumption of starting material. The solution was filtered through Florisil to remove triphenylphosphine oxide, and the solvent was removed by rotary evaporation. The resulting residue was purified by flash column chromatography (7:1 hexanes/EtOAc eluent) to afford dibromoolefin **2-77** (5.13 g, 95% yield, $R_f = 0.73$ in 4:1 hexanes/EtOAc) as a brown oil.

To a solution of dibromoolefin **2-77** (1.00 g, 2.84 mmol) in THF (10 mL, 0.28 M) at $-78\text{ }^\circ\text{C}$ was added $n\text{-BuLi}$ (2.38 mL, 2.5 M in hexanes, 5.96 mmol) dropwise, and the mixture was stirred for 1 h. The reaction was then warmed to $0\text{ }^\circ\text{C}$ and stirred at this temperature for 30 min. Next, the mixture was cooled to $-78\text{ }^\circ\text{C}$, acetaldehyde (0.160 mL, 2.84 mmol) was added dropwise, and the resulting mixture stirred for 1 h. The reaction mixture was warmed to $0\text{ }^\circ\text{C}$, dimethyl sulfate (0.300 mL, 3.17 mmol) was added, and the mixture was stirred at this temperature for 1 h. Upon completion, excess dimethyl sulfate was quenched by stirring with 10% aq. NH_4OH (10 mL) for 30 min, and the mixture was extracted with Et_2O ($3 \times 20\text{ mL}$). The combined organic layers were washed sequentially with H_2O (20 mL) and brine (20 mL), and the organic phase was dried over

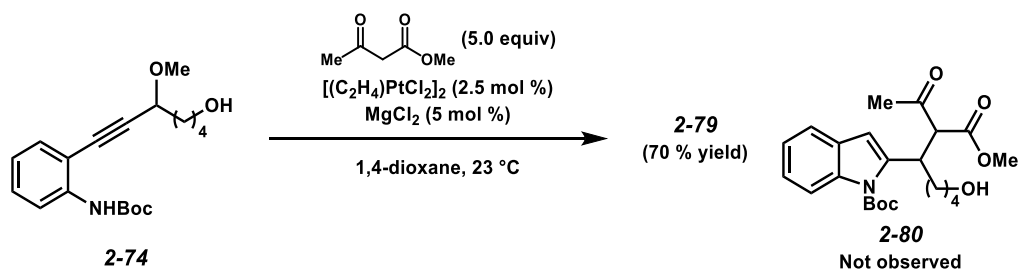
MgSO₄. The solvent was removed by rotary evaporation, and the resulting residue was purified by flash chromatography (9:1 hexanes/EtOAc eluent), affording ether **2-78** (254 mg, 36% yield, R_f = 0.50 in 4:1 hexanes/EtOAc) as a pale green oil.

To a solution of propargyl ether **2-78** (164 mg, 0.655 mmol) in MeOH (3.20 mL) at 23 °C was added 10% aq. HCl (1.70 mL) dropwise, and the mixture was stirred for 1 h at room temperature. Upon consumption of starting material, the reaction mixture was neutralized with sat. aq. NaHCO₃ and concentrated via rotary evaporation. The residue was redissolved in Et₂O (10 mL), washed with H₂O (10 mL), then brine (10 mL), and dried over MgSO₄. After removal of solvent by rotary evaporation, the crude material was purified by flash chromatography (17:3 hexanes/EtOAc eluent), affording alkyne **2-68k** (108 mg, 80% yield, R_f = 0.27 in 4:1 hexanes/EtOAc) as a yellow oil.

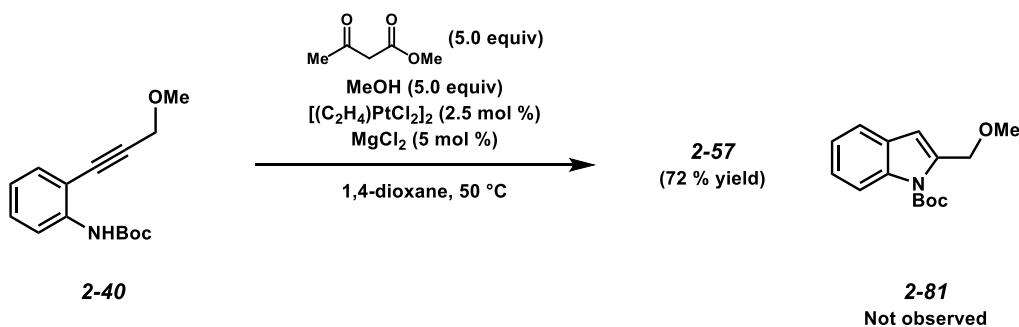
Alkyne 2-68k: ¹H NMR (400 MHz, CDCl₃) δ 6.87-6.81 (m, 3H), 5.51 (s, 1H), 4.33 (q, *J* = 6.7 Hz, 1H), 3.74 (s, 3H), 3.46 (s, 3H), 1.53 (d, *J* = 6.7 Hz, 3H); ¹³C NMR (100 MHz, CDCl₃) δ 152.9, 151.0, 117.5, 115.6, 115.5, 108.9, 95.8, 79.4, 67.4, 56.5, 55.8, 22.1; IR (film) 3351, 2986, 2935, 2832, 2220, 1613, 1494, 1465, 1418 cm⁻¹; HRMS (APCI) *m/z* calc'd for (M + H)⁺ [C₁₂H₁₄O₃ + H]⁺: 207.1016, found 207.1023.

¹H and ¹³C NMR spectra for **2-40** – **2-78** can be found online.³¹ A cross reference of numbering can be found in Appendix 1.

2.3.4. Competition Experiments



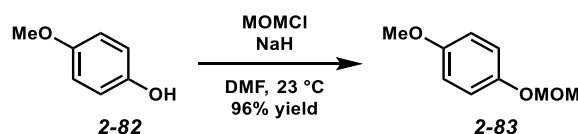
Following general procedure B, a 2-dram vial equipped with a magnetic stir bar and $MgCl_2$ (0.3 mg, 0.00263 mmol) was flame-dried under vacuum and cooled under a stream of argon. A solution of *N*-Boc aniline **2-74** (16.8 mg, 0.0504 mmol) and methyl acetoacetate (28.0 μ L, 0.259 mmol) in 1,4-dioxane (0.500 mL, 0.10 M in aniline) were added to the dried $MgCl_2$, and the resulting solution was stirred at 23 °C for 15 min. $[(C_2H_4)PtCl_2]_2$ (0.8 mg, 0.00128 mmol) was then added, and the reaction mixture was stirred at 23 °C for 10 h. Upon completion, the reaction mixture was filtered through a plug of silica gel (0.5 x 2.0 cm), washing with EtOAc (1 mL). The solvent was removed by rotary evaporation, and the resulting residue was purified by flash chromatography (5:1 hexanes/EtOAc eluent) to afford indole **2-79** (10.6 mg, 70% yield) as a colorless oil. All spectroscopic data were consistent with reported values.¹⁸ Indole **2-80** was not observed.



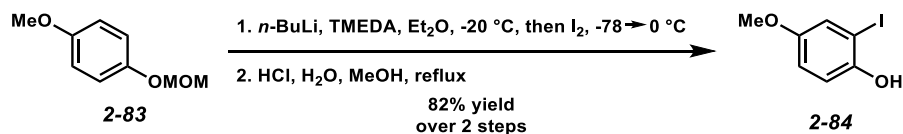
Following general procedure B, a 2-dram vial equipped with a magnetic stir bar and $MgCl_2$ (0.3 mg, 0.00263 mmol) was flame-dried under vacuum and cooled under a stream of argon. A solution of *N*-Boc aniline **2-40** (13.5 mg, 0.0517 mmol), methyl acetoacetate (28.0 μ L, 0.259 mmol), and

MeOH (10.1 μ L, 0.249 mmol) in 1,4-dioxane (0.500 mL, 0.10 M in aniline) were added to the dried MgCl_2 , and the resulting solution was stirred at 23 $^\circ\text{C}$ for 15 min. $[(\text{C}_2\text{H}_4)\text{PtCl}_2]_2$ (0.8 mg, 0.00129 mmol) was then added, and the reaction mixture was heated to 50 $^\circ\text{C}$ and stirred for 18 h. Upon completion, the reaction mixture was cooled to room temperature and filtered through a plug of silica gel (0.5 x 2.0 cm), washing with EtOAc (1 mL). The solvent was removed by rotary evaporation, and the resulting residue was purified by flash chromatography (5:1 hexanes/EtOAc eluent) to afford indole **2-57** (12.8 mg, 72% yield) as a colorless oil. Indole **2-81** was not observed.

2.3.5. Synthesis of Frondosin B



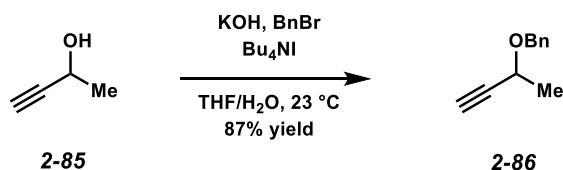
Methoxymethyl Ether 2-83. To a solution of 4-methoxyphenol (**2-82**, 12.4 g, 100 mmol) in DMF (100 mL) at 23 $^\circ\text{C}$ (with an external water bath) was added NaH (6.00 g, 60% dispersion in mineral oil, 150 mmol) portionwise at such a rate as to control H_2 evolution. Once the addition was complete, MOMCl (9.11 mL, 120 mmol) was added via additional funnel over approx. 10 min. Once the addition was complete, the reaction mixture was stirred an additional 1 h, at which point TLC indicated consumption of starting material. The reaction mixture was then poured into H_2O (300 mL) and extracted with pentane (3 x 75 mL). The combined organic extracts were washed sequentially with H_2O (100 mL) and brine (100 mL), dried with Na_2SO_4 , and concentrated. The crude residue was purified by flash column chromatography (hexanes \rightarrow 4:1 hexanes/ Et_2O eluent) to give methoxymethyl ether **2-83** as a colorless liquid (16.1 g, 96% yield, $R_f = 0.62$ in 7:3 hexanes/EtOAc). The spectroscopic data for methoxymethyl ether **2-83** matched those presented in the literature.³²



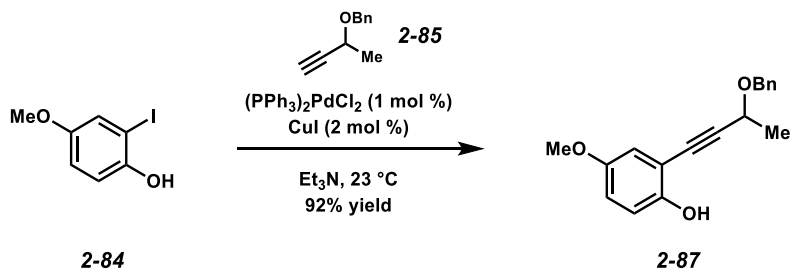
Phenol 2-84. To a 500 mL round bottom flask charged with a large stir bar and a solution of methoxymethyl ether **2-83** (16.8 g, 100 mmol) and TMEDA (18.0 mL, 120 mmol) in Et₂O (100 mL) at -78 °C was added *n*-BuLi (48.0 mL, 2.5 M in hexanes, 120 mmol) over 60 s. The reaction mixture was stirred at this temperature for 5 min and then allowed to warm to -20 °C and stirred for an additional 30 min. The reaction mixture was then cooled to -78 °C and a solution of I₂ (33.0 g, 130 mmol) in Et₂O (200 mL) was added via cannula over 10 min. During this addition, the reaction mixture became a thick slurry, and manual swirling was necessary to ensure full mixing. When the addition was complete, the reaction mixture was swirled an additional 5 min at -78 °C and then allowed to warm to ambient temperature with occasional swirling. Once the reaction mixture had reached ambient temperature, it was poured into a mixture of aq. NaHCO₃ (1 M, 100 mL) and sat. aq. Na₂S₂O₃ (100 mL). The organic layer was separated and washed sequentially with aq. HCl (1 M, 100 mL), aq. NaOH (1 M 100 mL) and brine (100 mL). The organic extract was dried with MgSO₄ and concentrated to give the aryl iodide ($R_f = 0.89$ in 9:1 hexanes/EtOAc) as a yellow oil that was used immediately without further purification.

To a solution of the crude aryl iodide (100 mmol, assumed) in MeOH (100 mL) at 23 °C was added 10% aq. HCl (30 mL, 100 mmol). The reaction mixture was heated to reflux for 20 min, at which point TLC indicated consumption of the iodide starting material. The reaction mixture was allowed to cool to ambient temperature and was then concentrated to remove MeOH. The resulting residue was partitioned between EtOAc (100 mL) and brine (100 mL). The organic layer was separated, and the aqueous layer was extracted with EtOAc (50 mL). The combined organic extracts were washed with brine (100 mL), dried with MgSO₄, and concentrated. The crude residue was purified

by flash column chromatography (19:1 hexanes/EtOAc eluent) to give phenol **2-84** as a colorless solid (20.4 g, 82% yield over 2 steps, $R_f = 0.27$ in 3:1 hexanes/EtOAc). The spectroscopic data for phenol **2-84** matched those presented in the literature.³³

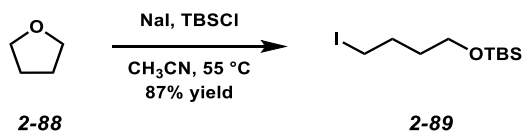


Benzyl Ether 2-86. To 3-butyn-2-ol (**2-85**, 13.5 g, 55% w/w in H₂O, 106 mmol) was added KOH pellets (85%, 14.0 g, 212 mmol). The solution was stirred until it partially solidified, at which point THF (20 mL) was added, followed by *n*-Bu₄NI (1.96 g, 5.30 mmol). A thermometer was placed directly into the reaction mixture, and BnBr (12.6 mL, 106 mmol) was added with vigorous stirring. When the reaction mixture reached 40 °C, the flask was submerged in an ice bath until the internal temperature reached 23 °C. The reaction was stirred an additional 1 h, then partitioned between pentane (150 mL) and H₂O (100 mL). The organic layer was washed sequentially with aq. HCl (1 M, 50 mL), H₂O (50 mL), and brine (50 mL). The organic extract was dried with Na₂SO₄ and concentrated. The resulting pale yellow residue was purified by flash column chromatography (19:1 hexanes/EtOAc eluent) to give benzyl ether **2-86** (14.7 g, 87% yield, $R_f = 0.36$ in 19:1 hexanes/EtOAc) as a colorless liquid. The spectroscopic data for ether **2-86** matched those previously reported.²⁸



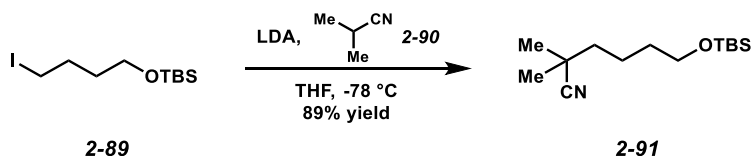
Alkyne 2-87. A mixture of aryl iodide **2-84** (5.01 g, 20.0 mmol), PdCl₂(PPh₃)₂ (140 mg, 0.200 mmol), and CuI (76.2 mg, 0.400 mmol) were stirred dry under vacuum until a fine powder resulted. The resulting powder was suspended/dissolved in Et₃N (40 mL) at 23 °C, and alkyne **2-85** (3.54 g, 22.0 mmol) was added neat via tared syringe. The reaction mixture became black and was stirred for 3 h at ambient temperature, at which point TLC indicated consumption of iodide **2-84**. Then H₂O (20 mL) was added and Et₃N was removed *in vacuo*. The resulting residue was suspended in aq. HCl (1 M, 100 mL) and extracted with Et₂O (3 × 50 mL). The organic extracts were then stirred with aq. Na₃EDTA (0.2 M, 100 mL) for 30 min, separated, washed with brine (100 mL), dried with MgSO₄, and concentrated. The crude residue was purified by flash column chromatography (9:1 hexanes/EtOAc eluent) and concentrated. This product was then allowed to stand 16 h at -10 °C to further precipitate Pd residue. This material was dissolved in Et₂O (20 mL) and filtered through a plug of SiO₂, rinsing with Et₂O (100 mL) to give alkyne **2-87** (5.22 g, 92% yield, R_f = 0.18 in 9:1 hexanes/EtOAc) as an orange oil.

Alkyne 2-87. ¹H NMR (400 MHz, CDCl₃): δ 7.41-7.27 (comp. m, 5H), 6.89-6.82 (comp. m, 3H), 5.41 (s, 1H), 4.83 (d, *J* = 11.7 Hz, 1H), 4.59 (d, *J* = 11.7 Hz, 1H), 4.49 (q, *J* = 6.3 Hz, 1H), 3.76 (s, 3H), 1.59 (d, *J* = 6.3 Hz, 3H). ¹³C NMR (100 MHz, CDCl₃): δ 153.2, 151.3, 137.9, 128.7, 128.2, 128.1, 117.8, 115.82, 115.76, 109.1, 96.4, 79.7, 71.1, 65.2, 56.1, 22.5. IR (film): 3383 (br), 2985, 2935, 2865, 2834, 1494, 1275, 1204, 1167, 1090, 1035, 814 cm⁻¹. MS (DART): *m/z* calc'd for (M + NH₄)⁺ [C₁₈H₁₈O₃ + NH₄]⁺: 300.1594, found 300.1605.



Alkyl iodide 2-89. Alkyl iodide **2-89** was synthesized according to the procedure described by Waldmann and coworkers.³⁴ To a solution of TBSCl (3.02 g, 20.0 mmol) and NaI (6.00 g, 40.0 mmol) in anhydrous CH₃CN (100 mL, 0.2 M in TBSCl) was added anhydrous tetrahydrofuran (**2-88**, 4.06 mL, 50.0 mmol) at 23 °C. The resulting mixture was heated to 55 °C and stirred for 12 h. The solution was then cooled to 23 °C, diluted with water (50 mL) and extracted into Et₂O (3 × 100 mL). The combined organic layers were washed with sat. aq. Na₂S₂O₃ (50 mL), then brine (50 mL) and dried over MgSO₄. The solvent was removed by rotary evaporation, and the residue was purified by flash column chromatography (19:1 hexanes/EtOAc eluent) to afford alkyl iodide **2-89** (13.7 g, 87% yield, R_f = 0.50 in 9:1 hexanes/EtOAc) as a light-sensitive colorless oil. The spectroscopic data for iodide **2-89** were consistent with those reported.³⁴

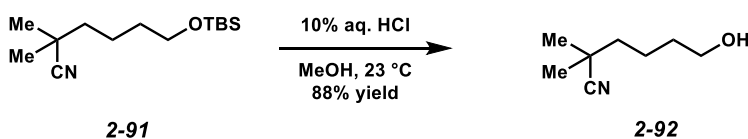
Alkyl iodide 2-89: ¹H NMR (300 MHz, CDCl₃): δ 3.63 (t, *J* = 6.2 Hz, 2H), 3.22 (t, *J* = 7.0 Hz, 2H), 1.90 (app. quintet, *J* = 7.0 Hz, 2H), 1.66 - 1.56 (m, 2H), 0.89 (s, 9H), 0.05 (s, 6H).



Nitrile 2-91. Nitrile **2-91** was synthesized according to the procedure described by Frontier and coworkers.³⁵ LDA was prepared *in situ* by addition of *n*-BuLi (3.60 mL, 2.48 M in hexanes, 8.91 mmol) to a solution of *i*-Pr₂NH (1.78 mL, 12.7 mmol) in anhydrous THF (22.3 mL) at 0 °C. The solution of LDA (1.4 equiv, 0.40 M in THF) was then cooled to -78 °C, isobutyronitrile (**2-90**, 0.800 mL, 8.91 mmol, 1.4 equiv) was added dropwise, and the resulting mixture was stirred for 1 h. A solution of alkyl iodide **2-89** (2.00 g, 6.36 mmol) in anhydrous THF (1.27 mL, 5.0 M) was then added dropwise, and the mixture was allowed to stir for an additional 2 h at -78 °C. After

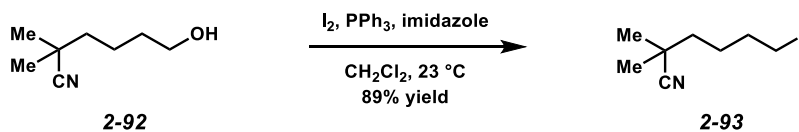
warming to 23 °C, the solution was diluted with water (20 mL) and extracted into CH₂Cl₂ (3 × 50 mL). The combined organic layers were washed with brine (50 mL) and dried over MgSO₄. The solvent was removed by rotary evaporation, and the crude residue was purified by flash column chromatography (9:1 hexanes/EtOAc eluent) to afford nitrile **2-91** (1.45 g, 89% yield, R_f = 0.58 in 9:1 hexanes/EtOAc) as a pale yellow oil. The spectroscopic data were consistent with those reported.³⁵

Nitrile 2-91: ¹H NMR (300 MHz, CDCl₃): δ 3.66 - 3.59 (m, 2H), 1.58 - 1.52 (m, 6H), 1.34 (s, 6H), 0.89 (s, 9H), 0.05 (s, 6H).



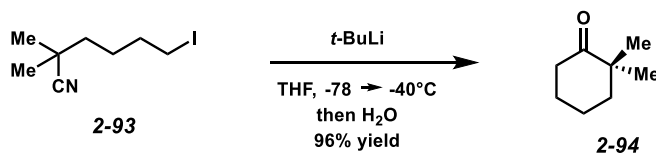
Alcohol 2-92. Nitrile **2-91** (1.00 g, 3.91 mmol) was dissolved in a mixture of MeOH (19.6 mL, 0.2 M) and 10% aq. HCl (9.78 mL, 0.4 M) at 23 °C, and the solution was allowed to stir for 30 min. Sat. aq. NaHCO₃ (50 mL) was then added to neutralize the mixture, and the solvent was removed by rotary evaporation. The crude residue was then dissolved in CH₂Cl₂ (20 mL) and washed with H₂O (20 mL), then brine (20 mL), dried over MgSO₄ and concentrated by rotary evaporation. The crude residue was then purified by flash column chromatography (1:1 hexanes/EtOAc eluent) to afford alcohol **2-92** (0.483 g, 88% yield, R_f = 0.38 in 1:1 hexanes/EtOAc) as a colorless oil.

Alcohol 2-92: ¹H NMR (300 MHz, CDCl₃): δ 3.68 (t, J = 7.9 Hz, 2H), 1.65 - 1.50 (m, 6H), 1.35 (s, 6H).



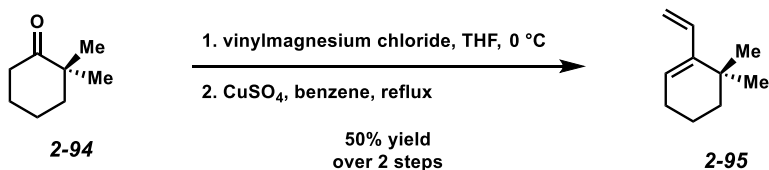
Iodonitrile 2-93. To a foil-wrapped flask containing a solution of triphenylphosphine (0.876 g, 3.34 mmol) in CH_2Cl_2 (4.1 mL, 0.82 M) was added imidazole (0.284 g, 4.73 mmol) and iodine (0.954 g, 3.76 mmol). To this mixture, a solution of alcohol **2-92** (0.393 g, 2.78 mmol) in CH_2Cl_2 (1.0 mL, 2.7 M) was added dropwise, and the reaction mixture was stirred at 23 °C for 1 h. The solvent was then removed by rotary evaporation, and the crude reaction mixture was purified by flash column chromatography (9:1 hexanes/EtOAc eluent) to afford pure iodonitrile **2-93** (0.621 g, 89% yield, $R_f = 0.36$ in 9:1 hexanes/EtOAc) as an extremely light-sensitive colorless oil.

Iodonitrile 2-93: $^1\text{H NMR}$ (300 MHz, CDCl_3): δ 3.21 (t, $J = 6.9$ Hz, 2H), 1.87 (app. quintet, $J = 6.9$ Hz, 2H), 1.68 - 1.49 (m, 6H), 1.36 (s, 6H).



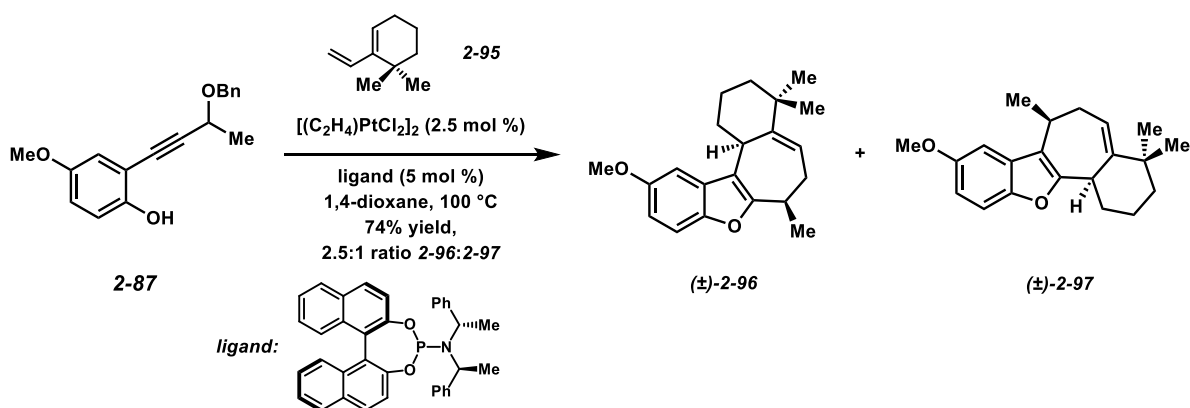
Cyclohexanone 2-94. To a solution of iodonitrile **2-93** (2.27 g, 9.02 mmol) in anhydrous THF (18 mL, 0.50 M) cooled to -78 °C was added *tert*-butyllithium (11.8 mL, 1.6 M in pentane) dropwise. The resulting mixture was allowed to warm to -40 °C and stirred for 10 min, and then the reaction was diluted with sat. aq. NH_4Cl (10 mL). Water (20 mL) was then added, and the mixture was extracted with CH_2Cl_2 (3 \times 50 mL). The combined organic layers were washed with brine (30 mL), dried over MgSO_4 , and concentrated by rotary evaporation. The crude residue was purified by flash column chromatography (9:1 hexanes/EtOAc eluent), affording cyclohexanone **2-94** (1.10 g, 96% yield, $R_f = 0.47$ in 9:1 hexanes/EtOAc) as a volatile colorless oil. The spectroscopic data matched those reported in the literature.³⁶

Cyclohexanone 2-94: ^1H NMR (300 MHz, CDCl_3): δ 2.39 (t, $J = 6.7$ Hz, 2H), 1.88 - 1.63 (m, 6H), 1.11 (s, 6H).



Diene 2-95. According to the reported literature procedure,³⁷⁻³⁸ to a solution of cyclohexanone **2-94** (0.915 g, 7.25 mmol) in anhydrous THF (18 mL, 0.4 M) cooled to 0 °C was added vinylmagnesium chloride (5.89 mL, 1.6 M in THF, 1.3 equiv) dropwise, and the resulting mixture was allowed to warm to 23 °C and stirred for 2 h. Saturated aq. NH_4Cl (5 mL) was then added dropwise to quench the reaction, and the solvent was removed by rotary evaporation. The crude residue was then dissolved in Et_2O (50 mL), washed with brine (30 mL), dried over MgSO_4 and concentrated by rotary evaporation. The crude residue was purified by flash column chromatography (9:1 hexanes/ EtOAc eluent) to afford the desired vinylcyclohexanol (0.757 g, 68% yield, $R_f = 0.70$ in 4:1 hexanes/ EtOAc) as a pale yellow oil. This alcohol was taken directly to the subsequent transformation.

To a solution of the obtained vinylcyclohexanol (0.105 g, 0.681 mmol) in benzene (3.00 mL, 0.25 M) was added anhydrous CuSO_4 (0.250 g, 1.56 mmol, 2.30 equiv) at 23 °C. The reaction vessel was then equipped with a Dean-Stark apparatus, and the resulting suspension was heated to reflux (bath temp. 90 °C) and stirred for 24 h. The system was then cooled to 23 °C, vacuum filtered to remove insoluble materials, and concentrated by rotary evaporation. The residue was purified using flash column chromatography (1:1 pentane/ Et_2O eluent) to afford diene **2-95** (0.0672 g, 73% yield, $R_f = 0.80$ in 1:1 pentane/ Et_2O) as a volatile colorless oil. The spectroscopic data for diene **2-95** matched those previously reported.³⁷⁻³⁸



Benzofuran (±)-2-96. To a solution of phosphoramidite ligand (3.3 mg, 0.00561 mmol) in 1,4-dioxane (0.50 mL, 0.2 M) at 23 °C under argon was added $[(C_2H_4)PtCl_2]_2$ (1.6 mg, 0.00272 mmol, 2.5 mol %), and the resulting solution was stirred for 10 min. A solution of phenol **2-87** (29.7 mg, 0.105 mmol) in 1,4-dioxane (0.50 mL, 0.2 M) was then added to the catalyst mixture. Diene **2-95** (29.1 mg, 0.214 mmol) was subsequently added, and the resulting mixture was heated to 100 °C and stirred for 15 h. The reaction mixture was then cooled to room temperature and filtered through a plug of SiO₂, eluting with EtOAc (3 mL). The filtrate was concentrated *in vacuo*, and the resulting residue was purified by flash column chromatography (9:1 hexanes/EtOAc eluent) to afford an inseparable 2.5:1 mixture of benzofuran (±)-**2-96** and benzofuran (±)-**2-97** (24.0 mg, 74% yield, $R_f = 0.45$ in 9:1 hexanes/EtOAc) as a pale yellow oil. The spectroscopic data for compound (±)-**2-96** matched those reported in the literature.³⁹⁻⁴⁰ The diastereomer drawn for compound (±)-**2-96** is consistent with the assignment of Xue and Li.³⁹

¹H and ¹³C NMR spectra for **2-82** – **2-97** can be found online.⁴¹

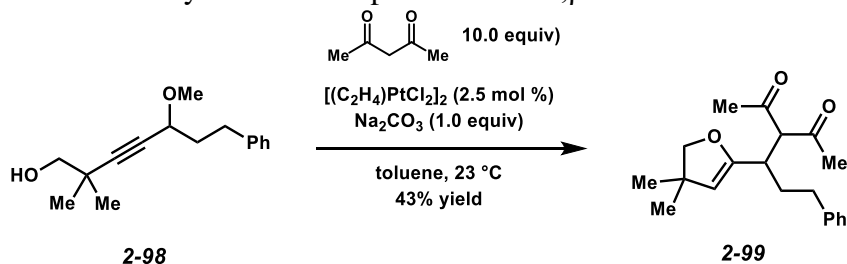
A cross reference of numbering can be found in Appendix 1.

2.4 Results and Discussion

2.4.1. Optimization and scope of dicarbonyl vinylogous additions

In order to expand the scope of carbon-based nucleophiles that can add vinylogously to our platinum carbenes, we examined the potential of using enols derived from β -dicarbonyl compounds. These are attractive candidates because in their enol tautomeric form they may be sufficiently nucleophilic to intercept the electrophilic intermediate in a Michael-type fashion. An initial discovery by Dr. Paul Allegretti showed that upon exposure of homopropargyl alcohol **2-98** to Zeise's dimer in the presence of acetylacetone and sodium carbonate, the nucleophilic addition product (**2-99**) was observed in 43% yield (Scheme 2.4.1).

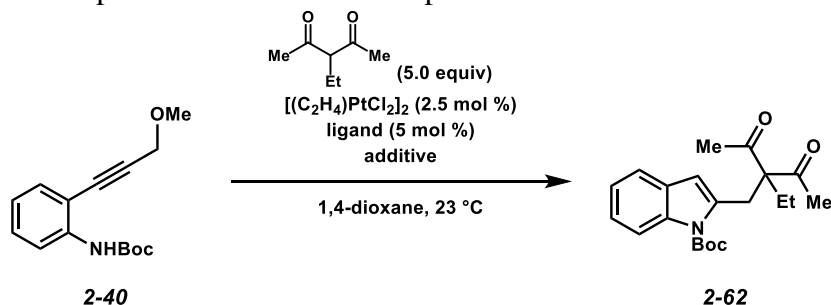
Scheme 2.4.1. Initial discovery of enol incorporation into α,β -unsaturated Pt carbene.



In order to optimize these reaction conditions, we first explored the effect of modifying the ligand additive on reactivity using more easily made *N*-Boc-aniline **2-40** and 3-ethyl-2,4-pentanedione (Table 2.4.1). Here, addition of triphenylphosphine (entry 1) attenuates reaction progress significantly, likely due to the electron rich nature of the platinum carbene intermediate. Switching the ligand to tris(pentafluorophenyl)phosphine restores reactivity, now giving indole **2-62** in 58% yield (entry 2). Surprisingly, addition of sodium carbonate (entries 3-4) also suppresses the reaction; however, addition of a Lewis acid significantly enhances reaction rate and yield (entries 5-9). Assessing various Lewis acid additives, we find that $MgCl_2$ and $La(OTf)_3$ promote conversion to indole **2-62** in improved yields (72 and 73%, respectively), and $MgCl_2$ was used for further optimization due to its relative low cost. Reducing the number of equivalents of β -diketone

also diminishes the yield (entries 10-11). Interestingly, when the phosphine is removed completely the yield is not affected, indicating that the $\text{P}(\text{C}_6\text{F}_5)_3$ ligand is not necessary for optimal reactivity (entry 12).

Table 2.4.1. Reaction optimization for enol incorporation.



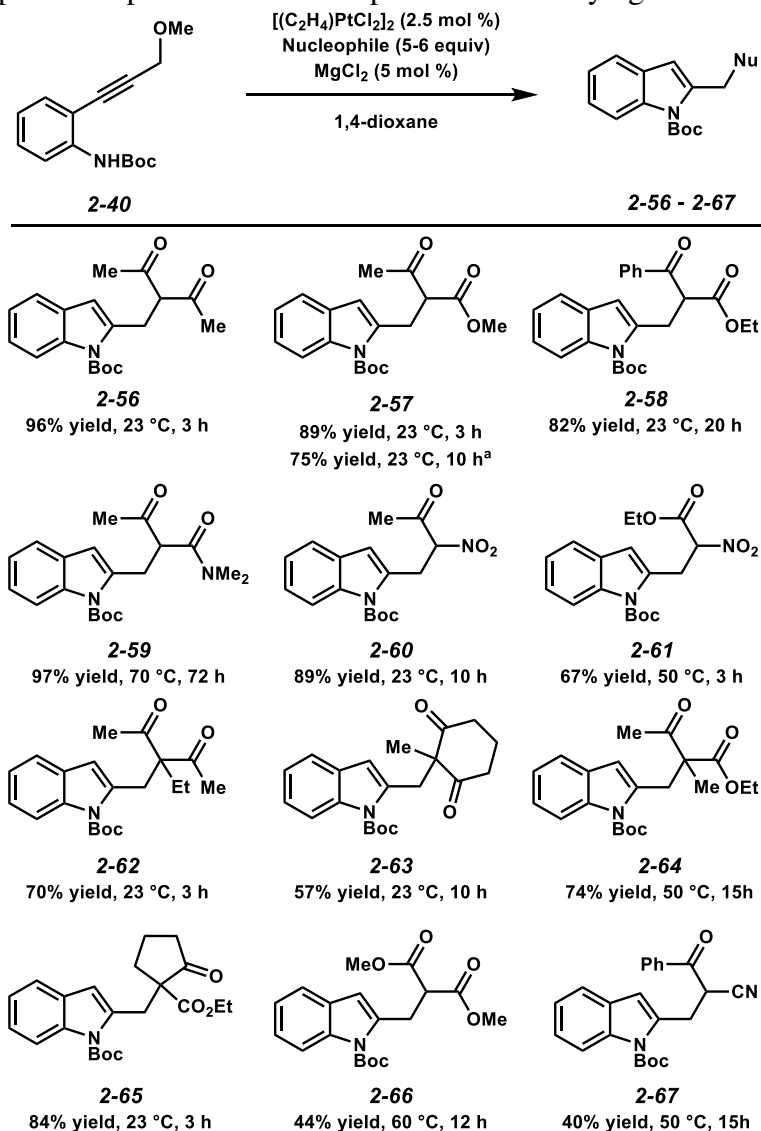
2-40				2-62	
entry	ligand	additive (mol %)	time (h)	yield 2-62 ^a	
1	PPh_3	none	5	8	
2	$\text{P}(\text{C}_6\text{F}_5)_3$	none	3	58	
3	$\text{P}(\text{C}_6\text{F}_5)_3$	Na_2CO_3 (100)	5	0	
4	$\text{P}(\text{C}_6\text{F}_5)_3$	Na_2CO_3 (10)	5	18	
5	$\text{P}(\text{C}_6\text{F}_5)_3$	MgCl_2 (5)	2	72	
6	$\text{P}(\text{C}_6\text{F}_5)_3$	$\text{La}(\text{OTf})_3$ (5)	2	73	
7	$\text{P}(\text{C}_6\text{F}_5)_3$	CuSO_4 (10)	4	68	
8	$\text{P}(\text{C}_6\text{F}_5)_3$	CeCl_3 (5)	0.5	65	
9	$\text{P}(\text{C}_6\text{F}_5)_3$	$\text{Sc}(\text{OTf})_3$ (5)	0.5	60	
10	$\text{P}(\text{C}_6\text{F}_5)_3$	MgCl_2 (5)	2	50 ^b	
11	$\text{P}(\text{C}_6\text{F}_5)_3$	MgCl_2 (5)	2	30 ^c	
12	none	MgCl_2 (5)	3	72 (70) ^d	

^a Yield determined by ^1H NMR using dibenzyl ether as an internal standard. ^b Used 2.0 equiv of diketone. ^c Used 1.1 equiv diketone. ^d Isolated yield in parentheses.

With the optimized conditions in hand, we set out to establish the generality of β -dicarbonyl partner with which this reaction can proceed (Scheme 2.4.2). Using *N*-Boc aniline **2-40**, we find that a variety of nucleophilic partners work, including β -diketones, ketoesters and ketoamides. Even α -nitro carbonyls are also competent in the reaction, giving indoles **2-60** and **2-61**. As seen in the reaction optimization, this method also allows for the formation of all-carbon quaternary centers (**2-62** – **2-65**). Less acidic pronucleophiles such as malonates and β -ketonitriles, for which the keto-enol tautomeric equilibrium shifts toward the carbonyl identity, give diminished yields

(2-66 – 2-67). Substrate **2-57** was also able to be synthesized using only 1.0 equiv of methyl acetoacetate, still giving the indole product in 75% yield (as opposed to 89% yield with 5.0 equiv).

Scheme 2.4.2. Scope of compatible enol nucleophiles for the vinylogous addition reaction.

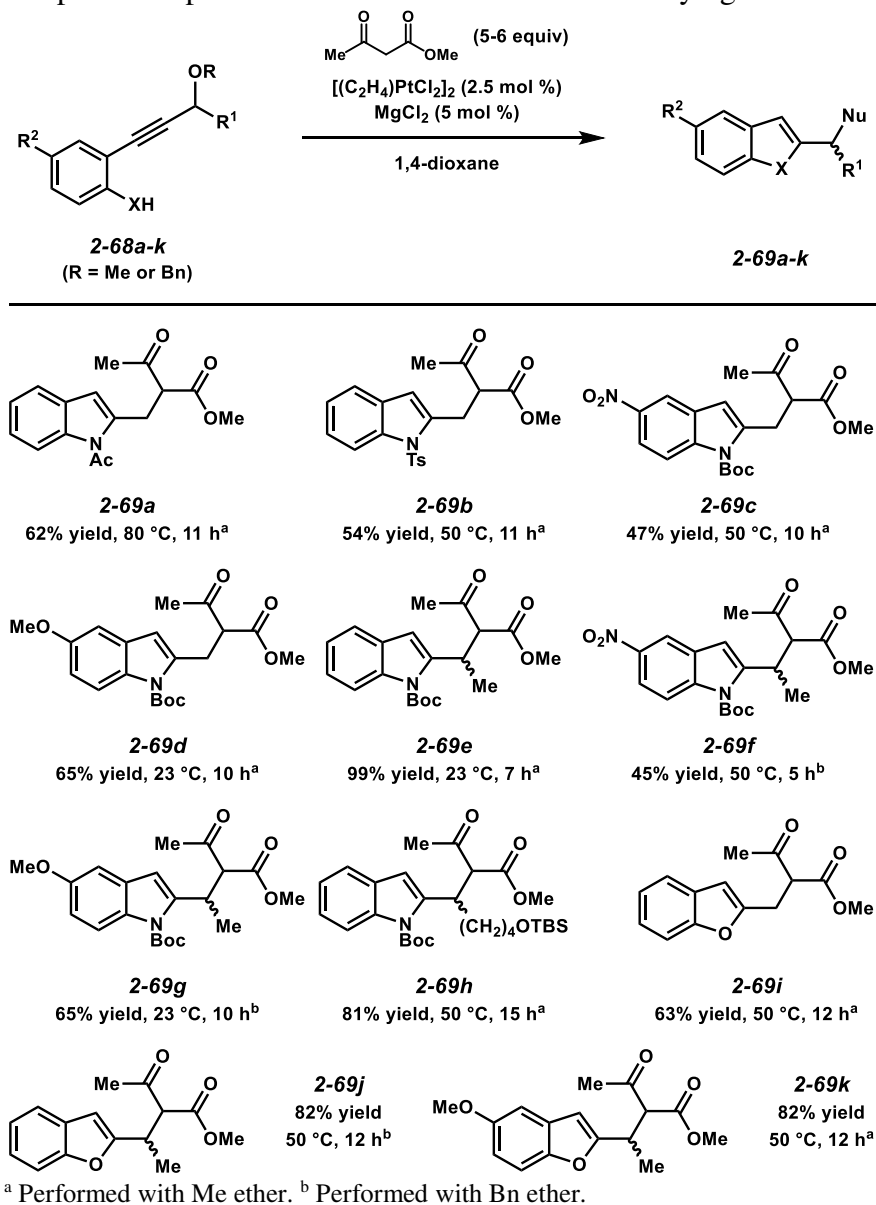


^a Using 1.0 equiv of methyl acetoacetate.

Next, we establish the generality of this method with respect to substitution on the carbene precursor (**2-68a-k**, Scheme 2.4.3). First, *N*-acetyl and *N*-tosyl-protected anilines are both compatible with this reactivity, though give slightly lower yields compared to when the *N*-Boc analog is used (X = NPG, **2-69a-b**). Further, electron withdrawing (-NO₂) and donating (-OMe) groups can be incorporated into the aniline *para* to the NHBoc (**2-69c-d**). Benzofuran formation

is also possible ($X = O$, **2-69i-k**), giving comparable yields to the indole products. Notably, secondary propargylic ethers can also be employed (**2-69e-h**, **2-69j-k**), though diastereoselectivity is not controlled (ranging from 1:1 to 2:1).

Scheme 2.4.3. Scope of compatible carbene substitution for the vinylogous addition reaction.

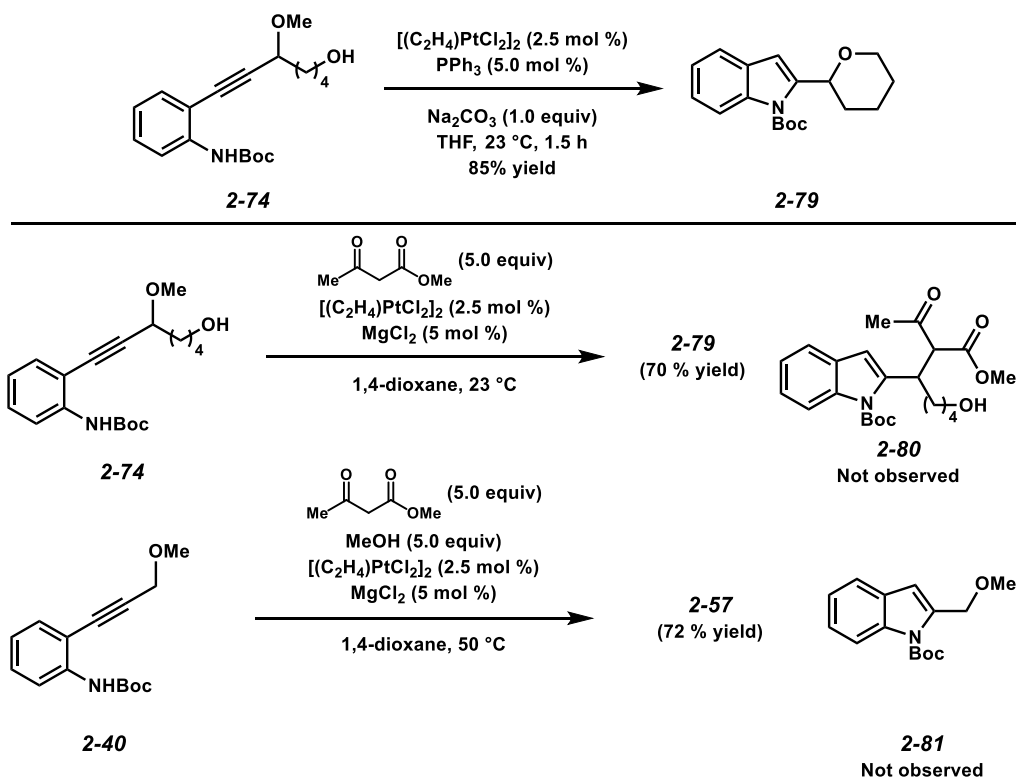


2.4.2. Competition Experiments

In order to glean mechanistic insights into the reactivity of these α,β -unsaturated carbenes with various nucleophiles, two competition experiments are performed. First, we want to

differentiate between direct vinylogous addition to the carbene and an alternative mechanism where ether ionization leads to an indolyl cation, which is then intercepted. In a previous report, we demonstrated that vicinal bisheterocyclizations of *N*-Boc aniline **2-74** was also possible under similar Pt conditions, given that it also contains an internal alcohol which could undergo a 6-*endo* cyclization (Scheme 2.4.4).¹⁸ When subjected to the dicarbonyl reaction conditions, substrate **2-74** should form solely bisheterocycle **2-79**, unless ether ionization is a viable pathway toward dicarbonyl adduct **2-80**. We also want to establish the difference in nucleophilic competency between alcohols and dicarbonyl enols, as alcohols are extruded during the formation of the unsaturated carbene intermediate.

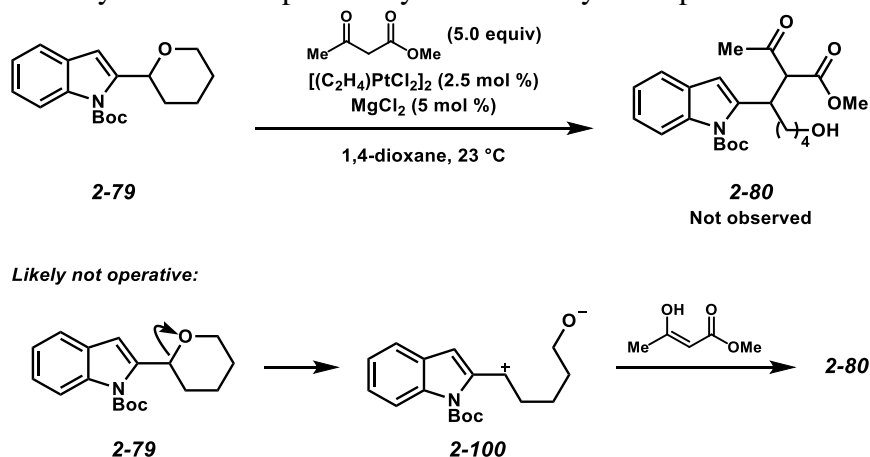
Scheme 2.4.4. Competition experiments between dicarbonyl and alcohol substrates.
Ferreira, 2013:



When aniline **2-74** is subjected to the optimized conditions for dicarbonyl incorporation in the presence of 5.0 equiv methyl acetoacetate, solely bisheterocycle **2-79** is formed with no

evidence of dicarbonyl incorporation. This supports our proposed mechanism of α,β -unsaturated carbene formation, as nucleophilic addition into an indolyl cation arising from ether ionization would eventually convert this product to the dicarbonyl adduct **2-80** (Scheme 2.4.5).

Scheme 2.4.5. Unlikely mechanistic possibility for dicarbonyl incorporation.



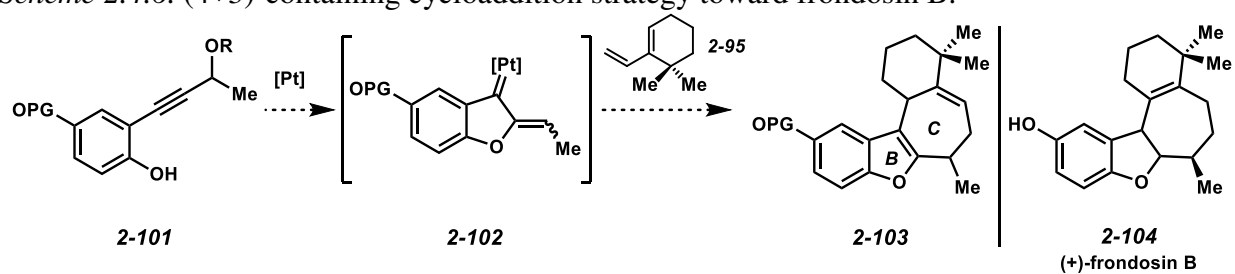
When competing external dicarbonyl and alcohol nucleophiles (in equimolar amounts) are combined with the carbene precursor and subjected to reaction conditions, dicarbonyl addition is the sole product observed (**2-57**). Given that ether ionization is likely not operative, this implies that while an internal nucleophile more quickly intercepts the electrophile, the enol is a better nucleophile when relying on intermolecular addition.

2.4.3. (4+3) cycloadditions enabled by diene incorporations

Having demonstrated that enols derived from β -dicarbonyls are competent in the nucleophilic interception of these catalytically-generated α,β -unsaturated Pt carbenes, we were surprised that no groups had reported the use of such powerful methodology in a natural product synthesis. Given the reports from the Tang and Iwasawa groups that dienes could undergo (4+3) cycloadditions with these carbene systems,¹²⁻¹³ we identified the natural product frondosin B as a candidate for testing the versatility of this reactivity. This tetracyclic sesquiterpenoid has been successfully synthesized by several groups since its isolation,^{33, 42-48} with the strategies by

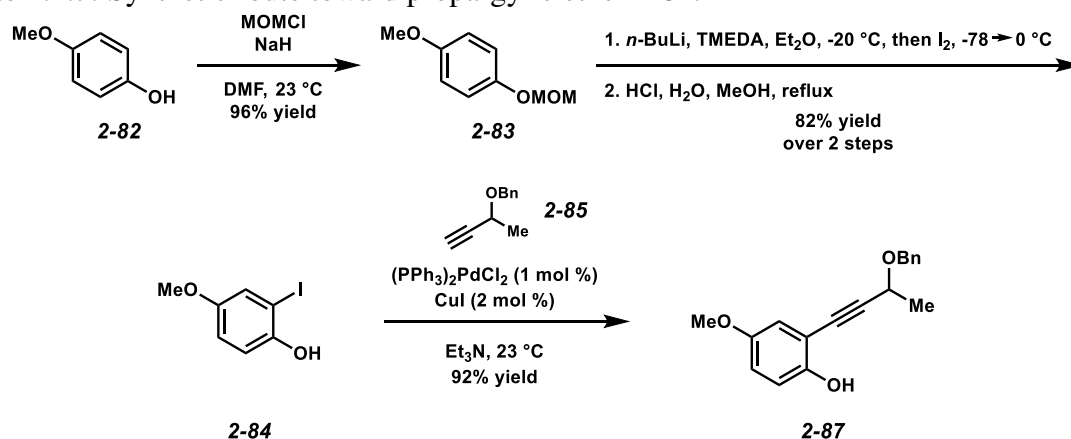
Davies,⁴⁹ Xue and Li,³⁹ as well as Winne⁵⁰ all employing a (4+3) cycloaddition to construct the cycloheptene core. This inspires a retrosynthesis where a key (4+3) step where carbene intermediate **2-102** could engage with an unactivated diene **2-95** to give a cycloheptene product (**2-103**), forming the B and C rings in frondosin B (**2-104**) concomitantly (Scheme 2.4.6).

Scheme 2.4.6. (4+3)-containing cycloaddition strategy toward frondosin B.



To this end, the two cycloaddition partners **2-87** and **2-95** were synthesized separately. The carbene precursor is readily accessed via a four-step synthesis starting from *p*-methoxyphenol (**2-82**, Scheme 2.4.7). First, the starting phenol is transformed into the methoxymethyl (MOM) acetal **2-83**. *Ortho*-iodination,⁵¹ followed by acid-promoted hydrolysis of the MOM acetal then gives iodophenol **2-84**. Sonogashira coupling⁵² with benzyl ether **2-85** then affords the targeted propargylic ether **2-87**.

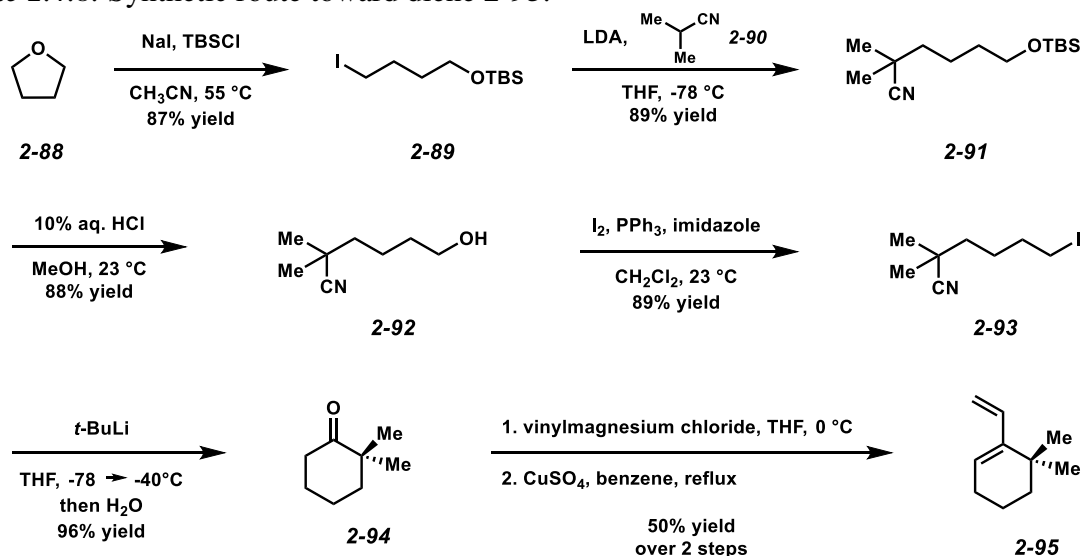
Scheme 2.4.7. Synthetic route toward propargylic ether **2-87**.



Next, the requisite diene can be synthesized according to literature precedent in two steps from 2,2-dimethylcyclohexanone (Scheme 2.4.8).³⁷ While this compound is commercially

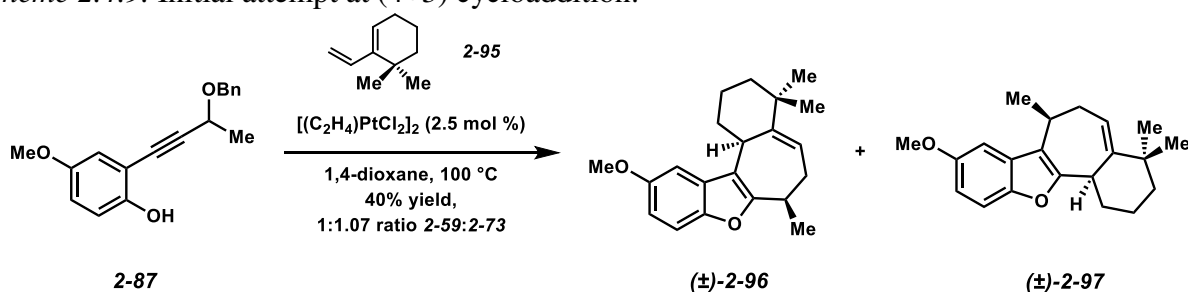
available, we find that a five step high yielding sequence is preferable for acquiring significant quantities. First, tetrahydrofuran (**2-88**) is ring-opened in the presence of sodium iodide and *in-situ* protected, giving alkyl iodide **2-89**.³⁴ This is then displaced by the enolate of isobutyronitrile (**2-90**),³⁵ and subsequent acid-mediated deprotection gives alcohol **2-92**. This is converted *via* Appel reaction to iodonitrile **2-93**, which then cyclizes upon lithium-halogen exchange with *tert*-butyllithium to give 2,2-dimethylcyclohexanone (**2-94**). Reaction with vinylmagnesium chloride followed by CuSO₄-mediated dehydration gives diene **2-95**.³⁷

Scheme 2.4.8. Synthetic route toward diene **2-95**.



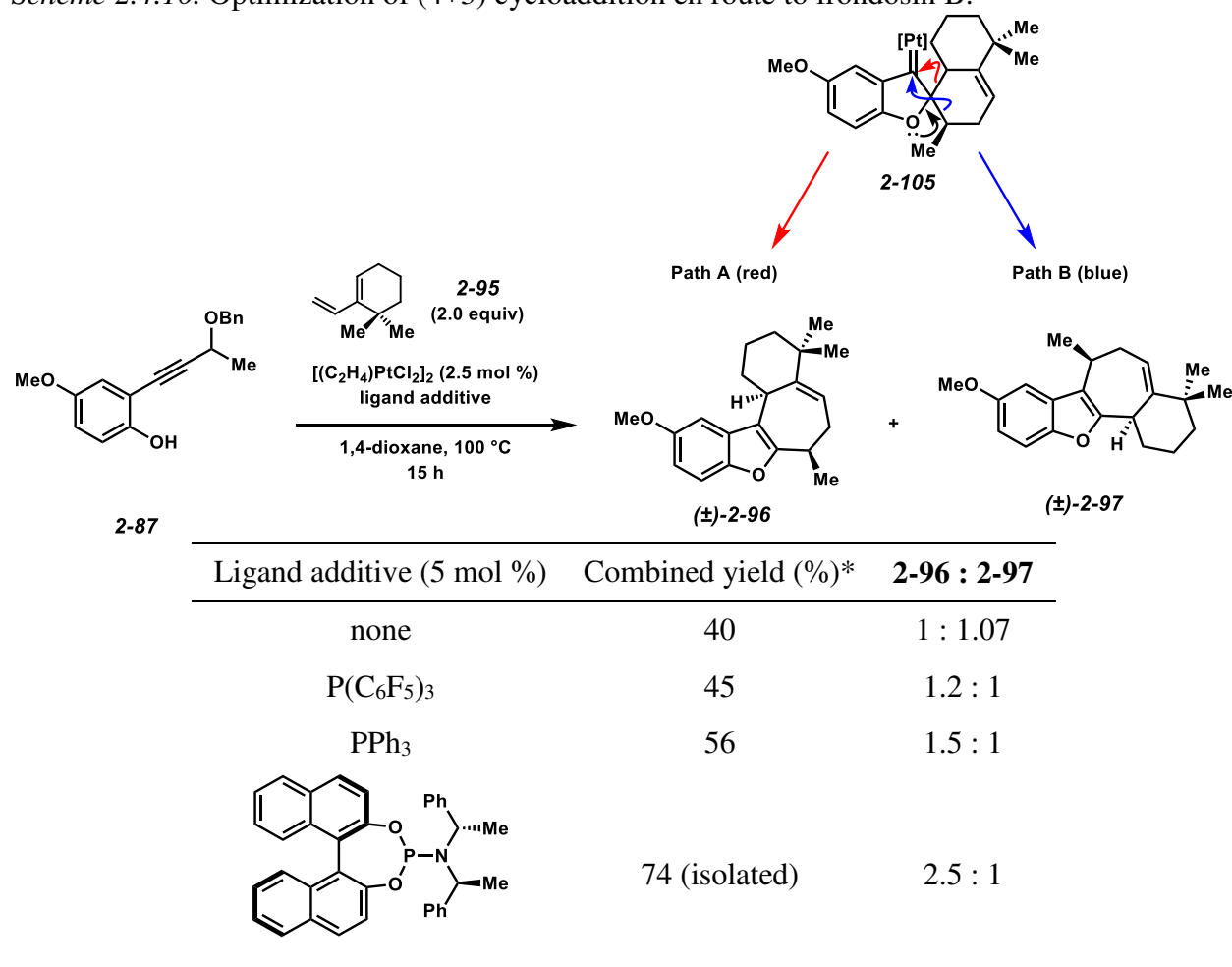
With the requisite coupling partners in hand, we set out to probe our initial hypothesis, namely that the C ring system of frondosin B could be formed concomitantly with benzofuran closure. To our delight, initial attempts to perform the (4+3) cycloaddition were met with success. When phenol **2-87** and diene **2-95** are treated with catalytic Zeise's dimer in 1,4-dioxane at 100 °C, conversion to tetracycle **2-96** is observed in 19% yield (Scheme 2.4.9). This reaction likely proceeds through a mechanism similar to that outlined in Scheme 2.1.4.

Scheme 2.4.9. Initial attempt at (4+3) cycloaddition.



We also find that side product **2-97** is formed in a nearly equal proportion to the desired tetracyclic product, which arises due to competing alkyl migrations (Paths A and B) from carbene intermediate **2-105** (Scheme 2.4.10). A brief optimization of this cycloaddition reaction reveals that inclusion of a ligand additive can significantly improve both yield and product ratios. Use of Feringa's phosphoramidite⁵³ results in a substantial increase in yield, and forms the desired product in a 2.5:1 ratio. This improvement in product distribution could be due to a change in electronics of the Pt carbene, as Iwasawa showed that ligand effects on product distribution in [4+3] cycloadditions can be significant.¹² Regardless, both **2-96** and **2-97** are formed as apparently single diastereomers in this reaction, implying that this reaction can be quite stereoselective. The formation of tetracycle **2-96** constitutes the formal synthesis of frondosin B, intercepting numerous syntheses at this point,^{40,49,51} alkene isomerization and demethylation affords the natural product.^{34,43,47}

Scheme 2.4.10. Optimization of (4+3) cycloaddition en route to frondosin B.



*NMR yield.

2.5 Conclusions

Overall, we have worked to both broaden the scope of carbon-based nucleophiles compatible with vinylogous addition to an unsaturated Pt carbene, as well as to probe the utility of cycloadditions enabled by this intermediate within the context of the total synthesis of frondosin B. Of note is the discovery that ligand additives to these cycloaddition reactions can affect product selectivities immensely, opening the door for potential expansion to stereoselective variants.

2.6 Acknowledgments

The National Institutes of Health (NIGMS, R01GM110560) is gratefully acknowledged for financial support of this work.

References

1. Marco-Contelles, J.; Soriano, E. *Chem. Eur. J.* **2007**, *13*, 1350.
2. Marion, N.; Lemière, G.; Correa, A.; Costabile, C.; Ramón, R. S.; Moreau, X.; de Frémont, P.; Dahmane, R.; Hours, A.; Lesage, D.; Tabet, J.-C.; Goddard, J.-P.; Gandon, V.; Cavallo, L.; Fensterbank, L.; Malacria, M.; Nolan, S. P. *Chem. Eur. J.* **2009**, *15*, 3243.
3. Blazykowski, C.; Harrak, Y.; Gonçalves, M.-H.; Cloarec, J.-M.; Dhimane, A.-L.; Fensterbank, L.; Malacria, M. *Org. Lett.* **2004**, *6*, 3771.
4. Mamane, V.; Gress, T.; Krause, H.; Fürstner, A.; *J. Am. Chem. Soc.* **2004**, *126*, 8654.
5. Fehr, C.; Galindo, J. *Angew. Chem. Int. Ed.* **2006**, *45*, 2901.
6. Mainetti, E.; Mouriès, V.; Fensterbank, L.; Malacria, M.; Marco-Contelles, J. *Angew. Chem. Int. Ed.* **2002**, *41*, 2132.
7. Bhanu Prasad, B. A.; Yoshimoto, F. K.; Sarpong, R. *J. Am. Chem. Soc.* **2005**, *127*, 12468.
8. Zheng, H.; Zheng, J.; Yu, B.; Chen, Q.; Wang, X.; He, Y.; Yang, Z.; She, X. *J. Am. Chem. Soc.* **2010**, *132*, 1788.
9. Pujanauski, B. G.; Bhanu Prasad, B. A.; Sarpong, R. *J. Am. Chem. Soc.* **2006**, *128*, 6786.
10. Phillips, A. J.; Allegretti, P. A.; Ferreira, E. M. Di- μ -chlorodichlorobis(η^2 -ethene)-diplatinum, in *Encyclopedia of Reagents for Organic Synthesis*, John Wiley & Sons, Inc., New York, 2014.
11. Saito, K.; Sogou, H.; Suga, T.; Kusama, H.; Iwasawa, N. *J. Am. Chem. Soc.* **2011**, *133*, 689.
12. Kusama, H.; Sogo, H.; Saito, K.; Suga, T.; Iwasawa, N. *Synlett* **2013**, *24*, 1364.
13. Shu, D.; Song, W.; Li, X.; Tang, W. *Angew. Chem. Int. Ed.* **2013**, *52*, 3237.
14. Yang, W.; Wang, T.; Yu, Y.; Shi, S.; Zhang, T.; Hashmi, A. S. K. *Adv. Synth. Catal.* **2013**, *355*, 1523.
15. Allegretti, P. A.; Ferreira, E. M. *Org. Lett.* **2011**, *13*, 5924.
16. Allegretti, P. A.; Ferreira, E. M. *Chem. Sci.* **2013**, *4*, 1053.
17. Shu, D.; Winston-McPherson, G. N.; Song, W.; Tang, W. *Org. Lett.* **2013**, *15*, 4162.

18. Allegretti, P. A.; Ferreira, E. M. *J. Am. Chem. Soc.* **2013**, *135*, 17266.
19. Kwon, Y.; Kim, I.; Kim, S. *Org. Lett.* **2014**, *16*, 4936.
20. Shen, W.-B.; Xiao, X.-Y.; Sun, Q.; Zhou, B.; Zhu, X.-Q.; Yan, J.-Z.; Lu, X.; Ye, L.-W. *Angew. Chem. Int. Ed.* **2017**, *56*, 605.
21. Tietze, L. F.; Böhnke, N.; Dietz, S. *Org. Lett.* **2009**, *11*, 2948.
22. Rudisill, D. E.; Stille, J. K. *J. Org. Chem.* **1989**, *54*, 5856.
23. Shen, Z.; Lu, X. *Adv. Synth. Catal.* **2009**, *351*, 3107.
24. Liao, Y.; Smith, J.; Fathi, R.; Yang, Z. *Org. Lett.* **2005**, *7*, 2707.
25. Nan, Y.; Miao, H.; Yang, Z. *Org. Lett.* **2000**, *2*, 297.
26. Wensbo, D.; Annby, U.; Gronowitz, S. *Tetrahedron* **1995**, *51*, 10323.
27. Kondo, Y.; Kojima, S.; Sakamoto, T. *J. Org. Chem.* **1997**, *62*, 6507.
28. Shade, R. E.; Hyde, A. M.; Olsen, J.-C.; Merlic, C. A. *J. Am. Chem. Soc.* **2010**, *132*, 1202.
29. Liu, Y.; Ma, S. *Org. Lett.* **2012**, *14*, 720.
30. Kumar, S. K.; Amador, M.; Hidalgo, M.; Bhat, S. V.; Khan, S. R. *Bioorg. Med. Chem.* **2005**, *13*, 2873.
31. Allegretti, P. A.; Huynh, K.; Ozumerzifon, T. J.; Ferreira, E. M. *Org. Lett.* **2016**, *18*, 64.
32. Bouzbouz, S.; Goujon, J.-Y.; Deplanne, J.; Kirschleger, B. *Eur. J. Org. Chem.* **2000**, 3223.
33. Inoue, M.; Carson, M. W.; Frontier, A. J.; Danishefsky, S. J. *J. Am. Chem. Soc.* **2001**, *123*, 1878.
34. Sommer, S.; Kühn, M.; Waldmann, H. *Adv. Synth. Catal.* **2008**, *350*, 1736.
35. Ciesielski, J.; Canterbury, D. P.; Frontier, A. J. *Org. Lett.* **2009**, *11*, 4374.
36. Gormisky, P. E.; White, M. C. *J. Am. Chem. Soc.* **2013**, *135*, 14052.
37. Tanis, S. P.; Abdallah, Y. M. *Synth. Commun.* **1986**, *16*, 251.
38. Mangel, N.; Mann, F. M.; Hillwig, M. L.; Peters, R. J.; Snider, B. B. *Org. Lett.* **2010**, *12*, 2626.

39. Zhang, J.; Li, L.; Wang, Y.; Wang, W.; Xue, J.; Li, Y. *Org. Lett.* **2012**, *14*, 4528.
40. Winne, J. M.; Catak, S.; Waroquier, M.; Van Speybroeck, V. *Angew. Chem. Int. Ed.* **2011**, *50*, 11990.
41. Huynh, K. Q.; Seizert, C. A.; Ozumerzifon, T. J.; Allegretti, P. A.; Ferreira, E. M. *Org. Lett.* **2017**, *19*, 294.
42. Hughes, C. C.; Trauner, D. *Angew. Chem. Int. Ed.* **2002**, *41*, 1569.
43. Kerr, D. J.; Willis, A. C.; Flynn, B. L. *Org. Lett.* **2004**, *6*, 457.
44. Li, X.; Ovaska, T. V. *Org. Lett.* **2007**, *9*, 3837.
45. Mehta, G.; Likhite, N. S. *Tetrahedron Lett.* **2008**, *49*, 7113.
46. Reiter, M.; Torssell, S.; Lee, S.; MacMillan, D. W. C. *Chem. Sci.* **2010**, *1*, 37.
47. Garayalde, D.; Krüger, K.; Nevado, C. *Angew. Chem. Int. Ed.* **2011**, *50*, 911.
48. Oblak, E. Z.; VanHeyst, M. D.; Li, J.; Wiemer, A. J.; Wright, D. L. *J. Am. Chem. Soc.* **2014**, *136*, 4309.
49. Olson, J. P.; Davies, H. M. L. *Org. Lett.* **2008**, *10*, 573.
50. Laplace, D. R.; Verbraeken, B.; Van Hecke, K.; Winne, J. M. *Chem. Eur. J.* **2014**, *20*, 253.
51. Townsend, C. A.; Bloom, L. M. *Tetrahedron Lett.* **1981**, *22*, 3923.
52. Chinchilla, R.; Nájera, C. *Chem. Rev.* **2007**, *107*, 874.
53. Teichert, J. F.; Feringa, B. L. *Angew. Chem. Int. Ed.* **2010**, *49*, 2486.

Chapter 3: Toward Steric Control of Guest Binding Modality: a Cationic Co(II) Complex Exhibiting Cation Binding and Zero-Field Relaxationⁱⁱ

3.1 Introduction

Cobalt(II)-containing complexes have been widely investigated for the development of novel single-molecule magnets (SMMs) due to the ion's large intrinsic magnetic anisotropy.¹⁻² While a variety of coordination numbers and geometries have been observed for Co(II) SMMs, few hexacoordinate systems have exhibited slow magnetic relaxation,³⁻¹² and fewer do so at zero applied dc field.¹³⁻¹⁸ Thus, the development of novel hexacoordinate Co SMMs is of great interest to understand the subtle geometrical differences that alter magnetic properties.

Previously, our group described a tris-(2-aminoethyl)amine (tren)-derived iminopyridine Fe(II) complex containing a trigonal pocket of *tert*-butylamide moieties.¹⁹ This ligand scaffold possessed enough inherent flexibility to accommodate an anionic guest (chloride), which was found to have little effect on the magnetic properties of the Fe complex. This motivated us to design a novel tripodal system also possessing a trigonal pocket for guest association using a more rigid backbone where a deviation from octahedral geometry could be achieved. Molecular systems possessing this geometry should have more anisotropy than an octahedral system, and are thus more likely to exhibit SMM properties.²⁰ Therefore, we employed the more rigid *cis*-, *cis*-1,3,5-triaminocyclohexane (tach) to replace the tren backbone in efforts to incur a deviation from

ⁱⁱ "Toward Steric Control of Guest Binding Modality: A Cationic Co(II) Complex Exhibiting Cation Binding and Zero-Field Relaxation." Ozumerzifon, T. J.; Bhowmick, I.; Spaller, W. C.; Rappé, A. K.; Shores, M. P. *Chem. Commun.* **2017**, 53, 4211 – Reproduced in part by permission of the Royal Society of Chemistry. <http://pubs.rsc.org/en/content/articlelanding/2017/cc/c7cc01172e#!divAbstract>

octahedral geometry. Presented herein are two structurally and magnetically characterized salts of a Co(II)-tach iminopyridine complex, as well as full syntheses of all ligands used.

3.2 Division of Labor

The tetraphenylborate salt $\{\text{Na}[\text{LCo}]\}(\text{BPh}_4)_3$ (**3.08**) was initially synthesized by William Spaller. UV-Vis and IR spectroscopy data were collected by William Spaller. Sequences for magnetic data collection were written with the help of Dr. Indrani Bhowmick. All theoretical computations were performed by Prof. Anthony Rappé. All other syntheses, crystallography and fitting of magnetic data were performed by Tarik Ozumerzifon.

3.3 Experimental Details

3.3.1. Materials and Methods

Synthetic details: All reactions were performed under ambient conditions (room temperature, normal benchtop atmosphere) unless otherwise stated. Qualitative thin layer chromatography (TLC) analysis was performed on 250 mm thick, 60 Å, glass backed, F254 silica (Silicycle, Quebec City, Canada). Visualization was accomplished using UV light. Flash chromatography was performed using Silicycle silica gel (230-400 mesh). Syringe filters were purchased from VWR International and were fitted with 0.2 µm PTFE membranes. Diethyl ether (Et_2O), tetrahydrofuran (THF) and acetonitrile (MeCN) were sparged with nitrogen, passed through an alumina column and degassed prior to use. Anhydrous methanol (MeOH) was purchased from Sigma Aldrich. All other chemicals were purchased from commercial vendors and used as received.

General Characterization: ^1H NMR spectra were obtained on a Varian 400 MR (at 400 MHz) and are reported relative to SiMe_4 (δ 0.00). Absorption spectra were obtained with a Hewlett-Packard 8453 spectrometer in quartz cuvettes with a 1 cm path length. Infrared spectra were measured with a Nicolet 380 FT-IR spectrometer. Mass spectrometry measurements were

performed in the positive ion mode on a Thermo LTQ mass spectrometer equipped with an analytical electrospray ion source and a quadrupole ion trap mass analyzer at 175 °C. Elemental analyses were performed by Robertson Microlit Laboratories, Inc. in Ledgewood, NJ.

Magnetic Measurements: DC magnetic data were collected for **3.9** and **3.10** using a Quantum Design MPMS XL SQUID magnetometer between 1.8 to 300 K and 0 to 50 kOe. AC magnetic measurements were performed between 0.1 to 1500 Hz using a 4 Oe oscillating field. Powdered microcrystalline samples were loaded into polyethylene bags (1 cm × 1.5 cm), sealed, and inserted into drinking straws for measurements. Ferromagnetic impurities were checked through a variable field measurement (0 to 20 kOe) of the magnetization at 100 K; linear fits of the M versus H data (Appendix 2) indicate the absence of ferromagnetic impurities. Data were corrected for the diamagnetic contributions of the sample holder and bag by subtracting empty containers; corrections for the sample were calculated from Pascal's constants.²¹ Fits of magnetic susceptibility data were performed using PHI²² according to the following Hamiltonian:

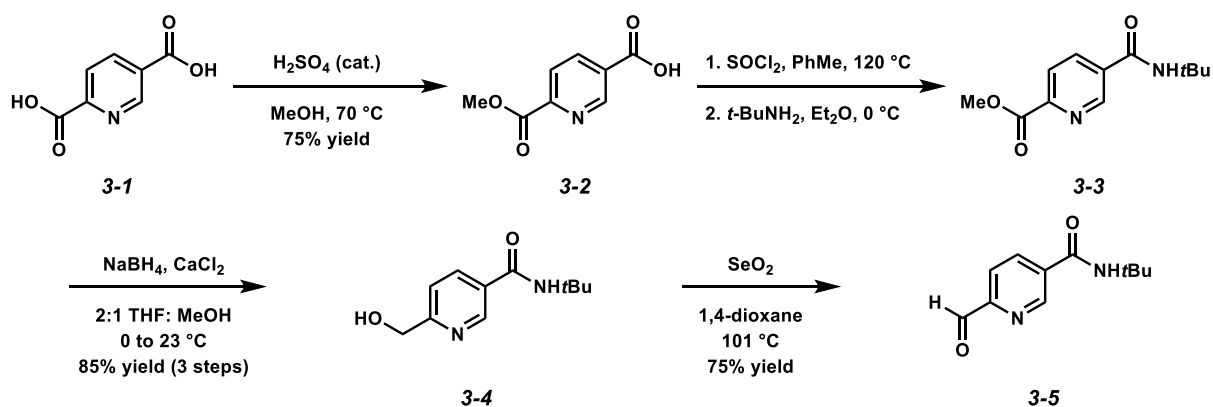
$$\hat{H} = \sum D_i [S_{z,i}^2 - 1/3S_i(S_i + 1) + E_i/D_i(S_{x,i}^2 - S_{y,i}^2)] + \sum g_{xx,i}\beta\check{S}_{x,i} \cdot \overline{B}_x + g_{yy,i}\beta\check{S}_{y,i} \cdot \overline{B}_y + g_{zz,i}\beta\check{S}_{z,i} \cdot \overline{B}_z$$

Crystallographic Measurements: Crystallographic parameters for the compounds are listed in Table 3.3.1. All crystals were coated in Paratone oil for data collection. The crystals were supported on Cryoloops, and then mounted on a Bruker Kappa Apex 2 CCD diffractometer under a stream of dinitrogen. Mo K α radiation and a graphite monochromator were used for data collection. Initial lattice parameters were determined from reflections found in 36 frames. Data sets were collected targeting complete coverage and threefold redundancy. Data were integrated and corrected for absorption effects with the APEX 2 software package.²³ Structures were solved and refined with the SHELXTL software package.²⁴ Unless noted otherwise, thermal parameters for all fully occupied, non-hydrogen atoms were refined anisotropically; hydrogen atoms were

added at the ideal positions and were refined using a riding model where the thermal parameters were set at 1.2 times those of the attached carbon or nitrogen atom (1.5 times that for methyl protons).

3.3.2. Synthesis of ligands and cobalt complexes

The precursor aldehyde **3-5** has been reported previously,¹⁹ however due to some complications with its synthesis, the details are presented here. Insufficient drying of **3-1** can lead to partial hydrolysis of the intermediate acid chloride en route to **3-2**, giving the bis(amide) species as a side product. Use of excess SeO₂ in the final step results in over-oxidation and failure to fully remove selenium-containing byproducts from **3-5** can result in undesired reactivity.



Monoester 3-2. To a suspension of 2,5-pyridinedicarboxylic acid (**3-1**) (5.68 g, 34.0 mmol) in MeOH (200 mL, 0.17 M) was added conc. aq. H₂SO₄ (5.0 mL, 0.0028 mmol) and the resulting mixture was heated to a gentle boil (~70 °C). When the reaction became transparent, it was poured on ice and filtered. The precipitate was then dissolved in wet THF (100 mL), dried over MgSO₄, filtered and concentrated *in vacuo* to isolate crude **3-2**. The crude compound was then dried overnight in a vacuum oven at 100 °C to give monoester **3-2** (4.65 g, 75% yield) as a pink solid which was used without further purification.

Monoester 3-2: ¹H NMR (400 MHz, CD₃OD): δ 9.21 (d, *J* = 1.6 Hz, 1H), 8.54 (dd, *J* = 8.0 Hz, 1.6 Hz, 1H), 8.25 (d, *J* = 8.0 Hz, 1H), 4.01 (s, 3H).

Amide 3-3. To a suspension of monoester **3-2** (4.63 g, 25.5 mmol) in anhydrous toluene (80 mL, 0.32 M) was added dropwise freshly distilled (from quinoline) SOCl₂ (5.57 mL, 76.6 mmol), and the resulting mixture was heated to reflux (~120 °C). Upon complete conversion to the acyl chloride (visually determined as when the mixture turns transparent yellow), excess SOCl₂ and solvent were removed by vacuum distillation to give the crude acid chloride. This residue was then redissolved in anhydrous Et₂O (160 mL, 0.16 M) and cooled to 0 °C, and *tert*-butyl amine (10.74 mL, 102.2 mmol) was added dropwise. The amide formation was immediate as evidenced by precipitation of the amine hydrochloride salt. The reaction was allowed to warm to 23 °C and stirred for 1 h. The mixture was filtered and the precipitate was washed with CH₂Cl₂ (2 × 100 mL). The combined filtrates were concentrated *in vacuo* to give crude amide **3-3** (R_f = 0.61 in EtOAc). This material was used without further purification.

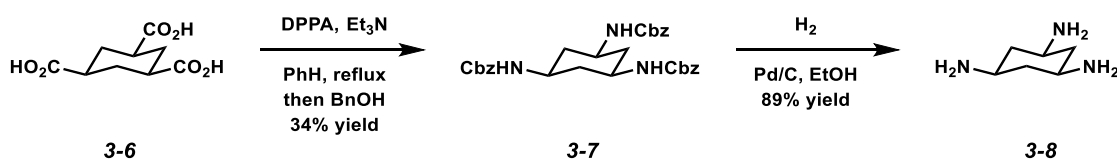
Amide 3-3: ¹H NMR (400 MHz, CDCl₃): δ 9.01 (s, 1H), 8.18 (s, 2H), 5.94 (br s, 1H), 4.03 (s, 3H), 1.50 (s, 9H).

Alcohol 3-4. To a solution of amide **3-3** (25.5 mmol assumed) in 2:1 MeOH:THF (426 mL, 0.06 M) at 0 °C was added anhydrous CaCl₂ (8.50 g, 76.6 mmol) and NaBH₄ (2.90 g, 76.6 mmol), the latter was added portionwise so as to control H₂ evolution. The reaction was allowed to warm to 23 °C and stirred overnight. Upon complete consumption of the starting material (as indicated by TLC), the reaction was filtered and concentrated *in vacuo* to give crude alcohol **3-4**. This residue was purified by flash column chromatography (CH₂Cl₂ to 19:1 CH₂Cl₂/MeOH gradient) to give alcohol **3-4** as a hygroscopic white solid (4.49 g, 85% yield over three steps).

Alcohol 3-4: ¹H NMR (400 MHz, CD₃OD): δ 8.82 (s, 1H), 8.18 (d, *J* = 8.0 Hz), 7.62 (d, *J* = 8.0 Hz, 1H), 4.73 (s, 2H), 1.46 (s, 9H).

Aldehyde 3-5. To a suspension of alcohol **3-4** (0.980 g, 4.69 mmol) in 1,4-dioxane (24 mL, 0.20 M) was added SeO₂ (0.260 g, 2.34 mmol) and the resulting mixture heated to a gentle reflux (~101 °C) overnight. After allowing to cool to 23 °C, the reaction mixture was filtered through Celite and the filtrate was concentrated *in vacuo* to give crude aldehyde **3-5**. The crude product was purified by flash column chromatography (1:1 hexanes/EtOAc eluent) to afford pure **3-5** as an off-white powder (0.730 g, 75% yield, R_f = 0.44 in 1:1 hexanes/EtOAc).

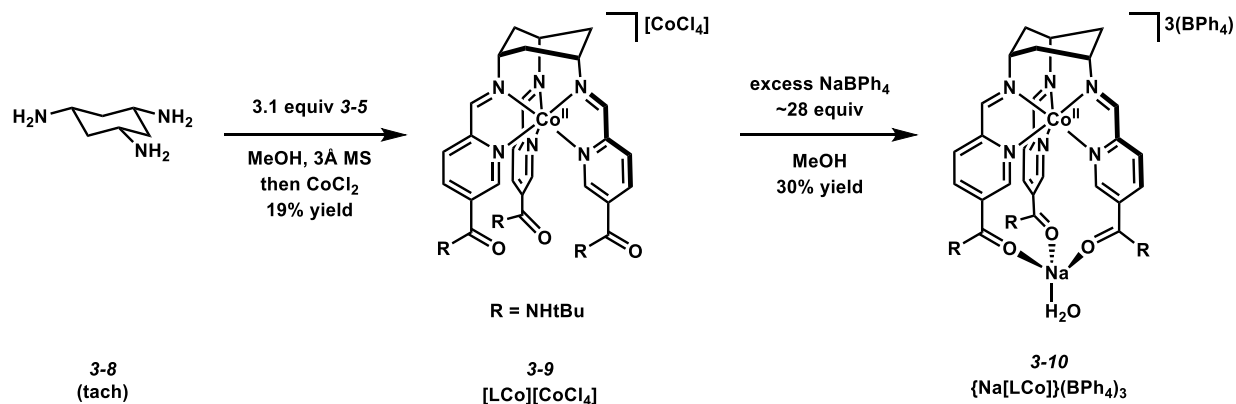
Aldehyde 3-5: ¹H NMR (400 MHz, CDCl₃): δ 10.12 (s, 1H), 9.07 (d, *J* = 1.2 Hz, 1H), 8.20 (dd, *J* = 8.0, 1.2 Hz, 1H), 8.01 (d, *J* = 8.0 Hz, 1H), 5.96 (br s, 1H), 1.51 (s, 9H).



Carbamate 3-7. Following a previous report,²⁵ the N,N',N''-tris(benzyl)carbamate of *cis*-, *cis*-1,3,5-cyclohexanetricarboxylic acid was prepared *via* Curtius rearrangement. To a solution of *cis*-, *cis*-1,3,5-cyclohexanetricarboxylic acid (4.17 g, 19.3 mmol) in anhydrous benzene (160 mL, 0.12 M) and freshly distilled triethylamine (8.14 mL, 58.5 mmol, 3.03 equiv) was added freshly prepared and distilled diphenylphosphoryl azide,²⁶ and the resulting mixture was stirred at room temperature for 0.5 h and then refluxed (80 °C) for an additional 0.5 h. Once the reaction mixture cooled to 23 °C, freshly distilled benzyl alcohol (6.66 mL, 64.4 mmol, 3.34 equiv) was added, and the reaction was refluxed for an additional 18 h. After cooling to ambient temperature, the reaction was vacuum filtered to isolate the white precipitate, washed with a minimal amount of cold benzene, giving *cis*-, *cis*-1,3,5-cyclohexanetricarboxybenzoyl amide (3.72 g, 34% yield) as a white powder, which was used without further purification.

Tach 3-8. The hydrogenolysis was performed according to Bialecki *et al.*²⁷ To a suspension of *cis*-, *cis*-1,3,5-cyclohexanetricarboxybenzoyl amide (0.400 g, 0.752 mmol) in absolute EtOH (100

mL) was added 10% palladium on carbon (0.300 g) and the resulting mixture was degassed with H₂ gas (2×) and then stirred for 48 h with a balloon of hydrogen affixed to provide a positive pressure during the reaction. After completion, as indicated by complete dissolution of the starting material, the reaction was filtered through Celite and concentrated *in vacuo* to give *cis*-, *cis*-1,3,5-triaminocyclohexane (tach, **3-8**, 0.124 g, 89% yield) as a white powder.



[LCo][CoCl₄] 3-9. To a solution of tach (0.060 g, 0.47 mmol) in MeOH (2 mL) was added a solution of aldehyde **3-5** (0.300 g, 1.44 mmol) in MeOH (2 mL), and the resulting mixture was stirred at 23 °C for 30 minutes in the presence of 3 Å molecular sieves. Then, a solution of CoCl₂ (0.060 g, 0.47 mmol) in MeOH (5 ml) was added, and the resulting orange solution was stirred at 23 °C for an additional hour. Then, Et₂O (10 mL) was added slowly to precipitate the crude product, which was isolated by vacuum filtration. Diffraction quality crystals were obtained from an Et₂O diffusion into a concentrated solution of the crude product in MeOH, giving **3-9** (0.091 g, 19% yield) as green needle-like crystals.

[LCo][CoCl₄] 3-9: UV-Vis (MeOH) λ , nm (ϵ , M⁻¹cm⁻¹): 226 (36200), 274 (21200), 355 (2300), 527 (140). MS (ESI⁺): m/z calcd for (M - CoCl₄ + Cl)⁺ [C₃₉H₅₁N₉O₃ClCo]⁺: 787.31, found 787.42, m/z calcd for (M - CoCl₄)²⁺ [C₃₉H₅₁N₉O₃Co]²⁺: 376.17, found 376.25. Anal. calcd (C₃₉H₅₁N₉O₃Co₂Cl₄ + 2(CH₄O): C: 48.39, H: 5.84, N: 12.39, found C: 48.04, H: 5.58, N: 12.36%.

{Na[LCo]}(BPh₄)₃ 3-10. To a solution of NaBPh₄ (0.220 g, 0.67 mmol) in MeOH (2 mL) was added dropwise a solution of **3-9** (0.024 g, 0.024 mmol) in MeOH (2 mL), immediately forming a suspension, which was stirred at 23 °C for 12 h. The reaction mixture was then filtered to isolate crude **3-10**, and diffraction quality crystals were grown by Et₂O diffusion into a concentrated acetonitrile solution of the crude product, giving yellow block-like crystals of **3-10** (0.013 g, 30% yield).

{Na[LCo]}(BPh₄)₃ 3-10: UV-Vis (MeCN) λ , nm (ϵ , M⁻¹cm⁻¹): 244 (92500), 276 (30500), 410 (4500). MS (ESI⁺): m/z calcd for (M - Na - 2BPh₄)⁺ [C₆₃H₇₁N₉O₃BCo]⁺: 1071.51, found 1071.25, m/z calcd for (M - Na - 3BPh₄)²⁺ [C₃₉H₅₁N₉O₃Co]²⁺: 376.17, found 376.25. Anal. calcd for (C₁₁₁H₁₁₁B₃N₉O₃Co + 1(C₂H₃N) + 1(C₄H₁₀O) + 2.5(H₂O): C: 74.21%, H: 6.87%, N: 7.40%, found C: 74.00%, H: 6.56%, N: 7.54%.

Discussion of reaction of L with CoI₂: L was generated *in-situ* in an identical manner as outlined in the syntheses of **3-9** and **3-10**, except the reaction was performed in a dinitrogen filled glovebox (MBRAUN Labmaster 130): to a solution of tach **3-8** (0.020 g, 0.15 mmol) in MeOH (3 mL) was added a solution of aldehyde **3-5** (0.090 g, 1.44 mmol) in MeOH (2 mL). The resulting mixture was stirred at 23 °C in the presence of 3Å molecular sieves. After 30 minutes, a solution of CoI₂ (0.049 g, 0.15 mmol) in MeOH (5 ml) was added and the resulting brown mixture was stirred for 12 h at 23 °C. Then, the mixture was passed through a syringe filter and the filtrate concentrated *in vacuo*, and X-ray diffraction quality crystals were obtained from a diethyl ether diffusion into a concentrated solution of acetonitrile, giving 0.056 g of brown crystals. Structural analysis indicates the formation of the triiodide salt of the tach-derived iminopyridine cobalt complex, **3-11** (Figure 3.3.4). Analysis of the crystalline product *via* mass spectrometry also indicates the expected formulation: m/z calcd for (M+I)⁺ [C₃₉H₅₁N₉O₃Co + I]⁺, 879.25, found 879.08; m/z calcd for (M -

$2\text{I}_3)^{2+}$, 376.17, found 376.25. Bulk purity combustion analyses, however, do not confirm absolute purity of this compound and efforts to further purify this species have been unsuccessful. Preliminary magnetic susceptibility studies suggested incomplete conversion of iodide to triiodide. However, efforts to fully convert iodide to triiodide using excess iodine (as has been shown previously for $[\text{Co}(\text{12-crown-4})_2](\text{I}_3)_2$,²⁸ do not afford complete reaction (0.0036 g isolated yield on a 0.046 mmol scale, 0.070 g theoretical yield) to form the triiodide salt. Therefore, the magnetic properties of this species will not be discussed.

[LCo][CoBr₄] 3-12. Following an identical procedure to the synthesis of **3-9** using CoBr_2 nominally leads to the formation of the tetrachlorocobaltate salt of the parent cobalt complex. This is assigned based on collection of a unit cell collection giving comparable parameters to **3-9**. Note that no bulk characterization was performed on this complex.

3.3.4. Crystallographic Results

Compound **3-10** crystallizes with partial occupancy and disorder of solvate molecules; this disorder was removed using SQUEEZE (model A). This process removed electron density corresponding to 73.81 electrons for a void space of 219.5 \AA^3 per unit cell. An explicit model (B), where the remaining electron density was modeled as two acetonitrile molecules (one at 0.333 occupancy, one at 0.666 occupancy) and one diethyl ether molecule (at 0.25 occupancy), gave slightly better agreement factors ($R_1 = 0.0583$), but with a larger number of parameters, such that model B was not a statistical enhancement of model A. In addition, relative to model A, the explicit disorder model (B) gave a disproportionate number of alerts in the checkcif due to overparameterization. Finally, three acetonitrile molecules and 0.75 ether molecules per unit cell correspond roughly to 97.5 electrons (275 \AA^3 , assuming $25 \text{ \AA}^3/\text{atom}$), higher than expected from the SQUEEZE analysis. Attempts to decrease the occupancy of any of the solvent sites

significantly deteriorate agreement with the data. Thus, the SQUEEZED model (A) was used as the final model.

In the structure of **3-10**, the H₂O molecule bound to the Na ion does not reside on the three-fold rotational axis, so the occupancy of the O atom was set to 0.333. Addition of H atoms causes the anisotropic thermal parameters of the O atom to become non positive definite, so the H atoms were omitted from the final model. The structures of **3-9** and **3-10** are shown in Figure 3.3.3.

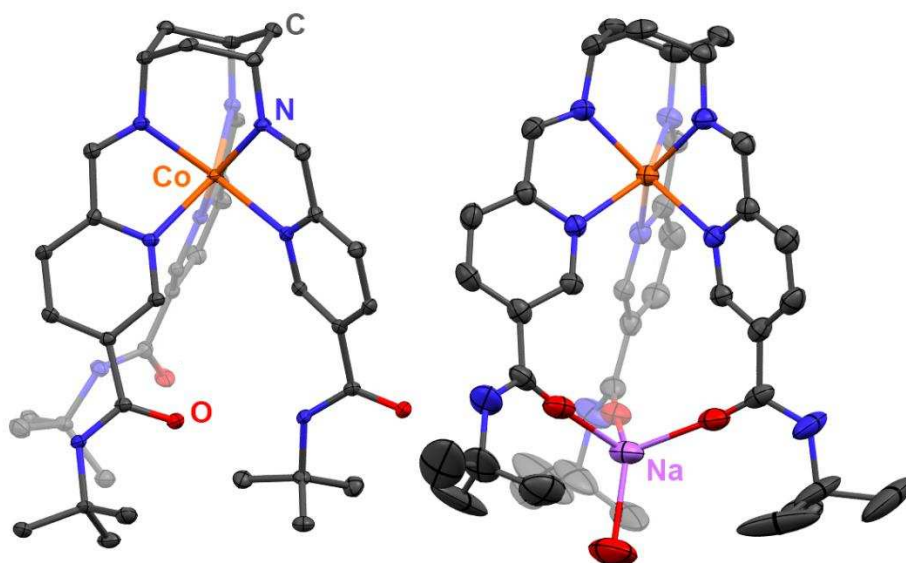


Figure 3.3.1. Crystal structures of the cationic complexes **3-9** (left) and **3-10** (right) rendered with 40% thermal ellipsoids. Orange, red, blue, grey and lavender ellipsoids represent Co, O, N, C and Na atoms, respectively. H atoms, solvent and charge balancing anions are omitted for clarity. The Co and Na atoms in **3-10** lie on a threefold rotation axis.

As described above (Section 3.3.3), an x-ray structure of **3-11** was obtained. It is shown in Figure 3.3.4.

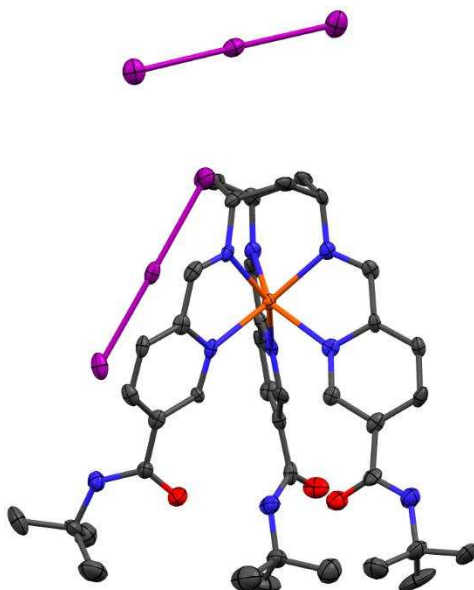


Figure 3.3.2. Crystal structure of **3-11** rendered with 40% thermal ellipsoids. Orange, red, blue, grey and purple ellipsoids represent Co, O, N, C and I atoms, respectively. H atoms and solvent are omitted for clarity.

Table 3.3.1. Crystallographic parameters for **3-9**, **3-10**, **3-11** and **3-12**.^a

	3-9	3-10	3-11	3-12
Formula	C ₄₁ H ₅₈ N ₉ O ₅ Co ₂ Cl	C ₁₁₅ H ₁₂₁ B ₃ N ₁₀ O _{4.5} CoNa	C ₄₃ H ₆₁ N ₉ O ₄ CoI ₆	-
Formula weight	1016.62	1749.43	1588.34	-
Color, habit	green needle	yellow block	brown block	green needle
<i>T</i> (K)	120	120	120	-
Space group	<i>P</i> $\bar{1}$	<i>R</i> 3 <i>c</i>	<i>P</i> 2 ₁ / <i>c</i>	-
<i>Z</i>	2	6	4	-
<i>a</i> (Å)	9.8899(12)	23.7294(15)	23.899(2)	9.94
<i>b</i> (Å)	10.4071(13)	23.7294(15)	17.3157(15)	10.47
<i>c</i> (Å)	25.652(3)	34.604(3)	13.5491(13)	25.75
α (°)	83.322(4)	90	90	92.65
β (°)	87.485(5)	90	95.028(3)	92.17
γ (°)	65.134(4)	120	90	115.56
<i>V</i> (Å ³)	2379.2(5)	16875(3)	5583.0(9)	2409
<i>d</i> _{calc} (g cm ⁻³)	1.419	1.033	1.890	-
GOF	1.042	1.066	1.147	-
<i>R</i> ₁ , <i>wR</i> ₂ ^b (%)	4.67, 13.40	6.04, 15.10	6.11, 13.05	-

^a Obtained with graphite-monochromated Mo K α ($\lambda = 0.71073$ Å) radiation.

^b $R_1 = \sum ||F_o| - |F_c|| / \sum |F_o|$, $wR_2 = \{ \sum [w(F_o^2 - F_c^2)^2] / \sum [w(F_o^2)^2] \}^{1/2}$ for $F_o > 4\sigma(F_o)$.

The crystal structures of **3-9**, **3-10** and **3-11** have been uploaded to the Cambridge Crystallographic Data Center (CCDC) as 1527921 - 1527923.

3.4 Results and Discussion

3.4.1. Synthesis of Co Complexes

Attempts to synthesize the chloride salt of the Co(II) complex of the Schiff base ligand (L) via *in situ* template complexation of CoCl_2 lead to the formation of the tetrachlorocobaltate salt, $[\text{LCo}][\text{CoCl}_4]$, **3-9** (Scheme 3.3.2). Crystallographic analysis shows that two of the pendant amides engage in a network of hydrogen bonds, while the third engages in a single hydrogen bond (2.852(1) Å) with a chlorine atom on the cobaltate anion (Figure 3.4.1). The closest intermolecular $\text{Co}\cdots\text{Co}$ distance in **3-9** is 5.862(1) Å.

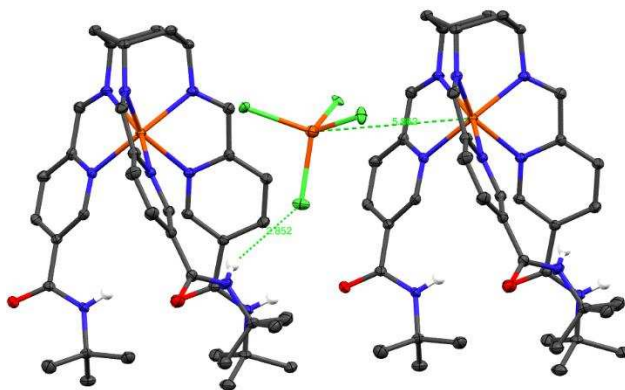


Figure 3.4.1. Short contacts in **3-9**. The structure is rendered with 40% thermal ellipsoids and orange, red, blue and grey ellipsoids represent Co, O, N and C atoms, respectively. Non-amide H atoms and solvent are omitted for clarity.

Combination of L with CoBr_2 leads to the tetrabromocobaltate salt, $[\text{LCo}][\text{CoBr}_4]$, as determined by single crystal x-ray crystallography (Section 3.3.4). Meanwhile, reaction with CoI_2 gives the bis(triiodido) **3-11** salt as the major isolable product (Section 3.3.2). Because the purity of this compound was not able to be confirmed, its magnetic properties will not be discussed. Interestingly, the successful exchange of the $[\text{CoCl}_4]^{2-}$ anion in **3-9** using excess sodium tetraphenylborate affords $\{\text{Na}[\text{LCo}]\}(\text{BPh}_4)_3$ (**3-10**), and single crystal x-ray crystallography reveals the ability of the $[\text{LCo}]^{2+}$ complex to bind one sodium cation through the three carbonyl oxygens of the amide groups (Figure 3.3.4).

The cationic cobalt centers in **3-9** and **3-10** have local geometries intermediate between trigonal prismatic and octahedral, where torsion of the N-N-N planes about the 3-fold rotational axis is 23.3(1) and 15.8(7)°, respectively (0° for an ideal trigonal prism). This is in contrast to the more flexible tren analog [Co(L^{5-OOMe})] [CoCl₄],²⁹ which is nearly octahedral (50.3(6)°; 60° for a perfect octahedron) and unsubstituted [Co(py₃tach)](ClO₄)₂, which exhibits trigonal prismatic geometry, 5.4(3)°.³⁰

The observed cation binding in complex **3-10** is intriguing, as *tert*-butylamide substituents have been observed only as anion-binding sites in related Fe(II) and Ru(II) complexes, the latter reported by Beer and coworkers.^{19, 31} Comparing the relevant amide groups in both **3-9** and **3-10** to those in {Cl[FeL^{5-OH*t*Bu}]}⁺, the C=O bond lengths are uniformly shorter than the corresponding C-N bonds (Table 3.4.1).

Table 3.4.1. Compiled crystallographic details regarding binding pockets in tripodal complexes.

Capping ligand	Guest	Complex	Area of pocket ^a (Å ²)	Amide C=O (Å)	Amide C-N (Å)
tach	None	3-9	13.40(3)	1.240(4)	1.346(5)
	Na ⁺	3-10	14.38(6)	1.218(1)	1.322(9)
tren	None ^b	[CoL ^{5-OOMe}] ²⁺	16.84(9)	None	-
	Cl ^{-c}	{Cl[Fe(L ^{5-OH<i>t</i>Bu})]} ⁺	19.65(8)	1.229(5)	1.335(3)

^a The area of the binding pocket is calculated from the triangle formed by the carbonyl carbons bound to pyridine 5-positions. ^b From ref. 29. ^c From ref. 19.

From this comparison, however, no obvious trend can be discerned regarding amide bond lengths between the bare, anion- and cation binding species. We note that complex **3-10** possesses shorter C-N bonds than **3-9**, signaling an increased contribution from an iminium-containing resonance structure. Rather, the preference for cation over anion association can be rationalized by noting the difference in ionic radii between Na⁺ (102 pm) and Cl⁻ (184 pm).³² This highlights the effect of the more geometrically constricting tach backbone, which imparts a smaller binding pocket than the tren analogs (Table 3.4.1).

3.4.2. DC Magnetic properties of **3-9** and **3-10**

The temperature dependencies of the magnetic susceptibility-temperature products of **3-9** and **3-10**, collected between 1.8 and 300 K under an applied dc field of 1000 Oe (Figure 3.4.2), show that both Co(II) complexes remain high spin throughout the temperature range. The CoCl_4^{2-} salt **3-9** displays a room temperature $\chi_M T$ value of $6.29 \text{ cm}^3 \text{ K mol}^{-1}$, consistent with the presence of two $S = 3/2$ Co(II) centers per formula unit. Upon cooling, the $\chi_M T$ value remains nearly constant until about 60 K, below which there is a pronounced downturn, eventually reaching a $\chi_M T$ value of $4.66 \text{ cm}^3 \text{ K mol}^{-1}$ at 1.8 K.

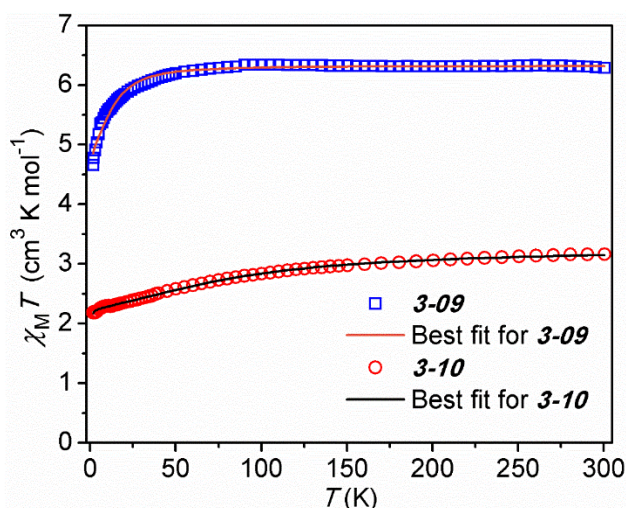


Figure 3.4.2. Variable temperature dc magnetic susceptibility data for **3-9** and **3-10** collected between 1.8 and 300 K at an applied dc field of 1000 Oe. The fit lines were determined using PHI²² with parameters found in Table 3.4.2.

This downturn could be attributed to magnetic anisotropy and/or intermolecular antiferromagnetic interactions, possibly through the hydrogen bond between one of the amides and the anion (Figure 3.4.1). The tetraphenylborate salt **3-10** shows a $\chi_M T$ value of $3.16 \text{ cm}^3 \text{ K mol}^{-1}$ at 300 K, consistent with the presence of a single $S = 3/2$ center. Upon cooling, the magnetic susceptibility product decreases gradually to $2.18 \text{ cm}^3 \text{ K mol}^{-1}$ at 1.8 K. Meanwhile, the field dependence of magnetization of **3-10**, collected at 2 K, nearly saturates at $2.37 \mu_B$ at 50 kOe (Figure

3.4.3), lower than the theoretical value for an $S = 3/2$ system when $g = 2$, but consistent with large magnetic anisotropy expected for a HS Co(II) center.

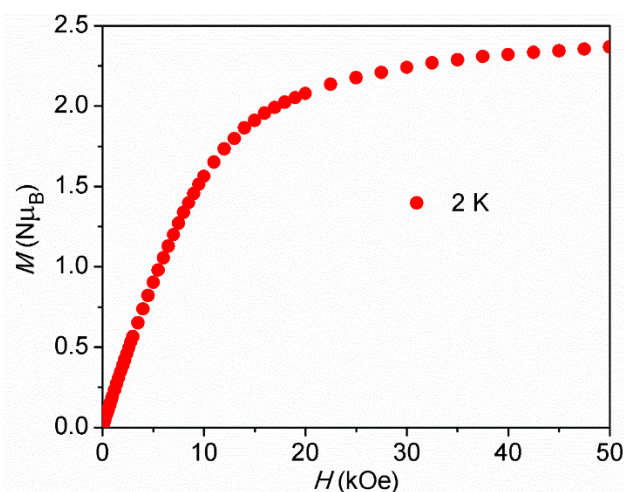


Figure 3.4.3. Field dependence of magnetization for **3-10** collected at 2 K.

The susceptibility data were modelled using PHI²² to determine g and anisotropy parameters for compounds **3-9** and **3-10** (Table 3.4.2). Addition of a mean field correction accounting for possible intermolecular antiferromagnetic coupling gives negligible values (entries 2 and 5), and thus was not included in the final model.

Table 3.4.2. Anisotropy values acquired from fitting magnetic susceptibility data and calculations. The calculated structures **3-9A** and **3-10A** are based on the cation complex, omitting anions and co-crystallized solvents.

Entry	Species	g	D (cm^{-1})	E (cm^{-1})	zJ (cm^{-1})	TIP ($\text{cm}^3 \text{mol}^{-1}$)	R^2
1	3-9*	2.84	-11.0	0.0084	-	-	0.9933
2	3-9	2.84	5.29	5.29	-0.0013	-	0.9999
3	3-9A	2.35	-104	0.050	-	-	-
4	3-10*	2.63 (\perp) 2.80 (\parallel)	-75.8	0.00090	-	0.000500	0.9999
5	3-10	2.63 (\perp) 2.80 (\parallel)	-76.0	0.013	-0.0043	0.000500	0.9999
6	3-10	2.84	-163	0.011	-	-	0.8931
7	3-10A	1.34 (\perp) ^a 3.45 (\parallel)	-142	0.021	-	-	-

*Optimized fit. ^a The calculated g_{\perp} value is the average of calculated g_{xx} and g_{yy} values.

The large g values found for **3-9** and **3-10** are reasonable for high spin Co(II) complexes that exhibit significant spin orbit coupling (SOC).¹⁵ The paramagnetic response of the tetrachlorocobaltate anion was modelled using $g_{\text{iso}} = 2.33$ ³³ and by constraining D and $|E/D|$ parameters to 0. Although the sign of D is not reliably obtained from fitting magnetic susceptibility data, the negative sign acquired from the fit is reasonable, given literature precedent of trigonal prismatic Co(II) systems as well as our computational results (Section 3.4.4).

The computed anisotropy parameters of *cations* **3-9A** and **3-10A** based on x-ray coordinates of **3-9** and **3-10** (Table 3.4.2) are comparable to those obtained from fits of the magnetic data in terms of sign as well as magnitude. With this protocol, we can show that the D value of **3-9A** (solely the cation, omitting CoCl_4^{2-}) is smaller in magnitude than **3-10A**; the discrepancy in magnitude between the obtained D value of **3-9** and the calculated value of **3-9A** likely arises from the omission of the dipolar interactions present in the salt.

3.4.3. AC Magnetic Properties of **3-9** and **3-10**

Although **3-9** and **3-10** both have coordination environments conducive to SMM properties, we found that **3-9** does not exhibit an out-of-phase ac susceptibility (χ'') response (Figure 3.4.4).

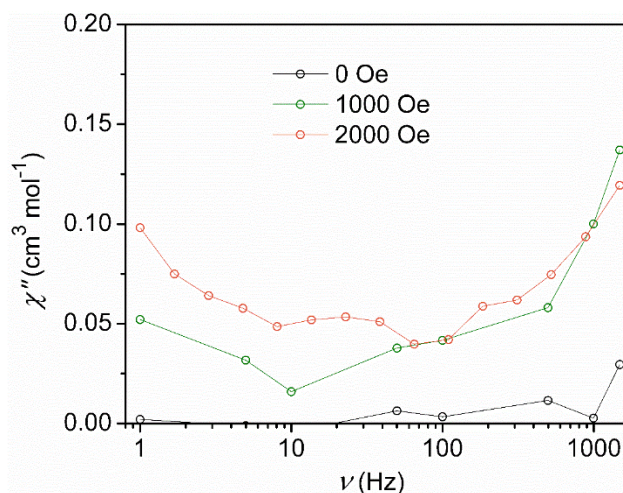


Figure 3.4.4. DC field scan of **3-9**. Application of 0, 1000 and 2000 Oe dc fields do not result in the detection of an out-of-phase (χ'') response (4 Oe oscillating field). Lines are guides for the eye.

Meanwhile, **3-10** shows slow magnetic relaxation both at zero field and under an applied external dc field (Figure 3.4.5). We attribute the lack of SMM properties in **3-9** mainly to dipolar interactions between the cation and the tetrachlorocobaltate anion, given the close intermolecular Co...Co distance of 5.862(1) Å, as has been detailed by Dunbar and coworkers,³⁴ though the smaller anisotropy value of the Co center in **3-9** may also play a role. The Co...Co is much larger in **3-10**, 14.864(6) Å.

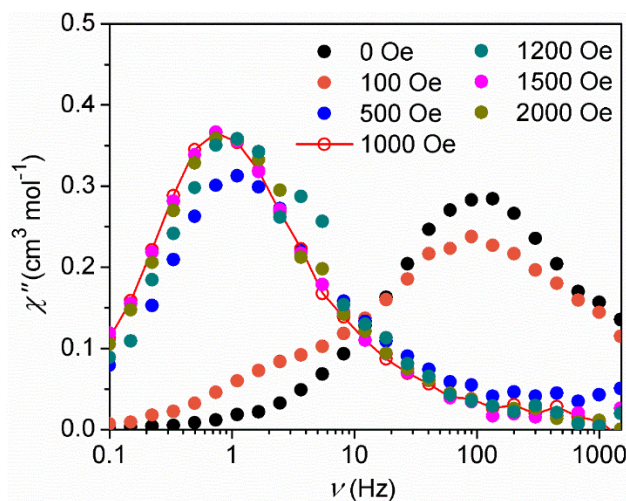


Figure 3.4.5. DC field scan of **3-10**. Optimal field is shown by solid red line (guide for the eye). Note the complete suppression of the higher frequency relaxation process upon application of sufficiently large dc field.

For **3-10**, we observe that the zero field $\chi''(\nu)$ response persists above 15 K (Figure 3.4.6, left). The temperature independence of χ'' maxima below ~ 5 K at zero field is characteristic of quantum tunneling of magnetization (QTM), while temperature dependence of magnetic dynamics is observed above 5 K. Application of a 1000 Oe dc field (Figure 3.4.6, right) quenches to a large extent the QTM, and reveals a slower temperature-dependent magnetic relaxation pathway. This slow relaxation is observed up to 15 K, though the maxima past 11 K are no longer detectable due to instrumental limitations.

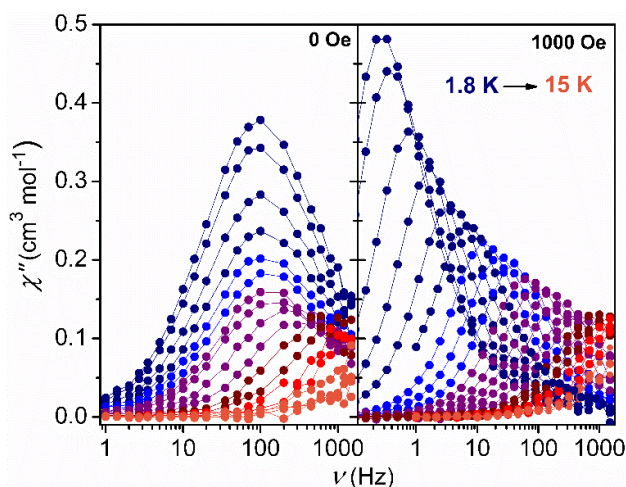


Figure 3.4.6. Out-of-phase magnetic susceptibility for compound **3-10**, collected at zero-applied dc field (left) and an applied dc field (1000 Oe, right) with an applied oscillating field of 4 Oe.

From the $\chi''(\nu)$ maxima, the temperature dependence of relaxation time, $\tau(T)$ is found and fit using the polynomial $\tau^{-1}(T) = AT^B + \tau_0^{-1}\exp(-U_{eff}/kT)$, where the two terms correspond to contributions from Raman and Orbach relaxation processes, respectively, and U_{eff} is the effective energy barrier for the relaxation process (Figure 3.4.7).

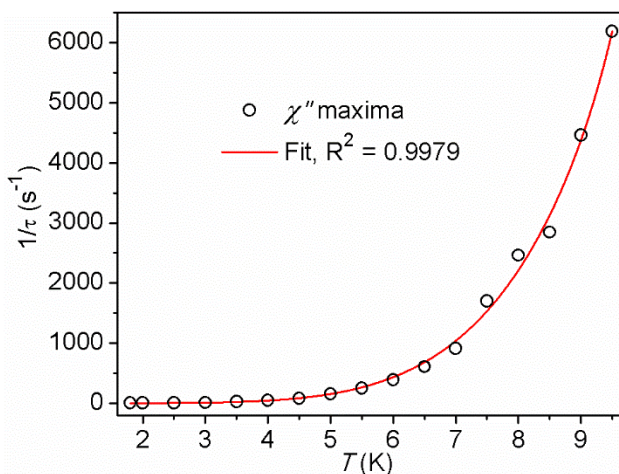


Figure 3.4.7. Fit of out-of-phase χ'' maxima (1000 Oe).

This analysis gives a value of $A = 0.053$, $B = 5$, $\tau_0 = 1.8 \times 10^{-7} \text{ s}^{-1}$ and $U_{eff} = 75.2 \text{ K}$; this barrier height is comparable to other Co(II) SMMs, but much lower than the anion-binding clathrochelate described by Novikov *et al.*, which also exhibited Raman and Orbach relaxation processes under an applied field.¹³ While performing this fit, inclusion of a term for a direct relaxation process results in a slightly better fit to the data ($R^2 = 0.99812$), however the values obtained for these parameters are physically unrealistic.

3.4.4. Theoretical Analysis of Anisotropy in Hexacoordinate System

In an effort to relate the anisotropy of these and related Co(II) systems with the torsion angle of the molecular structure, we can use HS $[\text{Co}(\text{NH}_3)_6]^{2+}$ as a model system to predict ZFS parameters for Co N_6 systems. With this treatment, we find that the axial anisotropy D varies greatly as a function of twisting the N-N-N planes; when the torsion is minimized, these values are large and negative, and the opposite is true for trigonal antiprismatic systems, where the D value is large and positive (Figure 3.4.8).

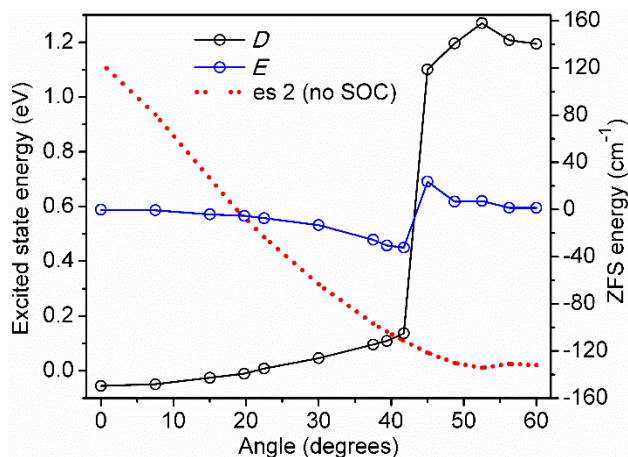


Figure 3.4.8. Calculated energy of the second excited state in $[\text{Co}(\text{NH}_3)_6]^{2+}$ and ZFS parameters (D , E) as a function of torsion angle.

The first excited state (es) is nearly degenerate with the ground state. Meanwhile, while the second es is sufficiently high in energy when the geometry is trigonal prismatic so as to not contribute significantly to the anisotropy of the system, twisting causes the energy of this state to drop and contribute significantly to D when octahedral. In all, this analysis supports our finding that a nearly trigonal prismatic system has a large negative D value and offers a platform for predicting anisotropies of Co systems based on their extent of trigonal distortion. For further information regarding this theoretical work, please consult the original publication and its supporting information (*Chem. Commun.* **2017**, 53, 4211).

3.5 Conclusions

Overall, we report two salts of a novel hexacoordinate tach-based iminopyridine Co(II) complex, **3-9** and **3-10**. Interestingly, **3-10** exhibits cationic guest association, counter to our original hypothesis that the pendant amide moieties would serve to bind anions. Whereas tetrachlorocobaltate **3-9** does not undergo slow relaxation of magnetization even under an applied dc field, the Na-bound tetraphenylborate salt **3-10** shows an out of phase ac response at both zero dc field and at 1000 Oe. We find that the rigidity of the tach backbone does not allow the cationic guest to impart significant distortion. The observation of new guest-binding modes informs the

design of externally-switchable magnetic materials, and further efforts to control host-guest interactions in Co(II) systems are underway.

3.6 Acknowledgments

This work was supported by Colorado State University and the NSF (CHE-1363274).

References

1. Frost, J. M.; Harriman, K. L. M.; Murugesu, M. *Chem. Sci.* **2016**, *7*, 2470.
2. Murrie, M. *Chem. Soc. Rev.* **2010**, *39*, 1986.
3. Herchel, R.; Váhovská, L.; Potočňák, I.; Trávníček, Z. *Inorg. Chem.* **2014**, *53*, 5896.
4. Zhang, Y.-Z.; Gomez-Cóca, S.; Brown, A. J.; Saber, M. R.; Zhang, X.; Dunbar, K. R. *Chem. Sci.* **2016**, *7*, 6519.
5. Chandrasekhar, V.; Dey, A.; Mota, A. J.; Colacio, E. *Inorg. Chem.* **2013**, *52*, 4554.
6. Vallejo, J.; Castro, I.; Ruiz-García, R.; Cano, J.; Julve, M.; Lloret, F.; De Munno, G.; Wernsdorfer, W.; Pardo, E. *J. Am. Chem. Soc.* **2012**, *134*, 15704.
7. Li, J.; Han, Y.; Cao, F.; Wei, R. M.; Zhang, Y. Q.; Song, Y. *Dalton Trans.* **2016**, *45*, 9279.
8. Villa-Pérez, C.; Oyarzabal, I.; Echeverría, G. A.; Valencia-Uribe, G. C.; Seco, J. M.; Soria, D. B. *Eur. J. Inorg. Chem.* **2016**, 4835.
9. Plenk, C.; Krause, J.; Rentschler, E. *Eur. J. Inorg. Chem.* **2015**, 370.
10. Wu, D. Y.; Zhang, X. X.; Huang, P.; Huang, W.; Ruan, M. Y.; Ouyang, Z. W. *Inorg. Chem.* **2013**, *52*, 10976.
11. Roy, S.; Oyarzabal, I.; Vallejo, J.; Cano, J.; Colacio, E.; Bauza, A.; Frontera, A.; Kirillov, A. M.; Drew, M. G. B.; Das, S. *Inorg. Chem.* **2016**, *55*, 8502.
12. Colacio, E.; Ruiz, J.; Ruiz, E.; Cremades, E.; Krzystek, J.; Carretta, S.; Cano, J.; Guidi, T.; Wernsdorfer, W.; Brechin, E. K. *Angew. Chem. Int. Ed.* **2013**, *52*, 9130.
13. Novikov, V. V.; Pavlov, A. A.; Nelyubina, Y. V.; Boulon, M. E.; Varzatski, O. A.; Voloshin, Y. Z.; Winpenny, R. E. P. *J. Am. Chem. Soc.* **2015**, *137*, 9792.
14. Karasawa, S.; Zhou, G. Y.; Morikawa, H.; Koga, N. *J. Am. Chem. Soc.* **2003**, *125*, 13676.
15. Zhu, Y. Y.; Cui, C.; Zhang, Y. Q.; Jia, J. H.; Guo, X.; Gao, C.; Qian, K.; Jiang, S. D.; Wang, B. W.; Wang, Z. M.; Gao, S. *Chem. Sci.* **2013**, *4*, 1802.
16. Peng, Y.; Bodenstein, T.; Fink, K.; Mereacre, V.; Anson, C. E.; Powell, A. K. *Phys. Chem. Chem. Phys.* **2016**, *18*, 30135.

17. Zhu, Y. Y.; Zhang, Y. Q.; Yin, T. T.; Gao, C.; Wang, B. W.; Gao, S. *Inorg. Chem.* **2015**, *54*, 5475.
18. Pavlov, A. A.; Nelyubina, Y. V.; Kats, S. V.; Penkova, L. V.; Efimov, N. N.; Dmitrienko, A. O.; Vologzhanina, A. V.; Belov, A. S.; Voloshin, Y. Z.; Novikov, A. V. *J. Phys. Chem. Lett.* **2016**, *7*, 4111.
19. McDaniel, A. M.; Klug, C. M.; Shores, M. P. *Eur. J. Inorg. Chem.* **2013**, 943.
20. Gomez-Cóca, S.; Cremades, E.; Aliaga-Alcalde, N.; Ruiz, E. *J. Am. Chem. Soc.* **2013**, *135*, 7010.
21. Bain, G. A.; Berry, J. F. *J. Chem. Educ.* **2008**, *85*, 532.
22. Chilton, N. F.; Anderson, R. P.; Turner, L. D.; Soncini, A.; Murray, K. S. *J. Comput. Chem.* **2013**, *34*, 1164.
23. *Apex 2*; Bruker Analytical X-Ray Systems, Inc.: Madison, WI, 2008.
24. G. M. Sheldrick *SHELXTL, Version 6.14*; Bruker Analytical X-Ray Systems, Inc.: Madison, WI, 1999.
25. Bowen, T.; Planalp, R. P.; Brechbiel, M. W. *Bioorg. Med. Chem. Lett.* **1996**, *6*, 807.
26. Davis, M. C. *Synth. Commun.* **2007**, *37*, 3519.
27. Bialecki, J. B.; Yuan, L.-H.; Gong, B. *Tetrahedron* **2007**, *63*, 5460.
28. Chen, L.; Wang, J.; Wei, J.-M.; Wernsdorfer, W.; Chen, X.-T.; Zhang, Y.-Q.; Song, Y.; Xue, Z.-L. *J. Am. Chem. Soc.* **2014**, *136*, 12213.
29. McDaniel, A. M.; Rappé, A. K.; Shores, M. P. *Inorg. Chem.* **2012**, *51*, 12493.
30. Wentworth, R. A. D.; Dahl, P. S.; Huffman, C. J.; Gillum, W. O.; Streib, W. E.; Huffman, J. C. *Inorg. Chem.* **1982**, *21*, 3060.
31. Beer, P. D.; Dent, S. W.; Wear, T. J. *J. Chem. Soc. Dalton Trans.* **1996**, 2341.
32. Greenwood, N. N.; Earnshaw, A. *Chemistry of the elements*; 2nd ed.; Butterworth-Heinemann, Oxford, Boston, 2nd ed., 1997.
33. Hillier, I. H.; Kendrick, J.; Mabbs, F. E.; Garner, C. D. *J. Am. Chem. Soc.* **1976**, *98*, 395.
34. Woods, T. J.; Ballesteros-Rivas, M. F.; Gómez-Coca, S.; Ruiz, E.; Dunbar, K. R. *J. Am. Chem. Soc.* **2016**, *138*, 16407.

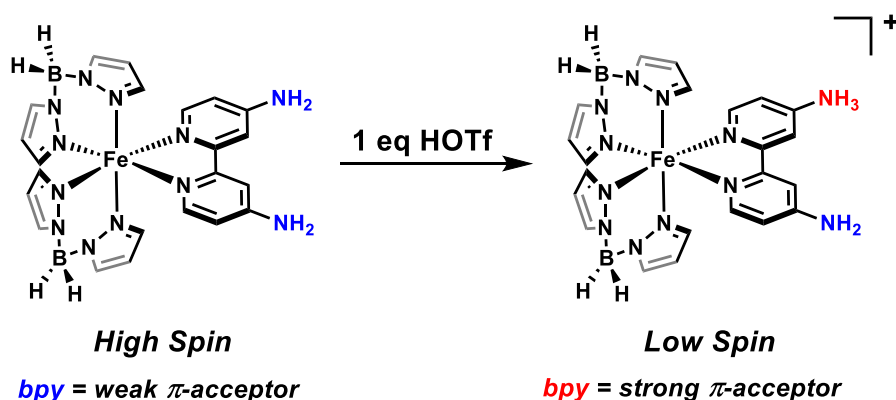
Chapter 4: Progress Toward Spin-State Switching Induced by Chemical Modifications to Ligands in an Fe(II) Tripodal System

4.1 Introduction

The ability to control spin in molecular systems has the potential to improve many types of devices with applications as sensors and memory devices.¹⁻³ Efforts to modulate the spin state in Fe(II) complexes have been multifaceted, and include modification of ligand steric hindrance⁴⁻⁹ as well as counter ion¹⁰⁻¹¹ and co-crystallized solvent.¹² This, of course, is due to the stark contrast in properties between the high spin (HS, $S = 2$) and low spin (LS, $S = 0$) states of the Fe(II) ion in an octahedral field (e.g., magnetism, absorptivity). As an example, progress has been made with regard to exploitation of hydrogen bonding for sensing applications with Fe(II) complexes in solution.¹³⁻¹⁵

One caveat of these sensing studies is that the binding of anions through hydrogen bonding interactions is in principle a reversible process. The use of irreversible post-synthetic modifications on Fe(II) systems could enable an alternative, more straightforward method for rapid analyte detection in solution; however, this remains underexplored in the field.¹⁶⁻¹⁹ Perhaps the most relevant examples of reversible spin switching in solution have used UV/visible light or protons as a “reagent-induced” spin switching triggers. In 2013, Khusniyarov and Oshio independently developed a diarylethene-based Fe system which showed reversible photoswitching between spin states caused by an electrocyclization event on the ligand.²⁰⁻²² More recently, Sun and Oshio demonstrated that a Fe complex bearing a 4,4'-diamino-2,2'-bipyridine ligand shifts from a HS to a LS state upon addition of triflic acid (Figure 4.1.1).²³

Scheme 4.1.1. Ligand protonation affects Fe(II) spin state in a 4,4'-diaminobpy system (ref. 23).



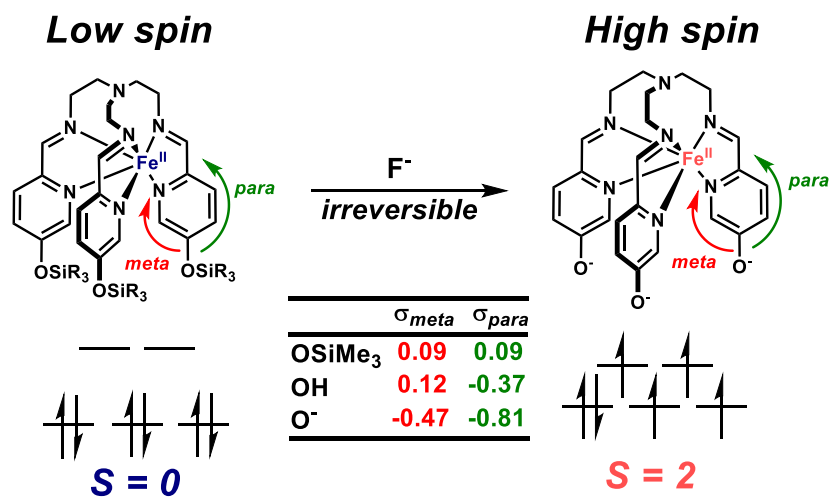
Previous studies concerning Hammett-type analyses of Fe(II) spin state have guided the rational development of sensing molecules.²⁴⁻²⁷ Several of these studies indicate that an increase in electron withdrawing character (more positive Hammett parameter, σ) at 4-pyridyl positions leads to stabilization of the LS state. This is rationalized as more electron withdrawing groups (EWG) will increase the π -accepting character of the ligand, stabilizing the t_{2g} orbitals to a greater extent than the e_g set, shifting $T_{1/2}$ to higher temperatures (where applicable in SCO systems).

In a study by Deeth and Halcrow concerning $[\text{Fe}(\text{bpp})_2]^{2+}$ systems (bpp = bis(pyrazolylpyridine)), subtle changes in electronics imparted significant changes in the spin state behavior of SCO Fe complexes. For example, the complex derived from a 4-Br substituted bpp ligand is HS, while the analogous 4-Cl system exhibits SCO ($T_{1/2} \sim 225$ K); the 4-NO₂ complex also undergoes SCO and has a $T_{1/2} \sim 300$ K. Thus, a relatively small change in electronic character (σ_{para} , Cl = 0.23; σ_{para} , NO₂ = 0.78)²⁸ can have a large effect on spin properties.

Previous studies from our group and others concerning ferrous podands derived from tris(2-aminoethyl)amine (tren) iminopyridines bearing 5-pyridyl substituents have shown high stability and singlet ground states in the absence of 6-pyridyl steric modifications.^{5-6, 29-30} Given the wealth of literature regarding this system, we aimed to install a fluoride-sensitive silyl ether moiety at the 5-position to generate a LS complex, which could ideally switch to a HS state upon

chemoselective reaction with fluoride. This might allow us to circumvent potential side reactivity with other reagents while enabling fluoride detection in solution (Figure 4.1.2).³¹

Scheme 4.1.2. Proposed method for spin state changing in Fe(II) podand complexes. Hammett values obtained from reference 28.²⁸



Thus, the large difference in electronics comparing a silyl ether to a corresponding phenoxide functional group (to a more negative σ value) could be sufficient to impart the envisioned spin-state change. Therefore, we set out to synthesize the two silyl ether-containing Fe podands (with and without 6-methylation) to evaluate the interplay of these effects on both LS and HS Fe(II) systems and the effect on Fe spin state during a desilylation reaction.

4.2 Division of Labor

The goal of using fluoride as a reagent trigger for desilylation-induced spin state switching was developed by Tarik Ozumerzifon and Matthew Shores. Design, synthesis and characterization of ligands were performed by Tarik Ozumerzifon. Crystallographic and magnetic characterizations of Fe complexes were also performed by Tarik Ozumerzifon. Electrochemical experiments were carried out by Robert Higgins. Desilylation and mass spectrometry experiments were carried out by Tarik Ozumerzifon and Robert Higgins.

4.3 Experimental Details

4.3.1. Materials and Methods

Synthetic Details: Reactions were performed under ambient conditions (room temperature, normal benchtop atmosphere) unless otherwise stated. Air-free manipulations were carried out in a dinitrogen filled glovebox (MBRAUN Labmaster 130). Qualitative thin layer chromatography (TLC) analysis was performed on 250 mm thick, 60 Å, glass backed, F254 silica (Silicycle, Quebec City, Canada). Visualization was accomplished using UV light. Flash chromatography was performed using Silicycle silica gel (230-400 mesh). Syringe filters were purchased from VWR International and were fitted with 0.2 µm PTFE membranes. Diethyl ether (Et₂O), dichloromethane (CH₂Cl₂) and acetonitrile (MeCN) were sparged with nitrogen, passed through an alumina column and degassed prior to use. Anhydrous ethanol (EtOH) and methanol (MeOH) were purchased from Sigma Aldrich. All other chemicals were purchased from commercial vendors and used as received.

General Characterization: ¹H NMR spectra were obtained on a Varian 400 MR spectrometer (at 400 MHz) and are reported relative to SiMe₄ (δ 0.00). ¹³C NMR spectra were obtained on a Varian 400 MR spectrometer (at 100 MHz) and are reported relative to SiMe₄ (δ 0.00). NMR acquisition sequences for metal species were changed to have a 1 ms relaxation delay, 90° pulse angle and acquisition time of 1 s. Elemental analyses were performed by Midwest Microlab, LLC in Indianapolis, IN.

Mass Spectrometry Measurements: Mass spectrometry samples were prepared in a dinitrogen filled glovebox and transported to the spectrometer in sealed vials prior to measurement, when they were exposed to air briefly (~3 s). Measurements were performed in the positive ion mode on a Thermo LTQ mass spectrometer equipped with an analytical electrospray ion source and a

quadrupole ion trap mass analyzer. Each measurement, unless otherwise noted, was performed with the capillary temperature = 175 °C, spray voltage = 5 kV and a spray current = 91 μA. All experiments were performed in methanol and the instrument was washed with 1 mL of solvent between scans. The peaks associated with Fe-containing complexes were identified and their relative abundances were summed into categories defined by loss of 0, 1, 2 or 3 TBS groups.

Electrochemical Measurements: Electrochemical experiments were performed in 0.1 M solutions of Bu₄NPF₆ in MeOH in a dinitrogen filled glovebox. Cyclic voltammograms (CVs) and square-wave voltammograms (SWVs) were obtained with a CH Instruments potentiostat (Model 1230A or 660C) using a 0.25 mm glassy carbon disk working electrode, Ag⁺/Ag reference electrode and a Pt wire counter electrode. Scans were collected at rates between 0.10 V s⁻¹ and 10 V s⁻¹ for CVs and at a step-size of 0.004 V and a frequency of 15 Hz for SWVs. Reported potentials are referenced to the [Cp₂Fe]⁺/[Cp₂Fe] (Fc⁺/Fc, where Cp = cyclopentadiene) redox couple, and were determined by adding ferrocenium tetrafluoroborate as an internal standard at the conclusion of each electrochemical experiment. Since all voltammograms were measured in MeOH, ferrocene could not be used as the internal standard as it is insoluble.

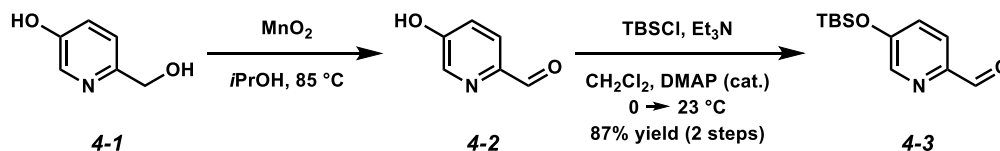
Crystallographic Measurements: Crystallographic parameters for [Fe(5-OTBSPy)₃tren](OTf)₂ **4-8** are listed in Table 4.3.1. All crystals were coated in Paratone oil for data collection. The crystals were supported on Cryoloops, and then mounted on a Bruker Kappa Apex 2 CCD diffractometer under a stream of dinitrogen. Mo Kα radiation and a graphite monochromator were used for data collection. Initial lattice parameters were determined from reflections found in 36 frames. Data sets were collected targeting complete coverage and threefold redundancy. Data were integrated and corrected for absorption effects with the APEX 2 software package.³² Structures were solved and refined with the SHELXTL software package.³³ Unless noted otherwise, thermal

parameters for all fully occupied, nonhydrogen atoms were refined anisotropically; hydrogen atoms were added at the ideal positions and were refined using a riding model where the thermal parameters were set at 1.2 times those of the attached carbon or nitrogen atom (1.5 times that for methyl protons).

Magnetic Measurements: DC magnetic data were collected for **4-9** using a Quantum Design MPMS XL SQUID magnetometer from 2 to 300 K and 0 to 20 kOe. In a dinitrogen-filled glovebox, powdered microcrystalline samples were loaded into polyethylene bags, sealed and inserted into drinking straws for measurements. Ferromagnetic impurities were checked through a variable field measurement (0 to 20 kOe) of the magnetization at 100 K; curvature in the M vs H data obtained between 0 and 2 kOe (Appendix 3) indicates the presence of ferromagnetic impurities. As a result, the magnetic susceptibility measurements were performed at a 5 kOe applied field, where the M vs H response was linear. Data were corrected for the diamagnetic contributions of the sample holder and bag by subtracting empty containers; corrections for the sample were calculated from Pascal's constants.³⁴ Evans' method determination of magnetic susceptibility in solution for **4-8** and **4-9** were carried out using SiMe_4 in a capillary as a reference.³⁵ The solution susceptibility of **4-9** during desilylation experiments was corrected for para/ferromagnetic impurities and temperature independent paramagnetism (TIP) according to the following equation: $\chi_{corr}(T) = (\chi_{raw} - \chi_{imp} - \chi_{TIP})(T)$. The para/ferromagnetic impurity was determined from the solid state susceptibility data (8%) and TIP subtracted was $6000 \times 10^{-6} \text{ cm}^3 \text{ mol}^{-1}$, as this gave values in agreement with a HS Fe(II) species with a g value of 2.11.²

4.3.2. Synthesis of Ligands and Fe Complexes

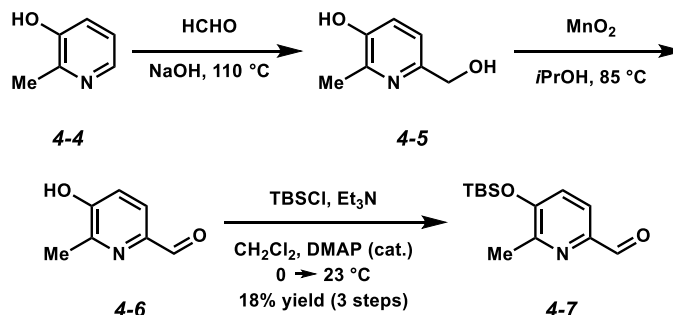
Diol **4-1** was synthesized according to Seredyuk *et al.*,⁵ with the only alteration being the use of 3M HCl (as opposed to concentrated HCl) to perform the last hydrolysis step to improve the yield.



Aldehyde 4-2. To a solution of diol **4-1** (1.17 g, 9.36 mmol) in $i\text{PrOH}$ (86 mL) was added MnO_2 (19.0 g, 220 mmol) and the resulting black suspension was refluxed for 24 h, until TLC analysis showed complete consumption of the starting material. Then, the reaction was filtered through Celite and subjected to centrifugation to pellet the excess MnO_2 . The supernatant was removed, and this extraction process was repeated with $i\text{PrOH}$ ($3 \times 15\text{ mL}$ per tube) until all crude **4-2** was extracted from the pellet as determined by TLC. The combined supernatants were then concentrated *in vacuo* to give crude **4-2**, which was used without further purification.

Silyl ether 4-3. Crude **4-2** (9.36 mmol, assumed), *tert*-butyldimethylchlorosilane (TBSCl, 3.00 g, 19.9 mmol) and *N,N*-dimethylaminopyridine (DMAP, 0.220 g, 1.8 mmol) were charged to a flame-dried flask, then dissolved in CH_2Cl_2 (36 mL) and cooled to $0\text{ }^\circ\text{C}$. Then, freshly distilled triethylamine (3.00 mL, 21.7 mmol) was added dropwise and the reaction was allowed to warm to $23\text{ }^\circ\text{C}$ and stirred for 1 h. The reaction mixture was then quenched with water, poured into a separatory funnel, and extracted with CH_2Cl_2 ($2 \times 20\text{ mL}$), washed with brine (20 mL), dried over MgSO_4 and filtered to give crude **4-3**. The desired compound was purified by flash column chromatography (4:1 hexanes:EtOAc eluent) to give pure silyl ether **4-3** (1.93 g, 87% yield over two steps, $R_f = 0.65$ in 4:1 hexanes:EtOAc) as a pale yellow oil.

Silyl ether 4-3: ^1H NMR (400 MHz, CDCl_3): δ 9.99 (s, 1H), 8.34 (d, $J = 2.3$ Hz, 1H), 7.91 (d, $J = 8.6$ Hz, 1H), 7.25 (app. dd, $J = 2.3$ Hz, 1H), 1.00 (s, 9H), 0.28 (s, 6H); ^{13}C NMR (100 MHz, CDCl_3): δ 192.0, 156.1, 146.7, 142.9, 126.8, 123.2, 25.5, 18.2, -4.4; IR (film): 2956, 2931, 2859, 1710, 1574, 1478, 1391, 1363, 1292, 1257, 1210, 1111, 1013 cm^{-1} ; HRMS (ESI $^+$): m/z calcd for $(\text{M} + \text{H})^+$ [$\text{C}_{12}\text{H}_{20}\text{NO}_2\text{Si} + \text{H}$] $^+$: 238.1263, found 238.1242.



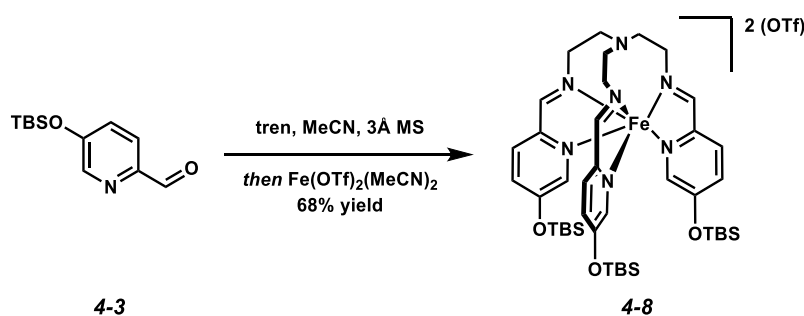
Diol 4-5. Following the procedure reported by Seredyuk, *et al.*,⁵ 3-hydroxy-2-methylpyridine **4-4** (5.12 g, 46.9 mmol) was dissolved in 10% aqueous NaOH (310 mL) and H_2O (150 mL), and then a solution of 37% aqueous formaldehyde (50 mL) was added and the resulting mixture was refluxed for 2 h. Then, the reaction was cooled and another portion of formaldehyde (50 mL) was added, and the reaction was heated at reflux for 10 h. After consumption of starting material as determined by TLC, the reaction was neutralized with conc. aq. HCl, and the solvent was removed *in vacuo*, giving crude diol **4-5**. The crude mixture was redissolved in *i*PrOH and was filtered to remove insoluble materials, then used without further purification.

Aldehyde 4-6. To a solution of crude diol **4-5** (6.53 g, 46.9 mmol, assumed) in *i*PrOH (200 mL) was added MnO_2 (40.8 g, 470 mmol) and the resulting black suspension was refluxed for 24 h, until the starting material was fully consumed (monitored by TLC). Then, the reaction was filtered through Celite and the filtrate was subject to centrifugation to remove MnO_2 , continuing this extraction process with *i*PrOH until all crude **4-6** was removed from the pellet as determined by

TLC. The combined supernatants were concentrated *in vacuo* to give crude **4-6**, which was used without further purification.

Silyl ether 4-7. Crude **4-6**, TBSCl (2.22 g, 14.7 mmol) and DMAP (0.160 g, 1.33 mmol) were charged to a flame dried flask, then dissolved in dichloromethane (27 mL) and cooled to 0 °C. Then, freshly distilled triethylamine (2.24 mL, 16.1 mmol) was added dropwise and the reaction was allowed to warm to 23 °C and stir for 1 h. The reaction mixture was then quenched with water, poured into a separatory funnel, and extracted with dichloromethane (2 × 20 mL), washed with brine (20 mL), dried over MgSO₄ and filtered to give crude **4-7**. The desired compound was purified by flash column chromatography (4:1 hexanes:EtOAc eluent) to give pure silyl ether **4-7** (2.13 g, 18% yield over three steps, R_f = 0.67 in 4:1 hexanes:EtOAc) as a pale yellow oil.

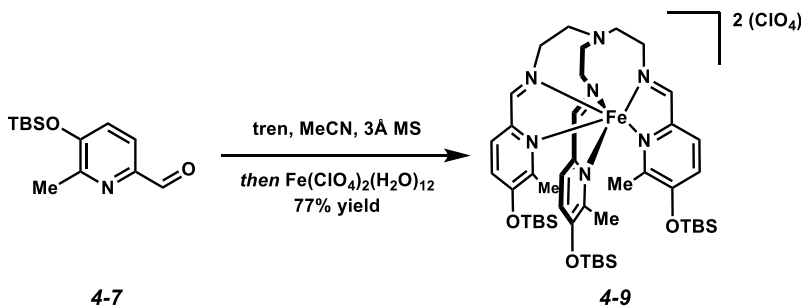
Silyl ether 4-7: ¹H NMR (400 MHz, CDCl₃): δ 9.95 (s, 1H), 7.76 (d, *J* = 8.2 Hz, 1H), 7.12 (d, *J* = 8.2 Hz, 1H), 2.53 (s, 3H), 1.03 (s, 9H), 0.28 (s, 6H); ¹³C NMR (100 MHz, CDCl₃): δ 192.3, 154.2, 152.0, 145.5, 124.3, 121.4, 25.5, 19.8, 18.2, -4.3; IR (film): 2956, 2931, 2859, 1702, 1566, 1456, 1347, 1303, 1278, 1257, 1245, 1170, 1112 cm⁻¹; HRMS (ESI⁺): *m/z* calcd for (M + H)⁺ [C₁₃H₂₂NO₂Si + H]⁺: 252.1420, found 252.1391.



[Fe(5-OTBSpy)₃tren](OTf)₂ 4-8. In a dinitrogen filled glovebox, to a solution of **4-3** (0.200 g, 0.84 mmol) in MeCN (2 mL) was added a solution of tren (0.040 g, 0.27 mmol) in MeCN (2 mL) and the resulting mixture was stirred in the presence of 3Å molecular sieves for 1 h at 23 °C. Then, a solution of Fe(OTf)₂(MeCN)₂ (0.119 g, 0.27 mmol) in MeCN (2 mL) was added dropwise and

the resulting dark red mixture was stirred for an additional 1 h at 23 °C. The reaction mixture was then passed through a syringe filter, and the desired Fe complex was precipitated by addition of Et₂O (20 mL) and stirred overnight. The suspension was then filtered and washed with Et₂O (2 × 5 mL) to afford **4-8** (0.215 g, 68% yield) as a dark red powder. Diffraction quality crystals were grown by diffusion of *i*Pr₂O into a concentrated solution of **4-8** in acetonitrile.

[Fe(5-OTBSPy)₃tren](OTf)₂ 4-8: MS (ESI⁺) *m/z* calcd for (M - OTf)⁺ [C₄₄H₆₉N₇O₉Si₃S₂F₆Fe - CF₃SO₃]⁺: 1008.36, found 1008.33, *m/z* calcd for (M - 2OTf)²⁺ [C₄₄H₆₉N₇O₉Si₃S₂F₆Fe - C₂F₆S₂O₆]²⁺: 429.71, found 429.83; Anal. calcd (C₄₄H₆₉N₇O₉Si₃S₂F₆Fe + 1.5C₂H₃N): C 46.28% H 6.07% N 9.76%, found C 45.83% H 5.65% N 10.09%; χ_{MT} (298 K, (CD₃)₂CO): 0.17 cm³ K mol⁻¹.



[Fe(6-Me-5-OTBSPy)₃tren](ClO₄)₂ 4-9. In a dinitrogen glovebox, to a solution of **4-7** (0.100 g, 0.40 mmol) in MeCN (2 mL) was added a solution of tren (0.019 g, 0.13 mmol) in MeCN (2 mL) and the resulting mixture was stirred in the presence of 3Å molecular sieves for 1 h at 23 °C. Then, a solution of Fe(ClO₄)₂(H₂O)₁₂ (0.060 g, 0.13 mmol) in MeCN (2 mL) was added dropwise and the resulting red mixture was stirred for an additional 1 h at 23 °C. The reaction mixture was then passed through a syringe filter, and the desired Fe complex was precipitated by addition of Et₂O (20 mL), stirred overnight and filtered to obtain crude **4-9**. The crude Fe complex was crystallized by placing a concentrated solution of **4-9** in ethanol into a freezer (-40 °C) overnight, giving pure

4-9 (0.109 g, 77% yield) as red needle-like crystals that are too brittle for single crystal x-ray structure determination.

Caution! While we have not encountered any difficulties with compound **4-9** at the scale described here, perchlorate salts are potentially explosive and should be handled in a careful manner in small quantities.

[Fe(6-Me-5-OTBSpy)₃tren](ClO₄)₂ 4-9: MS (ESI⁺) *m/z* calc'd for (M - ClO₄)⁺ [C₄₅H₇₅N₇O₁₁Cl₂Si₃Fe - ClO₄]⁺: 1000.41, found 1000.42, *m/z* calc'd for (M - 2ClO₄)²⁺ [C₄₅H₇₅N₇O₁₁Cl₂Si₃Fe - Cl₂O₈]²⁺: 450.73, found 450.75; Anal. calc'd (C₄₅H₇₅N₇O₁₁Cl₂Si₃Fe): C 49.09% H 6.87% N 8.90%, found C 48.94% H 6.75% N 8.97%; χ_{MT} (298 K, (CD₃)₂CO): 3.44 cm³ K mol⁻¹.

4.3.3 Crystallographic Results

Podand **4-8** was crystallographically characterized, showing the Fe atom is located within the N₆ pocket of the iminopyridine ligand (Figure 4.3.1).

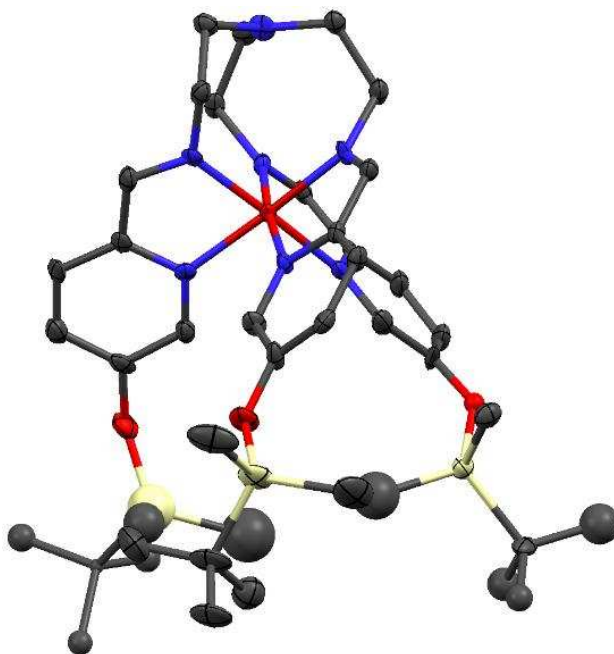


Figure 4.3.1. Crystal structure of the cationic complex **4-8**. Brick, grey, blue, red and beige ellipsoids represent Fe, C, N, O and Si atoms, respectively (40% probability).

The structure contains significant disorder within two of the arms, specifically regarding the TBS groups. There is positional disorder associated with one of the O atoms and this results in all Si and C atoms on this TBS group to be disordered over two positions. Another arm exhibits disorder within its Si and C atoms (over two positions). Thus, thermal parameters for nine carbons, one silicon and one oxygen in the main residue were refined isotropically. Nonetheless, the formation of the desired podand **4-8** is observed. Remaining crystallographic parameters of interest are listed in Table 4.3.1.

Table 4.3.1. Crystallographic parameters for **4-8**.^a

4-8	
Formula	C ₄₄ H ₆₉ F ₆ FeN ₇ O ₉ S ₂ Si ₃
Formula weight	1158.30
Color, habit	red block
<i>T</i> (K)	120
Space group	<i>P</i> 2 ₁ / <i>c</i>
<i>Z</i>	4
<i>a</i> (Å)	20.875(4)
<i>b</i> (Å)	19.541(4)
<i>c</i> (Å)	14.499(3)
α (°)	90
β (°)	105.91(3)
γ (°)	90
<i>V</i> (Å ³)	5688(2)
<i>d</i> _{calc} (g cm ⁻³)	1.353
GOF	1.259
<i>R</i> ₁ , <i>wR</i> ₂ ^b (%)	12.54, 28.32

^aObtained with graphite-monochromated Mo K α ($\lambda = 0.71073$ Å) radiation.

^b $R_1 = \sum ||F_o| - |F_c|| / \sum |F_o|$, $wR_2 = \{ \sum [w(F_o^2 - F_c^2)^2] / \sum [w(F_o^2)^2] \}^{1/2}$ for $F_o > 4\sigma(F_o)$.

4.4 Results and Discussion

4.4.1. Synthesis and Characterization of Fe Podands

The tripodal complexes **4-8** and **4-9** are prepared by first condensing the appropriate aldehyde (**4-3** or **4-7**, respectively) with tren and subsequent addition of the appropriate ferrous salt (Section 4.3.2). The use of iron(II) perchlorate is necessary in order to purify **4-9**; attempts to crystallize other salts (triflate, chloride, bromide, tetraphenylborate, tetrafluoroborate) of this

podand did not yield high purity material. The bulk purity of **4-8** and **4-9** have been confirmed through ESI-MS and elemental analyses.

Structural characterization of **4-8** was also accomplished (Figure 4.3.1), indicating that it crystallizes in the monoclinic space group $P2_1/c$. Further, NMR experiments indicate that **4-8** is LS at room temperature (298 K), therefore the solid state magnetic susceptibility data were not collected for this species. On the other hand, the 6-methylated species **4-9** shows a paramagnetic response consistent with a HS Fe(II) species at room temperature, as expected.^{4-6, 8-9} The temperature dependence of the magnetic susceptibility for **4-9** (Figure 4.4.1) also indicates that the species undergoes SCO.

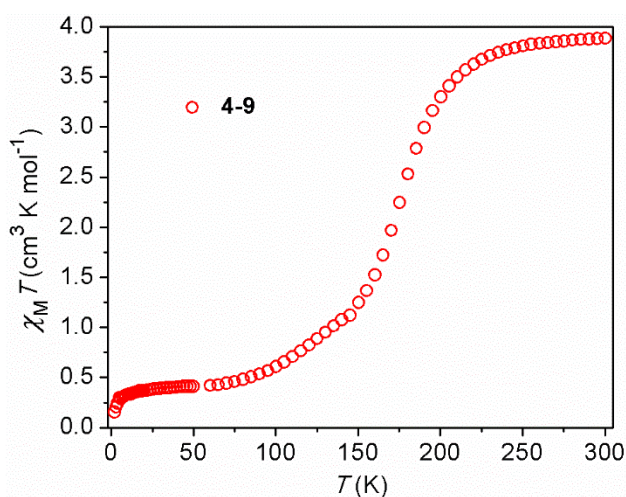


Figure 4.4.1. Temperature dependence of magnetic susceptibility for **4-9** measured with an applied dc field of 5000 Oe.

At 300 K, the $\chi_M T$ value for **4-9** is $3.89 \text{ cm}^3 \text{ K mol}^{-1}$, in agreement with a high spin Fe(II) complex ($S = 2$). Upon decreasing the temperature, the $\chi_M T$ product decreases slightly until ~ 215 K, where the decrease becomes more pronounced, indicative of a spin crossover (SCO) event ($T_{1/2} = 175$ K). This decrease continues until ~ 120 K where the $\chi_M T$ product begins to level out at $0.40 \text{ cm}^3 \text{ K mol}^{-1}$. The uncorrected magnetic susceptibility does not reach $0 \text{ cm}^3 \text{ K mol}^{-1}$ because of a paramagnetic impurity that is not separable from **4-9**, which is fairly common for Fe(II) SCO

materials.^{21, 36} The $T_{1/2}$ and low temperature magnetic susceptibility behavior observed here are consistent with other 6-methylated 5-alkoxy Fe(II) tren podands which undergo SCO behavior in the solid state.⁵⁻⁶

4.4.2. Mass Spectrometry and NMR Analysis of Desilylation Reaction

After establishing the identity and magnetic properties of **4-8** and **4-9**, we turned to probing the effects of desilylation on Fe spin state. In order to assess the physical changes that are occurring, several techniques must be employed due to the challenging nature of characterizing the species being formed. Therefore, *in situ* mass spectrometry, NMR and electrochemistry experiments of the desilylation reaction using CsF were performed.

The choice of fluoride source is critical for these experiments. At first, tetrabutylammonium triphenyldifluorosilicate (TBAT) was chosen because of its solubility in relatively aprotic solvents (*e.g.* tetrahydrofuran, acetonitrile). Unfortunately, addition of TBAT to solutions of **4-8** and **4-9** causes immediate decomposition, as evidenced by the most abundant peaks in the mass spectra showing demetalation of the complexes and a change in color to a pale yellow (Figure A3.15-A3.16). Therefore, CsF in methanol (for solubility) is employed, as preliminary mass spectrometry experiments show desilylation of the ligand without excessive demetalation (Figure 4.4.2).

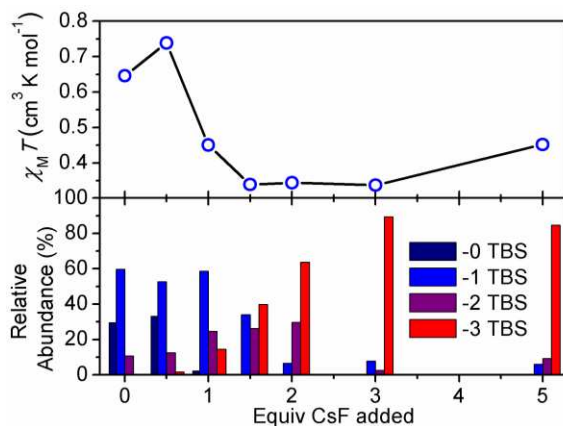


Figure 4.4.2. Top: solution state magnetic properties for **4-8** upon addition of CsF. Bottom: relative abundance of Fe-containing desilylated ions, as determined by mass spectrometry for **4-8**.

Even when no CsF is added, the major peaks in the mass spectrum that are observed for **4-8** indicate desilylation on one podand arm (-1 TBS). This observation indicates that even for soft ionization techniques such as ESI, the silyl ether moieties on the podand are quite labile. To our delight, upon addition of CsF, a greater extent of desilylation is seen, as the relative abundance of peaks associated with the loss of multiple TBS groups increases (-2 and -3 TBS). However, as increasing equivalents of CsF are added, decreased signal intensity of fewer species is observed, which presumably occurs for two different reasons. First, the addition of fluoride produces more neutral species in solution (e.g., a bis(desilylated) species bearing two phenoxides), and these neutral species should not ionize as readily as salts in an MS experiment. Second, desilylation would cause a large change in electronics about the iron center, likely causing the complex to be unstable and therefore inducing further reactivity, or eventual decomposition. Based on the mass spectrometry data obtained, it does not appear that complete desilylation is achieved even after the addition of five equivalents of CsF. A complete identification of all major species detected is provided in Table A3.1.

When the analogous reaction is performed with **4-9**, the mass spectrometry data indicate that only fully desilylated species are detected after 1.5 equivalents of CsF are added (Figure 4.4.3).

Upon further addition of CsF, bis-desilylated species are once again detected, however this observation is concomitant with loss of signal, suggesting that **4-9** may be decomposing further. The complete desilylation that is observed for **4-9** is perhaps unsurprising, given that its high-spin nature makes it more reactive.³⁷⁻³⁸ Additionally, fluoride cleavage may be superstoichiometric, in that it may generate a species that can also affect desilylation. An identification of all major species detected is provided in Table A3.2.

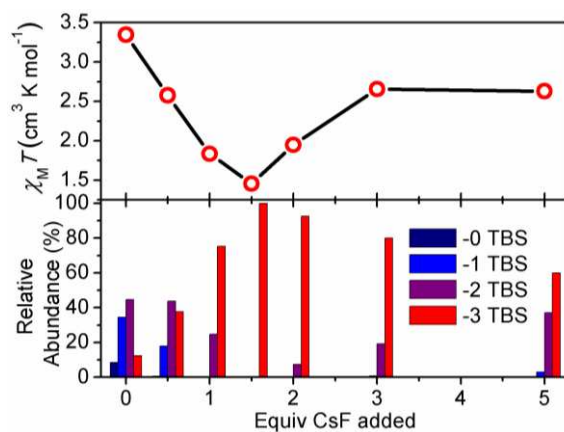


Figure 4.4.3. Top: solution state magnetic properties for **4-9** upon addition of fluoride. Bottom: relative abundance of desilylated products as determined by mass spectrometry for **4-9**.

Using Evans' method to determine the solution magnetic susceptibility of the samples, there is a decrease in $\chi_M T$ for both **4-8** and **4-9** upon addition of CsF; however, after 1.5 equivalents, the $\chi_M T$ values increase, which we attribute to decomposition of the samples. Of particular note is the discrepancy is observed $\chi_M T$ value of **4-9** when measured in MeOH (uncorrected) versus *d*₆-acetone (raw) (5.58 vs. 3.44 cm³ K mol⁻¹), indicating that this species exhibits decomposition shortly after solubilizing in MeOH. These results suggest that an increase in electron donating character of the 5-position substituent likely increases the ligand field (Δ), and thus affects the spin state. Previous reports in which post synthetic modifications have been performed on Fe(II) species have also described a propensity for decomposition.¹⁶⁻¹⁸ Considering the reactions being

performed in these other studies were arguably milder in nature with respect to change in ligand electronics (additions of alcohols into isocyanates, peptide couplings), we would expect our species to be less stable due to the drastic change in electronics of the ligand.

An in-depth analysis of the NMR spectra of the desilylation reactions of **4-8** offers additional insight into the speciation in solution. First, there are several sets of aromatic peaks associated with the pyridines present prior to addition of CsF and up until the addition of 3 equivalents (Figure A3.28). This suggests there may be multiple species present in solution until sufficient CsF has been added to induce complete cleavage of the silyl moiety, where the spectra indicate only one major species. Further, upon addition of CsF, the relative integration of the peaks associated with the TBS moiety relative to the aromatic region decreases, indicating that this group is being cleaved from the system. This analysis is more difficult with **4-9** as the spectra are extended over a larger range (δ -14 to 173 ppm).

4.4.3. Electrochemistry of **4-8** and **4-9**

In order to further assess the stability of the silylated podands, the electrochemical properties are probed in MeOH. The $E_{1/2}$ values for the Fe^{III/II} couple for **4-8** and **4-9** are +0.95 and +0.97 V vs Fc⁺/Fc, (as obtained from SWV measurements, Figures A3.20 and A3.22) respectively. These values compare well to $E_{1/2}$ values for the Fe^{III/II} couple in previously characterized Fe(II) iminopyridine tripodal systems.^{4, 30, 39} Compound **4-8** displays reversibility for the Fe^{III/II} couple at a scan rate of 0.10 V s⁻¹, whereas **4-9** shows seemingly irreversible behavior at the same scan rate (Figure 4.4.4). Upon increasing the scan rate to 10 V s⁻¹, the CV shows increased current being passed, thus **4-9** begins to show more reversible behavior, so this event is best described as quasi-reversible. Our group has reported that the 5-methylcarboxylated [FeL^{5-OOMe}](OTf)₂ compound

shows full reversibility;³⁰ however, Drago and others described the Fe^{III/II} couple the 6-methylated [FeL^{6-Me}](PF₆)₂ compound as only quasi-reversible.⁴

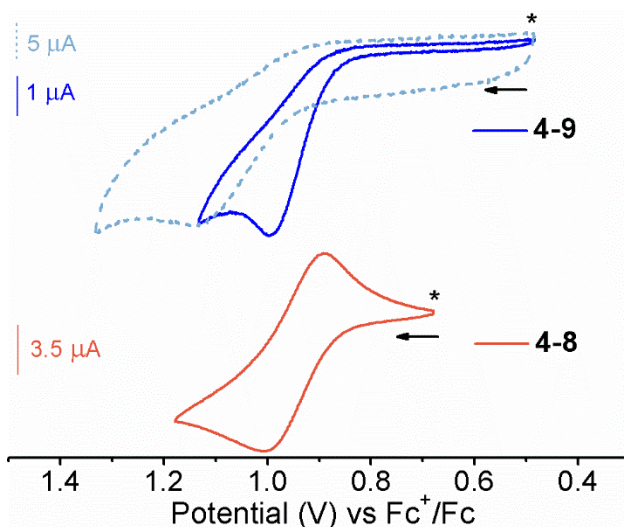


Figure 4.4.4. Cyclic voltammograms of **4-8** (bottom) and **4-9** (top) measured in 0.10 M Bu₄NPF₆ solutions in MeOH with scan rates of 0.10 V s⁻¹ (solid) or 10 V s⁻¹ (dashed). The asterisks indicate the open circuit potential while the arrows indicate the direction of the scan, which in all cases is anodic.

We rationalize the lack of electrochemical reversibility for **4-9** as arising from two separate but related considerations. First, the steric bulk imparted by the methyl substituents makes the formation of an Fe(III) species that has inherently shorter M-L lengths – ionic radii of 6-coordinate Fe(II) HS: 0.780 Å, Fe(III) LS: 0.55 Å, Fe(III) HS: 0.645 Å⁴⁰ – less favorable and likely induces further reactivity of the oxidized compound. Second, oxidation of the high spin d⁶ configuration likely results in an unstable species because the electron that is removed presumably resides in the e_g* set, giving an electronic configuration of t_{2g}⁴e_g*¹, which is extremely uncommon for non-heme octahedral Fe complexes,⁴¹⁻⁴² likely causing immediate relaxation of the e_g* electron to t_{2g} set. This would involve spin-flip and electron pairing energies, which could once again cause further side reactivity of the (transient) ferric complex.

Interestingly, after the addition of CsF into the electrochemical cell for **4-8**, the assigned Fe^{III/II} redox event shifts cathodically and maintains some reversibility (Figure 4.4.5). This result

likely indicates that a desilylated major species is formed in this experiment as the drastic shift in redox potential can be attributed to the large change in electronic properties of the substituent. Meanwhile, when CsF is added to the electrochemical cell for **4-9**, no redox events associated with an iron species are observed. These results also corroborate the greater stability of an iron-containing product derived from **4-8** upon desilylation.

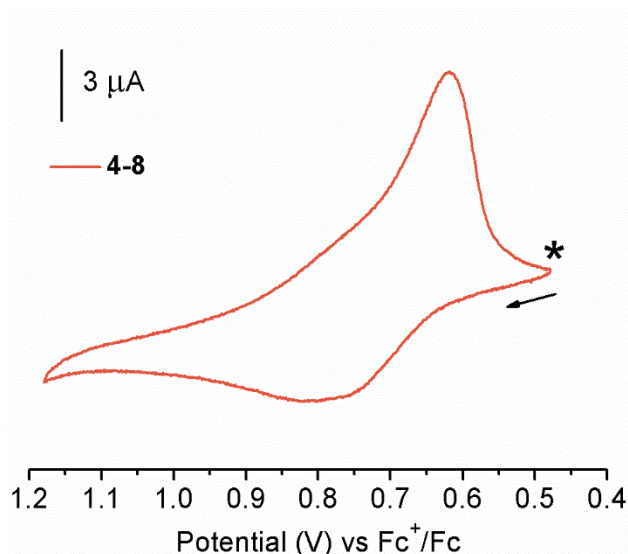


Figure 4.4.5. CV of **4-8** measured in a 0.10 M Bu₄NPF₆ solution of methanol with a scan rate of 0.10 V s⁻¹ after addition of excess CsF. The asterisk indicates the open circuit potential and the arrow indicates the direction of the scan.

To further assess the stability of **4-8** in solution, time-dependent electrochemical experiments are performed (Figure 4.4.6). This is probed by stirring **4-8** in a MeOH solution for extended periods of time. Comparing with the results shown in Figure 4.4.4, in as quickly as two hours, it is evident that some decomposition of **4-8** has occurred as additional redox events can be observed in the anodic regime. These are presented with caveat that the stability of **4-8** may differ between a methanolic solution and the salt solution in an electrochemical cell. The extent of decomposition increases significantly over time, however it is clear that after 2 h, the major species present is still **4-8**, while after 41 hours almost no signal attributed to the Fe^{III/II} event for **4-8** is observable. Additionally, after 25 hours of stirring an open circuit potential cannot be determined

as the recorded value fluctuates over a large potential regime, indicating that multiple species are present in solution. For consistency, each data set collection was begun at 0 V before referencing to Fc^+/Fc .

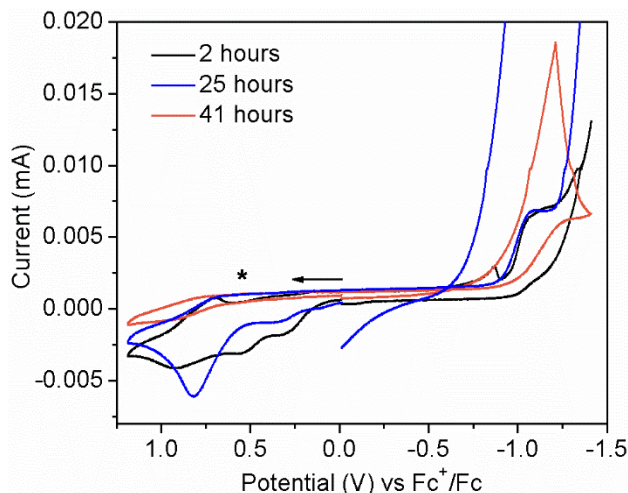


Figure 4.4.6. Electrochemical data for **4-8** at ~ 0.001 M in a 0.1 M Bu_4NPF_6 MeOH solution scanning at 0.1 V s^{-1} . The asterisk indicates the open circuit potential for the data after 2 h of stirring the electrochemical cell (black trace).

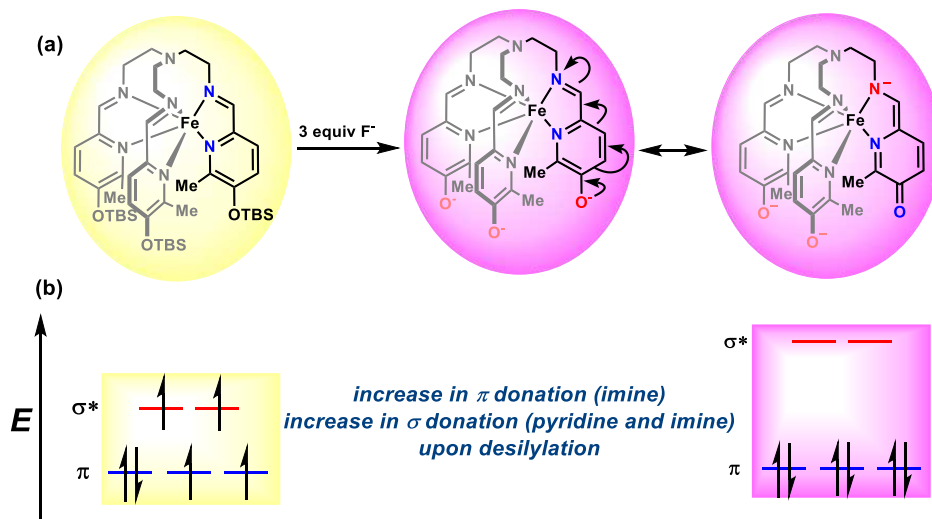
In all, these electrochemical data combined with the observation of desilylated species in the MS data when no CsF has been added, as well as the discrepancy between $\chi_{\text{M}}T$ values in MeOH vs. acetone suggest that these compounds are indeed quite sensitive to desilylation. This proves to be a double-edged sword, as functional group lability is crucial to accomplish reagent-induced spin state switching, but the solubility-driven requirements of this system prove inherently incompatible to achieve the desired chemoselective reactivity.

4.4.4. Discussion of Desilylation Reaction

We rationalize the observed stabilization of the LS state upon desilylation as the increase in electron density on the ligand should lead to an inductive effect which strengthens M-L σ donation, strengthening the ligand field. However, due to the bidentate nature of the iminopyridine arm, both the “*meta*” (pyridine) and “*para*” (imine) contributions from the (silyl) substituent must be considered separately. For instance, in the expected reaction where fluoride affects removal of

the TBS group(s), resonance delocalization of the resultant anionic ligand gives the imine nitrogen partial amide (N^- , X-type) character, increasing the π -donating ability at this site. This would cause a decrease in ligand field strength; however, considering the pyridyl portion of the ligand, upon desilylation there is no ability to delocalize the anionic charge on the pyridine N-atom. The effect on this N is therefore primarily an enhancement of the σ donating character, and since we observe a decrease in χ_{MT} value upon desilylation, this implies the “*meta*” effects on the pyridine are stronger than the “*para*” (imine N-atom) effects. This is consistent with the explanation given by Halcrow regarding the spin state properties of the $[Fe(bpp)_2]^{2+}$ system.⁴³

Scheme 4.4.1. (a) Depiction of ligand desilylation and (b) the effect on relative energies of metal d orbitals.



However, electrostatics must also be considered, as placing an anionic charge on the ligand will inherently destabilize the ligand orbitals required for σ overlap with the Fe bonding d orbitals, allowing for better overlap and favoring a LS state. This notion is supported by electrochemical experiments which indicate that an assigned “ $Fe^{3+/2+}$ couple” shifts cathodically upon addition of CsF to an electrochemical cell containing **4-8**. Thus, while it is difficult to separate the contributions of electrostatic and ligand field considerations in this system, as both are likely operative during this desilylation reaction, an overall stabilization of the LS state is observed.

4.5 Conclusions

This study probes whether a large change in electronic nature of the ligand around an Fe(II) center can impart a spin state change. Our results indicate that upon desilylation of **4-8** and **4-9**, a shift toward a lower overall spin state occurs, which is hypothesized to be a result of an increase in σ donating capability of the ligand. This observation is also accompanied by decomposition of the species, which casts doubt on the utility of these compounds as possible sensors. Notwithstanding, this is a scarcely investigated phenomenon which could lead to novel metal-organic scaffolds as spin state switching materials. Future directions are aimed at dampening the electronic change on the ligand to avoid decomposition of the Fe compound, while still imparting a spin state change.

4.6 Acknowledgments

This work is supported by Colorado State University and the NSF (CHE-1363274). We also thank the central instrument facility for assistance with mass spectrometry analysis and Dr. Jacek Kolanowski (University of Sydney) for helpful discussions.

References

1. Létard, J.-F.; Guionneau, P.; Goux-Capes, L. *Top. Curr. Chem.* **2004**, *235*, 221.
2. Halcrow, M. A. *Spin-crossover materials: properties and applications*; Wiley: West Sussex, UK, 2013.
3. Gütllich, P.; Gaspar, A. B.; Garcia, Y. *Beilstein J. Org. Chem.* **2013**, *9*, 342.
4. Hoselton, M. A.; Wilson, L. J.; Drago, R. S. *J. Am. Chem. Soc.* **1975**, *97*, 1722.
5. Seredyuk, M.; Gaspar, A. B.; Ksenofontov, V.; Galyametdinov, Y.; Kusz, J.; Gütllich, P. *J. Am. Chem. Soc.* **2008**, *130*, 1431.
6. Seredyuk, M.; Muñoz, M. C.; Ksenofontov, V.; Gütllich, P.; Galyametdinov, Y.; Real, J. A. *Inorg. Chem.* **2014**, *53*, 8442.
7. Fatur, S. M.; Shepard, S. G.; Higgins, R. F. Shores, M. P.; Damrauer, N. H. *J. Am. Chem. Soc.* **2017**, *139*, 4493.
8. Schultz, D.; Nitschke, J. R. *Angew. Chem. Int. Ed.* **2006**, *45*, 2453.
9. Schenker, S.; Hauser, A.; Wang, W.; Chan, I. Y. *J. Chem. Phys.* **1998**, *109*, 9870.
10. Lazar, H. Z.; Forestier, T.; Barrett, S. A.; Kilner, C. A.; Létard, J.-F.; Halcrow, M. A. *Dalton Trans.* **2007**, 4276.
11. Klug, C. M.; McDaniel, A. M.; Fiedler, S. R.; Schulte, K. A.; Newell, B. S.; Shores, M. P. *Dalton Trans.* **2012**, *41*, 12577.
12. Boča, R.; Baran, P.; Boča, M.; Dlhán, Ľ.; Fuess, H.; Haase, W.; Linert, W.; Papánková, B.; Werner, R. *Inorg. Chim. Acta* **1998**, *278*, 190.
13. Ni, Z.; Shores, M. P. *J. Am. Chem. Soc.* **2009**, *131*, 32.
14. Sahoo, D.; Quesne, M. G.; de Visser, S. P.; Rath, S. P. *Angew. Chem. Int. Ed.* **2015**, *54*, 4796.
15. Hasserodt, J.; Kolanowski, J. L.; Touti, F. *Angew. Chem. Int. Ed.* **2014**, *53*, 60.
16. Young, M. C.; Johnson, A. M.; Hooley, R. J. *Chem. Commun.* **2014**, *50*, 1378.

17. Roberts, D. A.; Castilla, A. M.; Ronson, T. K.; Nitschke, J. R. *J. Am. Chem. Soc.* **2014**, *136*, 8201.
18. Roberts, D. A.; Pilgrim, B. S.; Cooper, J. D.; Ronson, T. K.; Zarra, S.; Nitschke, J. R. *J. Am. Chem. Soc.* **2015**, *137*, 10068.
19. Clements, J. E.; Price, J. R.; Neville, S. M.; Kepert, C. J. *Angew. Chem. Int. Ed.* **2014**, *126*, 10328.
20. Nihei, M.; Suzuki, Y.; Kimura, N.; Kera, Y.; Oshio, H. *Chem. Eur. J.* **2013**, *19*, 6946.
21. Milek, M.; Heinemann, F. W.; Khusniyarov, M. M. *Inorg. Chem.* **2013**, *52*, 11585.
22. Rösner, B.; Milek, M.; Witt, A.; Gobaut, B.; Torelli, P.; Fink, R. H.; Khusniyarov, M. M. *Angew. Chem. Int. Ed.* **2015**, *54*, 12976.
23. Luo, Y.-H.; Nihei, M.; Wen, G.-J.; Sun, B.-W.; Oshio, H. *Inorg. Chem.* **2016**, *55*, 8147.
24. Wuts, P. G. M.; Greene, T. W. *Greene's protective groups in organic synthesis*; Wiley Interscience: Hoboken, NJ, **2007**.
25. Hansch, C.; Leo, A.; Taft, R. W. *Chem. Rev.* **1991**, *91*, 165.
26. Cook, L. J. K.; Kulmaczewski, R.; Mohammed, R.; Dudley, S.; Barrett, S. A.; Little, M. A.; Deeth, R. J.; Halcrow, M. A. *Angew. Chem. Int. Ed.* **2016**, *55*, 4327.
27. Lin, H.-J.; Siretanu, D.; Dickie, D. A.; Subedi, D.; Scepaniak, J. J.; Mitcov, D.; Clérac, R.; Smith, J. M. *J. Am. Chem. Soc.* **2014**, *136*, 13326.
28. Takahashi, K.; Hasegawa, Y.; Sakamoto, R.; Nishikawa, M.; Kume, S.; Nishibori, E.; Nishihara, H. *Inorg. Chem.* **2012**, *51*, 5188.
29. Prat, I.; Company, A.; Corona, T.; Parella, T.; Ribas, X.; Costas, M. *Inorg. Chem.* **2013**, *52*, 9229.
30. McDaniel, A. M.; Klug, C. M.; Shores, M. P. *Eur. J. Inorg. Chem.* **2013**, 943.
31. McDaniel, A. M.; Rappé, A. K.; Shores, M. P. *Inorg. Chem.* **2012**, *51*, 12493.
32. *Apex 2*; Bruker Analytical X-Ray Systems, Inc.: Madison, WI, 2008.
33. G. M. Sheldrick *SHELXTL, Version 6.14*; Bruker Analytical X-Ray Systems, Inc.: Madison, WI, 1999.
34. Bain, G. A.; Berry, J. F. *J. Chem. Educ.* **2008**, *85*, 532.

35. Evans, D. F. *J. Chem. Soc.* **1959**, 2003.
36. van der Meer, M.; Rechkemmer, Y.; Breitgoff, F. D.; Dechert, S.; Marx, R.; Dörfel, M.; Neugebauer, P.; van Slageren, J.; Sarkar, B. *Dalton Trans.* **2016**, 45, 8394.
37. Holland, P. L. *Acc. Chem. Res.* **2008**, 41, 905.
38. Chirik, P. J. *Angew. Chem. Int. Ed.* **2017**, 56, 5170.
39. Larsen, E.; LaMar, G. N.; Wagner, B. E.; Holm, R. H. *Inorg. Chem.* **1972**, 11, 2652.
40. Shannon, R. D.; Prewitt, C. T. *Acta. Cryst. B* **1969**, 925.
41. Sakai, T.; Ohgo, Y.; Ikeue, T.; Takahashi, M.; Takeda, M.; Nakamura, M. *J. Am. Chem. Soc.* **2003**, 125, 13028.
42. Simonato, J.-P.; Pécaut, J.; Le Pape, L.; Oddou, J.-L.; Jeandey, C.; Shang, M.; Scheidt, W. R.; Wojaczyński, J.; Wolowiec, S.; Latos-Grażyński, L.; Marchon, J.-C. *Inorg. Chem.* **2000**, 39, 3978.
43. Halcrow, M. A. *Crystals* **2016**, 6, 58.

Chapter 5: Investigation of Electronic Effect of 5-Pyridyl Substitution in Iron(II) Tren-Based Iminopyridines

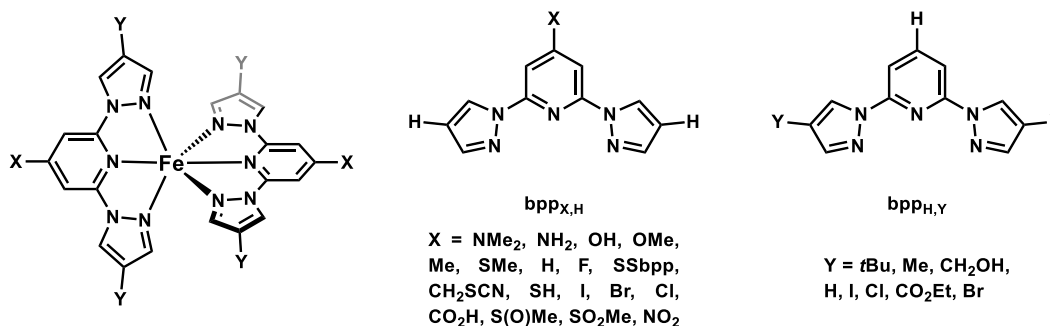
5.1 Introduction

Spin crossover compounds have the potential for applicability in devices, and recent studies using iron(II) complexes have rapidly advanced this field.¹⁻⁶ Iron(II) ions are of particular interest due to the large difference in physical properties between high spin (HS, $S = 2$) and low spin (LS, $S = 0$) species in an octahedral ligand field, given the drastic changes in magnetic as well as optical properties.

Toward increasing the usefulness of iron(II) complexes in such applications, several groups have explored ligand electronic effects in multidentate Fe(II) coordination complexes to modulate and control spin state. As an example, Company and Costas demonstrated that in $[\text{Fe}(\text{Pytacn})(\text{X})_2]^{n+}$ species, where either $\text{X} = \text{OTf}$, $n = 0$ or $\text{X} = \text{MeCN}$, $n = 2$, there is a linear relationship between room temperature μ_{eff} (magnetic susceptibility) and Hammett parameter (σ_{para}) of the 4-pyridyl substituent (tacn = 1,4,7-triazacyclononane).⁷ In addition, Kaizaki and coworkers observed a linear relationship between $T_{1/2}$ and the Hammett parameter of the substituent on a coordinated pyridine in a pyrazolato-bridged dinuclear SCO Fe(II) complex.⁸ A similar study by Clérac and Smith examined the effect of phenyl substituent in a phosphoraminate ligand on $T_{1/2}$ in a series of spin crossover (SCO) four-coordinate Fe(II) species, though it only includes three data points in the electron-rich regime, and the only electron poor substituent ($-\text{CF}_3$) does not undergo SCO.⁹ These studies indicated negative, positive and negative correlations, respectively, where a negative correlation implies that electron withdrawing groups (EWGs) stabilize the HS state.

Perhaps the most thorough of this type of studies was performed by Deeth and Halcrow on a family of substituted $[\text{Fe}(\text{bpp})_2]^{2+}$ complexes (bpp = bis(pyrazolyl)pyridine), several members of which are known to undergo SCO in the solid phase and in solution (Scheme 5.1.1).¹⁰ They analyzed only the effect of *para* substitution on the pyridine (denoted as X in Scheme 5.1.1) by leaving the pyrazole unsubstituted, and found that in that system, increasing electron withdrawing character at this position led to an increase in $T_{1/2}$. This gave a negative Hammett correlation and a greater HS fraction at room temperature. A similar relationship has also been seen in *para*-substituted 4-styryl $[\text{Fe}(\text{bpp})_2]^{2+}$ systems.¹¹ On the other hand, “*meta*” 4-pyrazole substitution effects were investigated on bpp ligands bearing no pyridyl substitution (denoted as Y in Scheme 5.1.1), which showed an inverse relationship as electron donating groups stabilized the HS state.

Scheme 5.1.1. Structure and substitution pattern of $[\text{Fe}(\text{bpp})_2]^{2+}$ complexes investigated by Halcrow and coworkers.



With these results in mind, we aim our focus on hexadentate ligands, which offer additional advantages, including reduced ligand scrambling and dissociation, as well as predictable coordination geometries. In fact, our group¹²⁻¹⁴ and others¹⁵⁻¹⁸ have studied tris(2-aminoethyl)amine (tren)-based iminopyridines as potential spin crossover systems, which has established that the installation of 6-alkyl substituents in these podand species gives rise to HS or SCO species. All known complexes bearing only 5-pyridyl substitution have been LS, however our work regarding desilylation-induced spin state changing in Chapter 4 suggested that it may be

possible to control Fe spin state by modulating ligand electronics. Thus, we wanted to perform a systematic study on the electronic character of 5-substitution in the tren iminopyridine system to evaluate if a HS (or SCO) species can be formed. Toward this goal, we will target functional groups with a wide range of σ value. We expect that the substituent effects might be complicated by the bidentate nature of each iminopyridine arm, so in an effort to separate these effects we will consider the *meta* effects (using σ_{meta}) of the pyridine N and the *para* effects on the imine (using σ_{para}). We envision that this analysis will inform future direction toward enabling spin state switching *via* host-guest interactions and possible use in devices.

5.2 Division of Labor

All work in this chapter has been carried out by Tarik Ozumerzifon.

5.3 Experimental Details

5.3.1. Materials and Methods

General Considerations: ^1H NMR spectra were obtained on a Varian 400 MR spectrometer (at 400 MHz) and are reported relative to SiMe_4 (δ 0.00). ^{13}C NMR spectra were obtained on a Varian 400 MR spectrometer (at 100 MHz) and are reported relative to SiMe_4 (δ 0.00). NMR acquisition sequences for paramagnetic species were changed to have a 1 ms relaxation delay, 90° pulse angle and acquisition time of 1 s. Evans' method determinations of magnetic susceptibility in solution for Fe complexes were carried out using SiMe_4 in a capillary as a reference.¹⁹ Absorption spectra were obtained with a Hewlett-Packard 8453 spectrometer in quartz cuvettes with a 1 cm path length. Infrared spectra were measured with a Nicolet 380 FT-IR spectrometer. Mass spectrometry measurements were performed in the positive ion mode on a Thermo LTQ mass spectrometer equipped with an analytical electrospray ion source and a quadrupole ion trap mass analyzer with

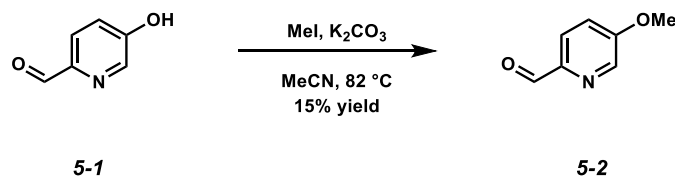
a capillary temperature of 175 °C. Elemental analyses were either performed by Robertson Microlit Laboratories, Inc. in Ledgewood, NJ or by Midwest Microlab, LLC in Indianapolis, IN.

Chemical Details: All reactions were performed under ambient conditions (room temperature, normal benchtop atmosphere) unless otherwise stated. Syringe filters were purchased from VWR International and were fitted with 0.2 µm PTFE membranes. Diethyl ether (Et₂O), tetrahydrofuran (THF), and acetonitrile (MeCN) were sparged with nitrogen, passed through an alumina column and degassed prior to use. 1,4-dioxane was distilled from sodium/benzophenone prior to use. Anhydrous methanol (MeOH) was purchased from Sigma Aldrich. 5-bromopicolinaldehyde and Xantphos were purchased from Oakwood Chemical. Dimethyl disulfide was passed through neutral alumina before use. Fe(OTf)₂ was purchased from Strem Chemical. Ni(OTf)₂ was purchased from Alfa Aesar. Fe(OTf)₂(MeCN)₂ was synthesized according to the literature preparation.²⁰ All other chemicals were purchased from commercial vendors and were used as received.

Crystallographic Measurements: Crystallographic parameters for the compounds measured are listed in Table 5.3.1. All crystals were coated in Paratone oil for data collection. The crystals were supported on Cryoloops, and then mounted on a Bruker Kappa Apex 2 CCD diffractometer under a stream of dinitrogen. Mo Kα radiation and a graphite monochromator were used for data collection. Initial lattice parameters were determined from reflections found in 36 frames. Data sets were collected targeting complete coverage and three-fold redundancy. Data were integrated and corrected for absorption effects with APEX 3 software.²¹ Structures were solved and refined with the SHELXTL software package.²² Unless noted otherwise, thermal parameters for all fully occupied, non-hydrogen atoms were refined anisotropically; hydrogen atoms were added at the

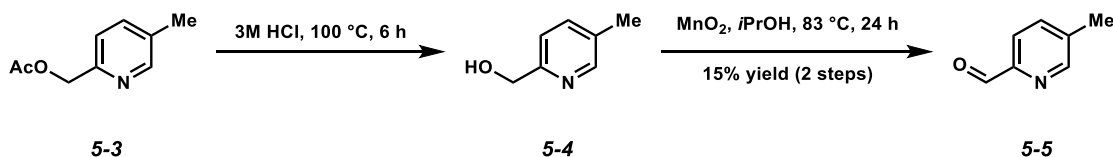
ideal positions and were refined using a riding model where the thermal parameters were set at 1.2 times those of the attached carbon or nitrogen atom (1.5 times that for methyl protons).

5.3.2. Syntheses of Ligands



Aldehyde 5-X. Following the preparation described in reference 23, 5-hydroxypicolinaldehyde **5-1**¹⁷ (0.180 g, 1.46 mmol) and potassium carbonate (0.290 g, 2.1 mmol) were charged to a flame dried flask and to this mixture was added MeCN (4.5 mL, 0.32 M) and methyl iodide (0.110 mL, 1.76 mmol) and the resulting suspension was heated to 82 °C under nitrogen for 12 h. Upon cooling, the reaction mixture was filtered, concentrated *in vacuo* and purified *via* flash column chromatography (1:1 hexanes:ethyl acetate (EtOAc) eluent), affording aldehyde **5-2** as an off-white solid (0.030 g, 15 % yield, $R_f = 0.57$ in 1:1 hexanes:EtOAc).

Aldehyde 5-2: ¹H NMR (400 MHz, CDCl₃): δ 9.99 (s, 1H), 8.44 (d, $J = 2.7$ Hz, 1H), 7.97 (d, $J = 8.6$ Hz, 1H), 7.30 (dd, $J = 8.6, 2.7$ Hz, 1H), 3.95 (s, 3H). The spectrum matches that reported in the literature.²³

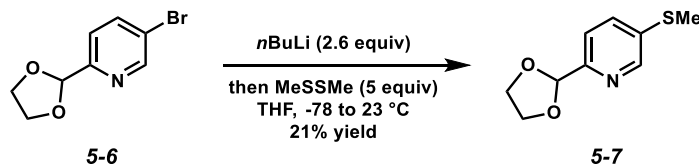


Alcohol 5-4. Following the preparation described in reference 25, acetate **5-3**²⁴ (0.744 g, 4.50 mmol) was dissolved in aq. HCl (3M, 3 mL) and heated to 100 °C for 6 hours. Then, the reaction mixture was neutralized (to pH 7) with aqueous NaOH (3M) and the solvent was removed *in vacuo* to give crude **5-4**. The residue was then redissolved in CH₂Cl₂ (50 mL), dried with MgSO₄, filtered

to remove insoluble material and then concentrated under reduced pressure. The crude product was used in the next step without further purification.

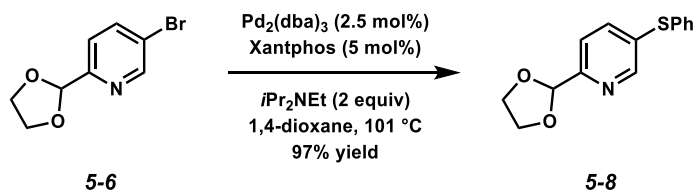
Aldehyde 5-5. Crude alcohol **5-5** was dissolved in *i*PrOH (22 mL, 0.2 M) and MnO₂ (4.70 g, 54 mmol) was added. The resulting suspension was heated to 83 °C for 24 hours. Upon cooling, the reaction was filtered through Celite and concentrated *in vacuo* to give crude 5-methylpicolinaldehyde **5-5**, which was further purified *via* flash column chromatography (1:1 hexanes:EtOAc eluent), affording **5-5** as a yellow oil (0.027 g, 15% yield over two steps from **5-3**, R_f = 0.65 in 1:1 hexanes:EtOAc).

Aldehyde 5-5: ¹H NMR (400 MHz, CDCl₃): δ 10.05 (s, 1H), 8.61 (s, 1H), 7.88 (d, *J* = 7.8 Hz, 1H), 7.67 (d, *J* = 7.8 Hz, 1H), 2.45 (s, 3H). The spectrum matches that reported in the literature.²⁵



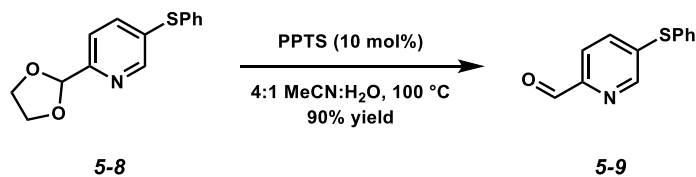
Thioether 5-7. Adapting a preparation described by Benjihad *et al.*,²⁶ to a solution of **5-6**²⁷ (0.302 g, 1.31 mmol) in THF (4.4 mL) at -78 °C was added dropwise a solution of *n*-butyllithium (*n*-BuLi) (1.50 M, 1.05 mL, 1.58 mmol), and the resulting mixture was stirred for 30 min. Then, a solution of dimethyl disulfide (0.175 mL, 1.97 mmol) in THF (2.6 mL) was added dropwise, and allowed to warm to 23 °C over 2 h. The reaction was quenched by addition of ~5 mL H₂O, and the mixture was extracted with Et₂O (3 × 50 mL), washed with water (50 mL) and brine (50 mL), dried over MgSO₄ before concentrating *in vacuo*. The crude product was purified by flash column chromatography (1:1 CH₂Cl₂:Et₂O eluent; note that there is an impurity that coelutes in 1:1 hexanes:EtOAc) to afford thioether **5-7** as a pale yellow oil (0.053 g, 21% yield, R_f = 0.61 in 1:1 CH₂Cl₂:Et₂O).

Thioether 5-7: $^1\text{H NMR}$ (400 MHz, CDCl_3): δ 8.49 (d, $J = 1.2$ Hz, 1H), 7.61 (dd, $J = 8.0, 2.1$ Hz, 1H), 7.44 (d, $J = 8.2$ Hz, 1H), 7.40-7.29 (comp. m, 5H), 5.83 (s, 1H), 4.21-4.03 (comp. m, 4H); $^{13}\text{C NMR}$ (100 MHz, CDCl_3): δ 165.0, 153.5, 147.7, 146.6, 136.1, 135.3, 134.1, 121.2, 120.1, 104.0, 102.8, 65.5; IR (film): 2885, 1554, 1384, 1369, 1211, 1107, 1085, 1018, 941 cm^{-1} ; HRMS m/z calcd for $(\text{M} + \text{H})^+$ [$\text{C}_9\text{H}_{11}\text{NO}_2\text{S} + \text{H}$] $^+$: 198.0583, found 198.0562.



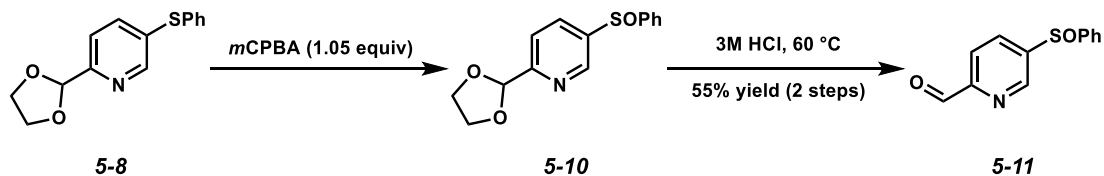
Acetal 5-8. Adapting a preparation described by Itoh *et al.*,²⁸ acetal **5-6**²⁷ (1.030 g, 4.49 mmol), $i\text{Pr}_2\text{NEt}$ (1.56 mL, 8.98 mmol) and freshly distilled 1,4-dioxane (9.3 mL) were successively charged to a flame dried round bottom flask. The mixture was then evacuated and refilled with nitrogen ($\times 3$). Then, $\text{Pd}_2(\text{dba})_3$ (0.103 g, 0.112 mmol), Xantphos (0.130 g, 0.224 mmol) and thiophenol (0.915 mL, 8.97 mmol) were added, and the resulting reaction mixture was degassed with nitrogen for 15 min. The mixture was then heated at reflux (101 °C) for 10 h, until TLC analysis indicated complete consumption of starting material. The reaction was then filtered through Celite, concentrated *in vacuo*, and purified *via* flash column chromatography (3:1 hexanes:EtOAc eluent), affording **5-8** as a yellow oil (1.120 g, 97% yield, $R_f = 0.36$ in 7:3 hexanes:EtOAc).

Acetal 5-8: $^1\text{H NMR}$ (400 MHz, CDCl_3): δ 8.53 (d, $J = 2.0$ Hz, 1H), 7.59 (dd, $J = 8.2, 2.3$ Hz, 1H), 7.44 (d, $J = 8.2$ Hz, 1H), 5.82 (s, 1H), 4.20-4.05 (comp. m, 4H), 2.50 (s, 3H); $^{13}\text{C NMR}$ (100 MHz, CDCl_3): δ 155.1, 150.2, 138.3, 134.2, 133.5, 131.9, 129.4, 127.9, 120.9, 103.2, 65.5; IR (film): 3056, 2882, 1580, 1554, 1475, 1439, 1383, 1303, 1287, 1211, 1130, 1101, 1087, 1016 cm^{-1} ; HRMS m/z calcd for $(\text{M} + \text{H})^+$ [$\text{C}_{14}\text{H}_{13}\text{NO}_2\text{S} + \text{H}$] $^+$: 260.0740, found 260.0734.



Aldehyde 5-9. Acetal **5-8** (0.200 g, 0.771 mmol) was dissolved in 4:1 MeCN:H₂O (5 mL) and to this solution was charged solid pyridinium *p*-toluenesulfonate (0.019 mg, 0.077 mmol). The resulting mixture was then stirred at 23 °C for 1 h until TLC analysis indicated complete consumption of starting material, then the reaction was basified with saturated aqueous NaHCO₃, extracted into EtOAc (2 × 20 mL), washed with brine (30 mL), dried over MgSO₄ and concentrated *in vacuo*, giving crude aldehyde **5-9**. The desired compound was purified by flash column chromatography (3:1 hexanes:EtOAc eluent), affording **5-9** as a yellow oil (0.150 g, 90% yield, *R_f* = 0.66 in 7:3 hexanes:EtOAc).

Aldehyde 5-9: ¹H NMR (400 MHz, CDCl₃): δ 10.0 (s, 1H), 8.51 (d, *J* = 2.0 Hz, 1H), 7.80 (d, *J* = 8.2 Hz, 1H), 7.57-7.43 (m, 5H); ¹³C NMR (100 MHz, CDCl₃): δ 192.5, 149.8, 147.9, 142.2, 134.7, 134.3, 130.1, 129.6, 121.6; IR (film): 3054, 2817, 1705, 1562, 1475, 1466, 1440, 1349, 1288, 1268, 1210, 1095, 1081, 1014 cm⁻¹; HRMS *m/z* calcd for (M + H)⁺ [C₁₂H₉NOS + H]⁺: 216.0478, found 216.0477.

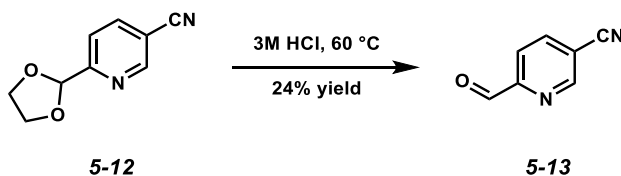


Sulfoxide 5-10. Acetal **5-8** (0.200 g, 0.774 mmol) was dissolved in CH₂Cl₂ (7.7 mL) and cooled to 0 °C. Then, a solution of *m*CPBA (81.2%, 0.173 g, 0.813 mmol) in CH₂Cl₂ (8.1 mL) was added dropwise and the reaction was stirred for 15 min at 0 °C, until TLC analysis indicated complete consumption of starting material. Then, saturated aqueous Na₂S₂O₃ (1 mL) was added to the solution, and the compound was extracted into EtOAc (30 mL), washed with saturated aqueous

NaHCO₃ (30 mL), brine (30 mL), dried over MgSO₄ and concentrated *in vacuo*. The crude sulfoxide **5-10** was used in the next step without further purification.

Aldehyde 5-11. Sulfoxide **5-10** (0.774 mmol, assumed) was dissolved in aqueous HCl (3M, 5 mL) and the resulting mixture was then heated to 60 °C for 30 min. Upon complete consumption of starting material, the reaction was basified with sat. aq. NaHCO₃, extracted into EtOAc (2 × 30 mL), washed with brine (30 mL) and dried over MgSO₄ and concentrated *in vacuo*. The crude aldehyde **5-11** was purified by flash column chromatography (1:1 hexanes:EtOAc eluent) to give **5-11** as an off-white powder (0.099 g, 55% yield over 2 steps from **5-8**, R_f = 0.46 in 1:1 hexanes:EtOAc).

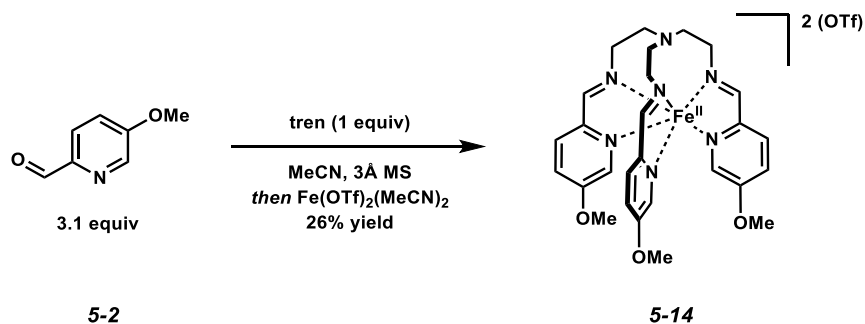
Aldehyde 5-11: ¹H NMR (400 MHz, CDCl₃): δ 10.1 (s, 1H), 8.93 (s, 1H), 8.18 (d, *J* = 8.2 Hz, 1H), 8.04 (d, *J* = 8.2 Hz, 1H), 7.74-7.67 (m, 2H), 7.56-7.49 (m, 3H); ¹³C NMR (100 MHz, CDCl₃): δ 192.2, 153.9, 146.9, 146.4, 144.0, 133.3, 132.1, 129.9, 124.8, 121.9; IR (film): 3054, 2835, 1713, 1572, 1444, 1360, 1206, 1092, 1070, 1051, 1013, 998 cm⁻¹; HRMS *m/z* calcd for (M + H)⁺ [C₁₂H₉NO₂S + H]⁺: 232.0427, found 232.0413.



Aldehyde 5-13. Acetal **5-12**²⁷ (0.630 g, 3.58 mmol) was dissolved in aq. HCl (3M, 11 mL) and heated to 60 °C for 10 min, until complete conversion was determined by TLC. Then, the reaction was basified with sat. aq. NaHCO₃, extracted into EtOAc (2 × 50 mL), washed with brine (50 mL), dried over MgSO₄ and concentrated *in vacuo*, giving crude aldehyde **5-13**. The crude material was purified *via* flash column chromatography (1:1 hexanes:EtOAc), affording **5-13** as a pale yellow solid (0.110 g, 24% yield, R_f = 0.50 in 7:3 hexanes:EtOAc).

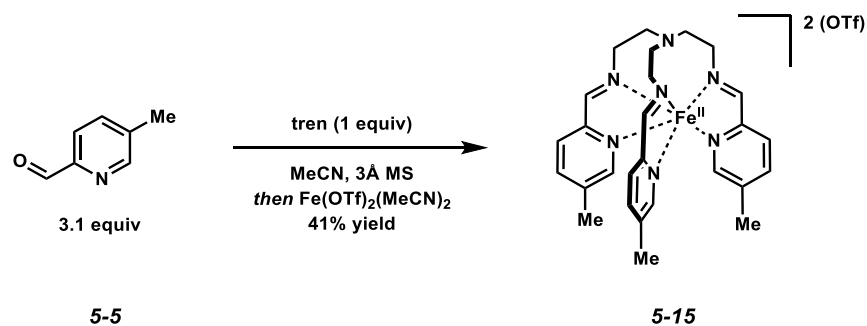
Aldehyde 5-13: ^1H NMR (400 MHz, CDCl_3): δ 10.12 (s, 1H), 9.05 (s, 1H), 8.17 (d, $J = 7.8$ Hz, 1H), 8.06 (d, $J = 7.8$ Hz, 1H). The spectrum matches that reported in the literature.²⁹

5.3.3. Synthesis of Metal Complexes



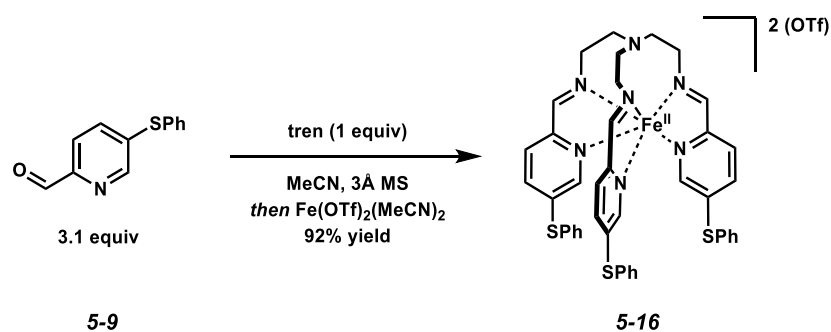
[Fe(5-OMepy)₃tren](OTf)₂ 5-14. To a solution of 5-methoxypicolinaldehyde **5-2** (0.030 g, 0.22 mmol) in MeCN (2 mL) was added a solution of tren (0.010 g, 0.068 mmol) in MeCN (2 mL), and the resulting mixture was stirred in the presence of 3Å molecular sieves for 1 h at 23 °C. Then, a solution of Fe(OTf)₂(MeCN)₂ (0.031 g, 0.071 mmol) in MeCN (2 mL) was added dropwise and the resulting dark purple mixture was stirred for an additional 1 h at 23 °C. The solvent was then concentrated *in vacuo* and crystals of the complex were grown from a diethyl ether diffusion into a concentrated acetonitrile solution, affording **5-14** (0.049 g, 26% yield) as dark red needles.

[Fe(5-OMepy)₃tren](OTf)₂ 5-14: IR (KBr): 3072, 3039, 2943, 2861, 1614, 1595, 1560, 1484, 1456, 1373, 1261, 1238, 1149, 1056, 1030 cm^{-1} ; MS (ESI⁺) m/z calcd for (M - OTf)⁺ [C₂₉H₃₃N₇O₉S₂F₆Fe - CF₃SO₃]⁺: 708.15, found 708.33, m/z calcd for (M - 2OTf)²⁺ [C₂₉H₃₃N₇O₉S₂F₆Fe - C₂F₆S₂O₆]²⁺: 279.60, found 279.67; Anal. calcd for C₂₉H₃₃N₇O₉S₂F₆Fe: C 40.62% H 3.88% N 11.43%, found C 40.72% H 3.62% N 11.40%; χ_{MT} (298 K, CD₃CN): 0.13 $\text{cm}^3 \text{K mol}^{-1}$.



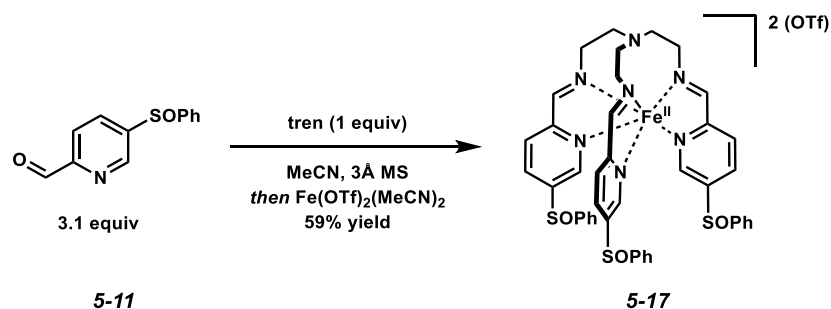
[Fe(5-Mepy)₃tren](OTf)₂ 5-15. To a solution of 5-methylpicolinaldehyde **5-5** (0.050 g, 0.41 mmol) in MeCN (2 mL) was added a solution of tren (0.020 g, 0.13 mmol) in MeCN (2 mL) and the resulting mixture was stirred in the presence of 3Å molecular sieves for 1 h at 23 °C. Then, a solution of Fe(OTf)₂(MeCN)₂ (0.058 g, 0.13 mmol) in MeCN (2 mL) was added dropwise and the resulting dark purple mixture was stirred for an additional 1 h at 23 °C. The reaction mixture was then passed through a syringe filter, the solvent volume was reduced to 1 mL, and Et₂O was slowly added to precipitate the complex, affording **5-15** (0.043 g, 41% yield) as a dark purple powder. Diffraction quality crystals were grown *via* Et₂O diffusion into a concentrated methanolic solution of **5-15**.

[Fe(5-Mepy)₃tren](OTf)₂ 5-15: IR (KBr): 3034, 2927, 2877, 1619, 1609, 1564, 1461, 1451, 1403, 1385, 1367, 1323, 1251, 1222, 1156, 1057, 1027 cm⁻¹; MS (ESI⁺) *m/z* calcd for (M - OTf)⁺ [C₂₉H₃₃N₇O₆F₆S₂Fe - CF₃SO₃]⁺: 660.17, found 660.25, *m/z* calcd for (M - 2OTf)²⁺ [C₂₉H₃₃N₇O₆F₆S₂Fe - C₂F₆S₂O₆]²⁺: 255.61, found 255.67; Anal. calcd (C₂₉H₃₃N₇O₆F₆S₂Fe: C 43.02% H 4.11% N 12.11%, found C 41.99% H 4.14% N 11.77%; $\chi_M T$ (298 K, CD₃CN): 0.05 cm³ K mol⁻¹.



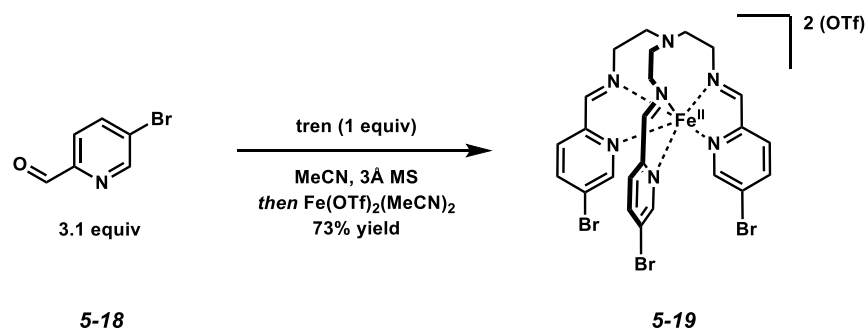
[Fe(5-SPhpy)₃tren](OTf)₂ 5-16. To a solution of 5-(phenylsulfide)picolinaldehyde **5-9** (0.020 g, 0.093 mmol) in MeCN (2 mL) was added a solution of tren (0.0044 mg, 0.030 mmol) in MeCN (2 mL) and the resulting mixture was stirred in the presence of 3Å molecular sieves for 1 h at 23 °C. Then, a solution of Fe(OTf)₂(MeCN)₂ (0.013 g, 0.030 mmol) in MeCN (2 mL) was added dropwise and the resulting dark purple mixture was stirred for an additional 1 h at 23 °C. The desired Fe complex was precipitated by addition of Et₂O (20 mL), and the resulting mixture was stirred overnight. The suspension was then filtered, washed with additional Et₂O (2 × 5 mL) and the resulting dark purple powder was crystallized *via* Et₂O diffusion into a concentrated MeCN solution, giving dark purple crystals of **5-16** (0.030 g, 74% yield).

[Fe(5-SPhpy)₃tren](OTf)₂ 5-16: IR (KBr): 3091, 2938, 2874, 2848, 1601, 1578, 1532, 1470, 1440, 1382, 1355, 1313, 1262, 1220, 1156, 1107, 1052, 1028 cm⁻¹; MS (ESI⁺) *m/z* calcd for (M - OTf)⁺ [C₄₄H₃₉N₇O₆S₅F₆Fe - CF₃SO₃]⁺: 942.13, found 942.25, *m/z* calcd for (M - 2OTf)²⁺ [C₄₄H₃₉N₇O₆S₅F₆Fe - C₂F₆S₂O₆]²⁺: 396.59, found 396.75; Anal. calcd for C₄₄H₃₉N₇O₆S₅F₆Fe: C 48.40% H 3.60% N 8.98%, found C 47.78% H 3.57% N 8.96%; χ_{MT} (298 K, CD₃CN): 0.05 cm³ K mol⁻¹.



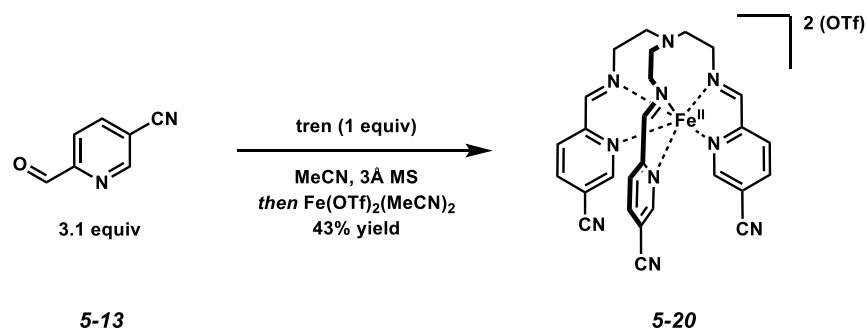
[Fe(5-SOPhy)₃tren](OTf)₂ 5-17. To a solution of 5-(phenylsulfoxide)picolinaldehyde **5-11** (0.050 g, 0.22 mmol) in MeCN (2 mL) was added a solution of tren (0.010 mg, 0.068 mmol) in 2 mL MeCN and the resulting mixture was stirred in the presence of 3 Å molecular sieves for 1 h at 23 °C. Then, a solution of Fe(OTf)₂ (0.024 g, 0.068 mmol) in MeCN (2 mL) was added dropwise and the resulting dark purple mixture was stirred for an additional 1 h at 23 °C. The desired Fe complex was then precipitated by addition of Et₂O (20 mL) and the mixture was stirred overnight. The suspension was then filtered, washed with additional Et₂O (2 × 5 mL) and the resulting dark purple powder was crystallized by placing a concentrated solution of **5-17** in 3:1 CH₂Cl₂:pentane at -40 °C, giving dark purple microcrystalline **5-17** (0.047 g, 59% yield). Fe(OTf)₂ was used in this preparation because Fe(OTf)₂(MeCN)₂ was not available; given the other results, this solvated salt should also generate the desired Fe complex.

[Fe(5-SOPhy)₃tren](OTf)₂ 5-17: IR (KBr): 3029, 2847, 1605, 1582, 1540, 1464, 1444, 1380, 1357, 1270, 1260, 1223, 1154, 1098, 1080, 1052, 1028 cm⁻¹; MS (ESI⁺) *m/z* calcd for (M - OTf)⁺ [C₄₄H₃₉N₇O₉S₅F₆Fe - CF₃SO₃]⁺: 990.11, found 990.25, *m/z* calcd for (M - 2OTf)²⁺ [C₄₄H₃₉N₇O₉S₅F₆Fe - C₂F₆S₂O₆]²⁺: 420.58, found 420.75; Anal. calcd for C₄₄H₃₉N₇O₉S₅F₆Fe: C 46.36% H 3.45% N 8.60%, found C 46.09% H 3.73% N 8.39%; χ_{MT} (298 K, CD₃CN): 0.20 cm³ K mol⁻¹.



[Fe(5-Brpy)₃tren](OTf)₂ 5-19. To a solution of 5-bromopicolinaldehyde **5-18** (0.050 g, 0.27 mmol) in MeCN (2 mL) was added a solution of tren (0.013 g, 0.089 mmol) in MeCN (2 mL) and the resulting mixture was stirred in the presence of 3Å molecular sieves for 1 h at 23 °C. Then, a solution of Fe(OTf)₂(MeCN)₂ (0.038 g, 0.087 mmol) in MeCN (2 mL) was added dropwise and the resulting dark purple mixture was stirred for an additional 1 h at 23 °C. The desired Fe complex was then precipitated by addition of Et₂O (20 mL) and the mixture was stirred overnight. The suspension was then filtered and washed with Et₂O (2 × 5 mL) to afford **5-19** (0.064 g, 74% yield) as a dark purple powder.

[Fe(5-Brpy)₃tren](OTf)₂ 5-19: IR (KBr): 3032, 2841, 1606, 1536, 1467, 1451, 1384, 1357, 1319, 1256, 1222, 1149, 1098, 1027 cm⁻¹; MS (ESI⁺) *m/z* calcd for (M - OTf)⁺ [C₂₆H₂₄N₇O₆Br₃F₆S₂Fe - CF₃SO₃]⁺: 851.85, found 852.08; Anal. calcd (C₂₆H₂₄N₇O₆Br₃F₆S₂Fe + 0.5C₂H₄N (MeCN): C 31.65% H 2.51% N 10.25%, found C 31.65% H 2.24% N 10.59%; χ_MT (298 K, CD₃CN): 0.31 cm³ K mol⁻¹.



[Fe(5-CNpy)₃tren](OTf)₂ 5-20. To a solution of 5-cyanopicolinaldehyde **5-13** (0.057 g, 0.43 mmol) in MeCN (2 mL) was added a solution of tren (0.020 g, 0.14 mmol) in MeCN (2 mL) and the resulting mixture was stirred in the presence of 3 Å molecular sieves for 1 h at 23 °C. Then, a solution of Fe(OTf)₂(MeCN)₂ (0.061 g, 0.14 mmol) in MeCN (2 mL) was added dropwise and the resulting dark blue mixture was stirred for an additional 1 h at 23 °C. The desired Fe complex was then precipitated by addition of Et₂O (20 mL) and the mixture was stirred overnight. The suspension was then filtered and washed with Et₂O (2 × 5 mL) to afford **5-20** (0.050 g, 43% yield) as a dark blue powder. The elemental analysis data obtained are from a powdered sample of **5-20**; attempts to crystallize this complex have not been successful. Further, the EA results listed below are from a too-small sample sent; a larger sample should be sent for re-analysis.

[Fe(5-CNpy)₃tren](OTf)₂ 5-20: IR (KBr): 3268, 2924, 2853, 2838, 1600, 1459, 1367, 1274, 1258, 1223, 1157, 1106, 1028 cm⁻¹; MS (ESI⁺) *m/z* calcd for (M - OTf)⁺ [C₂₉H₂₄N₁₀O₆F₆S₂Fe - CF₃SO₃]⁺: 693.11, found 693.17, *m/z* calcd for (M - 2OTf)²⁺ [C₂₉H₂₄N₁₀O₆F₆S₂Fe - C₂F₆S₂O₆]²⁺: 272.08, found 272.17; Anal. calcd (C₂₆H₂₄N₇O₆Br₃F₆S₂Fe: C 41.34% H 2.87% N 16.62%, found C 39.13% H 2.87% N 14.83%; χ_{MT} (298 K, CD₃CN): 0.37 cm³ K mol⁻¹.

General procedure for synthesis of nickel complexes: In a dinitrogen glovebox, to the requisite pyridine aldehyde (3.1 equiv) in MeOH (1 mL) was added a solution of tren (1 equiv) in MeOH (1 mL) and the resulting mixture was stirred in the presence of 3 Å molecular sieves for 1 h at 23 °C. Then, a solution of Ni(OTf)₂ (1 equiv) in MeOH (1 mL) was added, and the resulting yellow

mixture was stirred for an additional 1 h at 23 °C. The mixture was then passed through a syringe filter, the solvent was removed *in vacuo* and the residue was redissolved in MeCN for UV/Vis and MS analysis, the latter indicating that the major product formed as the title Ni complex.

Data obtained for **[Ni(5-OMepy)₃tren](OTf)₂ 5-14a**: MS (ESI⁺) *m/z* calcd for (M - OTf)⁺ [C₂₉H₃₃N₇O₉S₂F₆Ni - CF₃SO₃]⁺: 710.15, found 710.33, *m/z* calcd for (M - 2OTf)²⁺ [C₂₉H₃₃N₇O₉S₂F₆Ni - C₂F₆S₂O₆]²⁺: 281.15, found 280.67; UV/Vis (MeCN) λ_{max} = 851 nm.

Data obtained for **[Ni(5-Mepy)₃tren](OTf)₂ 5-15a**: MS (ESI⁺) *m/z* calcd for (M - OTf)⁺ [C₂₉H₃₃N₇O₆F₆S₂Ni - CF₃SO₃]⁺: 662.17, found 662.33, *m/z* calcd for (M - 2OTf)²⁺ [C₂₉H₃₃N₇O₆F₆S₂Ni - C₂F₆S₂O₆]²⁺: 256.61, found 256.75; UV/Vis (MeCN) λ_{max} = 819 nm.

Data obtained for **[Ni(5-SPhpy)₃tren](OTf)₂ 5-16a**: MS (ESI⁺) *m/z* calcd for (M - OTf)⁺ [C₄₄H₃₉N₇O₆S₅F₆Ni - CF₃SO₃]⁺: 944.13, found 944.25, *m/z* calcd for (M - 2OTf)²⁺ [C₄₄H₃₉N₇O₆S₅F₆Ni - C₂F₆S₂O₆]²⁺: 397.59, found 397.75; UV/Vis (MeCN) λ_{max} = 875 nm.

Data obtained for **[Ni(5-SOPhy)₃tren](OTf)₂ 5-17a**: MS (ESI⁺) *m/z* calcd for (M - OTf)⁺ [C₄₄H₃₉N₇O₉S₅F₆Ni - CF₃SO₃]⁺: 992.11, found 992.25, *m/z* calcd for (M - 2OTf)²⁺ [C₄₄H₃₉N₇O₉S₅F₆Ni - C₂F₆S₂O₆]²⁺: 421.58, found 421.75; UV/Vis (MeCN) λ_{max} = 865 nm.

Data obtained for **[Ni(5-Brpy)₃tren](OTf)₂ 5-19a**: MS (ESI⁺) *m/z* calcd for (M - OTf)⁺ [C₂₆H₂₄N₇O₆Br₃F₆S₂Ni - CF₃SO₃]⁺: 853.85, found 853.83; UV/Vis (MeCN) λ_{max} = 864 nm.

The MS data obtained for **[Ni(5-CNpy)₃tren](OTf)₂ 5-20a** were not saved when acquired, however calculated values are listed: MS (ESI⁺) *m/z* calcd for (M - OTf)⁺ [C₂₉H₂₄N₁₀O₆F₆S₂Ni - CF₃SO₃]⁺: 695.11, *m/z* calcd for (M - 2OTf)²⁺ [C₂₉H₂₄N₁₀O₆F₆S₂Ni - C₂F₆S₂O₆]²⁺: 273.08; UV/Vis (MeCN) λ_{max} = 872 nm.

NMR (¹H and ¹³C) and IR spectra are provided in Appendix 4.

5.3.4. Crystallographic Results

Three podands (5-OMe, 5-Me and 5-SPh) have been structurally characterized, and all three crystallize in a monoclinic space groups with minimal disorder. The structures of **5-14** and **5-15** are shown in Figure 5.3.1.

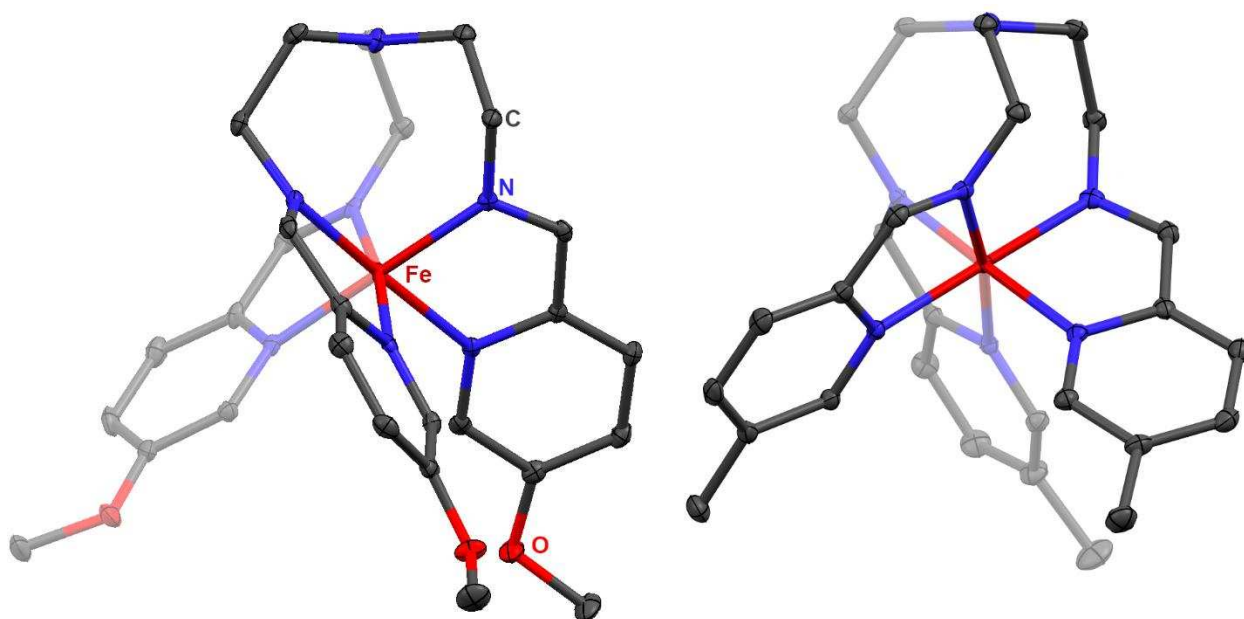


Figure 5.3.1. Crystal structures of the cationic complexes **5-14** (left) and **5-15** (right) depicted with 40% probability ellipsoids. Brick, grey, blue and red ellipsoids represent Fe, C, N and O atoms, respectively. Triflate anions and hydrogen atoms are omitted for clarity.

Meanwhile, the 5-phenylsulfide complex **5-16** exhibits inter-arm π stacking between the pyridine of one arm and the phenyl ring of another (Figure 5.3.2).

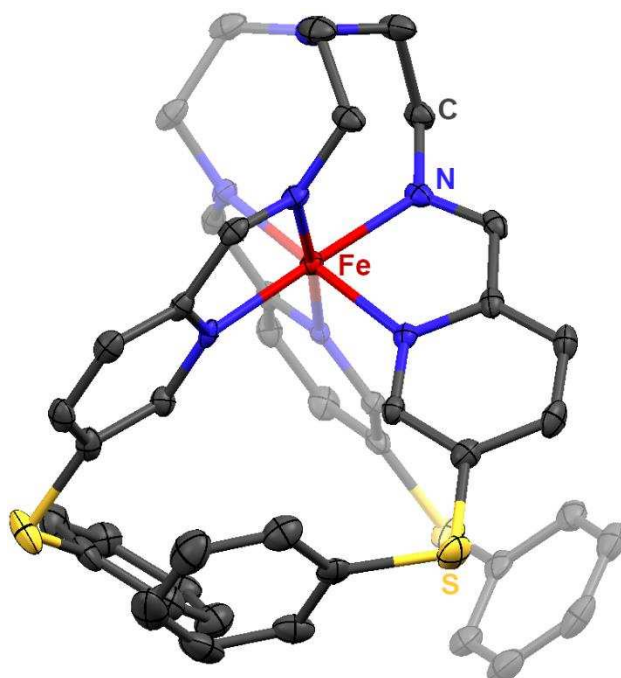


Figure 5.3.2. Crystal structure of **5-16** depicted with 40% probability ellipsoids. Brick, grey, blue, red and yellow ellipsoids represent Fe, C, N, O and S atoms, respectively. Triflate anions and hydrogen atoms are omitted for clarity.

Table 5.3.1. Crystallographic parameters for **5-14**, **5-15**, and **5-16**.^a

	5-14 (5-OMe)	5-15 (5-Me)	5-16 (5-SPh)
Formula	C ₂₉ H ₃₃ F ₆ FeN ₇ O ₉ S ₂	C ₂₉ H ₃₃ F ₆ FeN ₇ O ₆ S ₂	C ₄₄ H ₃₉ F ₆ FeN ₇ O ₆ S ₅
Formula weight	857.59	809.59	1091.97
Color, habit	red needles	purple needles	red needles
<i>T</i> (K)	100	100	100
Space group	<i>P</i> 2 ₁	<i>P</i> 2 ₁ / <i>c</i>	<i>C</i> 2/ <i>c</i>
<i>Z</i>	4	4	8
<i>a</i> (Å)	12.942(3)	13.795(3)	18.733(4)
<i>b</i> (Å)	19.961(4)	14.901(3)	13.026(3)
<i>c</i> (Å)	13.593(3)	16.482(3)	38.111(9)
α (°)	90	90	90
β (°)	98.32(3)	101.42(3)	98.108(8)
γ (°)	90	90	90
<i>V</i> (Å ³)	3474.6(13)	3321.0(12)	9207(4)
<i>d</i> _{calc} (g cm ⁻³)	1.639	1.619	1.576
GOF	1.02	1.017	1.018
<i>R</i> ₁ , <i>wR</i> ₂ ^b (%)	3.00, 6.77	5.60, 16.00	6.14, 15.13

^a Obtained with graphite-monochromated Mo K α ($\lambda = 0.71073$ Å) radiation.

^b $R_1 = \sum ||F_o| - |F_c|| / \sum |F_o|$, $wR_2 = \{ \sum [w(F_o^2 - F_c^2)^2] / \sum [w(F_o^2)^2] \}^{1/2}$ for $F_o > 4\sigma(F_o)$.

The CIF files for these three structures are available in the Shores Lab Documents Dropbox folder under Group Dissertations and Theses.

5.4 Results and Discussion

5.4.1. Synthesis of Fe complexes

The general method for preparation of the 5-pyridyl substituted iminopyridine complexes involves the condensation of each respective picolinaldehyde with tren, followed by subsequent metalation with $\text{Fe}(\text{OTf})_2(\text{MeCN})_x$ ($x = 0$ or 2). This procedure is successful for template-synthesis of each of the target Fe complexes (see section 5.3.3 for details). Compounds **5-14**, **5-15** and **5-16** were all characterized crystallographically, and from this analysis we can gain important structural information which is tabulated below (Table 5.4.1). The complex geometries found here are all distorted octahedral systems, as the Σ and Θ values vary from ideal values, which both equal 0 when perfectly octahedral.

Table 5.4.1. Compiled relevant crystallographic details for **5-14**, **5-15** and **5-16**.

	5-14^a	5-15	5-16
Fe-N _{bridge} (Å)	3.398(3), 3.423(3)	3.487(3)	3.410(4)
Average Fe-N _{imine} (Å)	1.964(4) ^b	1.956(2)	1.957(3)
Average Fe-N _{pyridine} (Å)	1.976(3) ^b	1.980(9)	1.974(7)
Σ (°)	57.0(7) ^b	61.3(4)	65.2(1)
Θ (°)	117.71 ^b	115.22	110.28
Average π stacking distance (Å) ^c	-	-	4.086

^a There are two podands in the asymmetric unit. ^b Averaged values of both podands in asymmetric unit. ^c Calculated from intra-centroid distances among three arms.

Using Evans' method,¹⁹ we can evaluate the spin state of each Fe podand in solution, the results of which are tabulated below (Table 5.4.2). These are raw susceptibility values, not corrected for TIP.

Table 5.4.2. Comparison of solution magnetic susceptibilities and Hammett parameters for Fe triflate salts.

	5-R	χ_{MT} (cm ³ K mol ⁻¹) ^a	$3\sigma_{meta}$	$3\sigma_{para}$
5-14	OMe	0.13	0.36	-0.81
5-15	Me	0.05	-0.21	-0.51
5-16	SPh	0.05	0.69	0.21
5-17	SOPh	0.20	1.50	1.32
5-19	Br	0.31	1.17	0.69
5-20	CN	0.37	1.68	1.92
5-21^b	H	0.03 ^c	0.00	0.00
5-22	CO ₂ Me	0.11 ^d	1.11	1.35

^a Acquired in MeCN at 298 K using SiMe₄ as an internal standard (Evans' method). ^b PF₆ salt. ^c From reference 15. ^d From reference 13.

All eight Fe salts described in Table 5.4.2 exhibit small solution χ_{MT} values, allowing us to label them as “mostly LS.” Nitrile-containing **5-20** has the largest molar susceptibility value of 0.37 cm³ K mol⁻¹; this is also the most electron withdrawing substituent (most positive Hammett parameter) in both *meta* and *para* contributions to the bidentate ligand arm. Thus, we can make a qualitative argument (Figure 5.4.1) that an electron withdrawing group at the 5-position increases the HS fraction of the tren podand; however, the susceptibility values are still quite low and thus a strong argument cannot be made without further analysis. To evaluate if these complexes exhibit thermal SCO above room temperature, the 5-CN Fe complex was heated to ~80 °C (boiling point of MeCN) – a persistence of deep blue color is indicative that the compound remains LS.

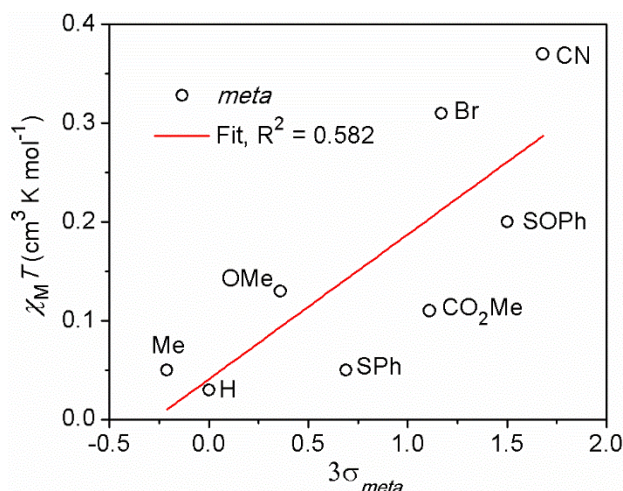


Figure 5.4.1. Plot of $\chi_M T$ as a function of Hammett parameter for the eight Fe complexes. Data for 5-21 (H) and 5-22 (CO₂Me) are from references 15 and 13, respectively.

5.4.2. Analysis of Ni(II) Analogs

To analyze the ligand field splitting (Δ) in these podands, the analogous Ni(II) complexes are also synthesized. This is a technique employed to evaluate Δ in transition metal complexes which exhibit strong charge transfer bands that obscure the lower intensity d-d excitations in electronic spectra.³⁰ While the initial report from Busch and coworkers suggest that Ni(II) Dq values ranging between 1160-1340 cm⁻¹ should give rise to SCO Fe(II) species ($\Delta = 10Dq$),³¹ Goodwin has refined that range to 1120-1240 cm⁻¹.³⁰ As discussed earlier, 5-pyridyl substituents should have an effect on both the pyridine N (*meta*) and imine (*para*) binding sites, so we analyze the effects individually.

First, the *meta* effects are isolated by tracking Ni(II) Dq values as a function of the *meta* Hammett parameter (σ_{meta}). The traditional σ parameters are being used in these analyses, as an alternative (σ^+ , for example, used by Deeth and Halcrow¹⁰) gave a worse correlation. There is a pseudo linear relationship between these quantities (Figure 5.4.2), which indicates that electron withdrawing groups at this position lead to smaller Dq values. While the correlation coefficient is relatively low for a Hammett fit (0.671), we note that two complexes (H and SPh) lie significantly

off the fit line. In fact, omission of these two points results in an R^2 value of 0.940. Ideally, the acquired linear functions would enable predictive synthesis targeting the substituent with a Hammett parameter suitable for SCO, however given that these Dq values all lie within the SCO range, there is likely no physical meaning to these relationships outside of the sign of the slope (relation). Along these lines, the nonzero y-intercepts of these functions should line up with the H data point ($\sigma_{para/meta} = 0$), indicating a baseline ligand field in the absence of substitution, but clearly this is not the case.

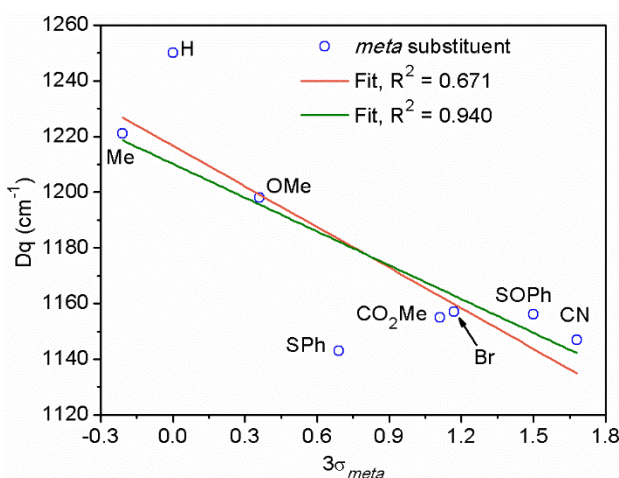


Figure 5.4.2. Dependence of the Ni(II) analog ligand field splitting (Dq) as a function of ligand substituent ($3\sigma_{meta}$). The orange fit line includes all data points ($Dq = -50 \times 3\sigma_{meta} + 1220$, $R^2 = 0.671$). The green fit line omits the H and SPh data points ($Dq = -40 \times 3\sigma_{meta} + 1210$, $R^2 = 0.940$). Data for **5-21** (H) and **5-22** (CO₂Me) are from references 15 and 13, respectively.

The SPh podand is unique in that it clearly exhibits inter-arm π stacking (between phenyl and pyridine rings on adjacent arms) in the solid state, leading to a more compact molecular structure (Figure 5.4.3). This effect may serve to increase the ligand field of the phenylsulfide-bound species more than would be expected from a strict electronics argument, resulting in the observed outlier behavior. Meanwhile, the deviation of the parent ($R = H$) podand is less understood, however it may be due to reduced steric size (H is the smallest substituent of any).

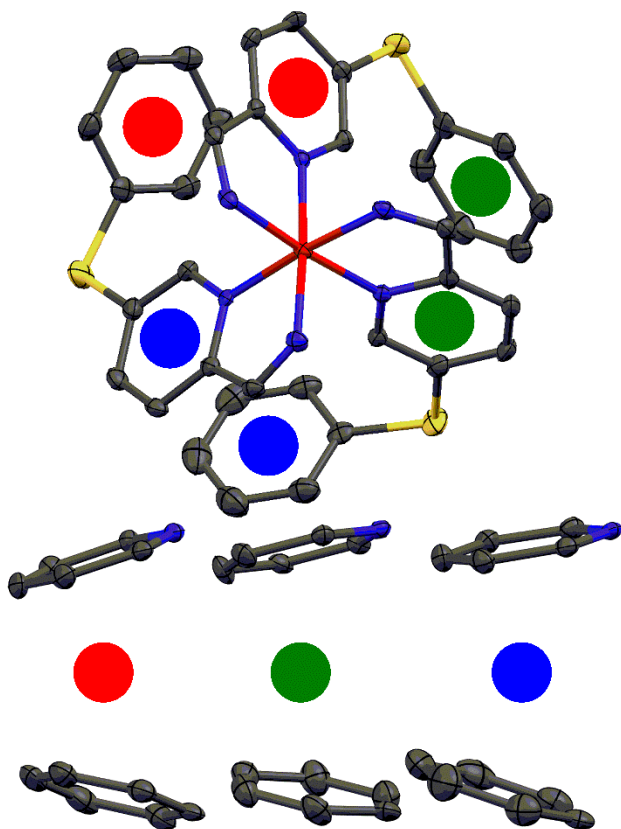


Figure 5.4.3. Intramolecular π stacking in **5-16**. Brick, grey, blue, red and yellow ellipsoids represent Fe, C, N, O and S atoms, respectively. All tren backbone atoms (1N, 6C), triflate anions and hydrogen atoms are omitted for clarity.

Next, we analyze the *para* effects separately. Once again, we see a pseudo linear relationship between Ni(II) Dq and σ_{para} (Figure 5.4.4). The lower slope of this correlation indicates that there is a slightly weaker *para* influence of the electronic nature of 5-pyridyl substituent. Thus, the slight increase in spin state (and Ni(II) Dq) is likely primarily due to the dampening of σ donation ability of the pyridine.³² In this plot, it can be seen that the R = H and SPh-containing complexes once again lie significantly off the regression fit; omission of these points again results in a much higher R^2 value (0.790). The linear functions obtained have nearly equal intercepts (the identical to three significant figures), however the function that includes the H and SPh data points is slightly higher (red). In all, we can conclude that there is indeed a pseudo

linear relationship between Ni(II) Dq value (and therefore Fe(II) spin state) based on varying electronics at the 5-pyridyl position.

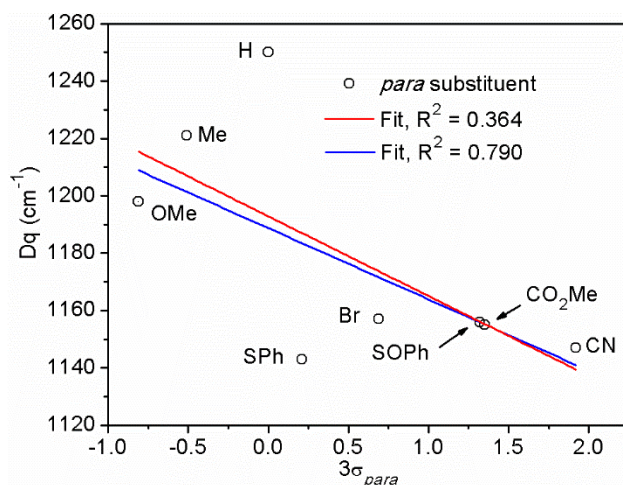


Figure 5.4.4. Dependence of Ni(II) analog Dq as a function of $3\sigma_{para}$. The red fit line includes all data points ($Dq = -30 \times 3\sigma_{para} + 1190$, $R^2 = 0.364$). The blue fit line omits the H and SPh data points ($Dq = -25 \times 3\sigma_{para} + 1190$, $R^2 = 0.790$). Data for **5-21** (H) and **5-22** (CO₂Me) are from references 15 and 13, respectively.

Given Goodwin's prediction that Fe(II) species whose Ni(II) analogs have Dq values between 1120-1240 cm^{-1} should undergo SCO, we are left to consider why the eight Fe(II) complexes described here are LS even though their Dq values all reside at the center of this range (Table 5.4.3).

Table 5.4.3. Tabulated Ni(II) Dq values for **5-14a – 5-17a, 5-19a – 5-22a**.

	5-R	Ni(II) Dq (cm^{-1}) ^a	$3\sigma_{meta}$	$3\sigma_{para}$
5-14a	OMe	1200	0.36	-0.81
5-15a	Me	1220	-0.21	-0.51
5-16a	SPh	1140	0.69	0.21
5-17a	SOPh	1155	1.50	1.32
5-19a	Br	1160	1.17	0.69
5-20a	CN	1150	1.68	1.92
5-21a ^b	H	1250 ^c	0	0
5-22a ^c	CO ₂ Me	1155 ^d	1.11	1.35

^a Acquired in MeCN at 23 °C. ^b PF₆ salt. ^c From ref. 15. ^d From ref. 13.

In the initial report by Busch and coworkers, it is discussed that there is a scalar variable which is needed to balance the Ni(II) and Fe(II) Dq values. In the complexes studied in their report

this varied from 1.02 to 1.21, though it was observed that this scalar “constant” approaches 1 as Dq increases. For instance, the two highest Ni(II) Dq values of 1080 and 1120 cm⁻¹ (for the hexaammine and tris(ethylenediamine) species, respectively) have scalars of 1.03 and 1.02, respectively. This implies that our Ni compounds, which vary in Dq between 1100 and 1250 cm⁻¹, might possess nearly equal values for their Fe(II) analogs, if this hypothesis is applicable here.

5.4.3. Discussion of SCO Fe(II) tren Podands

We are prompted to review the literature concerning Fe(II) tren-capped podands, in an effort to understand the LS nature of our compounds. Analysis of several SCO systems of this nature offers some insight into the phenomenon we were expecting to observe. First, it has been demonstrated that in both tren-capped iminopyrazole and iminothiazole podands, the central nitrogen in tren puckers toward the Fe when in the HS state.³³⁻³⁵ This is in contrast to the LS species, including the iminopyridines described here, where the central nitrogen remains nearly trigonal planar (Figure 5.4.5). This observation is also consistent with a recently reported iminotriazole species.³⁶



Figure 5.4.5. Overlay of the HS (grey) and LS (black) crystal structures of $[\text{Fe}(\text{pz}_3\text{tren})](\text{NO}_3)_2 \cdot \text{CH}_3\text{NO}_2$. This figure is reproduced from reference 33.

While this may be the most marked difference between LS and HS structures, Halcrow describes in detail the structural distortions that occur during the SCO transition. This includes an expansion of the imine N-N-N plane (*via* increase in Fe- N_{imine} bond lengths) as well as an increase in Fe- $\text{N}_{\text{pyridine}}$ bond lengths in the HS structure. Additionally, there is a large change in the Σ (deviation from octahedral) and Θ (distortion toward trigonal prismatic) structural parameters, signaling a distortion from the capped trigonal antiprismatic geometry in the LS state (Table 5.4.4).³⁷ This also manifests in a nearly 0.13 Å difference in intra-arm $\text{N}_{\text{imine}} \cdots \text{N}_{\text{pyridine}}$ distance between the 300 K (HS) and 30 K (LS) structures in the iminopyrazole system, a parameter which can determine spin state, as recently discussed by Shatruk and coworkers.³⁸

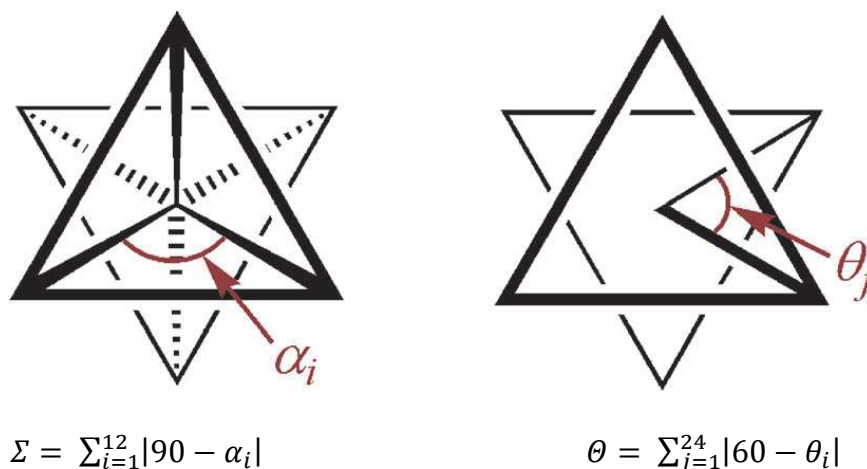


Table 5.4.4. Summary of structural changes upon SCO in Fe(II) tren-capped tripodal systems.

Species	$T_{1/2}$ (K)	$\Delta\text{Fe-N}_{\text{bridge}}$ (Å)	$\Delta\Sigma$ (°)	$\Delta\Theta$ (°)	Ref.
[Fe(6-Mepy) ₃ tren](ClO ₄) ₂	233	0.362(3)	27(1)	70	16
[Fe(6-Me-5-OC ₆ H ₁₃ py) ₃ tren](ClO ₄) ₂	146	0.357	34.5(4)	79	17
[Fe(pz ₃)tren](NO ₃) ₂ · CH ₃ NO ₂	139	0.474(3)	25.0(5)	64	33
[Fe(4-imid) ₃ tren](BF ₄) ₂ · 3H ₂ O	210	0.634(7)	49.0(8)	81	40
{[Fe(2-Me-4-imid) ₃ tren]Cl}(PF ₆)	122	0.372(3)	22.4(4)	87	43
[Fe(2-imid) ₃ tren](BF ₄) ₂ · H ₂ O	^a	0.497(2)	54.3(3)	88	42
[Fe(6-CH ₂ OHpy) ₃ tren](OTf) ₂	173	0.535(9)	35.0(1)	77	14
[Fe(thiazole) ₃ tren](BF ₄) ₂	208	0.687(1)	61.1(1)	95	35
[Fe(triazole) ₃ tren](NTf ₂) ₂	280	0.354(8)	25.0(5)	53	36

^a Magnetic susceptibility data were not collected in the report.

Further, several hexadentate Fe iminoimidazole species have also displayed similar behavior. Three different substitution patterns (4-imidazolyl, 2-imidazolyl and 2-alkyl-4-imidazolyl) have given rise to SCO compounds.³⁹⁻⁴³ As is the case with the pyrazolyl-bound species, these imidazole podands exhibit a high degree of hydrogen-bonding interactions between co-crystallized solvents or anions and the additional N in the heterocycle. Therefore, changing the counter anion can affect the SCO properties significantly in these systems.

These less basic heterocycles (weaker σ donor ligands) can likely access their HS states because of increased ligand flexibility due to the non-ideal Fe-N_{heterocycle} angles. The iminopyridines, in the absence of 6-methylation, are all LS; this is rationalized as a deviation from the ideal bonding angle would cause an increase in energy, meaning the system cannot

accommodate the structural changes necessary for a LS \rightarrow HS transition. This assertion is supported by the phenylsulfide-containing **5-16** described here, which exhibits intramolecular π stacking and a lower than expected $\chi_M T$ value (and also higher than expected Dq value in its Ni(II) congener). In all, it seems in the current iminopyridine scaffold, the LS state will be favored indifferent of ligand electronics, and either lowering the molecular symmetry or increasing ligand flexibility (by 6-alkylation, removing the tren capping ligand or imine reduction) may be required to achieve SCO in these systems.

5.5 Conclusions

In all, we describe here six novel Fe(II) tren iminopyridine salts which are all LS at room temperature. Assessment of the electronic effect of 5-substitution was accomplished with the Ni(II) analogs by tracking Dq as a function of substituent Hammett parameter. This analysis reveals a linear relationship, where electron withdrawing groups give rise to smaller Dq values and stronger *meta* effects on the pyridine N. Comparison to other SCO tren Fe(II) podands suggests that either removal of the tren capping ligand or increase in ligand flexibility will allow for formation of a HS (or SCO) species. This would open the door for their use in potential sensing applications.

5.6 Acknowledgments

This work is supported by Colorado State University and the NSF (CHE-1363274). Devon Shircliff is thanked for bringing up starting materials necessary to synthesize **5-11** and **5-13** for compound characterization.

References

1. Halcrow, M. A. *Spin-crossover materials: properties and applications*; Wiley: West Sussex, UK, 2013.
2. Kahn, O.; Martinez, C. J. *Science* **1998**, *279*, 44.
3. Létard, J.-F.; Guionneau, P.; Goux-Capes, L. *Top. Curr. Chem.* **2004**, *235*, 221.
4. Kumar, K. S.; Ruben, M. *Coord. Chem. Rev.* **2017**, *346*, 176.
5. Jeon, I.-R.; Park, J. G.; Haney, C. R.; Harris, T. D. *Chem. Sci.* **2014**, *5*, 2461.
6. Thorarinsdottir, A. E.; Gaudette, A. I.; Harris, T. D. *Chem. Sci.* **2017**, *8*, 2448.
7. Prat, I.; Company, A.; Corona, T.; Parella, T.; Ribas, X.; Costas, M. *Inorg. Chem.* **2013**, *52*, 9229.
8. Nakano, K.; Suemura, N.; Yoneda, K.; Kawata, S.; Kaizaki, S. *Dalton Trans.* **2005**, 740.
9. Lin, H.-J.; Siretanu, D.; Dickie, D. A.; Subedi, D.; Scepaniak, J. J.; Mitcov, D.; Clérac, R.; Smith, J. M. *J. Am. Chem. Soc.* **2014**, *136*, 13326.
10. Kershaw Cook, L. J.; Kulmaczewski, R.; Mohammed, R.; Dudley, S.; Barrett, S. A.; Little, M. A.; Deeth, R. J.; Halcrow, M. A. *Angew Chem. Int. Ed.* **2016**, *55*, 4327.
11. Takahashi, K.; Hasegawa, Y.; Sakamoto, R.; Nishikawa, M.; Kume, S.; Nishibori, E.; Nishihara, H. *Inorg. Chem.* **2012**, *51*, 5188.
12. McDaniel, A. M.; Klug, C. M.; Shores, M. P. *Eur. J. Inorg. Chem.* **2013**, 943.
13. McDaniel, A. M.; Rappé, A. K.; Shores, M. P. *Inorg. Chem.* **2012**, *51*, 12493.
14. Klug, C. M.; McDaniel, A. M.; Fiedler, S. R.; Schulte, K. A.; Newell, B. S.; Shores, M. P. *Dalton Trans.* **2012**, *41*, 12577.
15. Wilson, L. J.; Georges, D.; Hoselton, M. A. *Inorg. Chem.* **1975**, *14*, 2968.
16. Seredyuk, M.; Gaspar, A. B.; Kusz, J.; Bednarek, G.; Gütllich, P. *J. Appl. Cryst.* **2007**, *40*, 1135.
17. Seredyuk, M.; Gaspar, A. B.; Ksenofontov, V.; Galyametdinov, Y.; Kusz, J.; Gütllich, P. *J. Am. Chem. Soc.* **2008**, *130*, 1431.

18. Hoselton, M. A.; Wilson, L. J.; Drago, R. S. *J. Am. Chem. Soc.* **1975**, *97*, 1722.
19. Evans, D. F. *J. Chem. Soc.* **1959**, 2003.
20. Hagen, K. S. *Inorg. Chem.* **2000**, *39*, 5867.
21. *Apex 3*; Bruker Analytical X-Ray Systems, Inc.: Madison, WI, 2015.
22. G. M. Sheldrick *SHELXTL, Version 6.14*; Bruker Analytical X-Ray Systems, Inc.: Madison, WI, 1999.
23. Faulkner, A. D.; Kaner, R. A.; Abdallah, Q. M. A.; Clarkson, G.; Fox, D. J.; Gurnani, P.; Howson, S. E.; Phillips, R. M.; Roper, D. I.; Simpson, D. H.; Scott, P. *Nat. Chem.* **2014**, *6*, 797.
24. Stock, N. S.; Bain, G.; Zunic, J.; Li, Y.; Ziff, J.; Roppe, J.; Santini, A.; Darlington, J.; Prodanovich, P.; King, C. D.; Baccei, C.; Lee, C.; Rong, H.; Chapman, C.; Broadhead, A.; Lorrain, D.; Correa, L.; Hutchinson, J. H.; Evans, J. F.; Prasit, P. *J. Med. Chem.* **2011**, *54*, 8013.
25. Wang, Q.; Zhang, S.; Guo, F.; Zhang, B.; Hu, P.; Wang, Z. *J. Org. Chem.* **2012**, *77*, 11161.
26. Benjahad, A.; Oumouch, S.; Guillemont, J.; Pasquier, E.; Mabire, D.; Andries, K.; Nguyen, C. H.; Grierson, D. S. *Bioorg. Med. Chem. Lett.* **2007**, *17*, 712.
27. Roberts, D. A.; Pilgrim, B. S.; Cooper, J. D.; Ronson, T. K.; Zarra, S.; Nitschke, J. R. *J. Am. Chem. Soc.* **2015**, *137*, 10068.
28. Itoh, T.; Mase, T. *Org. Lett.* **2004**, *6*, 4587.
29. Sterckx, H.; De Houwer, J.; Mensch, C.; Caretti, I.; Tehrani, K. A.; Herrebout, W. A.; Van Doorslaer, S.; Maes, B. U. W. *Chem. Sci.* **2016**, *7*, 346.
30. Goodwin, H. A. *Top. Curr. Chem.* **2004**, *233*, 59.
31. Robinson, M. A.; Busch, D. H.; Curry, J. D. *Inorg. Chem.* **1963**, *2*, 1178.
32. Halcrow, M. A. *Crystals* **2016**, *6*, 58.
33. Lazar, H. Z.; Forestier, T.; Barrett, S. A.; Kilner, C. A.; Létard, J.-F.; Halcrow, M. A. *Dalton Trans.* **2007**, *38*, 4276.
34. Struch, N.; Wagner, N.; Schnakenburg, G.; Weisbarth, R.; Klos, S.; Beck, J.; Lützen, A. *Dalton Trans.* **2016**, *45*, 14023.

35. Kulmaczewski, R.; Cespedes, O.; Halcrow, M. A. *Inorg. Chem.* **2017**, *56*, 3144.
36. Hagiwara, H.; Minoura, R.; Okada, S.; Sunatsuki, Y. *Chem. Lett.* **2014**, *43*, 950.
37. Halcrow, M. A. *Chem. Soc. Rev.* **2011**, *40*, 4119.
38. Phan, H.; Hrudka, J. J.; Igimbayeva, D.; Lawson Daku, L. M.; Shatruk, M. *J. Am. Chem. Soc.* **2017**, *139*, 6437.
39. Brewer, C.; Brewer, G.; Patil, G.; Sun, Y. Q.; Viragh, C.; Butcher, R. J. *Inorg. Chim. Acta* **2005**, *358*, 3441.
40. Sunatsuki, Y.; Ohta, H.; Kojima, M.; Ikuta, Y.; Goto, Y.; Matsumoto, N.; Iijima, S.; Akashi, H.; Kaizaki, S.; Dahan, F.; Tuchagues, J.-P. *Inorg. Chem.* **2004**, *43*, 4154.
41. Hagiwara, H.; Matsumoto, N.; Iijima, S.; Kojima, M. *Inorg. Chim. Acta* **2011**, *366*, 283.
42. Alvarado, L.; Brewer, C.; Brewer, G.; Butcher, R. J.; Straka, A.; Viragh, C. *CrystEngComm* **2009**, *11*, 2297.
43. Yamada, M.; Hagiwara, H.; Torigoe, H.; Matsumoto, N.; Kojima, M.; Dahan, F.; Tuchagues, J.-P.; Re, N.; Iijima, S. *Chem. Eur. J.* **2006**, *12*, 4536.

Appendix 1: Supporting Information for Chapter 2

Cross referencing of dissertation numbering with numbering from published work.

Reference 1: *Org. Lett.* **2016**, 18, 64.

Reference 2: *Org. Lett.* **2017**, 19, 294.

Dissertation Number	Publication Number	Reference (1 or 2)	Dissertation Number	Publication Number	Reference (1 or 2)
2-40	1a	1	2-69j	3kc	1
2-56	3ab	1	2-69k	3lc	1
2-57	3ac	1	2-70	S1	1
2-58	3ad	1	2-71	S2	1
2-59	3ae	1	2-72	S3	1
2-60	3af	1	2-73	S4	1
2-61	3ag	1	2-74	4	1
2-62	3aa	1	2-75	S5	1
2-63	3ah	1	2-76	S6	1
2-64	3ai	1	2-77	S7	1
2-65	3aj	1	2-78	S8	1
2-66	3ak	1	2-79	5	1
2-67	3al	1	2-80	6	1
2-68a	1b	1	2-81	7	1
2-68b	1c	1	2-82	7	2
2-68c	1d	1	2-83	8	2
2-68d	1e	1	2-84	9	2
2-68e	1f	1	2-85	S1	2
2-68f	1g	1	2-86	10	2
2-68g	1h	1	2-87	3a	2
2-68h	1i	1	2-88	S6	2
2-68i	1j	1	2-89	S7	2
2-68j	1k	1	2-90	S8	2
2-68k	1l	1	2-91	S9	2
2-69a	3bc	1	2-92	S10	2
2-69b	3cc	1	2-93	S11	2
2-69c	3dc	1	2-94	11	2
2-69d	3ec	1	2-95	5a	2
2-69e	3fc	1	2-96	6aa	2
2-69f	3gc	1	2-97	12	2
2-69g	3hc	1			
2-69h	3ic	1			
2-69i	3jc	1			

Appendix 2: Supporting Information for Chapter 3

IR and Electronic Spectral Characterization of Co Complexes

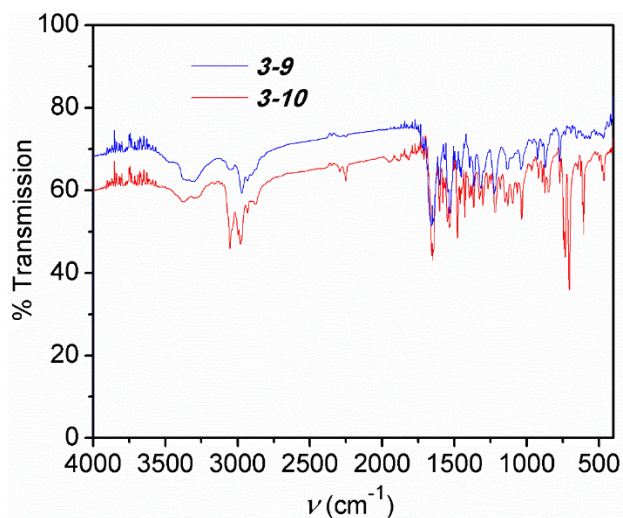


Figure A2.1. Stacked IR spectra of **3-9** and **3-10**. Spectra were obtained using KBr pellets.

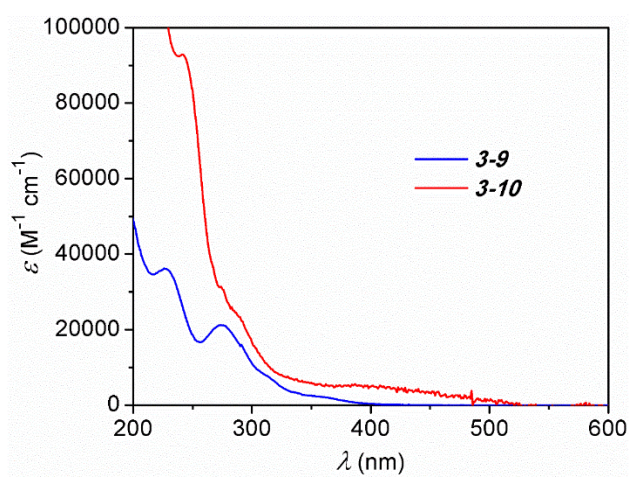


Figure A2.2. Stacked UV-Vis spectra of **3-9** and **3-10**. Spectra were taken in either MeOH (for **3-9**) or MeCN (for **3-10**).

Magnetic Data of Co Complexes

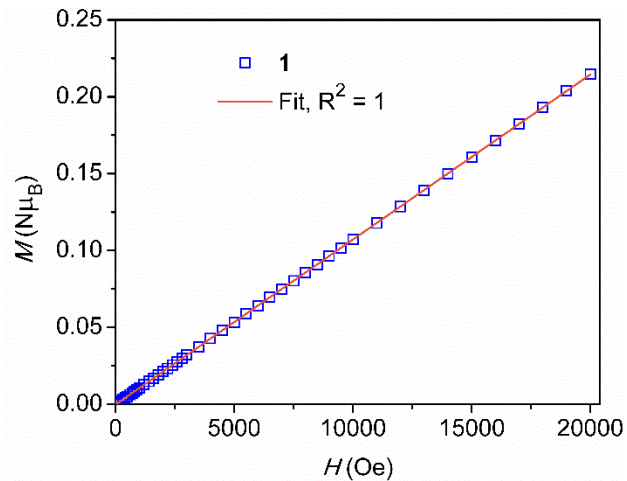


Figure A2.3. Field dependence of magnetization for **3-9** collected at 100 K. Fit: $y = 1.07 \times 10^{-5}(x) - 1.84 \times 10^{-4}$ ($R^2 = 1$).

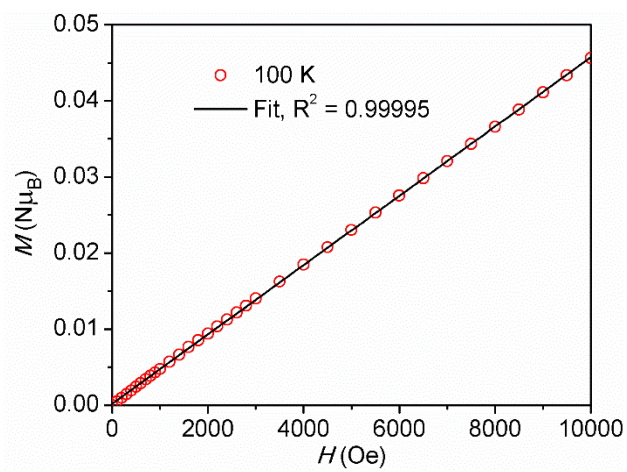


Figure A2.4. Field dependence of magnetization for **3-10** collected at 100 K. Fit: $y = 4.55 \times 10^{-6}(x) - 2.02 \times 10^{-4}$ ($R^2 = 0.99995$).

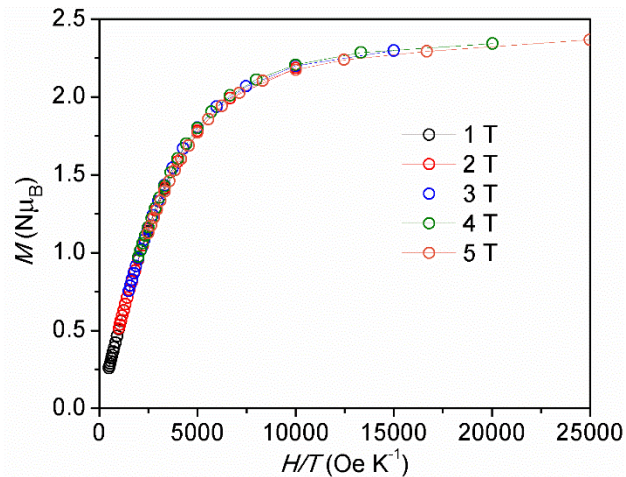


Figure A2.5. Reduced magnetization of **3-10**. The connecting lines are guides for the eye.

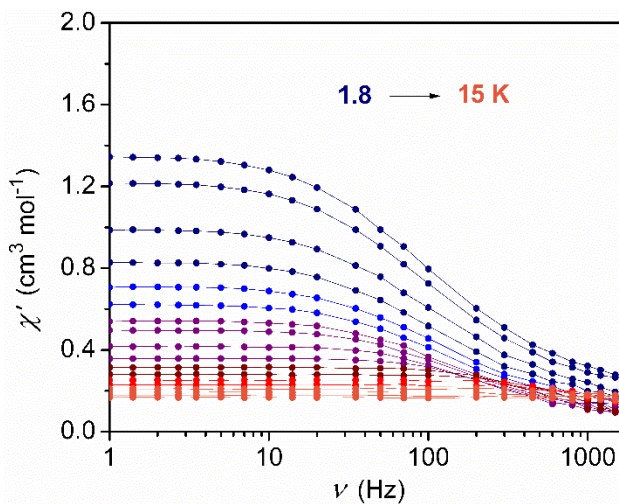


Figure A2.6. χ' vs. ν under 0 applied DC field for **3-10**. The temperature was increased in 0.5 K increments from 2 K to 5 K, and 1 K increments from 6 K to 13 K. Data were acquired using an oscillating field of 4 Oe. The lines are guides for the eye.

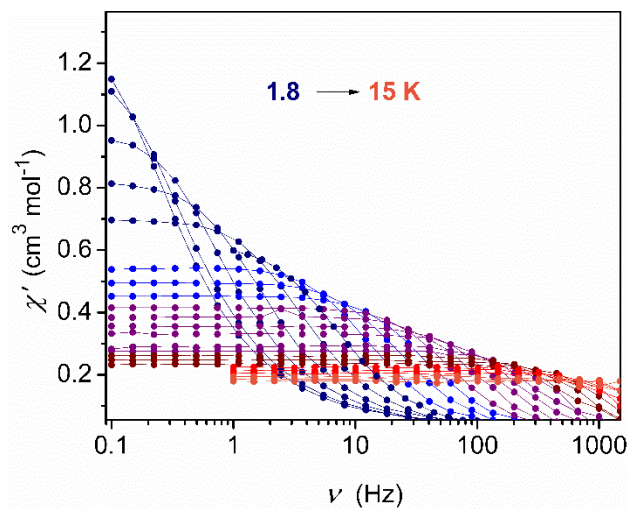


Figure A2.7. χ' vs. ν under 1000 Oe applied DC field for **3-10**. The temperature was increased in 0.5 K increments from 2 K to 13 K, and 1 K increments from 14 to 15 K. Data were acquired using an oscillating field of 4 Oe. The lines are guides for the eye.

Appendix 3: Supporting Information for Chapter 4

A3.1. Mass Spectrometry Data

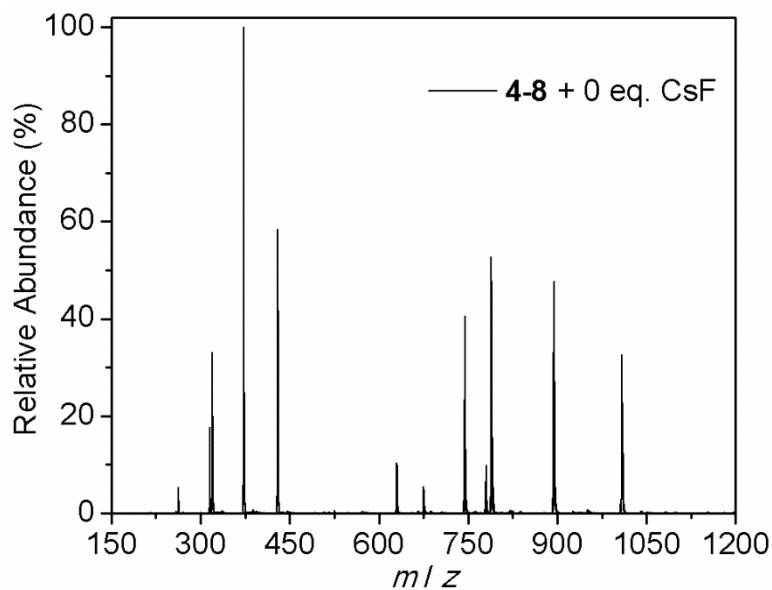


Figure A3.1. Full MS (positive ion mode) of **4-8** with 0 equivalents of CsF added in CD₃OD.

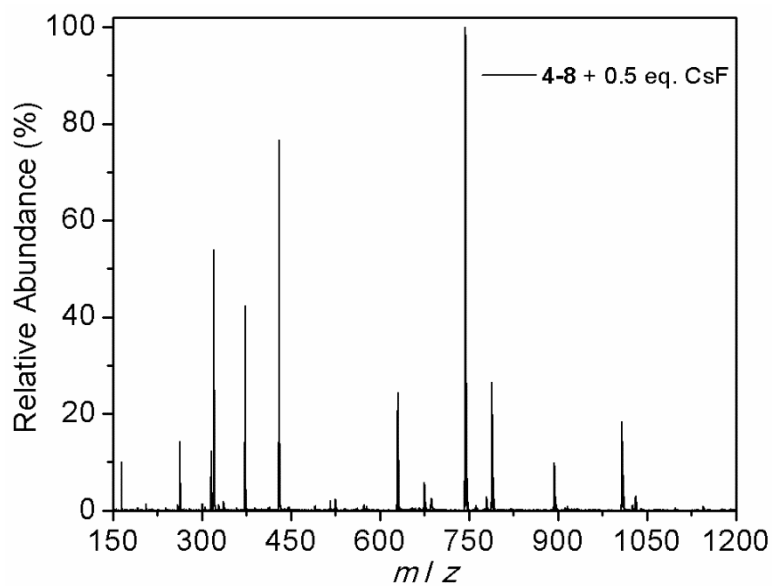


Figure A3.2. Full MS (positive ion mode) of **4-8** with 0.5 equivalents of CsF added in CD₃OD.

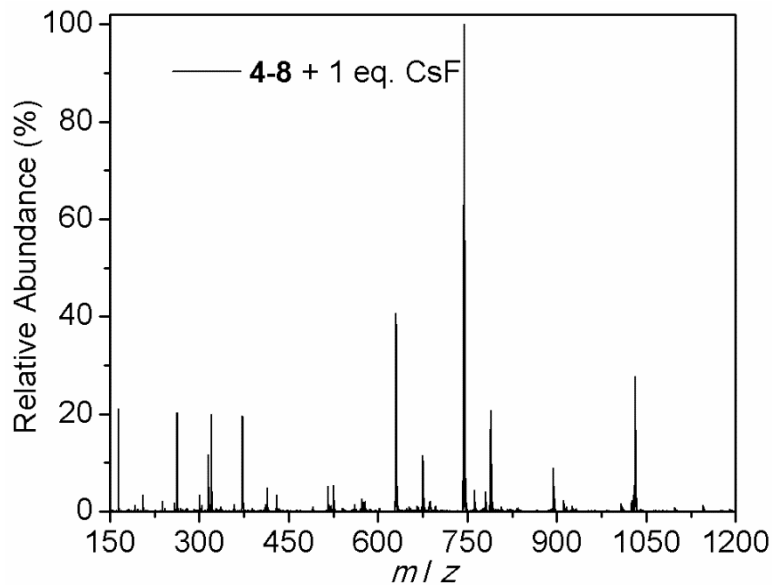


Figure A3.3. Full MS (positive ion mode) of **4-8** with 1 equivalent of CsF added in CD_3OD .

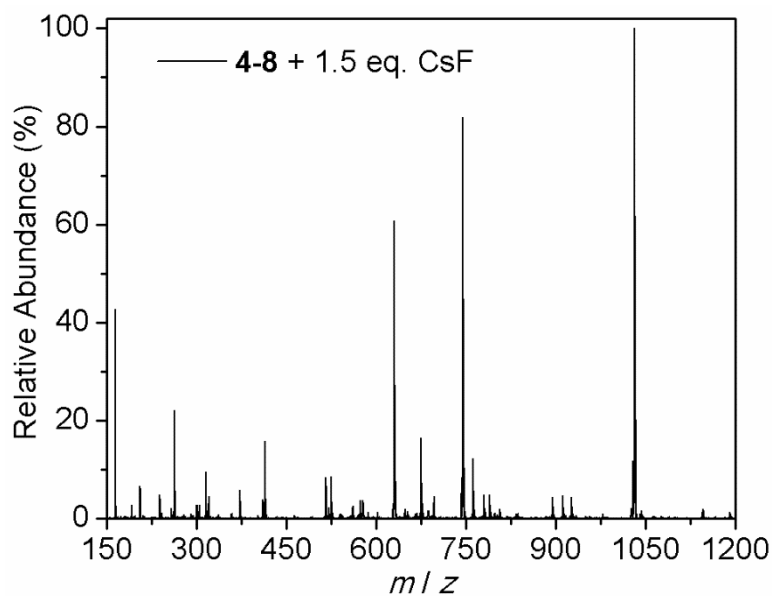


Figure A3.4. Full MS (positive ion mode) of **4-8** with 1.5 equivalents of CsF added in CD_3OD .

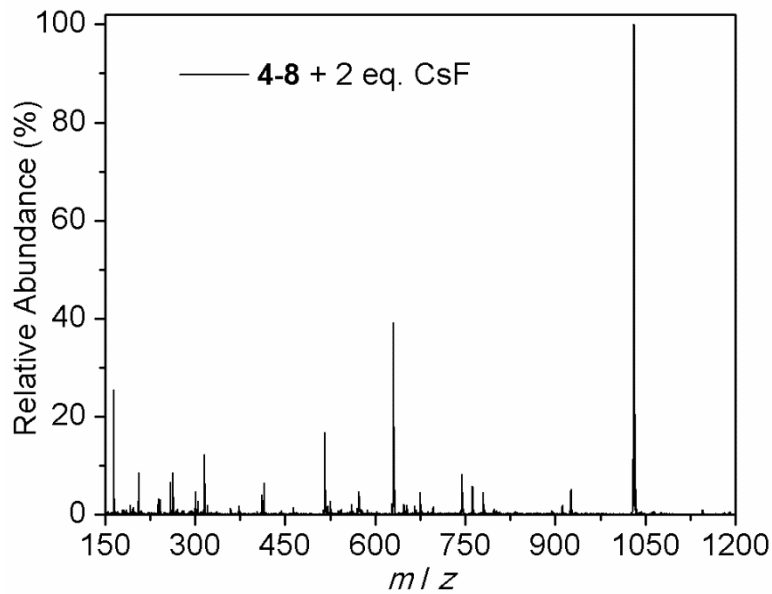


Figure A3.5. Full MS (positive ion mode) of **4-8** with 2 equivalents of CsF added in CD_3OD .

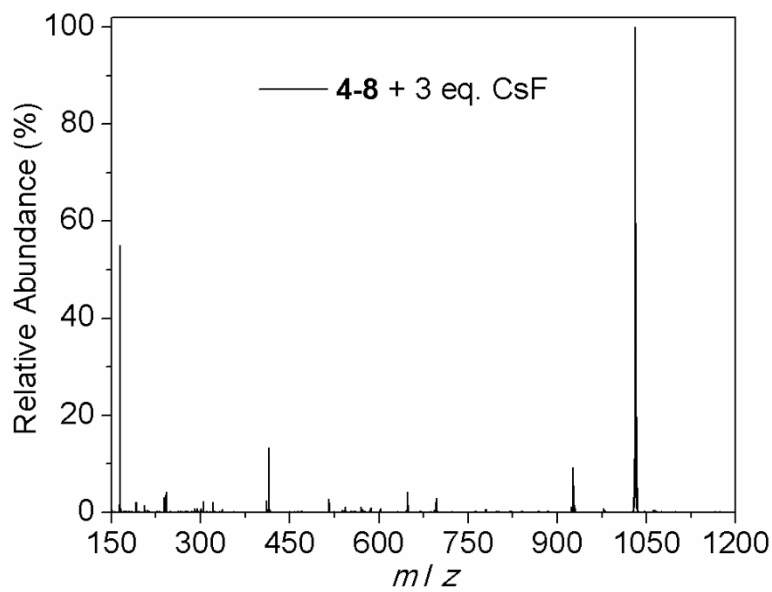


Figure A3.6. Full MS (positive ion mode) of **4-8** with 3 equivalents of CsF added in CD_3OD .

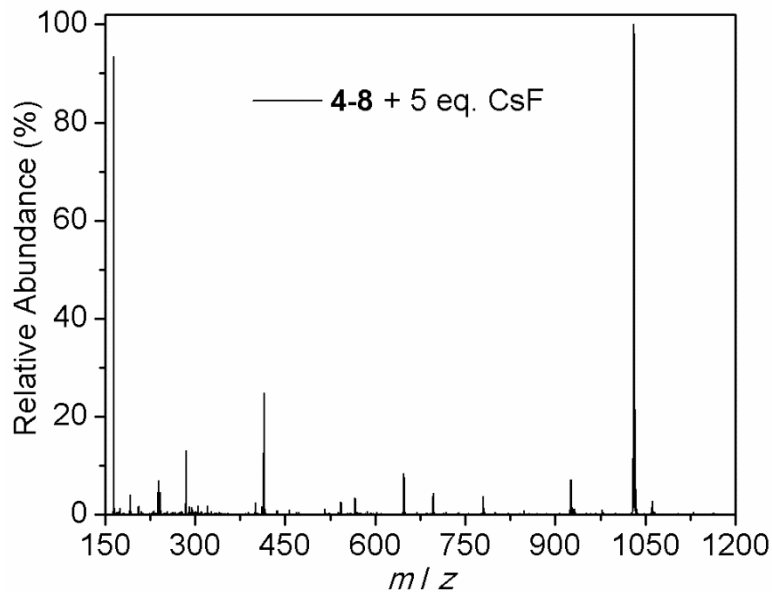


Figure A3.7. Full MS (positive ion mode) of **4-8** with 5 equivalents of CsF added in CD_3OD .

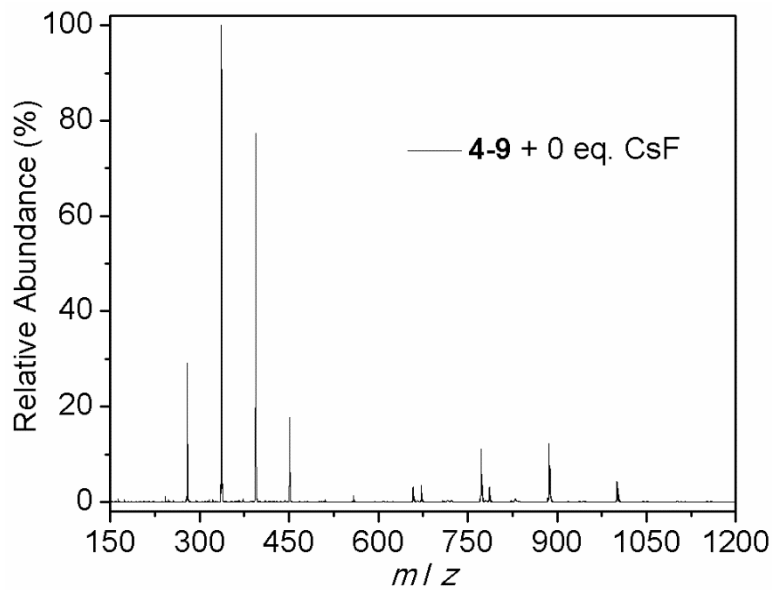


Figure A3.8. Full MS (positive ion mode) of **4-9** with 0 equivalents of CsF added in CD_3OD .

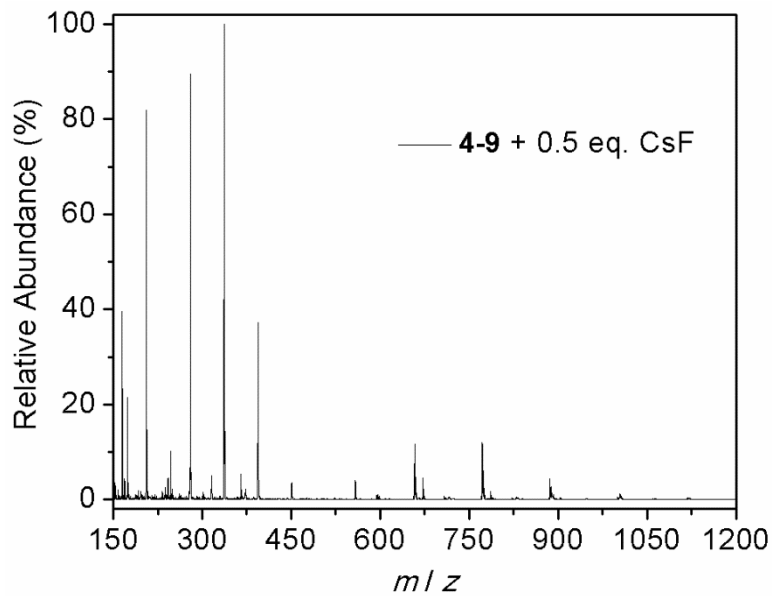


Figure A3.9. Full MS (positive ion mode) of **4-9** with 0.5 equivalents of CsF added in CD_3OD .

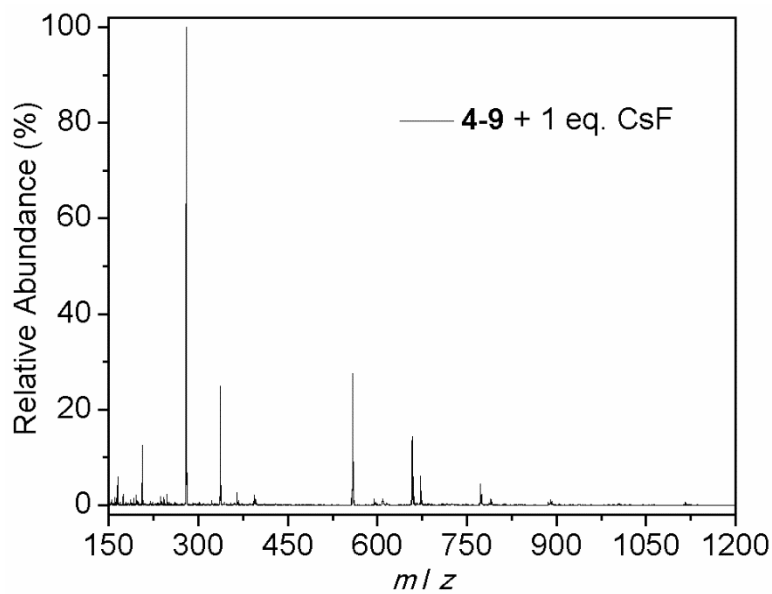


Figure A3.10. Full MS (positive ion mode) of **4-9** with 1 equivalent of CsF added in CD_3OD .

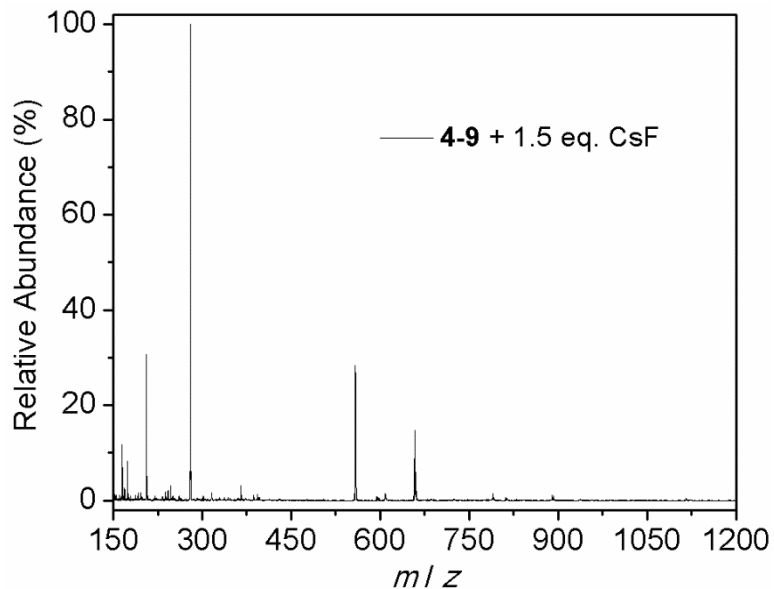


Figure A3.11. Full MS (positive ion mode) of **4-9** with 1.5 equivalents of CsF added in CD_3OD .

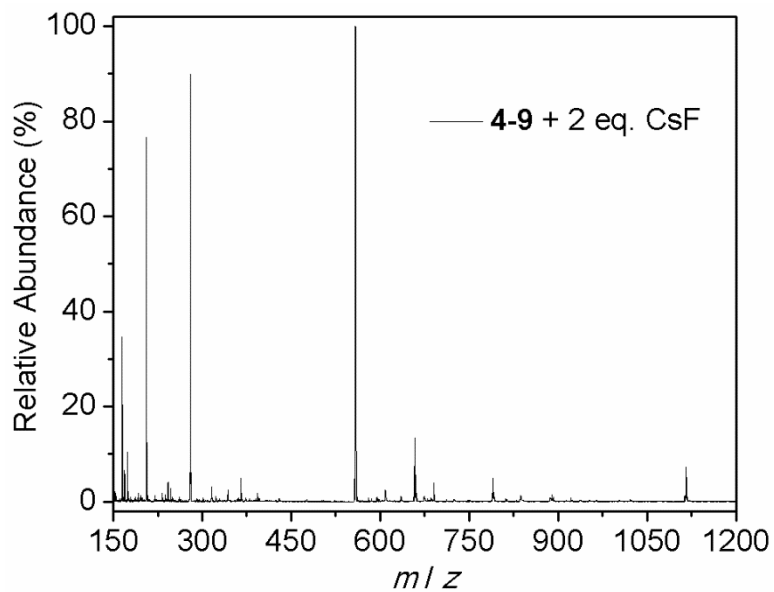


Figure A3.12. Full MS (positive ion mode) of **4-9** with 2 equivalents of CsF added in CD_3OD .

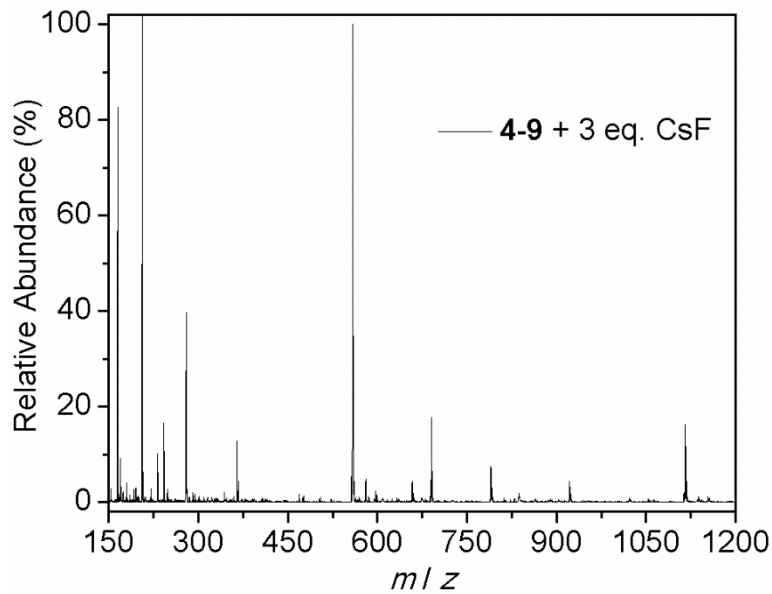


Figure A3.13. Full MS (positive ion mode) of **4-9** with 3 equivalents of CsF added in CD₃OD.

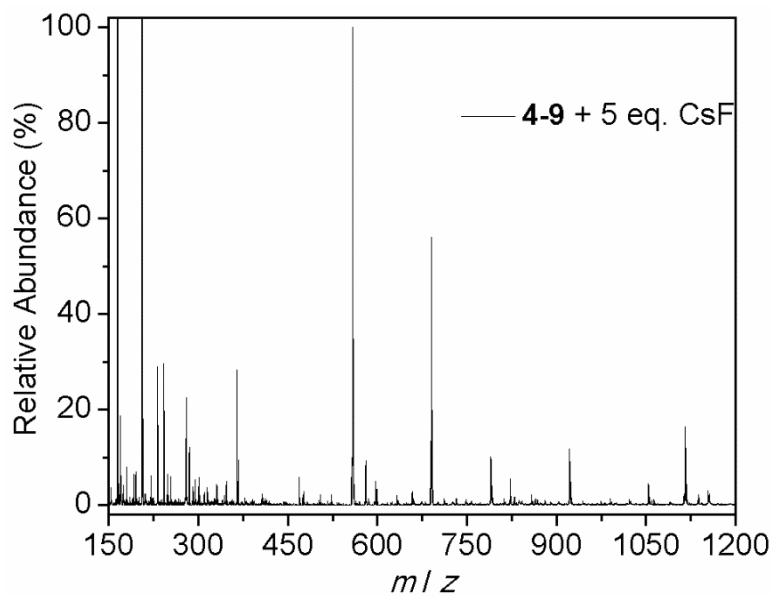


Figure A3.14. Full MS (positive ion mode) of **4-9** with 5 equivalents of CsF added in CD₃OD.

Table A3.1. Major peaks in the ESI-MS spectra for **4-8** before and after addition of CsF.

species	Observed m/z	Expected m/z
$[\text{Cs} + \text{MeOH}]^+$	164.92	164.93
$[\text{L} + \text{Fe} - \text{arm} - \text{TBS} + \text{H}]^{2+}$	263.17	263.11
$[\text{L} + \text{Fe} - 2\text{TBS} + 2\text{H}]^{2+}$	315.67	315.62
$[\text{L} + \text{Fe} - \text{arm}]^{2+}$	320.92	320.65
$[\text{L} + \text{Fe} - \text{TBS} + \text{H}]^{2+}$	372.75	372.66
$[\text{L} + \text{Cs} - 2(\text{arm}) - \text{TBS} + \text{MeOH}]^+$	414.75	415.10
$[\text{L} + \text{Fe}]^{2+}$	429.83	429.71
$[\text{L} + \text{Fe} - 3(\text{TBS}) + 2(\text{H})]^+$	516.33	516.27
$[\text{L} + \text{Fe} - 2(\text{TBS}) + \text{H}]^+$	630.42	630.23
$[\text{L} + \text{Fe} - 2(\text{TBS}) + \text{H} + \text{H}_2\text{O}]^+$	648.25	648.24
$[\text{L} + \text{Fe} - \text{arm} - \text{TBS} + \text{H} + \text{OTf}]^+$	675.17	675.17
$[\text{L} + \text{Fe} - \text{TBS}]^+$	744.50	744.32
$[\text{L} + \text{Fe} - 2(\text{TBS}) + 2(\text{H}) + \text{OTf}]^+$	780.42	780.19
$[\text{L} + \text{Fe} - \text{arm} + \text{OTf}]^+$	789.25	789.26
$[\text{L} + \text{Fe} - \text{TBS} + \text{H} + \text{OTf}]^+$	894.25	894.28
$[\text{L} + \text{Fe} - \text{TBS} + \text{H} + \text{MeOH} + \text{OTf}]^+$	926.42	926.30
$[\text{L} + \text{Fe} + \text{OTf}]^+$	1008.33	1008.36
$[\text{L} + \text{Fe} - 3(\text{TBS}) + 2.5(\text{H})]_2^+$	1031.42	1031.41

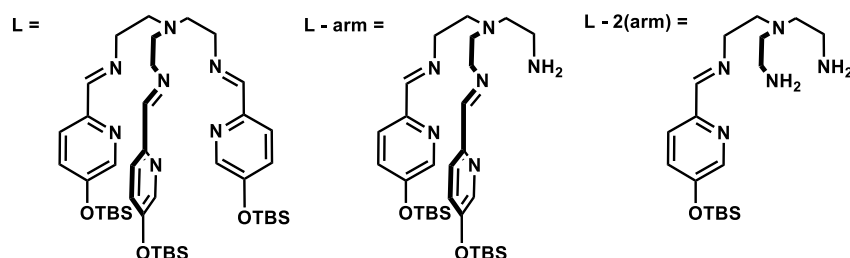


Table A3.2. Major peaks in the ESI-MS spectra for **4-9** before and after addition of CsF.

species	Observed m/z	Expected m/z
$[\text{L} + \text{Fe} - 3(\text{TBS}) + 3(\text{H})]^{2+}$	279.67	279.60
$[\text{L} + \text{Fe} - 2(\text{TBS}) + 2(\text{H})]^{2+}$	336.67	336.64
$[\text{Cs} + 3(\text{MeOH}) + \text{ClO}_4 + \text{H} + 2(\text{H}_2\text{O})]^+$	364.83	364.96
$[\text{L} + \text{Fe} - \text{TBS} + \text{H}]^{2+}$	393.67	393.69
$[\text{L} + \text{Fe} - \text{TBS} + \text{H}]^{2+}$	450.75	450.73
$[\text{L} + \text{Fe} - 3(\text{TBS}) + 2(\text{H})]^+$	558.17	558.19
$[\text{L} + \text{Fe} - 3(\text{TBS}) + 3(\text{H}) + \text{ClO}_4]^+$	658.25	658.15
$[\text{L} + \text{Fe} - 2(\text{TBS}) + \text{H}]^+$	672.17	672.28
$[\text{L} + \text{Fe} - 2(\text{TBS}) + \text{H} + \text{H}_2\text{O}]^+$	690.29	690.17
$[\text{L} + \text{Fe} - 2(\text{TBS}) + 2(\text{H}) + \text{ClO}_4]^+$	772.23	772.08
$[\text{L} + \text{Fe} - 2(\text{TBS}) + 2(\text{H}) + \text{H}_2\text{O} + \text{ClO}_4]^+$	789.92	790.24
$[\text{L} + \text{Fe} - \text{TBS} + \text{H} + \text{ClO}_4]^+$	886.17	886.32
$[\text{L} + \text{Fe} - \text{TBS} + \text{H} + 2(\text{H}_2\text{O}) + \text{ClO}_4]^+$	922.00	922.34
$[\text{L} + \text{Fe} + \text{ClO}_4]^+$	1000.42	1000.41
$[\text{L} + \text{Fe} - 3(\text{TBS}) + 2.5(\text{H})]_2^+$	1115.54	1115.42

Table A3.3. Relative abundance (%) of the major peaks in the ESI-MS spectra for **4-8** with different equivalents of CsF added.

<i>m / z</i>	0 eq.	0.5 eq.	1 eq.	1.5 eq.	2 eq.	3 eq.	5 eq.
263	5	13	20	22	6	0	0
315	14	10	12	8	11	0	0
320	33	54	20	4	1	2	0
372	100	42	20	5	0	0	0
415	0	0	5	16	5	12	25
429	58	77	3	0	0	0	0
516	0	2	4	8	16	2	0
630	10	23	39	58	39	0	0
648	0	0	0	0	1	3	8
675	5	5	12	15	4	0	0
744	34	100	100	79	8	0	0
780	8	3	3	5	3	0	3
789	51	26	20	5	0	0	0
894	46	9	9	4	0	0	0
926	0	0	0	4	4	9	7
1008	31	18	2	0	0	0	0
1031	0	3	28	100	100	100	100

Table A3.4. Relative abundance (%) of the major peaks in the ESI-MS spectra for **4-9** with different equivalents of CsF added.

<i>m / z</i>	0 eq.	0.5 eq.	1 eq.	1.5 eq.	2 eq.	3 eq.	5 eq.
279	29	90	100	100	90	35	23
336	100	100	23	0	0	0	0
393	77	37	0	0	0	0	0
450	18	3	0	0	0	0	0
558	0	4	26	28	100	100	100
658	3	12	14	15	13	4	0
672	4	4	6	0	0	0	0
690	0	0	0	0	3	17	54
772	11	12	4	0	0	0	0
790	0	0	0	0	5	7	8
886	12	4	0	0	0	0	0
922	0	0	0	0	0	4	8
1000	4	0	0	0	0	0	0
1115	0	0	0	0	7	16	16

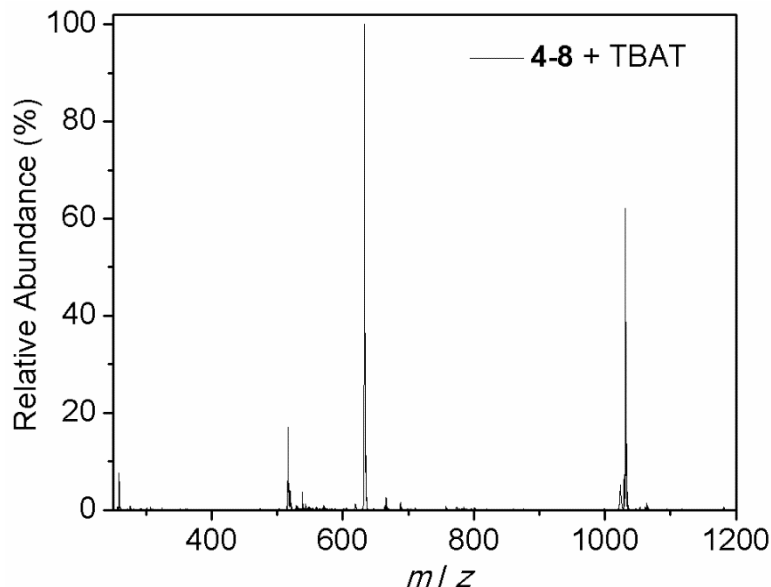


Figure A3.15. Full MS (positive ion mode) of **4-8** in MeOH with excess TBAT added. The largest peak (633 m/z) is identified as $[L - 2(\text{TBS}) + 2\text{H} + \text{Na} + 2\text{H}_2\text{O}]^+$ expected m/z : 633.31 found m/z : 633.25. The peak at 258 m/z corresponds to $[L + \text{Fe} - 2(\text{arm}) + 3(\text{MeOH})]^{2+}$, expected m/z : 258.64, found m/z : 258.67.

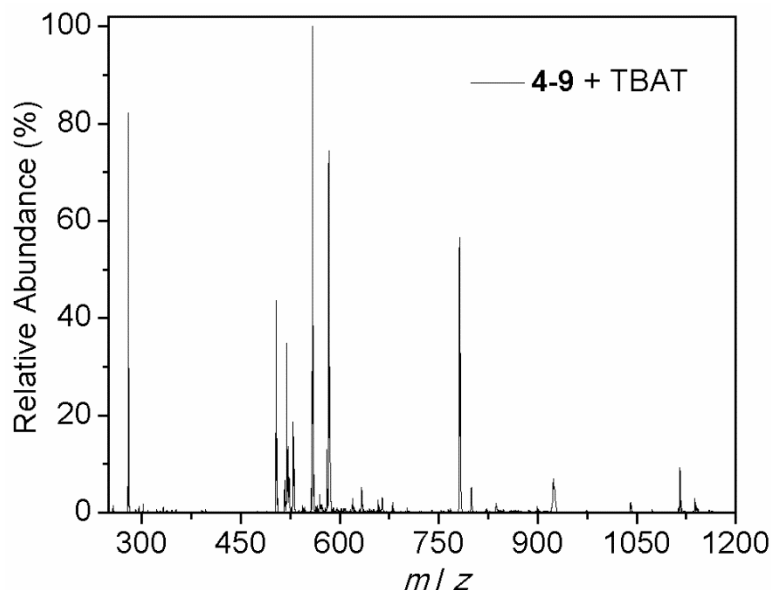


Figure A3.16. Full MS (positive ion mode) of **4-9** in MeOH with excess TBAT added. The identity of peaks at m/z 558 and 279 are in Table A3.2. The 583.42 m/z peak corresponds to $[L + \text{Fe} - 2(\text{TBS}) + 2\text{Na} - \text{arm} + \text{ClO}_4]^+$, expected m/z : 583.07. The 781.50 m/z peak corresponds to $[2(\text{Bu}_4\text{N}) + \text{Ph}_3\text{SiF}_2]^+$, expected m/z : 781.66. The 503.67 m/z peak corresponds to $[2(\text{Bu}_4\text{N}) + \text{F}]^+$, expected m/z : 503.57.

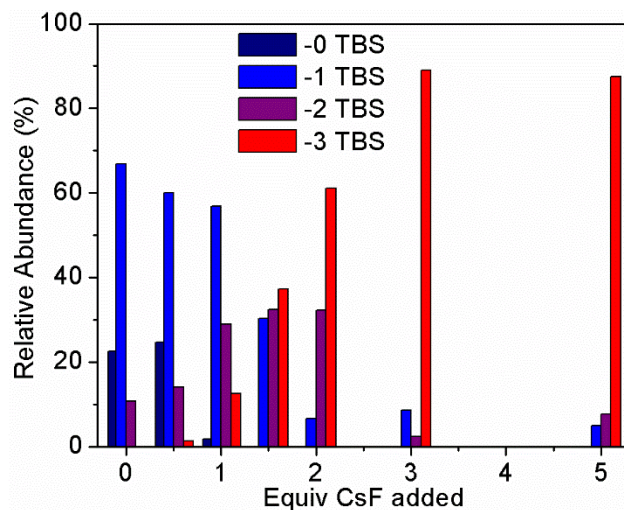


Figure A3.17. Relative abundance of desilylated products as determined by MS for 4-8, desilylated fractions are normalized within each spectrum.

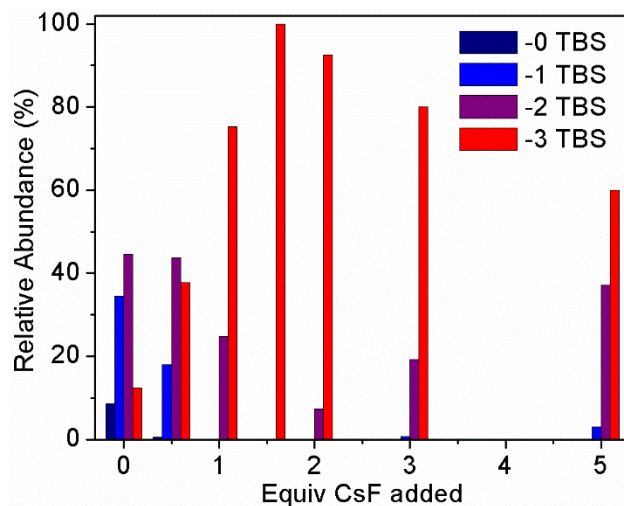


Figure A3.18. Relative abundance of desilylated products as determined by MS for 4-9, desilylated fractions are normalized within each spectrum.

Electrochemical Data

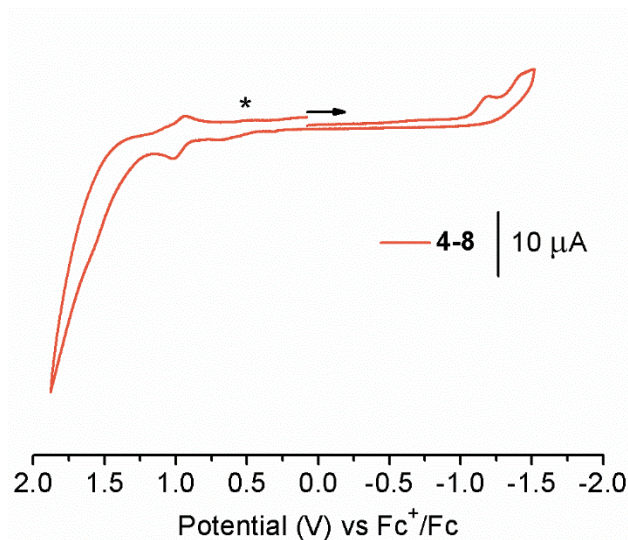


Figure A3.19. Full CV of **4-8** measured in a 0.1 M Bu_4NPF_6 solution of methanol with a scan rate of 0.10 V s^{-1} . The asterisk indicates the open circuit potential and the arrow indicates the direction of the scan. The small anodic current being passed at $\sim 0.75 \text{ V}$ only appears after scanning cathodically to $\sim 1.25 \text{ V}$.

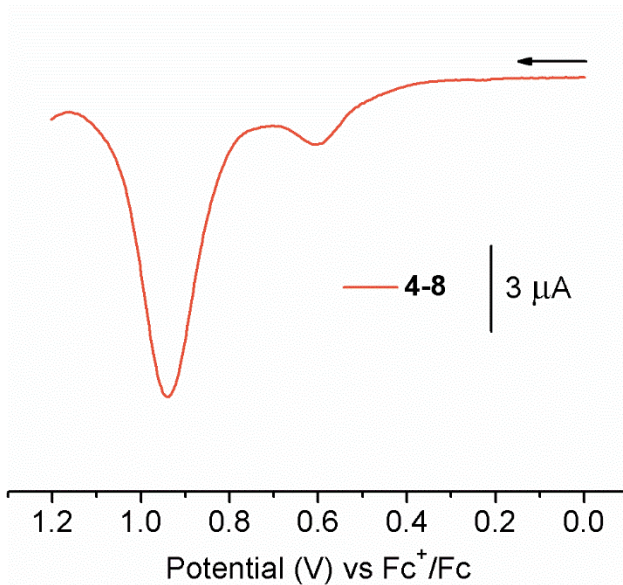


Figure A3.20. A portion of the SWV of **4-8** measured in a 0.10 M Bu_4NPF_6 solution of methanol with a step size of 0.004 V . The arrow indicates the direction of the scan. The small anodic current being passed at $\sim 0.6 \text{ V}$ only appears after scanning cathodically.

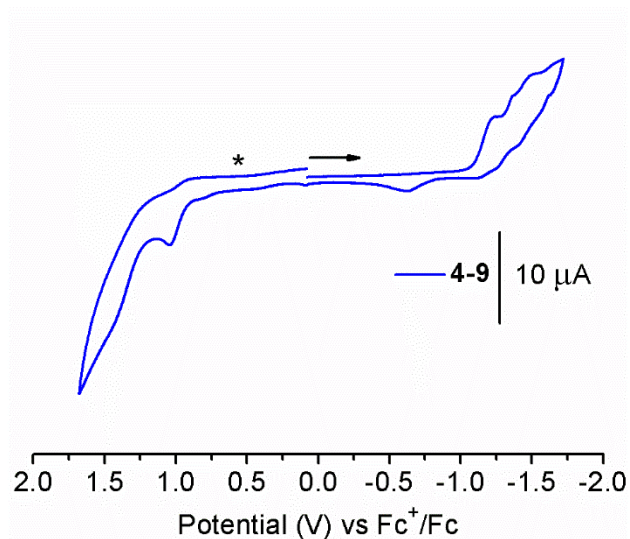


Figure A3.21. Full CV of **4-9** measured in a 0.1 M Bu₄NPF₆ solution of methanol with a scan rate of 0.10 V s⁻¹. The asterisk indicates the open circuit potential and the arrow indicates the direction of the scan.

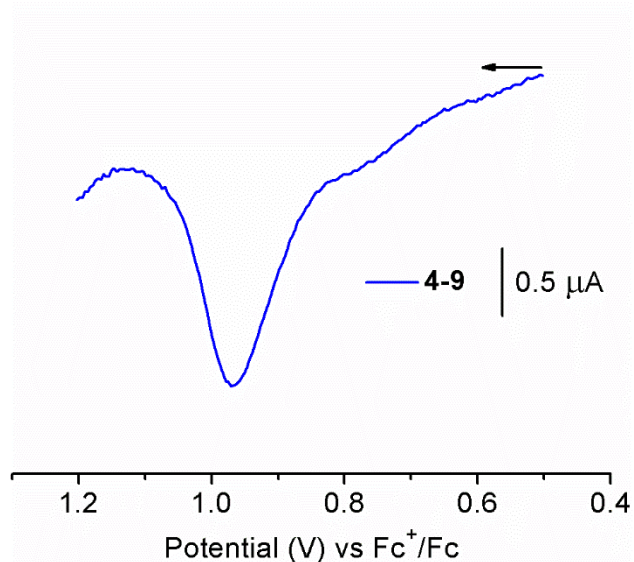


Figure A3.22. A portion of the SWV of **4-9** measured in a 0.10 M Bu₄NPF₆ solution of methanol with a step size of 0.004 V. The arrow indicates the direction of the scan.

Magnetic Data

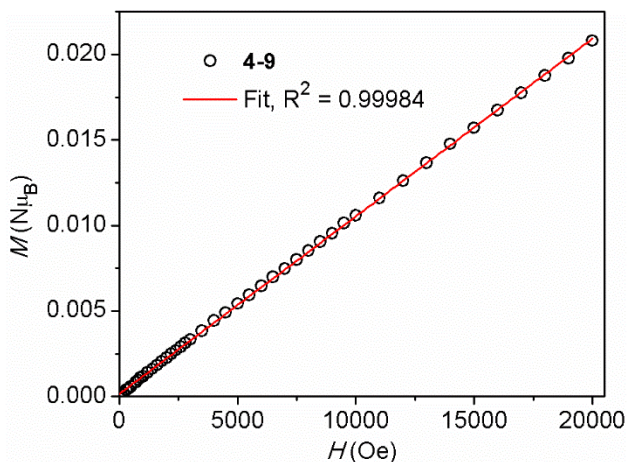


Figure A3.23. Field dependence of magnetization for **4-9** collected at 100 K. Fit: $y = 1.04 \times 10^{-6}(x) + 1.56 \times 10^{-4}$ ($R^2 = 0.99984$).

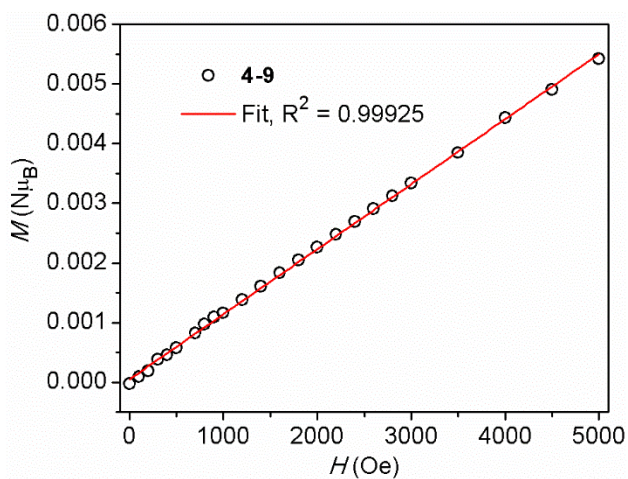
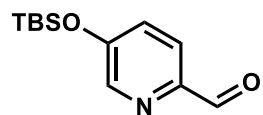


Figure A3.24. Zoom of field dependence of magnetization for **4-9** collected at 100 K. Fit: $y = 1.09 \times 10^{-6}(x) + 5.33 \times 10^{-5}$ ($R^2 = 0.99925$). Note that potential ferromagnetic impurities are quenched with application of a dc field >2000 Oe.

NMR and IR Spectroscopic Data



4-3
¹H NMR
(400 MHz, CDCl₃)

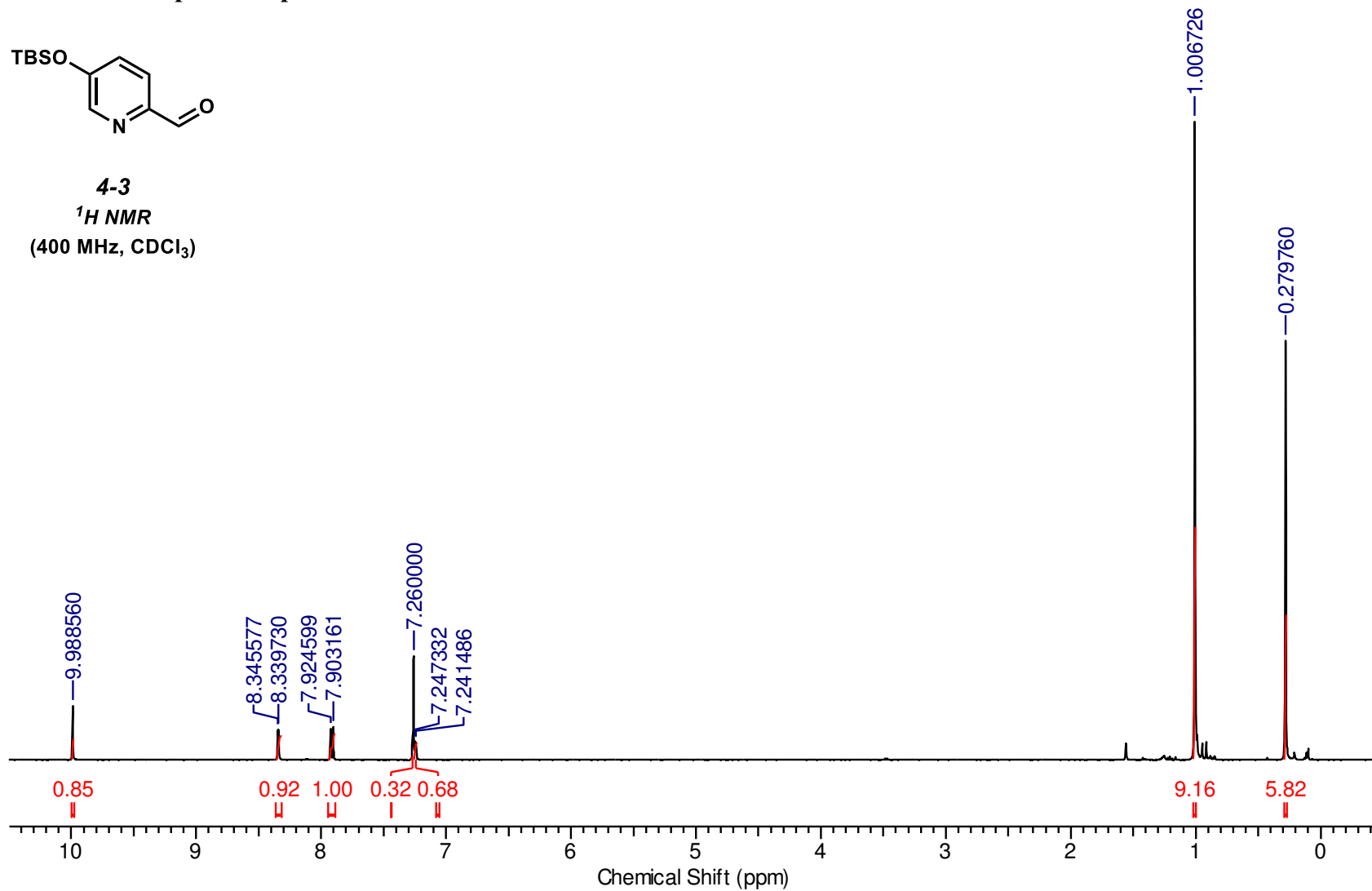


Figure A3.25. ¹H NMR spectrum of 4-3.

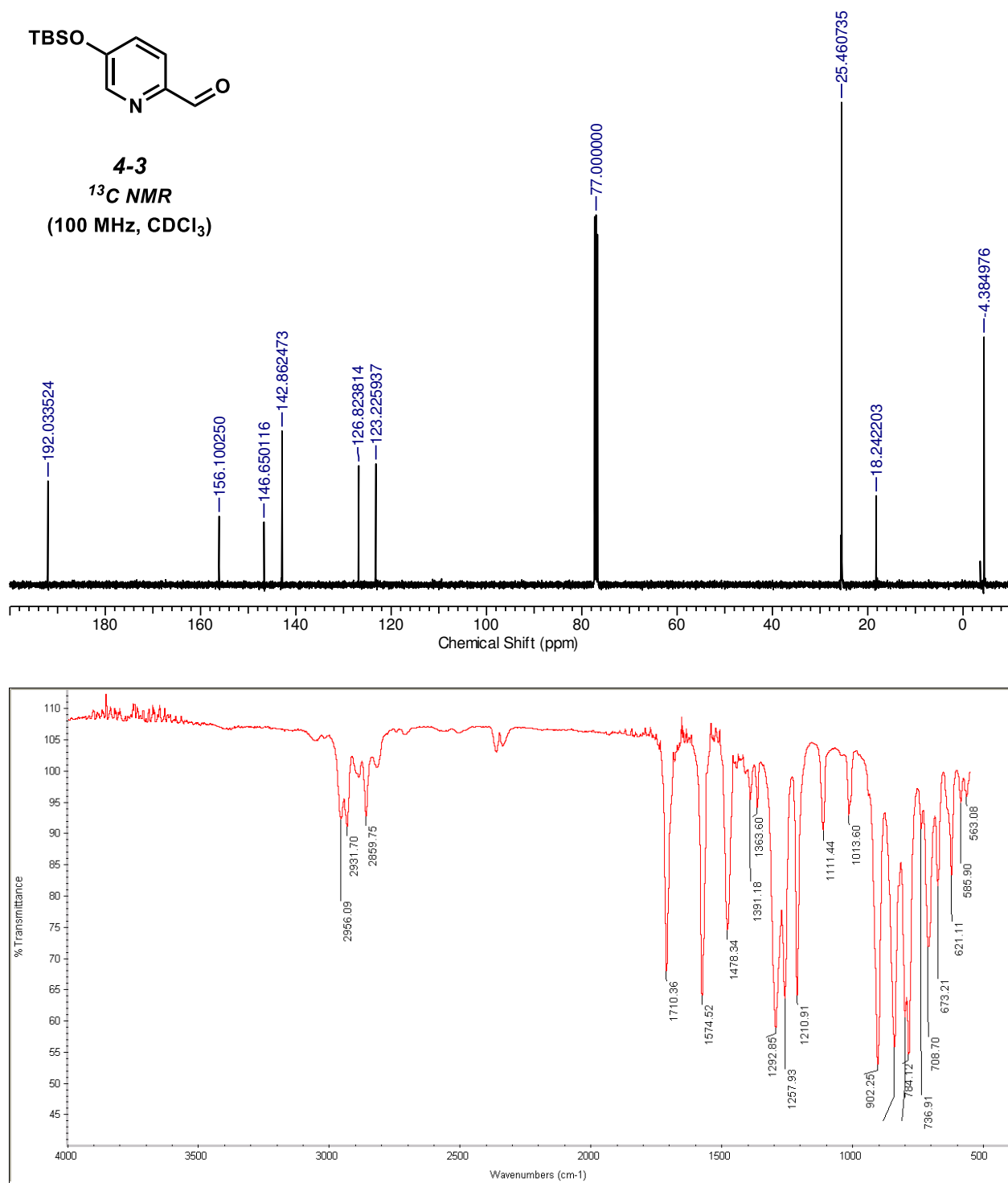
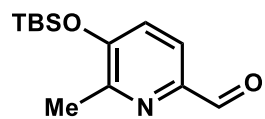


Figure A3.26. ¹³C NMR (top) and IR (bottom) spectra of **4-3**.



4-7
¹H NMR
(400 MHz, CDCl₃)

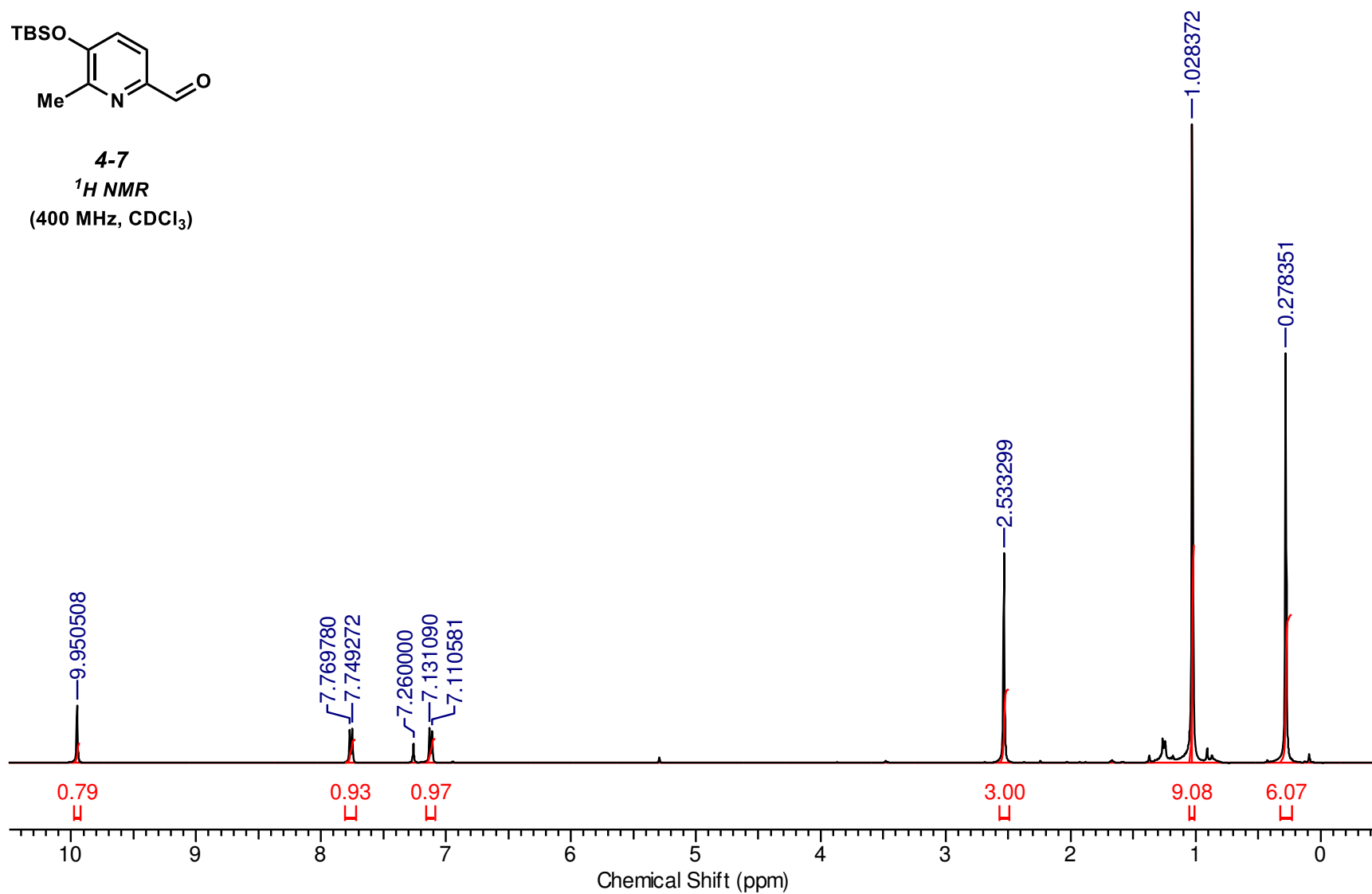
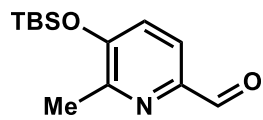


Figure A3.27. ¹H NMR spectrum of 4-7.



4-7
 ^{13}C NMR
 (100 MHz, CDCl_3)

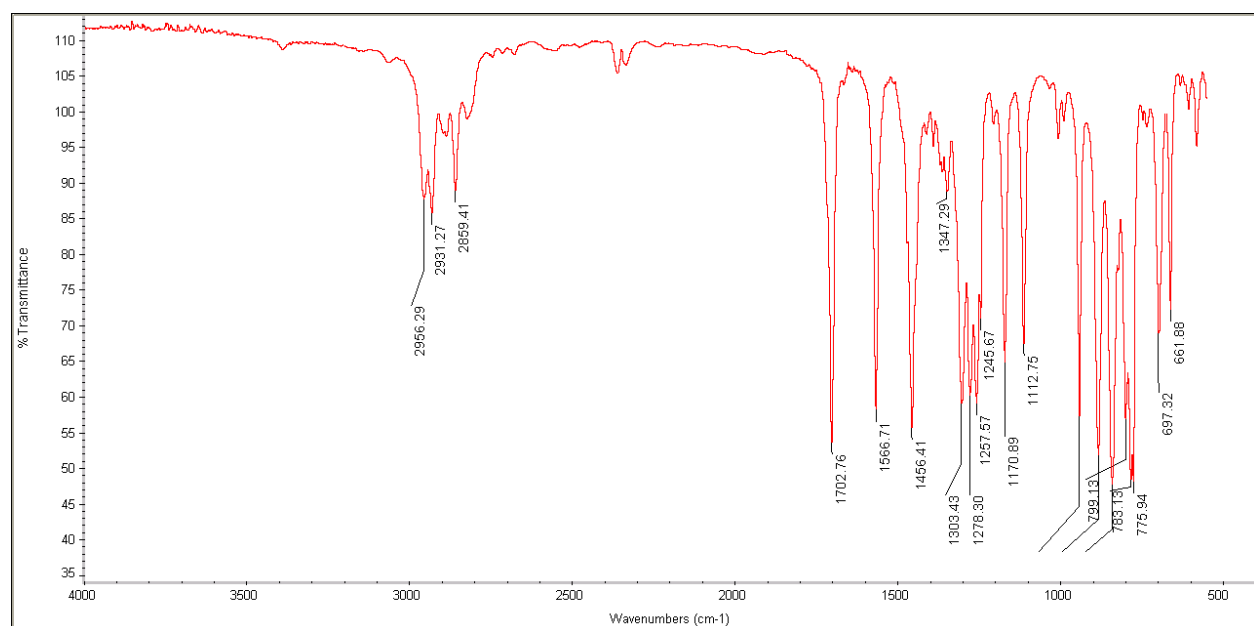
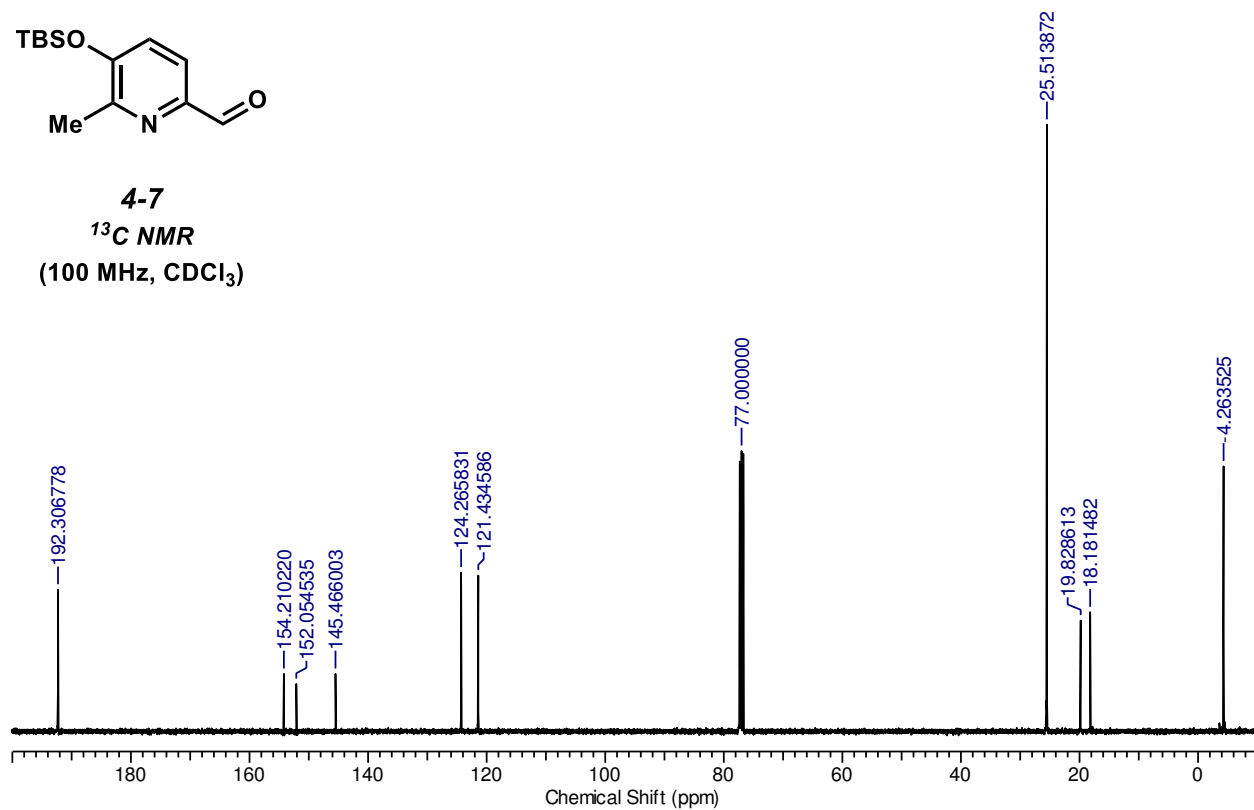


Figure A3.28. ^{13}C NMR (top) and IR (bottom) spectra of **4-7**.

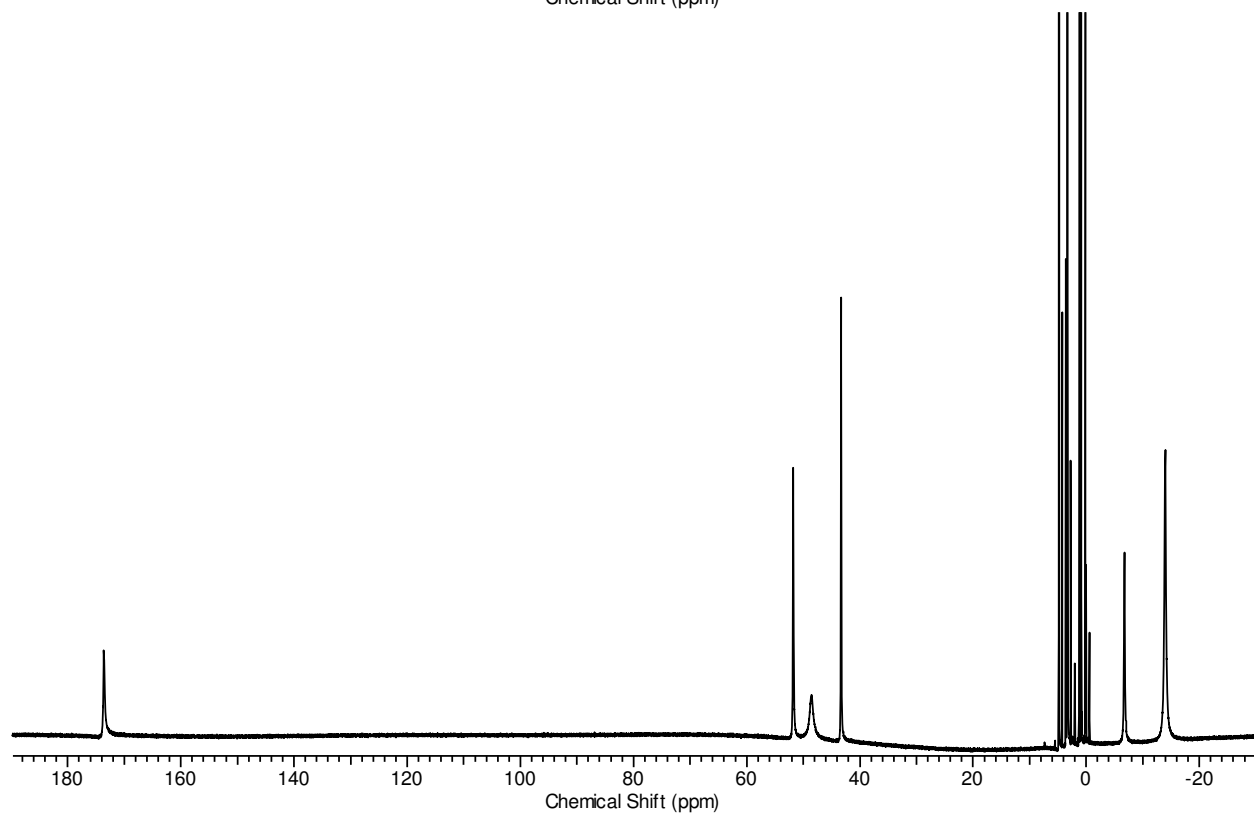
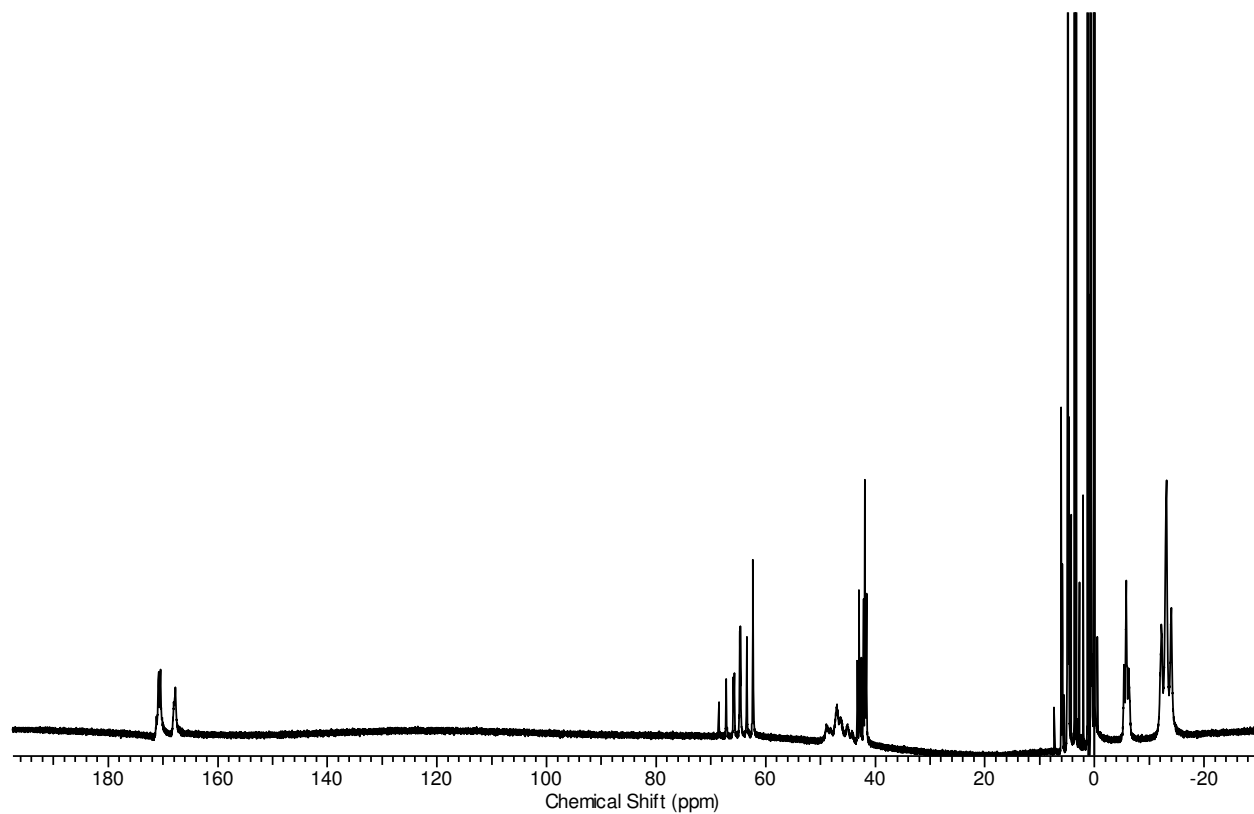


Figure A3.28. ^1H NMR spectrum of 4-8 before (top) and after (bottom) addition of 5 equivalents of CsF in CD_3OD .

Appendix 4: Supporting Information for Chapter 5

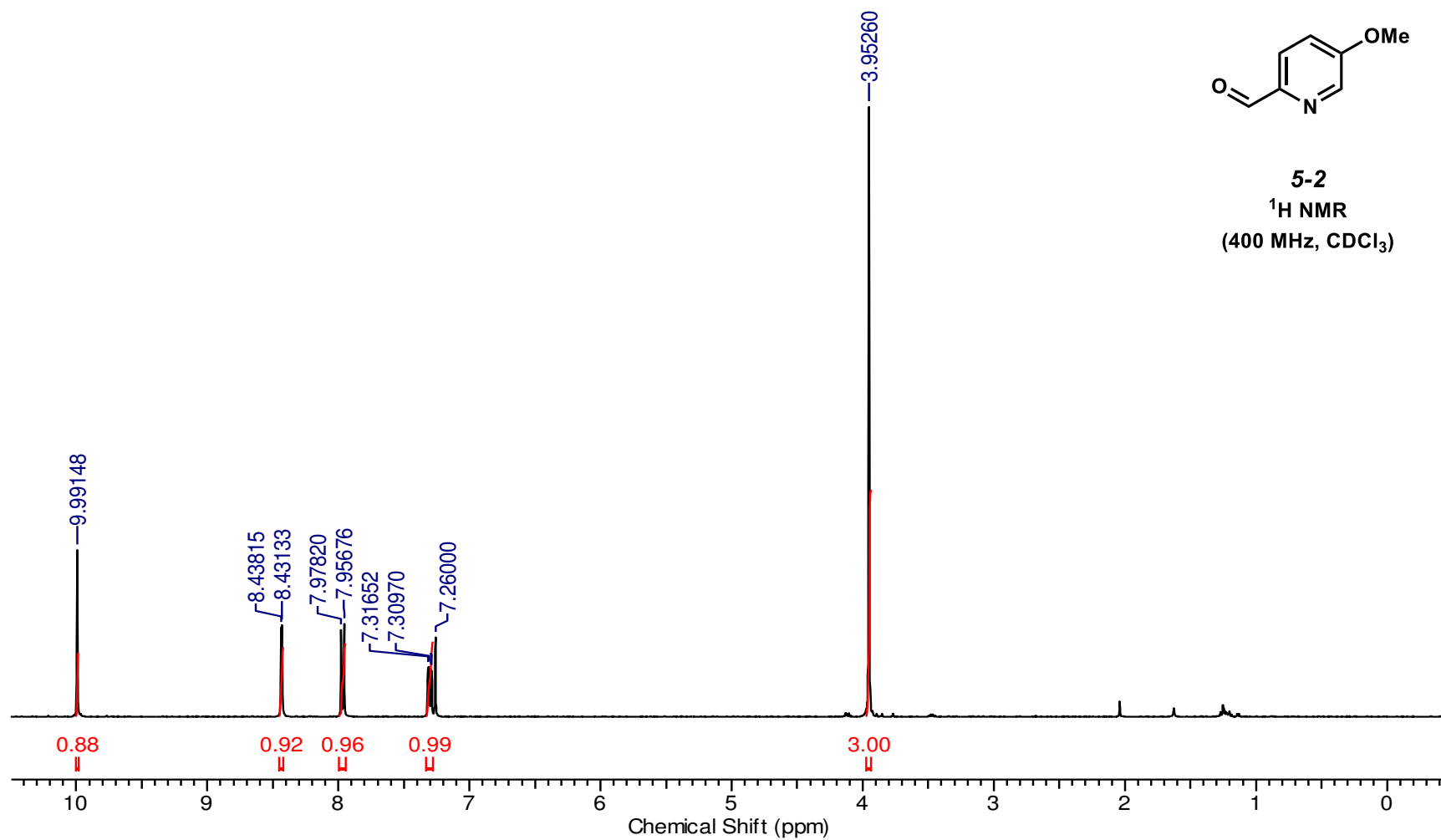


Figure A4.1. ¹H NMR spectrum of **5-2**.

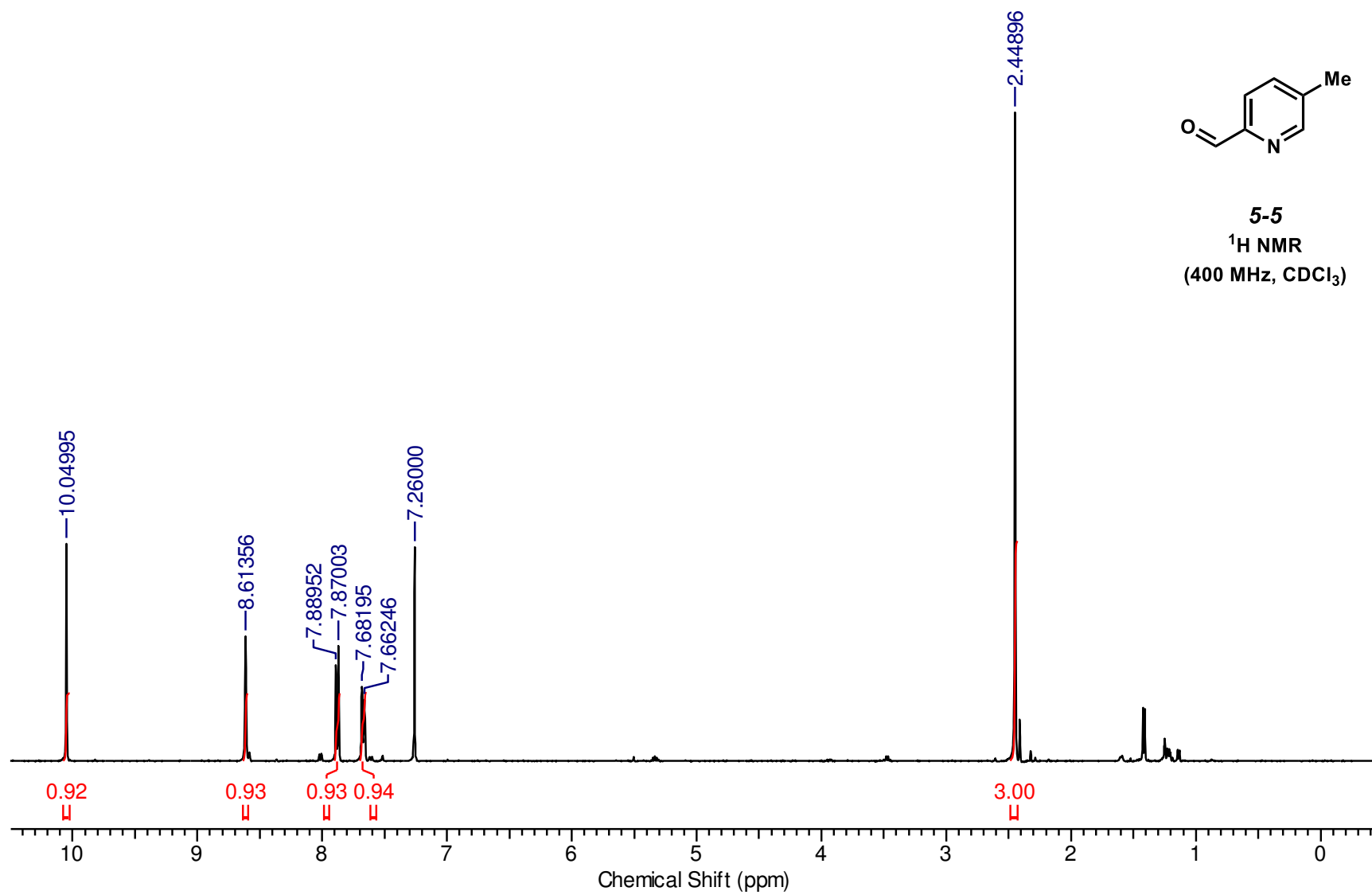
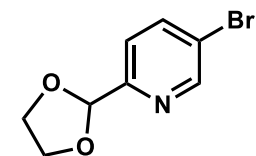


Figure A4.2. ¹H NMR spectrum of **5-5**.



5-6
¹H NMR
(400 MHz, CDCl₃)

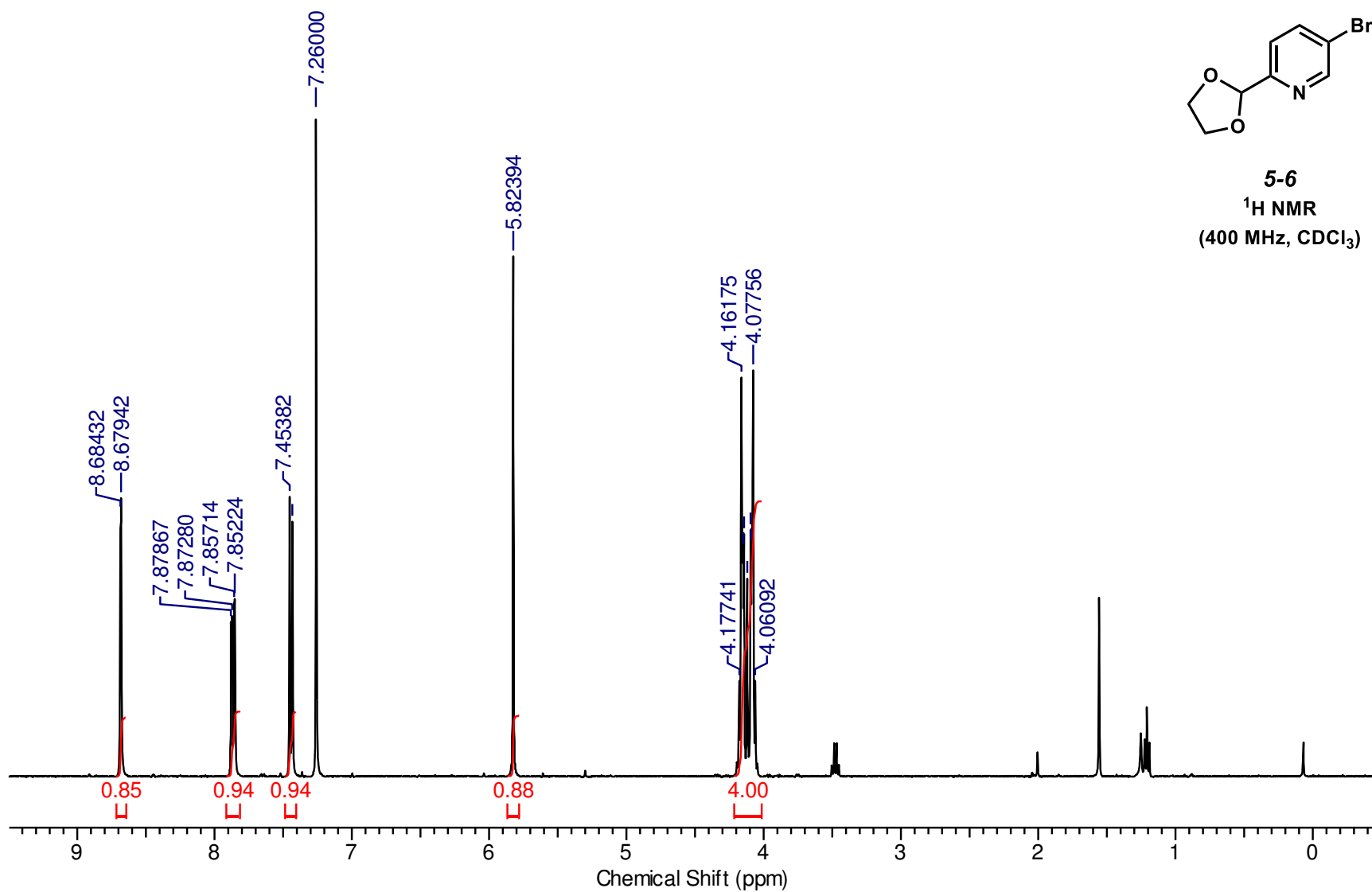


Figure A4.3. ¹H NMR spectrum of **5-6**.

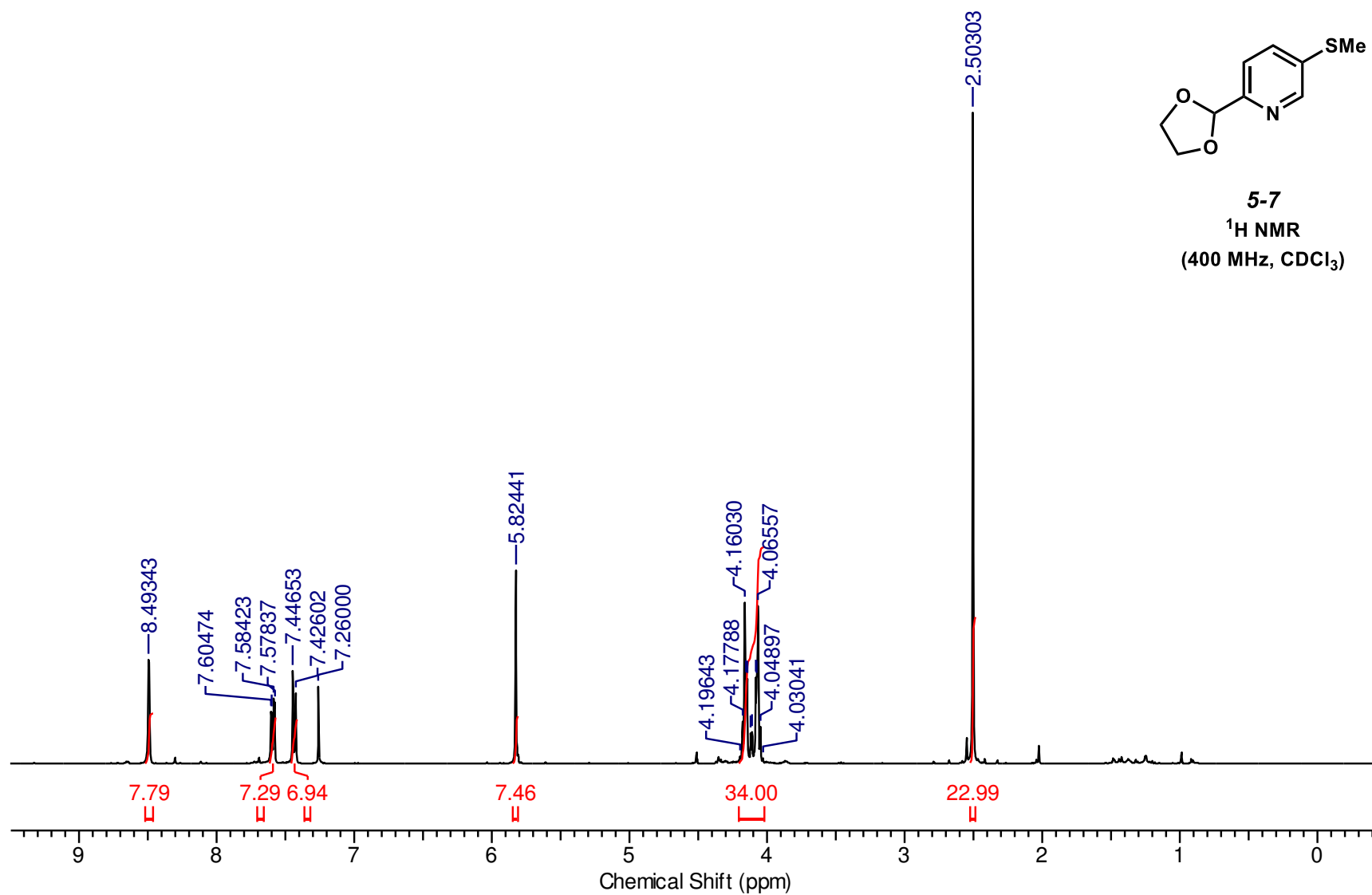


Figure A4.4. ¹H NMR spectrum of **5-7**.

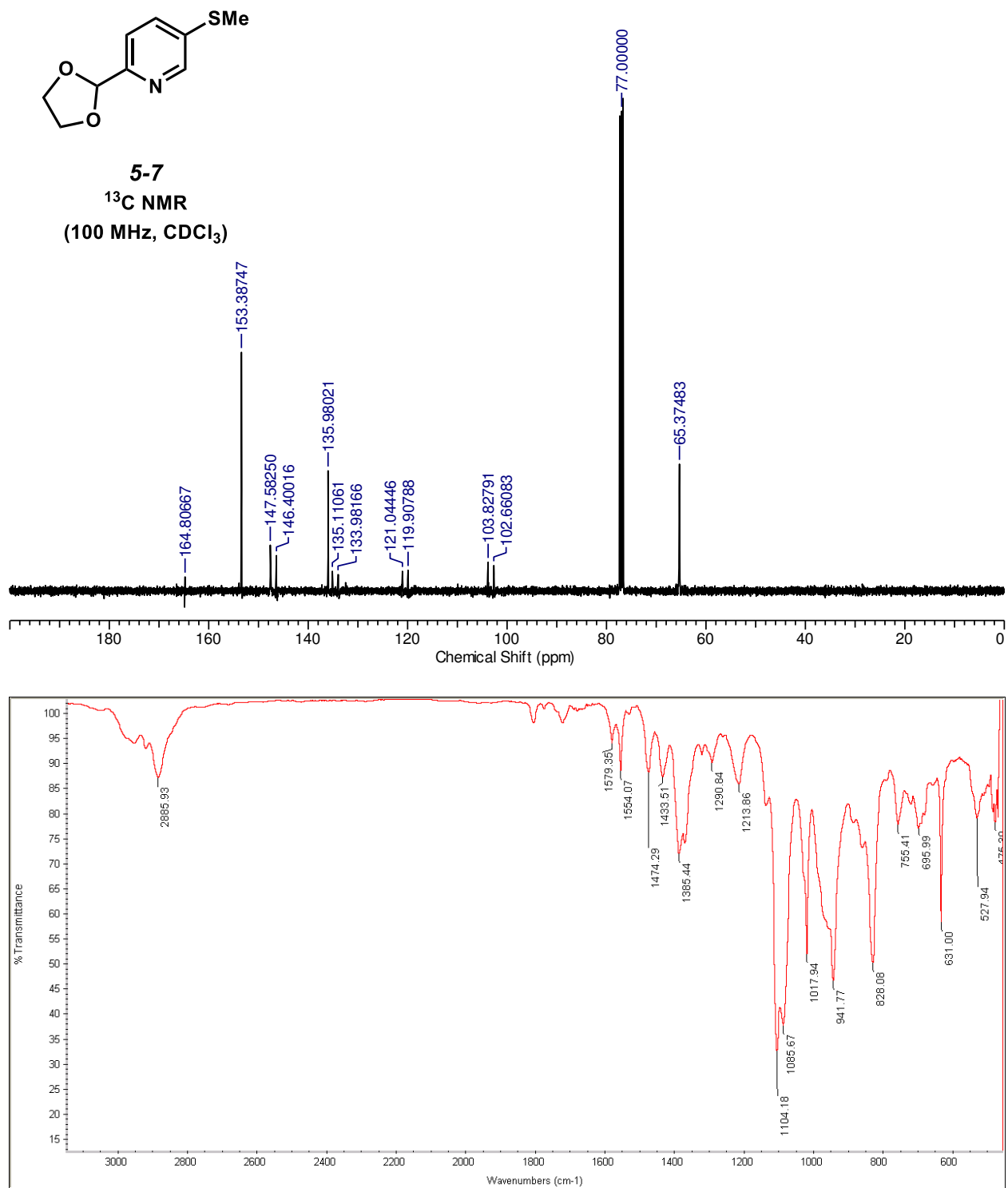


Figure A4.5. ¹³C NMR (top) and IR (bottom) spectra of **5-7**.

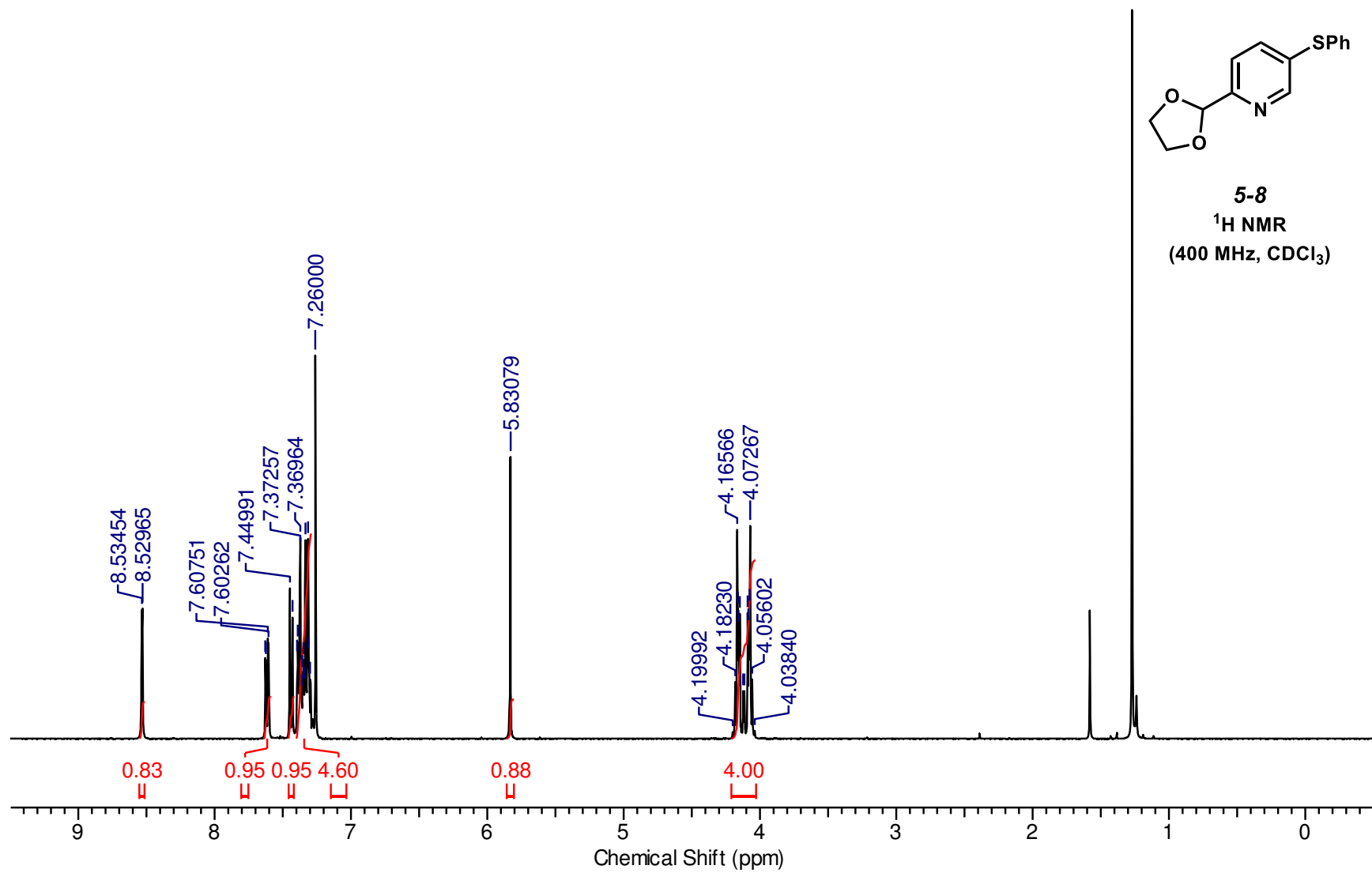


Figure A4.6. ¹H NMR spectrum of **5-8**.

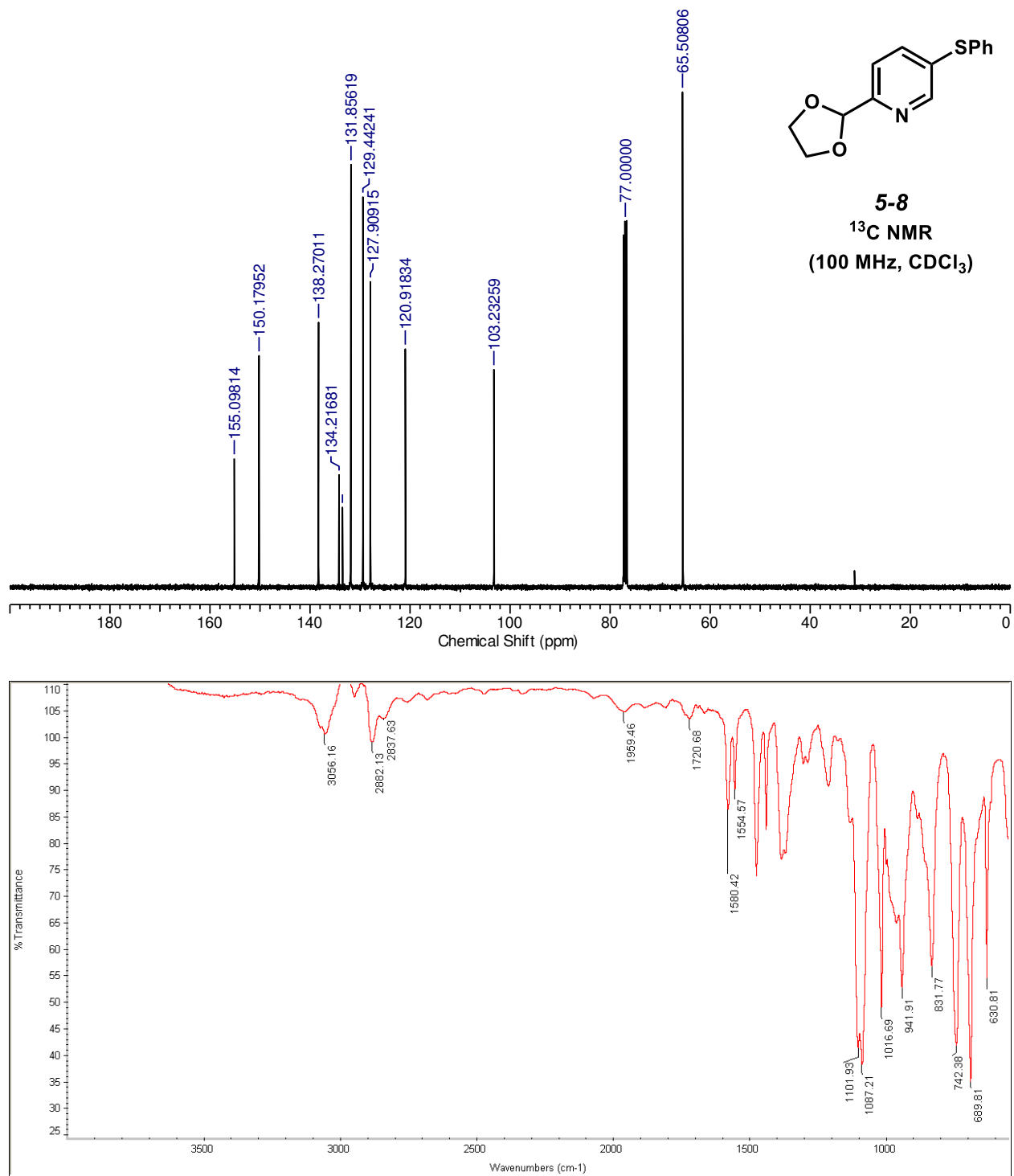
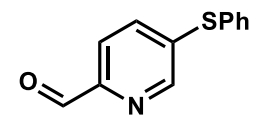


Figure A4.7. ¹³C NMR (top) and IR (bottom) spectra of **5-8**.



5-9
¹H NMR
(400 MHz, CDCl₃)

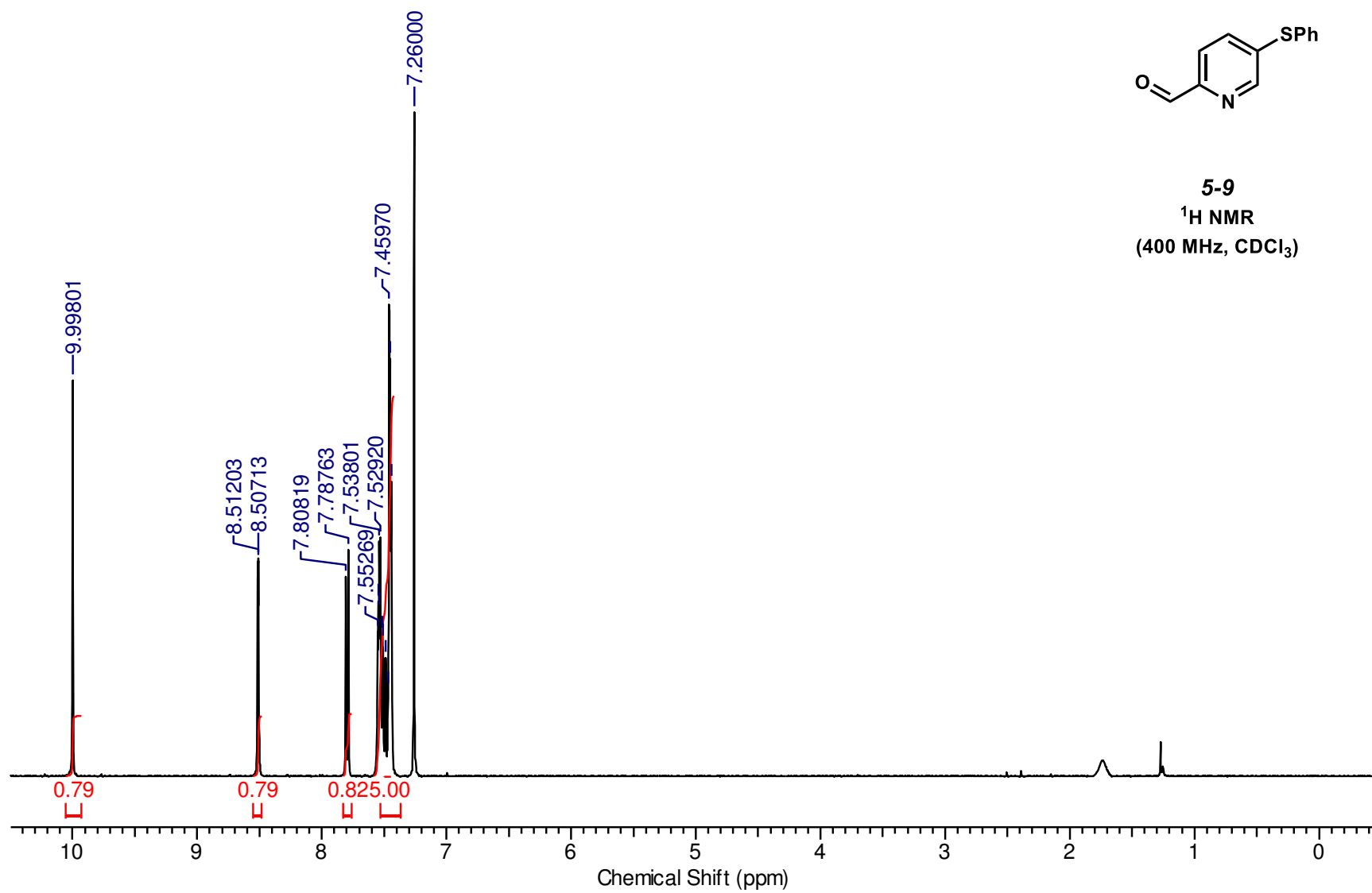


Figure A4.8. ¹H NMR spectrum of **5-9**.

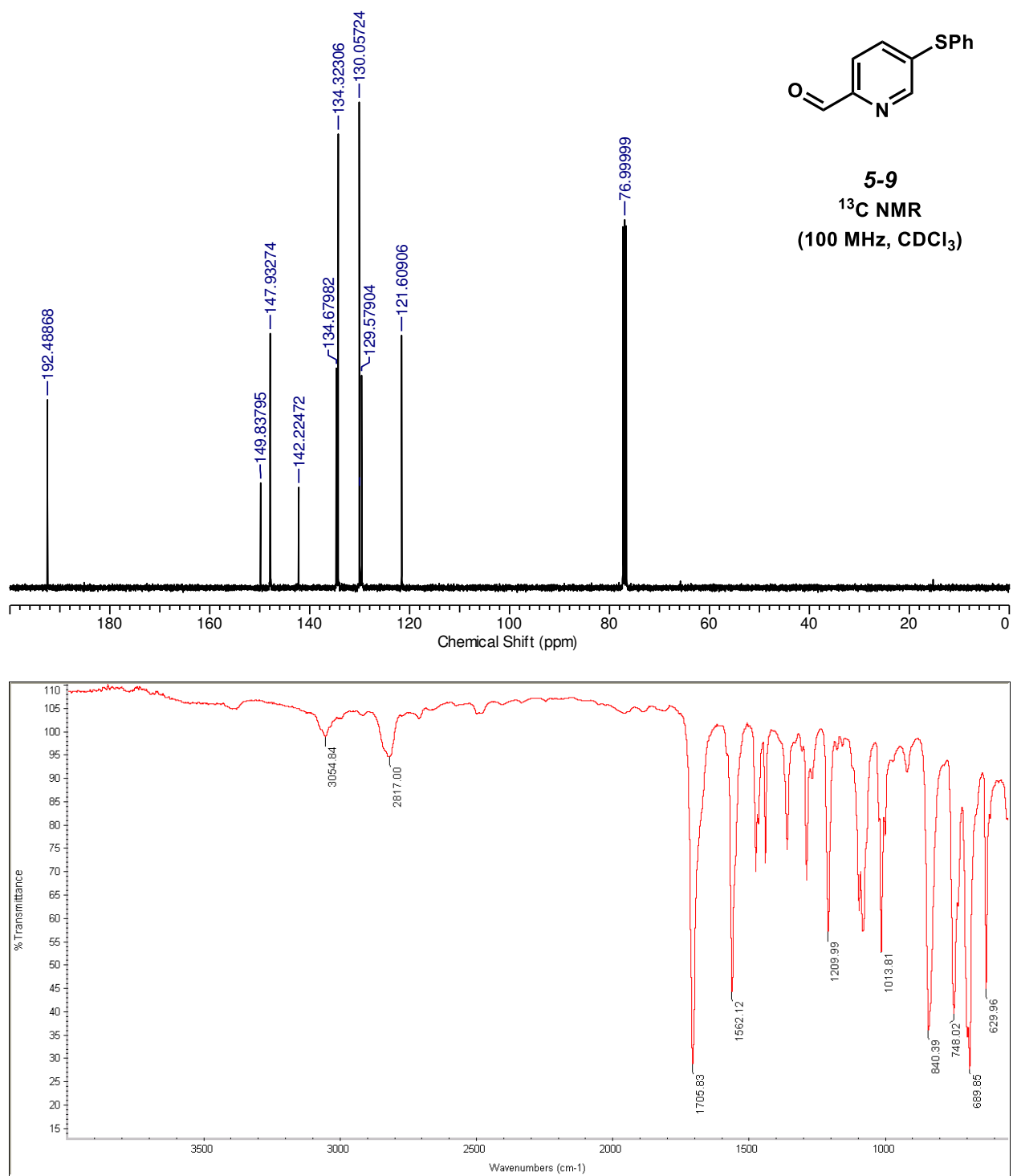
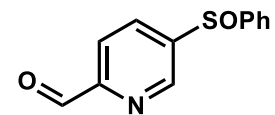


Figure A4.9. ¹³C NMR (top) and IR (bottom) spectra of **5-9**.



5-11
¹H NMR
(400 MHz, CDCl₃)

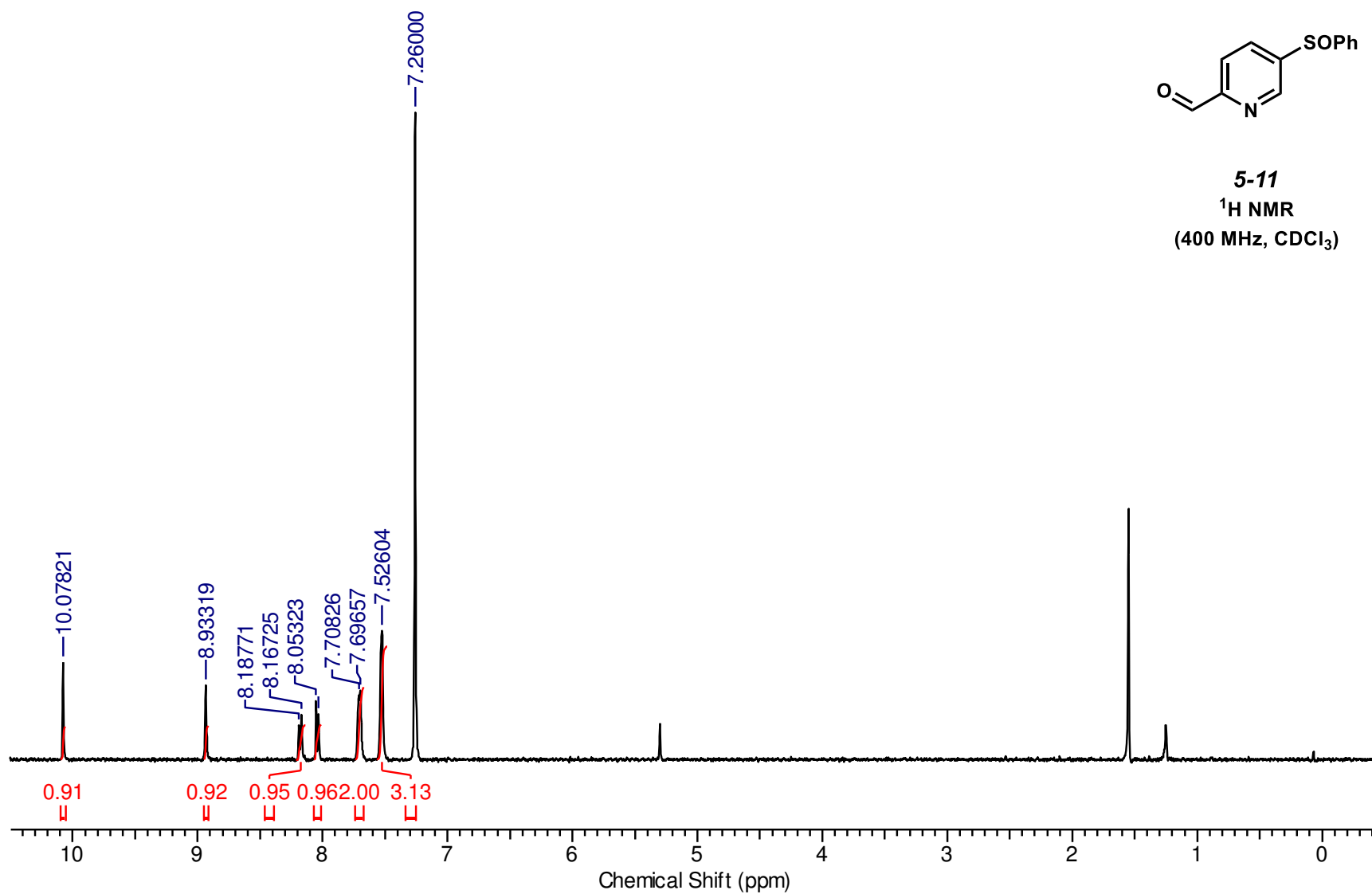


Figure A4.10. ¹H NMR spectrum of **5-11**.

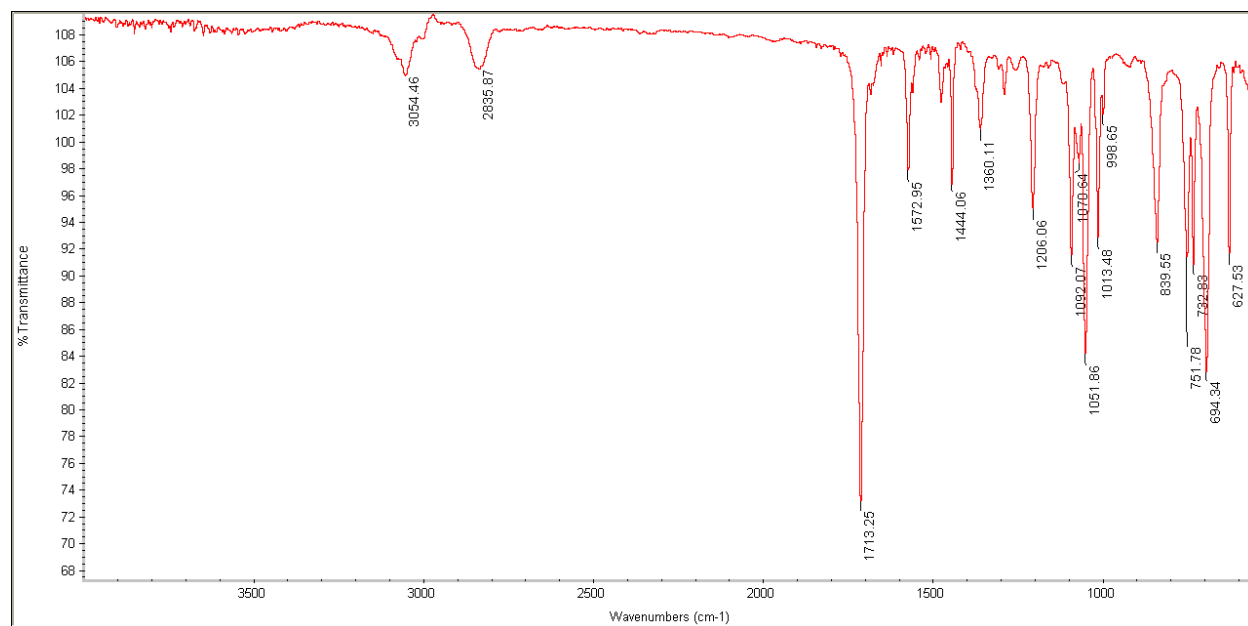
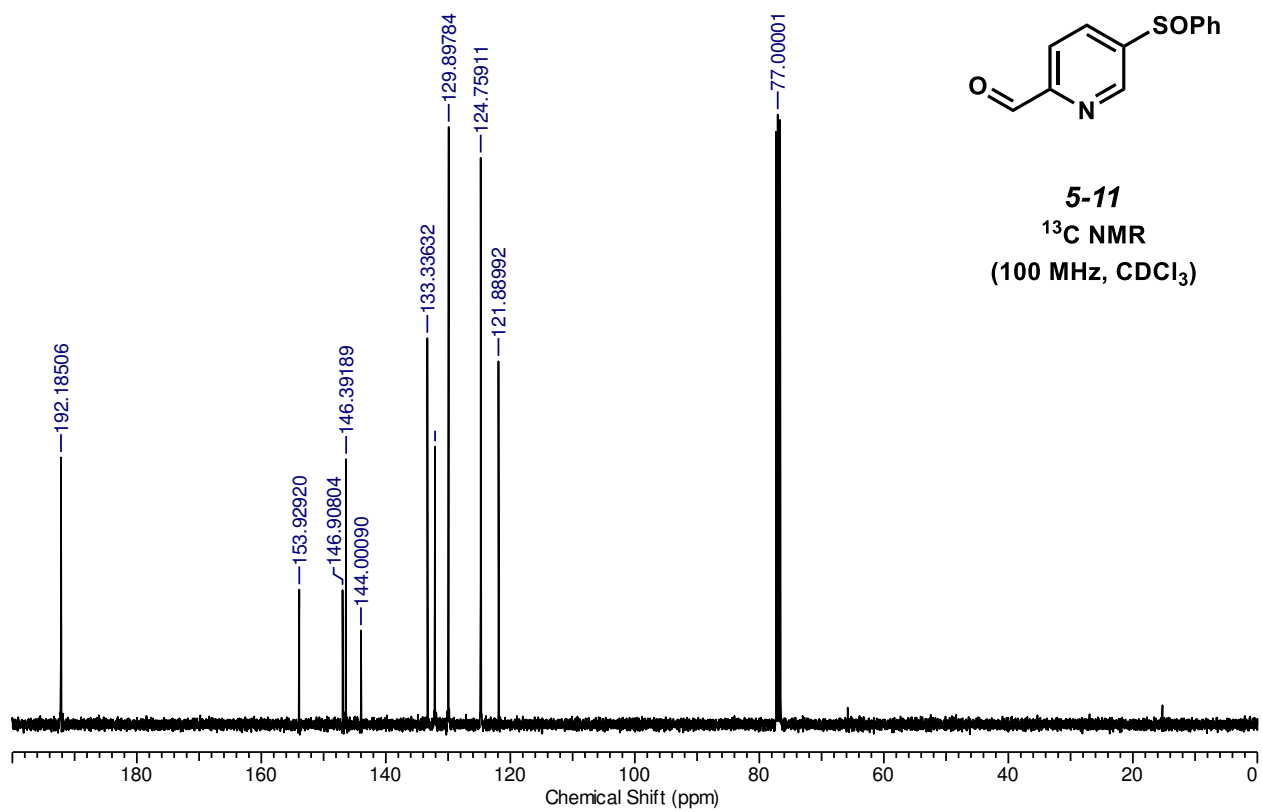
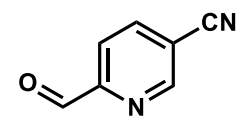


Figure A4.11. ¹³C NMR (top) and IR (bottom) spectra of **5-11**.



5-13
¹H NMR
(400 MHz, CDCl₃)

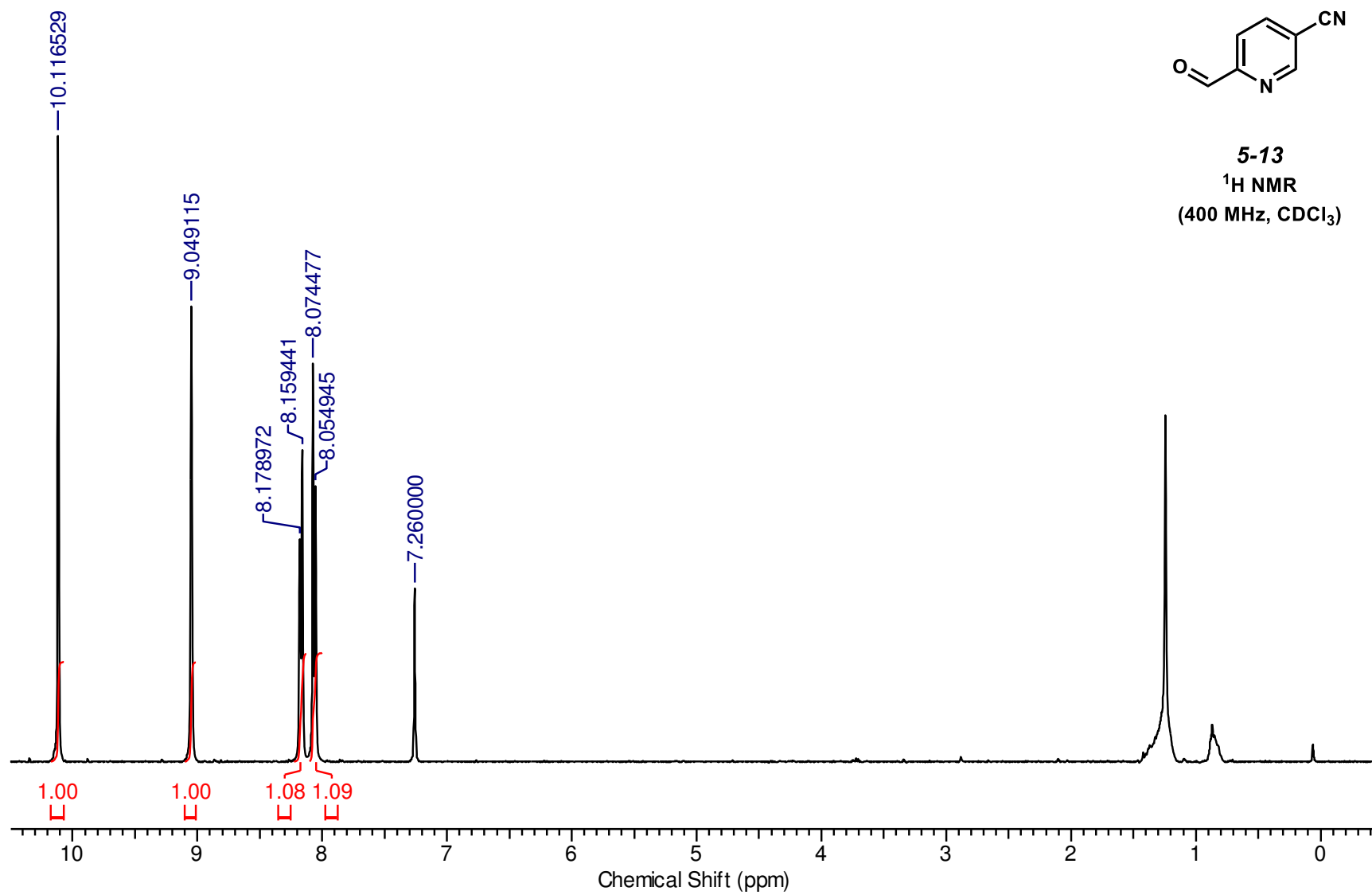


Figure A4.12. ¹H NMR spectrum of **5-13**.

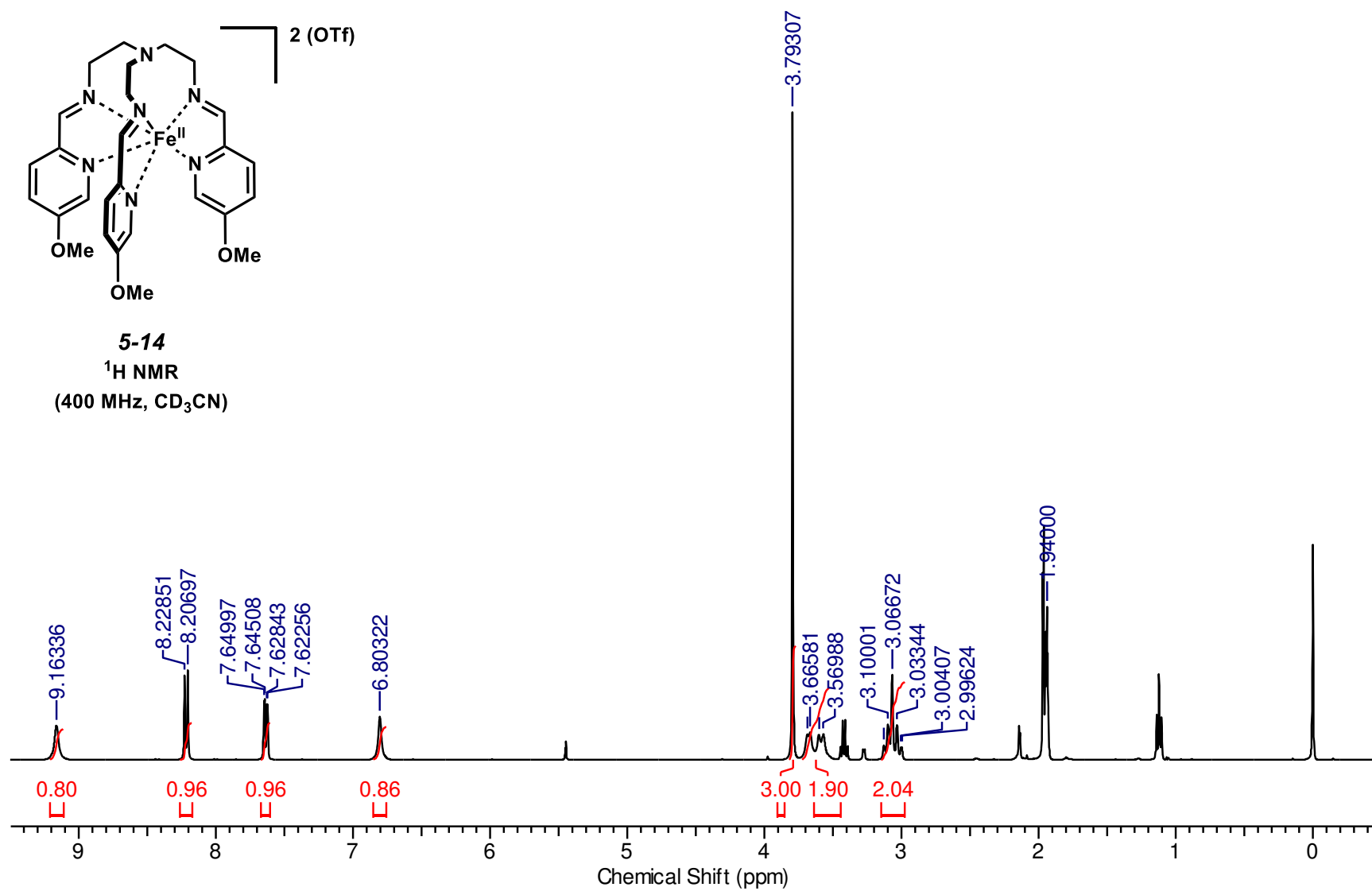


Figure A4.13. Paramagnetic ¹H NMR spectrum of **5-14**.

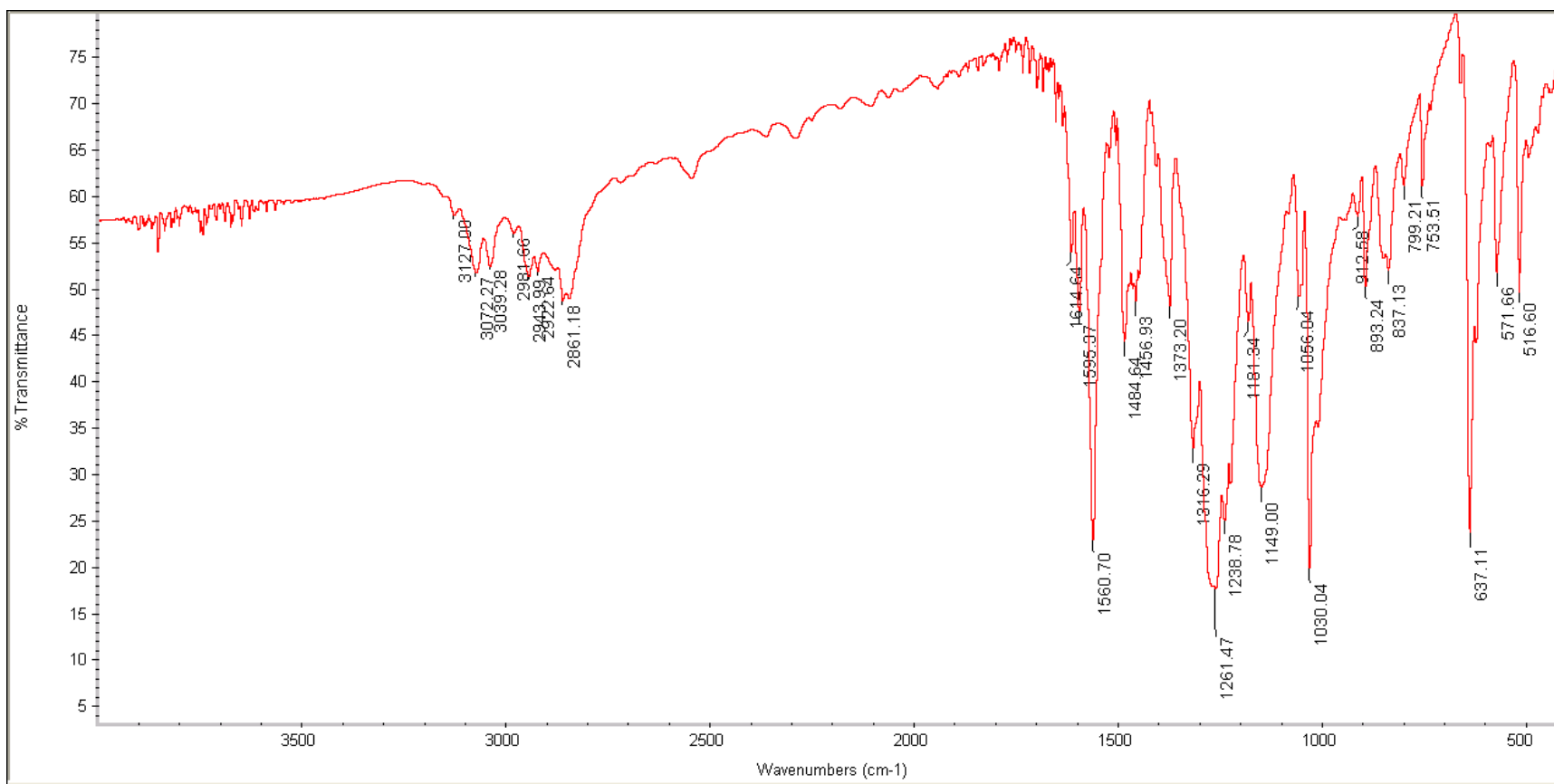


Figure A4.14. IR spectrum of 5-14.

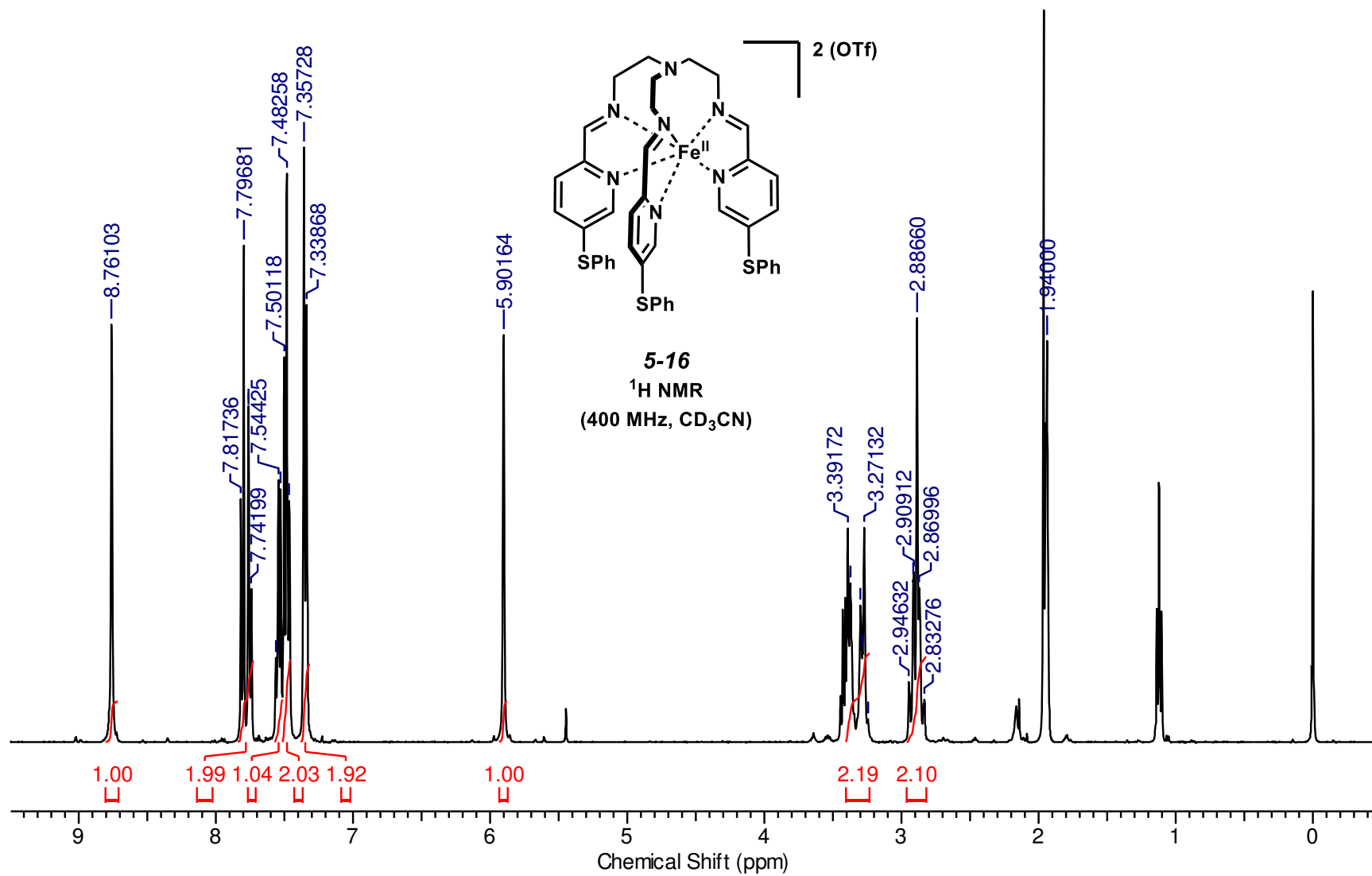


Figure A4.15. Paramagnetic ¹H NMR spectrum of **5-16**.

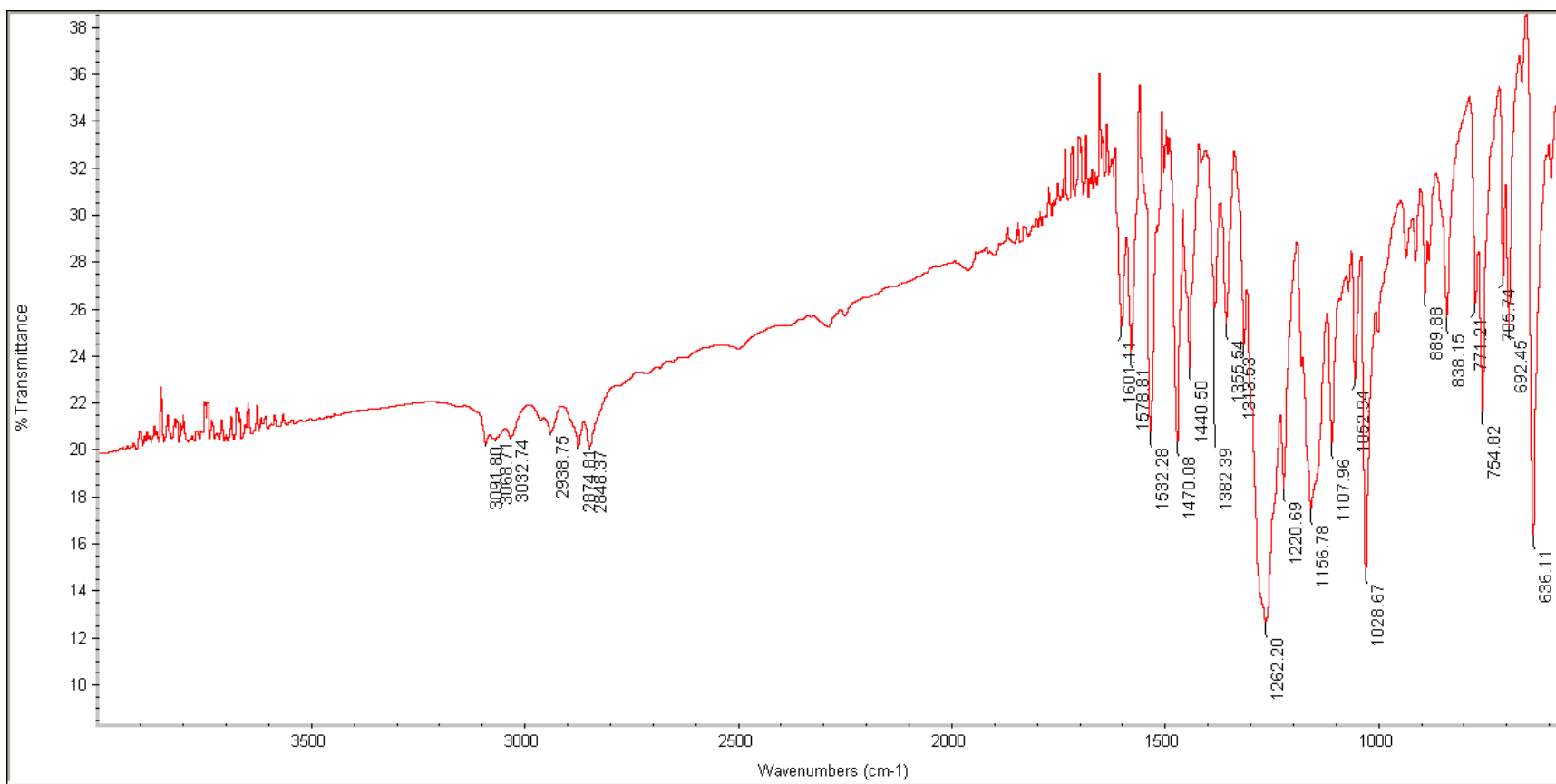
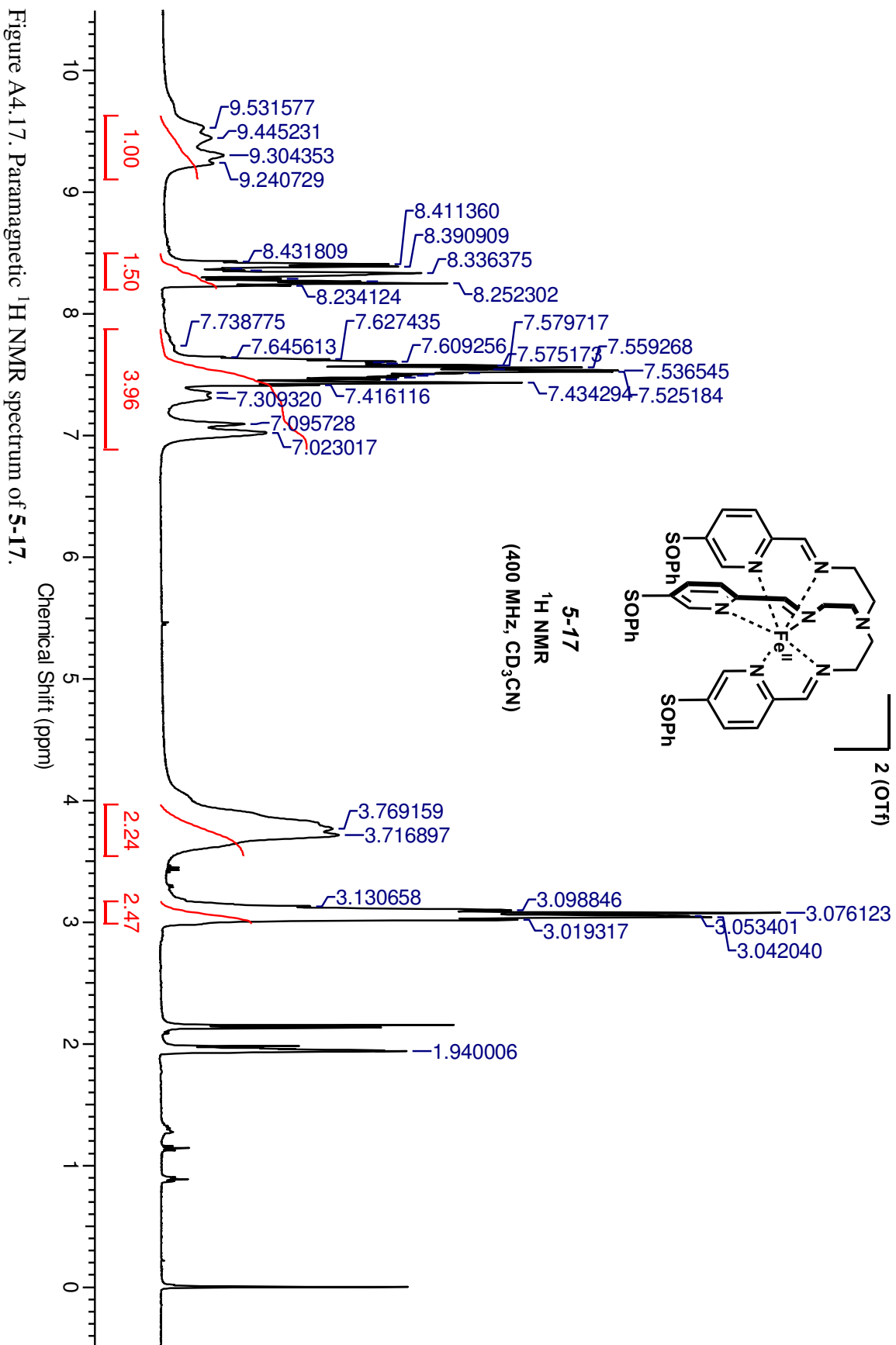


Figure A4.16. IR spectrum of 5-16.



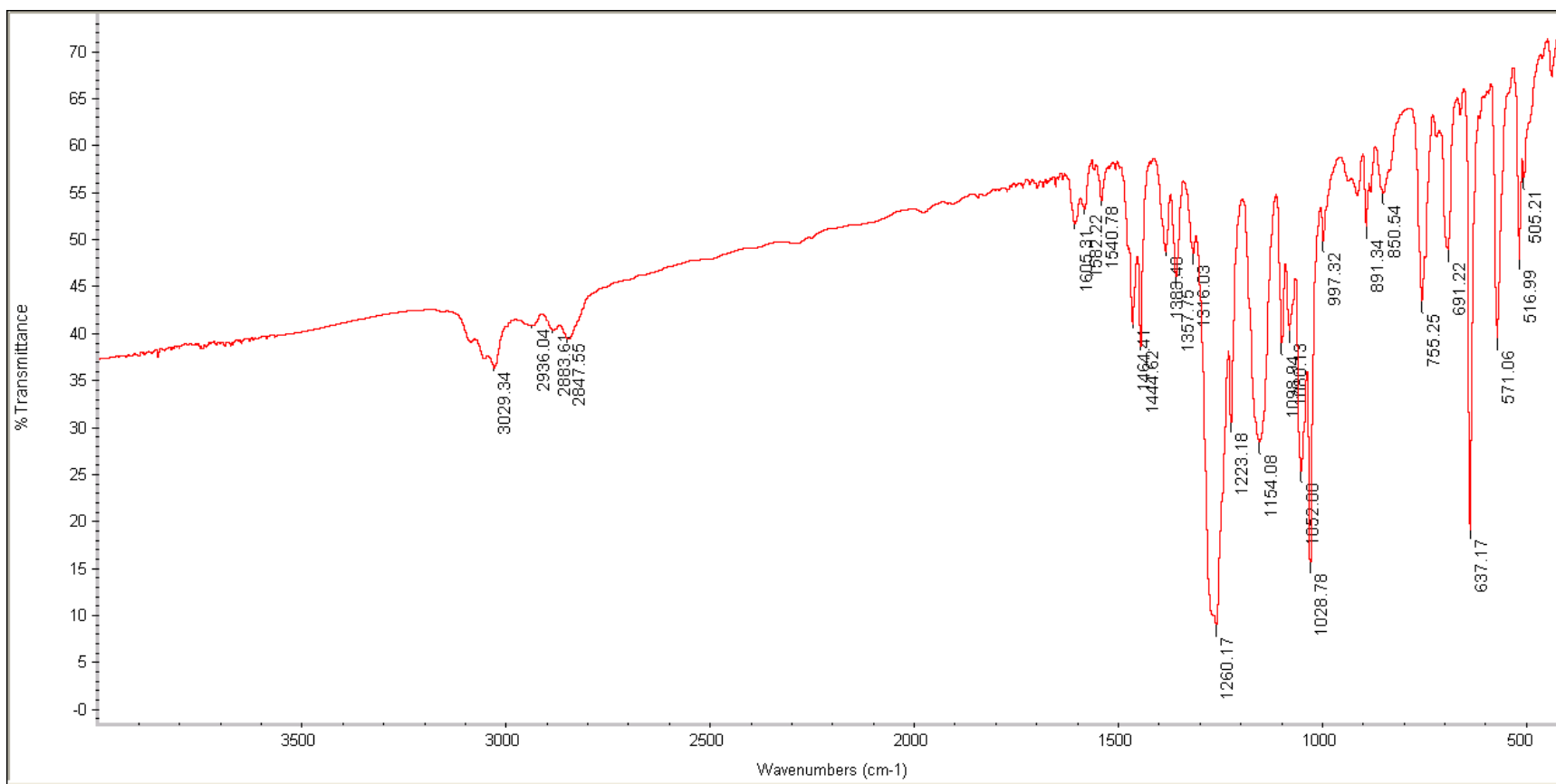
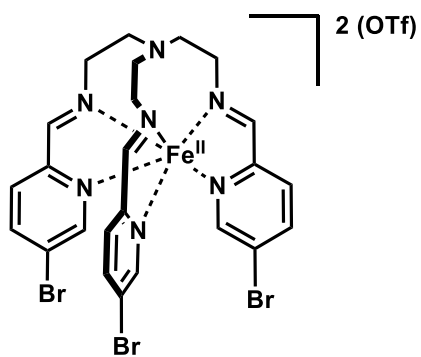


Figure A4.18. IR spectrum of 5-17.



5-19
¹H NMR
 (400 MHz, CD₃CN)

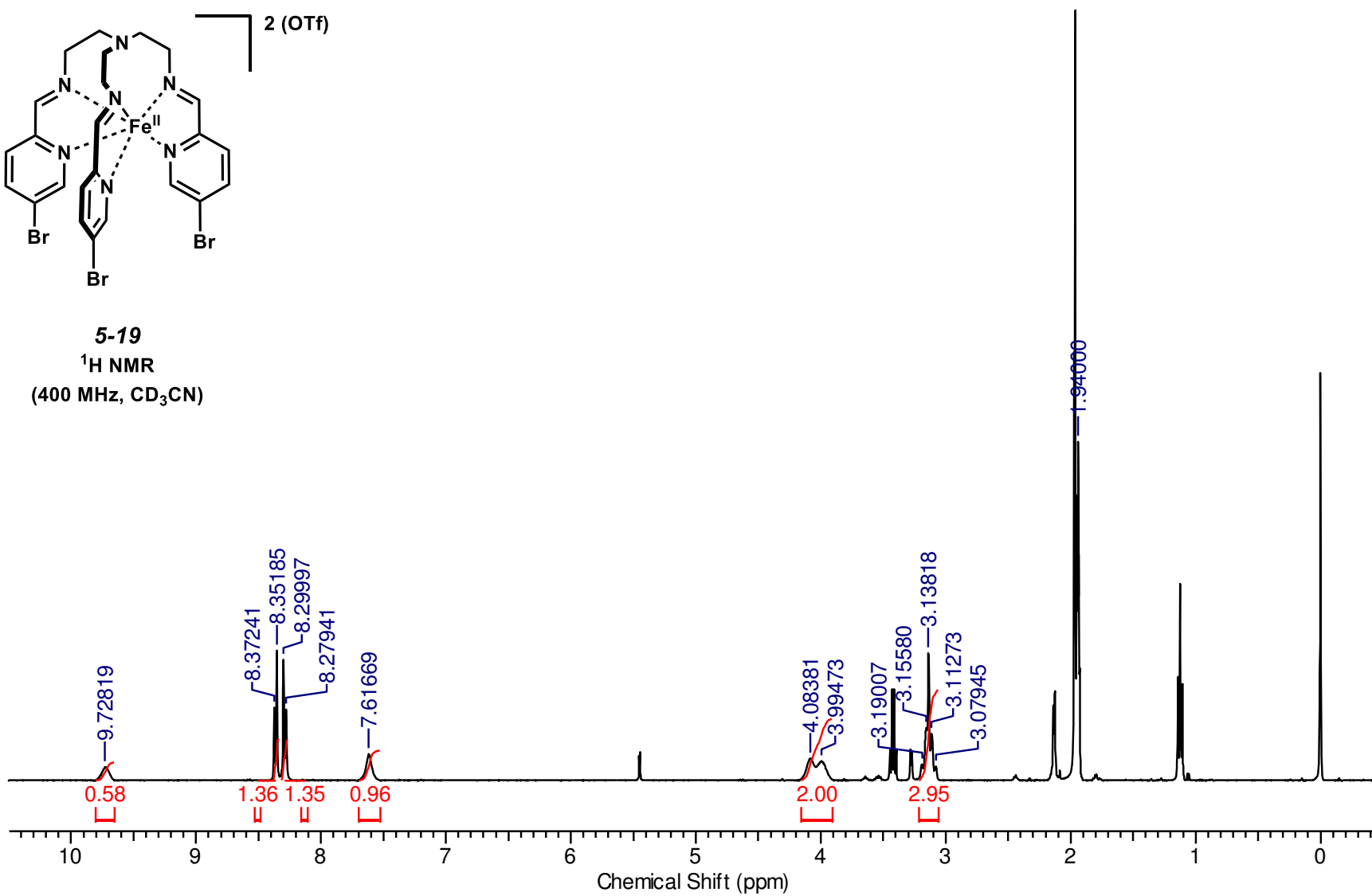


Figure A4.19. Paramagnetic ¹H NMR spectrum of **5-19**.

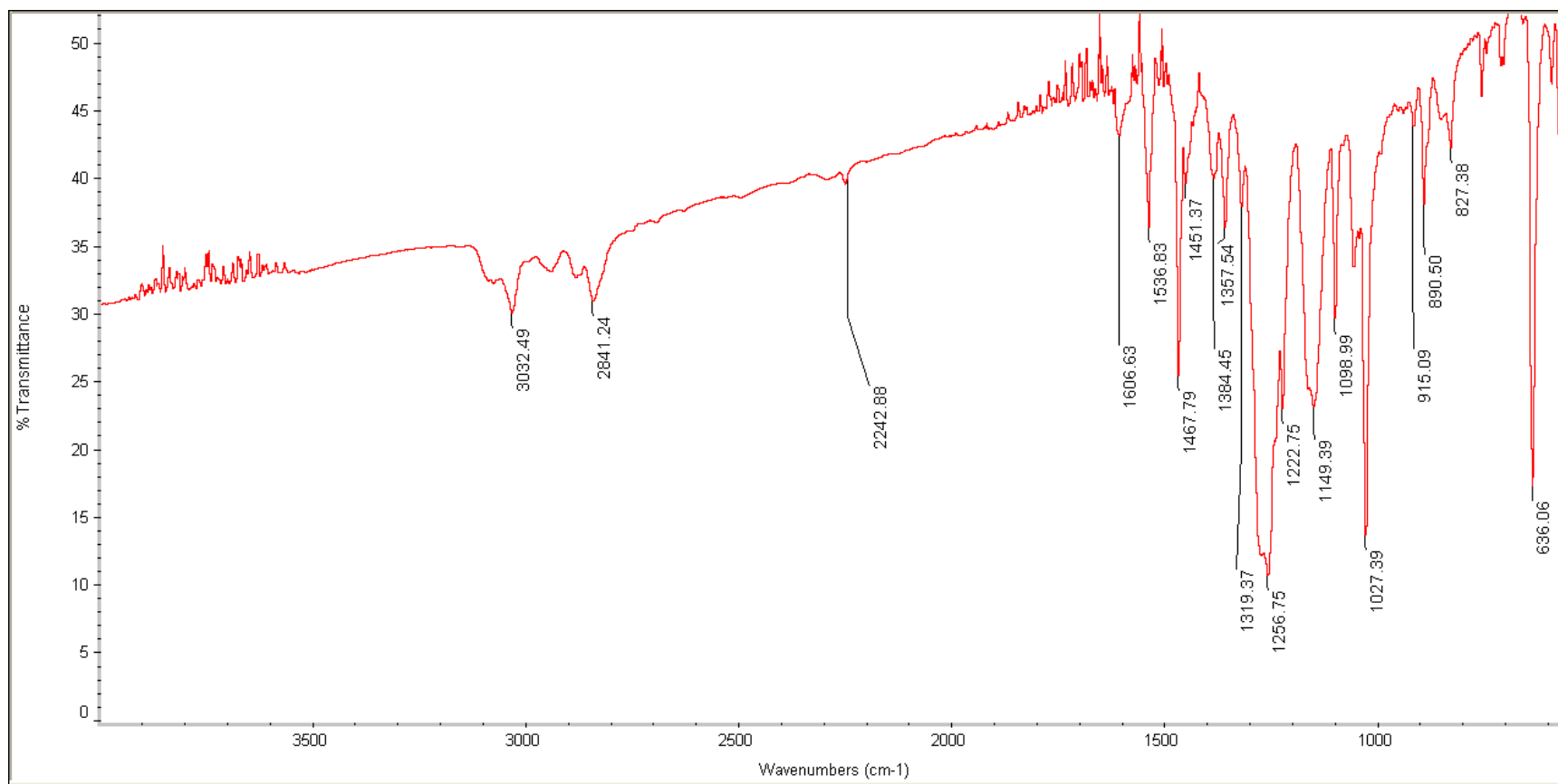


Figure A4.20. IR spectrum of **5-19**.

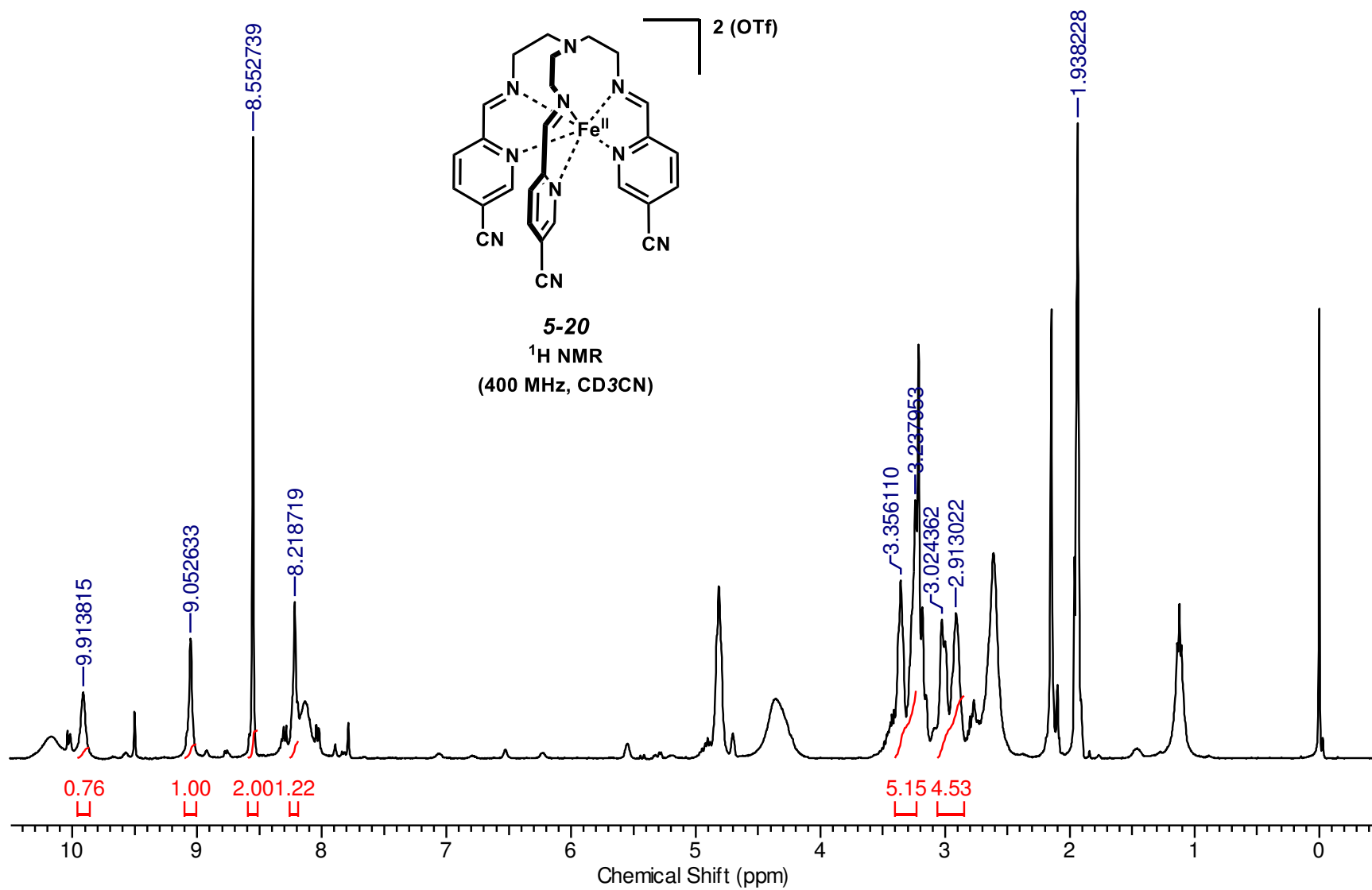


Figure A4.21. Paramagnetic ^1H NMR spectrum of **5-20**.

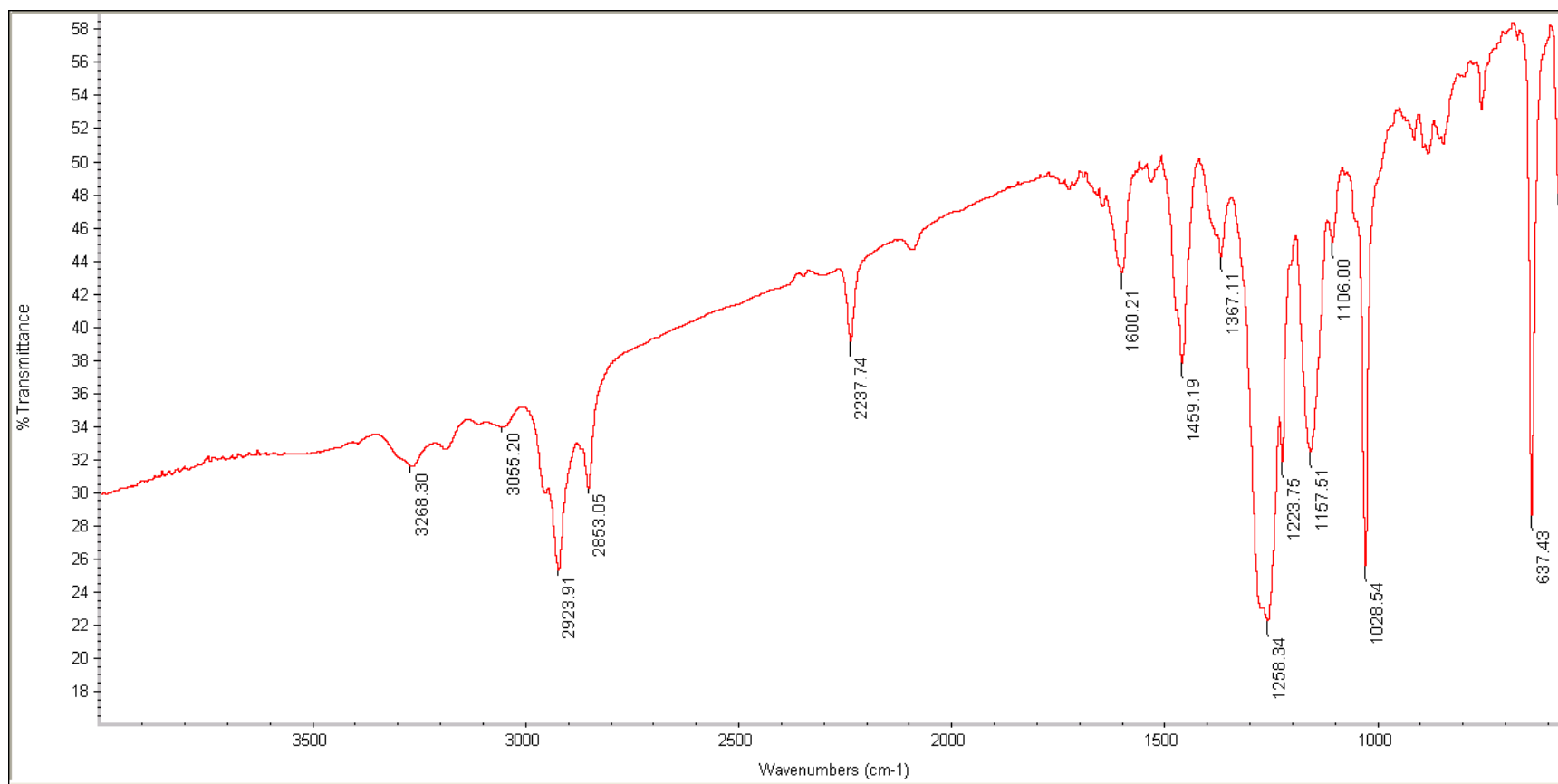


Figure A4.22. IR spectrum of **5-20**.